ABSTRACT

Title of Dissertation: TREATMENT OF STORMWATER RUNOFF BY GEOTEXTILE FILTERS VIA SUSPENDED SOLIDS CAPTURE

Carmen Ann Franks, Doctor of Philosophy, 2012

Dissertation directed by: Professor Allen P. Davis
Associate Professor Ahmet H. Aydilek
Department of Civil and Environmental Engineering

Suspended solids in stormwater runoff create a range of water quality problems; their removal lessens the deleterious impact of stormwater runoff on aquatic ecosystems. In this study, three geotextiles were tested in laboratory column tests with influent suspensions having hydraulic loading rates, total suspended solids (TSS) concentrations, and particle size distributions (PSDs) similar to those reported for urban highway stormwater runoff. After a short ripening period, the geotextile filters removed TSS from 100-200 mg/L to below a target concentration of 30 mg/L. A lower geotextile permittivity resulted in an increased percentage of TSS captured by the filter; however, the total mass of solids captured was unaffected because lower permittivity resulted in lower total solids loaded to the filter overall. In general, the effectiveness of the geotextile filter at retaining suspended solids increased as filter opening sizes decreased and as influent particle sizes increased. The hydraulic conductivity of a geotextile filter,

which was related to TSS captured via a power function, was higher for geotextiles with higher permittivity and larger opening sizes and for larger influent particle sizes. Overall, the filter with the second highest permittivity (0.8 s^{-1}), NW2, was the most successful geotextile tested. TSS removal in the geotextile laboratory tests was comparable to reported values from sand filters in literature under similar loading conditions. Sand filters in laboratory tests had greater TSS removal than geotextile filters. However, the sand filters clogged at a lower total solids loading than the geotextiles. The applicability of existing filtration criteria for geotextiles for stormwater treatment is addressed, and four new retention criteria ratios specifically for stormwater filtration which use two filter opening sizes and two particle diameters, such as $(0_{95}/D_{60})/(O_{30}/D_{10}) > 0.05$, are introduced. Results from field testing are analyzed; the geotextile filter reduced TSS concentrations in runoff by an average of 84% with input TSS event mean concentrations (EMCs) ranging from 22 – 185 mg/L and output EMCs ranging from 1.7 – 22 mg/L. A mathematical model is developed which estimates hydraulic conductivity as a function of solids captured. The model and filtration criteria are used to assess the field testing results.

TREATMENT OF STORMWATER RUNOFF BY GEOTEXTILE FILTERS VIA
SUSPENDED SOLIDS CAPTURE

by

Carmen Ann Franks

Dissertation submitted to the Faculty of the Graduate School of the
University of Maryland, College Park in partial fulfillment
of the requirements for the degree of
Doctorate of Philosophy
2012

Advisory Committee:

      Professor Allen P. Davis, Chair
      Associate Professor Ahmet H. Aydilek
      Professor Robert L. Hill
      Assistant Professor Baoxia Mi
      Professor Alba Torrents

ACKNOWLEDGEMENTS

TABLE OF CONTENTS

LIST OF TABLES

LIST OF FIGURES

LIST OF ABBREVIATIONS AND SYMBOLS

α	statistical level of significance
α_C	critical level of significance
α_s	sticking coefficient
γ_w	specific weight of water
ε	porosity
η	single collector collision efficiency
Θ	angle of triangular weir
μ	dynamic viscosity
θ	transmissivity
ρ	density of liquid
ρ_f	density of fibers
τ	time
ψ	permittivity
a	dimensionless model parameter
A	area of filter
AOS	apparent opening size (O_{95})
b	dimensionless model parameter
b_0	y-intercept of linear trend line
b_1	slope of linear trend line
B_C	clogging ratio
B_R	retention ratio
BMP	best management practice
BOD	biochemical oxygen demand
C	concentration of particles/pollutant
C_0	concentration of particles/pollutant in influent suspension
C_C	coefficient of curvature
C_f	flume coefficient
C_U	coefficient of uniformity
C_{wt}	triangular weir constant
D	particle diameter
D_c	collector diameter
D_{50}	diameter at which 50% of the particles by mass have a smaller diameter than that value
$\bar{e}$	bias
EMC	event mean concentration
EPA	Environmental Protection Agency

EV	explained variance
FOS	filtration opening size
g	gravitational acceleration
h	head loss
H	weir head
HLR	hydraulic loading rate
k	cross-plane permeability
K	hydraulic conductivity
K_0	initial hydraulic conductivity of the clean filter
k_i	permeability of elementary element i of filter media
k_{in}	in-plane permeability
L	length of flow in filter
LID	Low Impact Development
m	mass of accumulated particles in and on filter
m_1	critical value of mass of accumulated particles
m_c	cumulative mass of solids loaded to the filter
M_i	mass of pollutant in event i
m_L	mass of solids loaded to the filter per each 75 minute test
m_n	mass of solids at end of final test (test n)
MTBE	methyl-tertiary-butyl ether
n	number of tests in test set
N	weighting coefficient
O	opening diameter
O_{large}	average of (O_{95}, O_{100})
O_{small}	average of (O_{10}, O_{20}, O_{30})
p	pressure measured when filter is exposed to suspension
p_0	pressure measured when filter is exposed to clear water
δp	excess pressure
ΔP	pressure drop across media
ΔP_0	initial pressure drop across the filter before solids loading occurs
PSD	particle size distribution
q	flow rate
q_{in}	flow rate of the influent runoff
r	empirical flow-through constant
R	correlation coefficient
R^2	coefficient of determination
RPM	rotations per minute
S_e	standard error

S_y	standard deviation
t	thickness/depth of filter
TMDL	Total Maximum Daily Load
TSS	total suspended solids
TV	total variance
u	flume exponent
UV	unexplained variance
v	flow velocity
v_{in}	influent flow velocity
V_i	volume of sample for event i
w	mass per unit area
x	empirical exponential constant
X	$\alpha_{s*}\,\eta\,/\,D_C$
$\hat{y}$	predicted values of y
$\bar{y}$	mean of y
z	water level in channel

Chapter I: INTRODUCTION

<u>**PURPOSE OF RESEARCH**</u>

Current urban infrastructure is highly reliant on impervious surfaces, including roadways, parking lots, and building rooftops. Rainfall that strikes these surfaces cannot infiltrate into the soil and subsurface and rapidly becomes surface runoff. This runoff is conveyed away from the source via the storm drain infrastructure system to minimize flooding and resulting safety concerns. As this rainfall and runoff is transported across these impervious surfaces, it mobilizes and transports particulate matter and other pollutants. These particulates include soil matter as well as anthropogenic particulate matter resulting from the attrition of pavements, vehicle wear materials, and building materials. The enhanced flows and particulate loads are directed into local receiving bodies, causing erosion problems, toxicity concerns, and general overall detriment to stream ecosystems.

Major technological and regulatory advances are being made to address urban stormwater challenges, primarily with Low Impact Development and related natural technologies. However, most of these technologies require significant land area commitments and are difficult to retrofit in highly urbanized areas. An efficient technology to address stormwater quality in highly urbanized areas could have major impact on managing runoff in these areas. One current stormwater runoff treatment system used in urban areas is a sand filter, as shown in Figure 1. Sand filters effectively capture the particulate pollutants which are mobilized by stormwater runoff. However, as sand filters clog, some or all of the sand must be replaced to ensure adequate drainage through the treatment system. Removal of filtration media such as sand is highly labor-

intensive. Therefore, in order to reduce labor costs, development of a new type of stormwater treatment system with a longer lifespan is needed.

In order to respond to this need, a research project was initiated to determine if synthetic filters and drain elements, namely geosynthetics, can effectively remove suspended solids from urban runoff through a filtration mechanism, and maintain the drainage capacity of the drain system. Geosynthetics can replace the traditional sand filters and gravel in stormwater runoff treatment systems in urban areas, while minimizing the need for cleaning or material replacement. The influence of certain influent factors, such as hydraulic loading rates, suspended solids' particle sizes, and event mean concentrations of suspended solids, as well as characteristics of the filter material such as permittivity and opening sizes, on the filtration ability of the geotextile filters have been evaluated in this research. The filtration ability of geotextile was compared with that of a sand filter. Observations have also been made to define the impact of a build-up of solids on overall filter performance, and a theoretical model was created to define the hydraulic behavior of the filter as a function of solids build-up and various important geotextile and runoff characteristics. These important characteristics along with empirical laboratory data were also used to establish new geotextile filtration criteria for treatment of stormwater runoff.
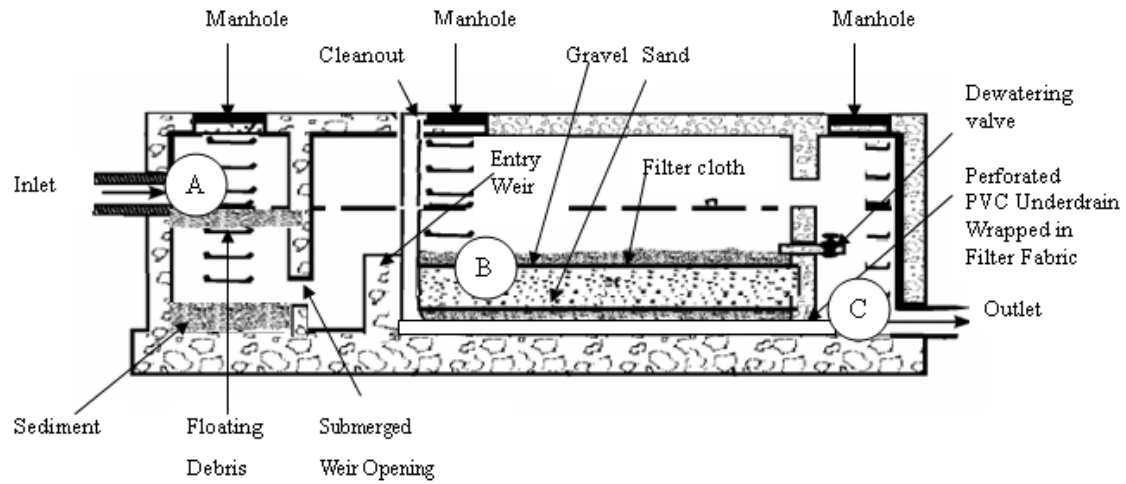
Figure 1. Typical subsurface sand filter for stormwater runoff treatment found in the District of Columbia area.

INTENT OF RESEARCH

HYPOTHESES

The current research intends to address the following hypotheses:

1. A geosynthetic filter can perform filtration of suspended solids that are of roughly the same particle size as pollutants found in urban highway stormwater runoff as adequately as a sand filter, while maintaining hydraulic capacity.

2. Filtration criteria established for geotextiles can be used to select the type of geotextile for effective stormwater filtration. If not, new criteria can be developed for this purpose.

3. A power model can be established to predict the hydraulic conductivity of a geotextile stormwater filter as a function of the solids loaded to or the solids retained by the filter.

4. The geotextile filter can perform filtration of suspended solids in actual stormwater runoff to meet established water quality criteria.

OBJECTIVES

The following objectives have been developed in order to address the above hypotheses:

1. To experimentally determine the type of geotextile that is most effective at capturing suspended solids in urban stormwater while maintaining hydraulic capacity.

2. To develop new retention and clogging criteria (if necessary) for use of geotextiles in stormwater filtration which correlate with the experimental filtration results.

3. To show that a geotextile filter performs as well as a sand filter in terms of suspended solids removal and maintenance of drainage capacity in a stormwater filtration system.

4. To develop a mathematical model that describes the hydraulic conductivity of the geotextile filter as a function of suspended solids captured by the filter.

5. To show that a geotextile filter performs suspended solids filtration in a field setting with actual stormwater runoff.

IMPACTS

The stormwater filtration system proposed in this research will have important impacts on the environment, and public health. The filtration system will also contribute to a greener highway infrastructure and create a better understanding of the filtration mechanisms of geosynthetic filters.

Suspended solids are an important pollutant, and have direct and indirect effects on water bodies. One direct effect of increased TSS is increased turbidity, the cloudiness of the water or a measurement of the amount of light which gets absorbed or deflected by the solids rather than transmitted (Walker et al. 2006). As turbidity increases, less light can reach photosynthetic organisms present in the water column. Thus, it is important to reduce the amount of suspended solids which reach aquatic ecosystems in order prevent disruption of photosynthesis.

Another direct result of increasing TSS levels is increased sedimentation. As water velocities decrease, more particles leave suspension and deposit onto stream beds. As the stones and rocks within the stream become covered, areas where some aquatic species hide from predators or fast-flowing water can be eliminated. The sediment can also smother macroinvertebrates and fish eggs which dwell on or near stream beds causing them to suffocate (Walker et al. 2006).

The greatest indirect effect of TSS is the input of various pollutants that may be attached to the solids into the water column. One specific example that could cause toxicity is adsorption of heavy metals. In particular, cadmium, zinc, copper, chromium, iron, and lead have all been detected in urban pavement runoff. Tires, brakes, frames and bodies, fuel, and oil of automobiles are responsible for producing much of these metal pollutants in highway stormwater runoff (Sansalone and Buchberger 1997). If these metals exceed levels beyond water quality standards for surface water discharges, they can pose serious health risks to aquatic species that come into contact with or ingest the contaminated waters (Mulligan et al. 2009).

In addition to heavy metals, particles in runoff can carry nutrients (Mulligan et al. 2009). An abundance of nutrients, or eutrophication, in a water body often results in increased algal blooms (Walker et al. 2006). Once these masses of algae die, their presence creates a large oxygen demand, and their degradation can result in large-scale oxygen depletion (Madigan and Martinko 2006). Therefore, it is important to avoid releasing high particulate loads into water bodies in order to protect aerobic aquatic species.

Not only can suspended solids negatively impact aquatic ecosystems, they can also impair human health. As stated previously, the particles in urban stormwater runoff can carry sorbed heavy metals into water bodies. If metal-contaminated surface waters are intentionally or accidentally ingested by humans, they can pose serious health risks. Additionally, as metals bioaccumulate in aquatic biota, they can build to a level that would be harmful to humans if these animals, such as fish and shellfish, are consumed (Mulligan et al. 2009).

Another category of pollutants of concern in urban stormwater runoff includes petroleum-based fuels such as gasoline and diesel fuel. Unleaded gasoline can contain benzene and toluene which are hazardous to organisms when released into aquatic ecosystems and dangerous to humans if contamination of a drinking water source such as groundwater, occurs. In addition, some fuels may contain potentially dangerous additives such as methyl-tertiary-butyl ether (MTBE) a derivative added to gasoline to boost oxygen content in the fuel. MTBE is resistant to biodegradation and produces a foul taste and odor in water, making it undrinkable (Pepper et al. 2006).

According to the Federal Highway Administration, there are over 10^6 miles of paved highway in urban areas of the United States. In most urban areas, stormwater is unable to infiltrate into the ground because of the vast amount of impervious surface present. If urban infrastructure increases, which in the US it inevitably will, the amount of rainwater becoming highway runoff will increase as well. Since stormwater runoff is recognized under the Clean Water Act as non-point source pollution which must be remediated by best management practices (BMPs), future increases in runoff flows will lead to a greater demand of treatment options for stormwater runoff. Certainly a more

cost-effective and less labor-intensive stormwater treatment system such as the one proposed in this research will be very beneficial to those regulated by stormwater BMPs.

By capturing suspended solids from runoff before they reach receiving waters, this stormwater filtration system will lessen the risks of problems associated with increased turbidity and metal and nutrient concentrations in aquatic ecosystems. Additionally, the risk of human exposure to waters or food contaminated with heavy metals will decrease due to lower concentrations of solids with sorbed heavy metals reaching surface waters.

Chapter II: TOTAL SUSPENDED SOLIDS REMOVAL AND HYDRUALIC

CONDUCTIVITY: LABORATORY COLUMN STUDIES

INTRODUCTION / BACKGROUND

The primary function of the geotextile filter was to remove and retain suspended solids while allowing adequate drainage of water. It was necessary to study the characteristics of suspended solids in highway stormwater runoff for this research project in order to accurately simulate stormwater runoff for laboratory testing of a geosynthetic filter. Particle size and concentration are two factors that impact filtration efficiency greatly, and existing work on these factors is discussed below.

PARTICLE SIZE DISTRIBUTION

Particle sizes in urban highway runoff waters can range from a diameter of 1 μm to over 1 cm (Sansalone et al. 1998). The particle size distribution (PSD) of stormwater runoff depends on the characteristics of the runoff surface and its surroundings. Kim and Sansalone (2008) reported that 25-80% by weight of the dry particles on highway pavements are fine particulate matter (>75 μm) and gravel-size particles (>2 mm) make up only 0.5-30% by weight of the particles. Similar observations were made in a study during collection of highway runoff for seven different runoff events in Los Angeles. Of the particles between 2 and 1000 μm in the runoff samples, more than 90% by number were less than 10 μm (Li et al., 2006). Kim and Sansalone (2008) indicated that the particles with diameters less than 8 μm are usually washed away rapidly in high flow

events, while the coarse particulate matter (>75μm) can easily be separated from runoff by mechanical means.

Gironas et al. (2008) employed a particle size range of 10 to 300 μm for simulated stormwater runoff with a mean particle diameter (the diameter at which 50% of the particles by mass have a smaller diameter than that value, D_{50}) of 100 μm. Siriwardene et al. (2007) also used a semi-artificial stormwater solution to evaluate clogging of stormwater infiltration systems in the laboratory environment. The particles in the stormwater solution had a D_{50} of 25-60 μm, which they claim to be a typical characteristic of urban stormwater.

In another study, Furumai et al. (2002) established a relationship between particle size distribution and suspended solids concentration. The samples analyzed in this study came from the runoff of a Swiss highway, characterized by heavy traffic en route to Zurich. Particles larger than 250 μm were eliminated, and total suspended solids (TSS) concentrations were determined for several urban runoff events. As seen in Figure 2, larger TSS concentrations typically have a smaller fraction of particles which are less than 20 μm in diameter and a larger fraction of coarser particles which are at least 45 μm in diameter.

SETTLING VELOCITY

The settling velocity of discrete particulate matter is one of the most important parameters in stormwater treatment. In the case of the typical sand filter treatment system in the Washington D.C. area, a retention basin precedes the sand filter in order to allow larger particles to settle out of the influent suspension before reaching the filter. In

the previous section, the particle size distribution of urban highway stormwater runoff

was addressed. However, this is not an entirely accurate assessment of the size of

particles that will reach the filter if a retention basin is present. The sizes of the particles

that will settle before reaching the filter can be more accurately determined if the area of

the retention basin, suspended particle density, and flow rate of the influent are known.

In case of a geotextile filter (like the one used in the current study), reliable information

on the sizes of the particles that reach the filter is essential for choosing the apparent

opening size (AOS) of the geotextile filter.
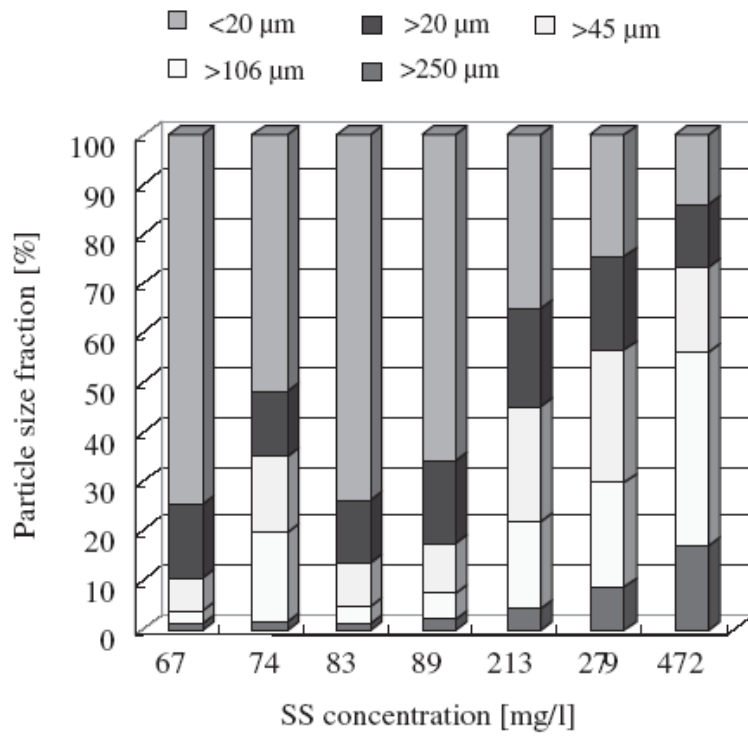
Figure 2. Particle size distributions at several TSS concentrations for urban highway runoff events in Winterthur, Switzerland (Furumai et al. 2002).

EVENT MEAN CONCENTRATION

The event mean concentration (EMC) is a typical measurement of runoff events. It is often used for quantifying the suspended solids concentration in urban runoff, and represents the time-weighted average concentration of the pollutant in the runoff volume.

$$EMC = \frac{\sum_{i=1}^{N} C_i q_i \Delta \tau_i}{\sum_{i=1}^{N} q_i \Delta \tau_i} = \frac{\sum_{i=1}^{N} \Delta M_i}{\sum_{i=1}^{N} \Delta V_i} \qquad (1)$$

where C_i represents the pollutant concentration of each sample within an event i, q_i is the runoff volume flow rate of the sample, M_i is the mass of pollutant in event i, V_i is the volume of sample for event i, and $\Delta \tau$ is the time interval between the samples (Taebi and Droste 2004).

In a field study performed in Maryland, the average EMC for total suspended solids (TSS) was found to be 420 mg/L. This concentration is 2.4 to 8.6 times larger than TSS concentrations in many other areas (Flint and Davis 2007). In Stockholm, Sweden, researchers found that out of 44 consecutive rainfall events that were monitored, 35 events had TSS EMCs in highway runoff that exceeded the European Union discharge regulation of 60 mg/L. The concentrations in the 44 events ranged from 38 to 970 mg/L (Hallberg and Renman 2008). In a study performed in the late 1990s in Ohio, the EMC range for TSS was found to be 44-259 mg/L (Sansalone et al. 1998). The range of EMC values for several studies are listed in Table 1.

Table 1. Event mean concentrations for total suspended solids in urban highway stormwater runoff

EMC$_{mean}$ (mg/L)	EMC$_{min}$ (mg/L)	EMC$_{max}$ (mg/L)	Location	Source
131	44	259	Cincinnati, OH	Sansalone et al. (1998)
128	NA	NA	Winterthur, Switzerland	Furumai et al. (2002)
161	43	467	Isfahan, Iran	Taebi and Droste (2004)
272	138	561	Baton Rouge, LA	Sansalone et al. (2005)
420	41	1600	Mount Rainier, MD	Flint and Davis (2007)
283	38	970	Stockholm, Sweden	Hallberg and Renman (2007)
110	47	272	Baton Rouge, LA	Kim and Sansalone (2008)
118	44	209	Austin, TX	Barrett et al. (2006)

NA: Not available

HYDRAULIC CONDUCTIVITY

Hydraulic conductivity is an important parameter of the geotextile because it is a measure of the ability of the material to drain fluids. A low hydraulic conductivity indicates that the material is not allowing fluid to flow through it quickly and could be clogged. The hydraulic conductivity normal to a material K is defined as:

$$K = \frac{qt}{hA} \tag{2}$$

where q is the flow rate, t is the thickness of the material, h is the head loss, and A is the total area of the material (Koerner 2005).

Urbonas (1999) stated that the flow velocity through a soil media, such as a sand filter, is directly impacted by the amount of sediment accumulated on the filter's surface. This relationship is described by a power function.

$$v = r \cdot \left(\frac{m}{A}\right)^{-x} \tag{3}$$

where v is the flow velocity, r is an empirical flow-through constant, x is an empirical exponential constant, and *(m/A)* is the cumulative unit TSS load accumulated on the filter surface.

Clark and Pitt (2009) verified that this power equation could be applied to a mixed-media stormwater filter as well. However, the laboratory test results indicated that the concentration of the influent solution and the diameter of the filter alter the filter performance. This is an indication of the parameters that could predict the constants r and x without collecting empirical data.

Gironas et al. (2008) applied Equation 3 to laboratory test results on stormwater treatment by a perlite filter. They found that the model applied to their empirical data

15

when the conditions (type of expanded perlite, thickness, and head) remained identical. When the conditions were varied, however, the constants r and x varied. They also discovered a tendency for the model to overestimate the filtration rates at the beginning and end of the tests, which could be a result of the different removal mechanisms of perlite and sand. A sand media filtration system is controlled more by the filtration of the cake layer than a perlite system.

Because the geotextile filter system is believed to behave similarly to a sand filter, it is hypothesized that the hydraulic function of a geotextile filter will depend greatly on the amount of solids accumulated in and on the filter, and this relationship can be expressed as a power equation. Besides unit flow rate, the hydraulic conductivity of the filter system can be described as a power model as a function of solids captured by the filter as well. Additionally, the hydraulic conductivity as a function of the solids that reach the filter or the solids loaded onto the system will be described by a power function in the form of Equation 3.

METHODOLOGY AND MATERIALS

A laboratory column set-up was assembled to test the efficiency of geotextile filtration for stormwater runoff. The set-up included a pump, a mixer, a 40-L plastic tub, tubing, 500-mL plastic sampling containers, the nonwoven geotextile filter, a rubber screen for filter support, and a Plexiglas column. Figure 3 shows a sketch of the laboratory column set-up, where a simulated stormwater solution was pumped into the top of the Plexiglas column containing a geotextile filter and effluent samples were collected at the bottom of the column.

Silty soil collected from a landfill cover in Polson County, Montana, was used to prepare a suspended solids material with a particle size distribution similar to that of suspended solids in urban stormwater runoff. A hydrometer test was conducted on the soil to determine the particle sizes of the fine-grained soil passing through Standard Sieve No. 200 (75 μm). Then, the soil was sieved through U.S. Standard Sieves No. 80, 100, 120, 140, 170 and 200 and combined to obtain a particle size distribution (PSD) of 0-180 μm with a D_{50} of 106 μm (P1) and of 0-106 μm with a D_{50} of 50 μm and 25 μm (P2 and P3, respectively). The D_{50} value for P1 was chosen because it closely resembles the typical D_{50} value for urban stormwater highway runoff reported in existing literature (Siriwardene et al. 2007; Gironas et al. 2008; Kim and Sansalone 2008). The D_{50} values for P2 and P3 were chosen to represent stormwater runoff after flowing through a retention basin common to a typical urban stormwater treatment systems (Li et al. 2006). Coefficients of uniformity (C_U) for P1, P2, and P3 are 12, 35, and 34, respectively, and coefficients of curvature (C_C) are 2.1, 4.8, and 2.0, respectively.

Nonwoven geotextiles were chosen for use in this study as opposed to woven geotextiles. In general, nonwoven geotextiles are more commonly used for filtration applications because of their smaller opening sizes and larger thicknesses. The fibers in a woven geotextile are organized in a quasi-regular pattern while those of nonwoven geotextile are organized in a quasi-random pattern (Aydilek 2011).

The geotextiles used in this study were chosen because of their pore sizes. The apparent opening size (AOS), the size at which 95% of the openings are that size or smaller, and other relevant properties of each geotextile are given in Table 2. The ratios produced by the geotextile pore sizes and the particle sizes in the simulated stormwater

suspension are generally within the ranges established by existing filtration criteria for geotextiles, which are listed in Table 3. Because the ratios developed for P1 and P2 and all three geotextiles (NW1, NW2, and NW3) are within the ranges established by the existing filtration criteria, the filtration criteria imply that NW1, NW2, and NW3 will be successful at retaining particles in particle size distributions P1 and P2. If the filters are not successful at retaining the particles, then the existing criteria are not adequate for use in stormwater treatment. Applicability of existing criteria and development of new criteria will be discussed in greater detail in Chapter III.

Approximately 8 g of soil were added to a container of 40 L filled with tap water at room temperature to achieve a TSS concentration of approximately 200 mg/L, which is slightly higher than the average event mean concentration (EMC) for TSS in stormwater runoff events occurring in urban areas. Tests were also performed using 100 mg/L, which is slightly lower than the average TSS EMC for stormwater runoff events in urban areas (Sansalone et al. 1998; Furumai et al. 2002; Taebi and Droste 2004; Sansalone et al. 2005; Barrett et al. 2006; Flint and Davis 2007; Hallberg and Renman 2008; Kim and Sansalone 2008; Li and Davis 2008). A mixer powered by a Minarik motor vigorously mixed the simulated stormwater solution at approximately 100 RPM in order to keep the soil particles suspended. The simulated stormwater was then applied to the column at an influent flow rate of approximately 6 mL/s. For a circular geotextile filter with a diameter of 127 mm, the influent flow rate corresponded to a hydraulic loading rate (HLR) of 0.49 mm/s (69 in/hr). Assuming a runoff area-to-drainage area ratio of 50, the HLR corresponds to an approximate rainfall rate of 3.6 cm/hr (1.4 in/hr), approximately 10 times greater than the rainfall rate for the highest frequency of rainfall events for the

18

state of Maryland. Two tests were performed using an influent flow rate of

approximately 3 mL/s which would correspond to an HLR of 1.8 cm/hr, approximately 5

times greater than the rainfall rate for the highest frequency of rainfall events in the state

of Maryland (0-0.254 cm, 1 hr; Kreeb 2003).

Several measurements were taken during testing. Head losses were measured as

water levels rose in the column. Outlet flow rates were calculated by measuring the

volume of water exiting the column in a given amount of time. After the suspension

passed through the geotextile filter, samples of effluent were collected in plastic

containers every 8 minutes, and TSS concentration measurements were conducted using

Standard Method 2540 B (Eaton et al. 1995). Each test run with an influent flow rate of 6

mL/s was run for 75 minutes because rainfall events between 0 and 2 hours occur at a

higher frequency than all other rainfall events in the state of Maryland (Kreeb 2003). The

tests run with an influent flow rate of 3 mL/s were run for 150 minutes in order to

maintain the same influent volume as the previous tests. Nine effluent samples were

collected during each test, and the TSS concentrations of all nine samples were used to

calculate an effluent TSS EMC value for each test. EMC is defined by Equation 1, given

earlier. In order to calculate the EMC, TSS concentration, C, and effluent flow rate, q,

were approximated for each instance, i, by assuming a linear relationship between two

sampling points (Hallberg and Renman 2008).   After 75 (or 150) minutes of treatment,

the test was stopped and the filter was allowed to dry by exposing the surface to the

atmosphere for 2 or more days. Subsequently, the suspension loading was continued for

another 75 (or 150) minutes, and effluent samples were collected. The process was

repeated for many tests, i.e., an average of about 21 tests for all 16 sets of tests, stopping

at 75 (or 150) minutes or whenever the ponded water level reached the top of the column (30 cm), until the filter clogged. Clogging was defined to occur when the height of standing water on the filter reached the top of the column within 20 minutes of testing. Assuming a linear increase in head loss, reaching the top of the 30 cm column within 20 minutes is approximately equivalent to reaching the typical vertical clearance (1 m) in an underground sand column system within the average duration of a rainfall event (1 hr) (Barrett 2003; Kreeb 2003). Each complete set of tests addressed in this work is labeled as Test A.B, where A is the geotextile indicator and B is the particle size distribution of the influent suspension indicator. For example, Test 3.P2 indicates that the test involved the NW3 geotextile filter, and the particle size distribution P2 for the influent suspension. Unless otherwise indicated by parentheses following the test name, the influent flow rate was 6 mL/s and the influent TSS concentration was 200 mg/L. A test involving NW2, PSD P1, 200 mg/L, and 3 mL/s would be named 2.P1(3). Likewise, a test involving NW3, PSD P2, 100 mg/L, and 6 mL/s would be named 3.P2(100).

Statistical analysis was performed in order to compare the results of the cumulative tests. To compare a parameter of one test with that of another, two hypothesis tests were performed using two-tailed t-tests, one with a level of significance equal to 1%, and one with a 5% level of significance. The null hypothesis stated that one parameter is equal to the other, and the level of significance (α) was defined as the probability of rejecting the null hypothesis when it was actually true. Therefore, the critical α value (α_C) for a hypothesis test was the rejection probability, and it was safe to reject the null hypothesis if the α_C was very small.
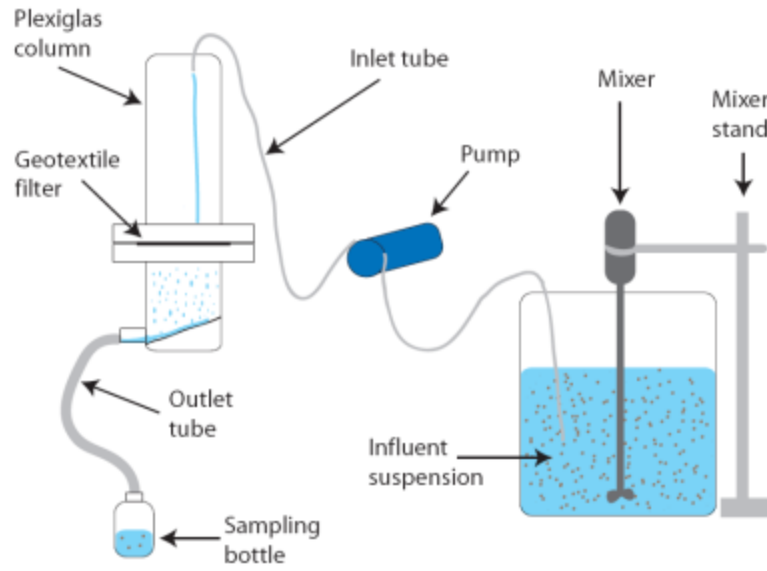
Figure 3. A schematic diagram of the laboratory set-up for geotextile filtration testing.

Table 2. Physical and hydraulic properties of the geotextiles used in this study.

Name	Structure, manufacturing and polymer type	Hydraulic Properties					Physical Properties		
		Apparent opening size, AOS (mm)	Porosity, ε (%)	Hydraulic conductivity, K (mm/s)	Permittivity, ψ (s^{-1})	Flow rate (L/min/m^2)	Mass/unit area (g/m^2)	Thickness (mm)	Grab tensile strength (N)
NW1	NW, NP, STF, PP	0.18	87	2.76	1.2	3866	278	2.3	900
NW2	NW, NP, STF, PP	0.15	86	2.40	0.8	2648	400	3	1340
NW3	NW, NP, STF, PP	0.15	86	1.73	0.54	2037	509	3.2	1691

Note: NW: nonwoven, NP: needle punched, STF: Staple fiber, PP: polypropylene. All properties are the manufacturer's minimum average roll value (MARV) for each geotextile. Tensile strengths are the machine direction values. Permittivity is equal to hydraulic conductivity normalized by thickness.

TOTAL SUSPENDED SOLIDS CONCENTRATION REDUCTION

Since stormwater runoff is a non-point source discharge without current numeric discharge criteria, the effluent TSS concentrations were compared to effluent restrictions commonly imposed upon point source dischargers, 30 mg/L, which was selected as the water quality goal. Figure 4 shows an example of the influent and effluent TSS concentrations found for one 75 minute test (from Test 1.P1). The influent concentrations were constant at approximately 200 mg/L. The first effluent concentration measured at 8 minutes was above the target concentration of 30 mg/L, while all others were below the 30 mg/L limit. This phenomenon, i.e., the highest concentration observed in the earliest effluent sample and then a decrease in effluent concentration with time, was observed in most of the 75 minute tests because the filter cake was disturbed by the initial influent flow and with time, the soil particles settled back onto the filter.

Effluent concentrations were determined to decrease as the total solids loading increased. Figure 5 shows both influent and effluent TSS EMCs as a function of total cumulative solids loading for tests 1.P1, 2.P1, and 3.P1. Each point represents an EMC for each 75 min test. For both NW2 and NW3 filters, the effluent EMCs drop below the target concentration (30 mg/L) between a solids loading of 1 and 2 kg/m^2, and beyond this loading, the effluent TSS EMCs remained below the target value, at about 5 mg/L. Before this concentration drop, a ripening process for the filter occurred where particles built up in and on the filter and enhanced the retention capacity of the filter (Mao et al. 2006). As shown in Figure 5, a ripening period occurred for all three filters. While TSS removal was good, the effluent EMC for NW1 did not fall below the target concentration. The differing result for NW1 as compared with NW2 and NW3 can be attributed to the

larger AOS and the larger permittivity (the hydraulic conductivity divided by the thickness) of the filter (Table 2). Similar behavior was exhibited in a study by Kutay and Aydilek (2004), where the percentage of solids piping, i.e., passing through the geotextiles, increased with increasing AOS and permittivity.

Another difference among the three filters was the total solids loaded at the end of the test set, i.e., at the final clogging point (as defined in the METHODOLOGY AND MATERIALS section). Clogging occurred at the lowest total solids loading for NW3 (4.2 kg/m^2), followed by NW2 (6.4 kg/m^2), and last for NW1 (>10.8 kg/m^2) (Figure 5). These results correlate directly with the permittivities of the filters; NW3, NW2, and NW1 had permittivities of 1.2 s^{-1}, 0.8 s^{-1}, and 0.54 s^{-1} respectively. A higher permittivity indicates that a greater mass of solids can be loaded to the filter before clogging occurs. Maximizing the mass of solids loaded to the filter before clogging occurs lengthens the lifespan of the filter system. However, as discussed earlier, a larger permittivity results in larger effluent TSS concentrations. Therefore, the filtration criteria which will be discussed in depth later in this study are very important in order to choose a geotextile that can retain suspended solids while maintaining adequate drainage for as long as possible.

Test 1.P1 was repeated to ensure that the NW1 filter does not reduce the TSS concentrations to the target value as the other filters had done. The results of the repeated test are given in Figure 6. The results were similar, but some slight differences in the concentrations are seen in Figure 6. During the repeated test, the ripening period lasted longer and concentrations were higher during this period than for Test 1.P1. After the ripening period occurred, concentrations did drop to below the target, but increased back

up to values approaching the target before clogging occurred. Also, the test had to be ended before a final clogging point occurred because water seepage in the bottom portion of the column indicated that the filter may have slipped out of its proper position in the column. Therefore, the value of total solids loading at the end of the test cannot be used as an indication of when clogging occurs for the NW1 filter.

Figure 7 shows the TSS concentrations in the influent and effluent suspensions as a function of the total solids loaded for the three geotextiles using particle size distribution, P2. Similar to the results in Figure 5, for both NW2 and NW3 filters, the effluent concentrations dropped below the target concentration (30 mg/L) between a solids loading of 1 and 2 kg/m^2, and beyond this loading, the effluent TSS concentrations remained below the target value. Before this concentration drop, a ripening process occurs for both filters. Like the observations made in P1 tests, NW2 reached a greater solids loading than NW3 at its clogging point when loaded with soil particles of particle size distribution P2. Again, the higher permittivity for NW2 allowed the filter to be loaded to a greater degree than NW3 before clogging. Unlike the P1 test results shown in Figure 5, however, NW1 did not experience a ripening period and the effluent TSS concentrations never consistently dropped below the influent TSS concentration of 200 mg/L. NW1 has a larger AOS than the other two filters and as a result, is unable to retain particles of P2 due to their smaller diameters.

Test 1.P2 was repeated to ensure that the NW1 filter was not able to reduce the TSS concentrations or complete a ripening period for particle size distribution P2. Figure 8 shows that the effluent TSS concentrations of the repeated test were nearly identical to those of 1.P2. Therefore, the NW1 filter does not experience a ripening period for

particle size distribution 2 or reduce TSS concentrations below the influent value of 200 mg/L.

Figure 9 shows the TSS concentrations in the influent and effluent suspensions as a function of the total solids loaded for the NW2 and NW3 geotextiles using the smallest particle size distribution, P3. No tests were performed on NW1 with particle size distribution P3 because NW1 was unable to capture the particles in P2 in Test 1.P2 and the 1.P2 test (repeat). The particles in P2 were in the range of 0-106 μm with a D_{50} of 50 μm. The particles in P3 were in the same range, 0-106 μm, but had a D_{50} of 25 μm. It was assumed that if NW1 is unable to retain particles in P2, it would not be able to retain the particles in P3 because P3 consisted of larger percentages by mass of finer particles.

Similar to the results in Figures 5 and 7, for both NW2 and NW3 filters, the effluent concentrations dropped below the target concentration (30 mg/L) between a solids loading of 1 and 2 kg/m^2, and beyond this loading, the effluent TSS concentrations remained below the target value (Fig. 9). Before this concentration drop, a ripening process occurred for both filters. Like the observations made for P1 and P2 tests, NW2 reached a slightly greater solids loading than NW3 at its clogging point when loaded with soil particles of particle size distribution P3. Again, the higher permittivity for NW2 allowed the filter to be loaded to a greater degree than NW3 before clogging.

26
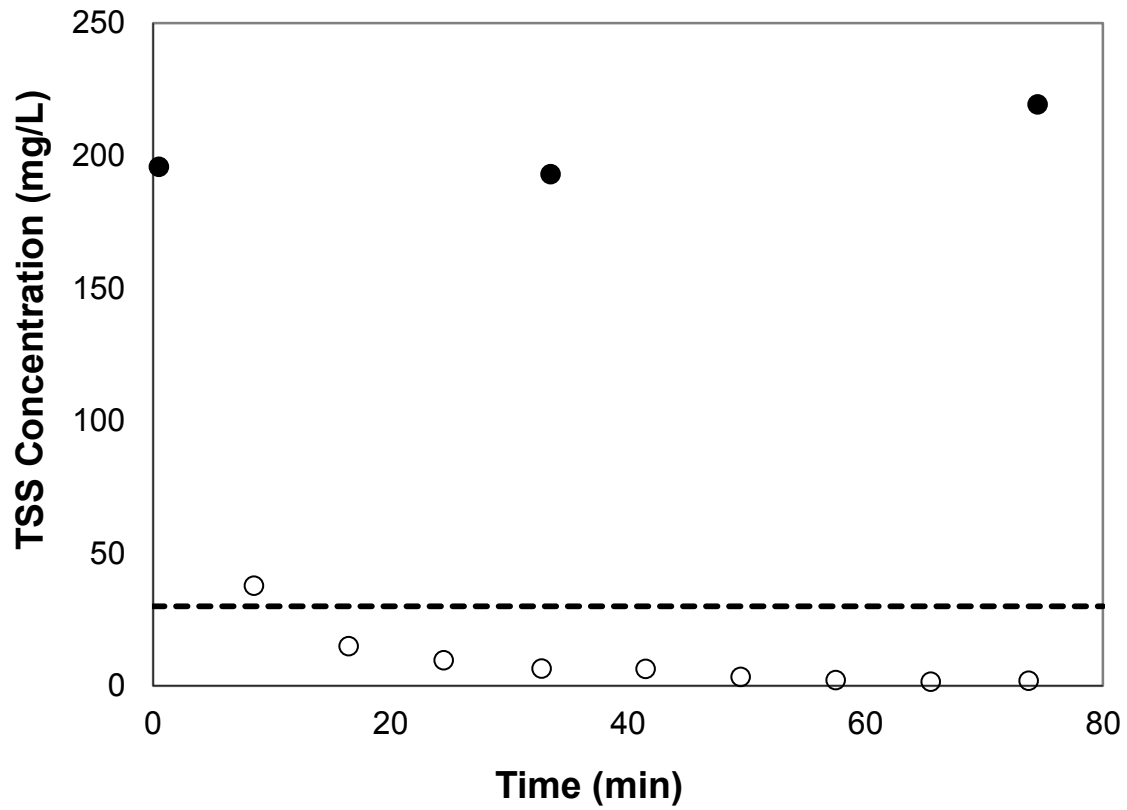
Figure 4. TSS concentration as a function of time during the fifth test of Test 1.P1.
Closed symbols indicate influent values. Open symbols indicate effluent values. Dashed
line indicates the target concentration of 30 mg/L.
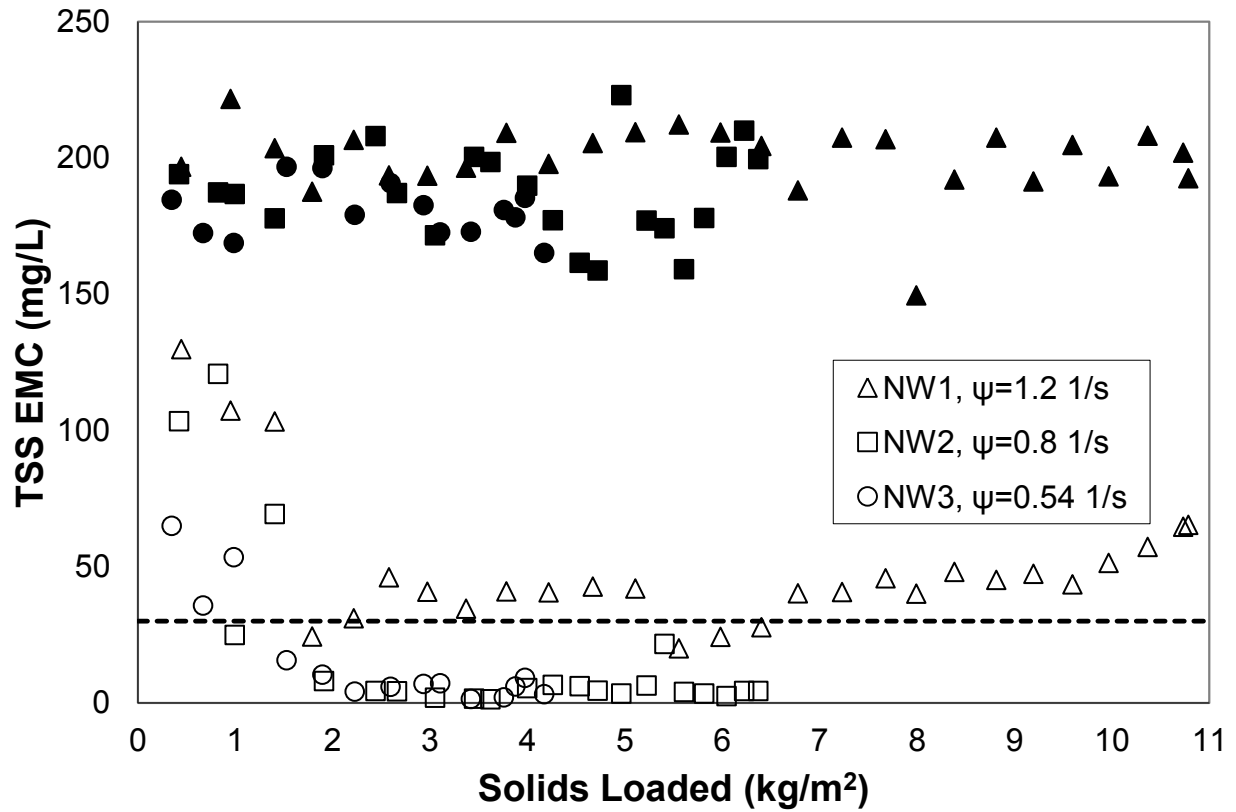
Figure 5. Effect of total solids loaded to each filter on TSS concentration for particle size distribution P1. Closed symbols indicate influent values. Open symbols indicate effluent values. Initial permittivity values are given in the legend for each geotextile. Dashed line indicates the target concentration of 30 mg/L.
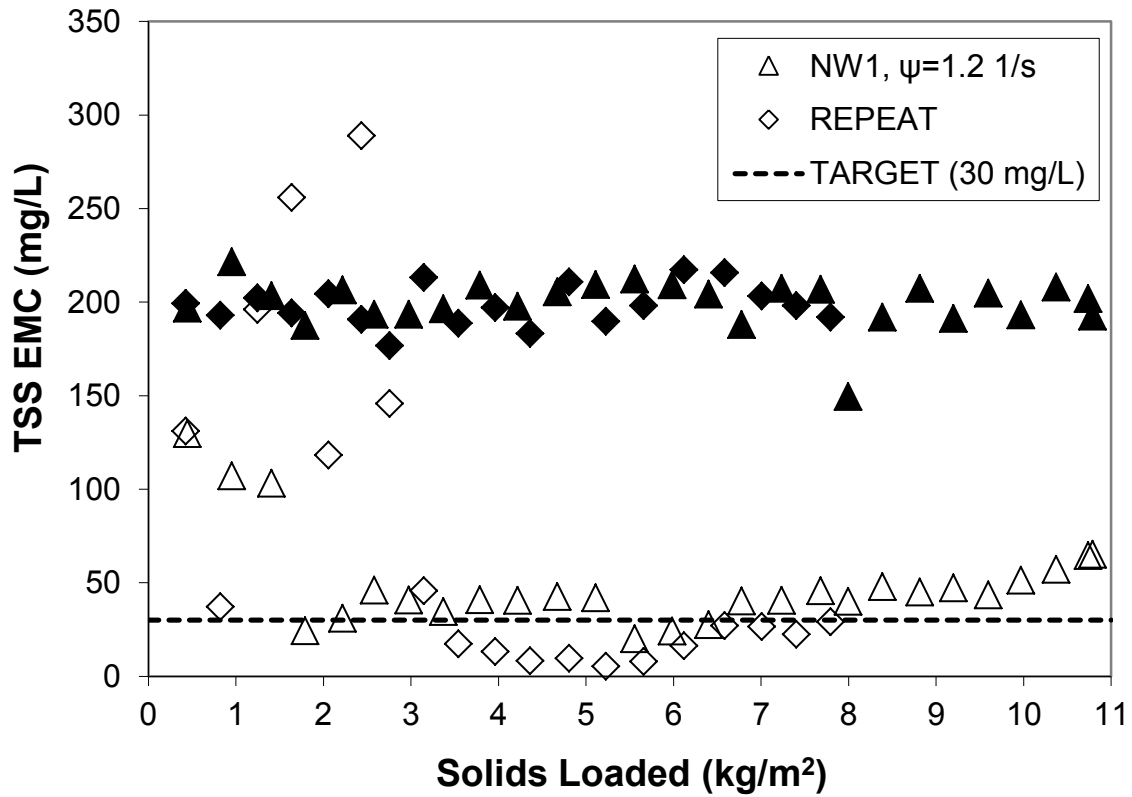
Figure 6. Effect of total solids loaded to NW1 filter on TSS concentration for particle size distribution P1. Closed symbols indicate influent values. Open symbols indicate effluent values. Initial permittivity values are given in the legend for each geotextile. Dashed line indicates the target concentration of 30 mg/L.
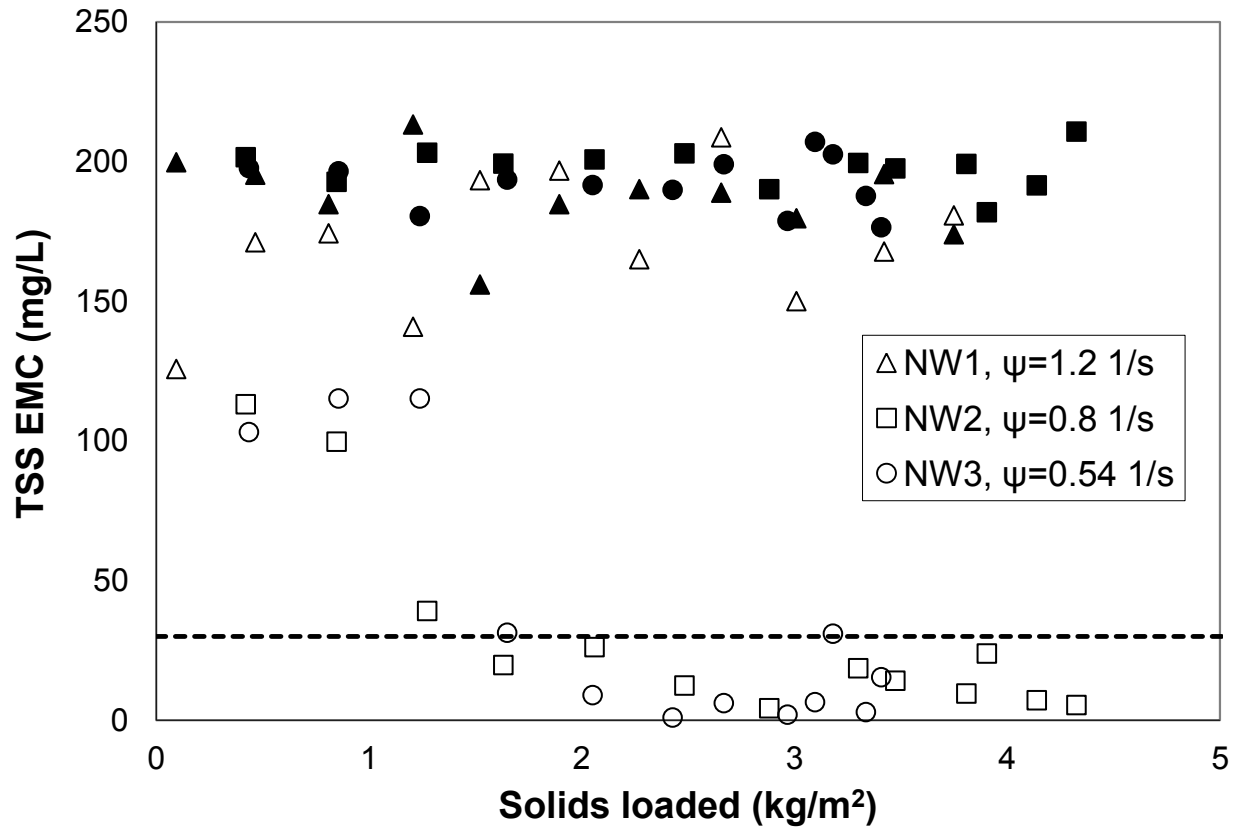
Figure 7. Effect of total solids loaded to each filter on TSS concentration for particle size distribution P2. Closed symbols indicate influent values. Open symbols indicate effluent values. Initial permittivity values are given in the legend for each geotextile. Dashed line indicates the target concentration of 30 mg/L.
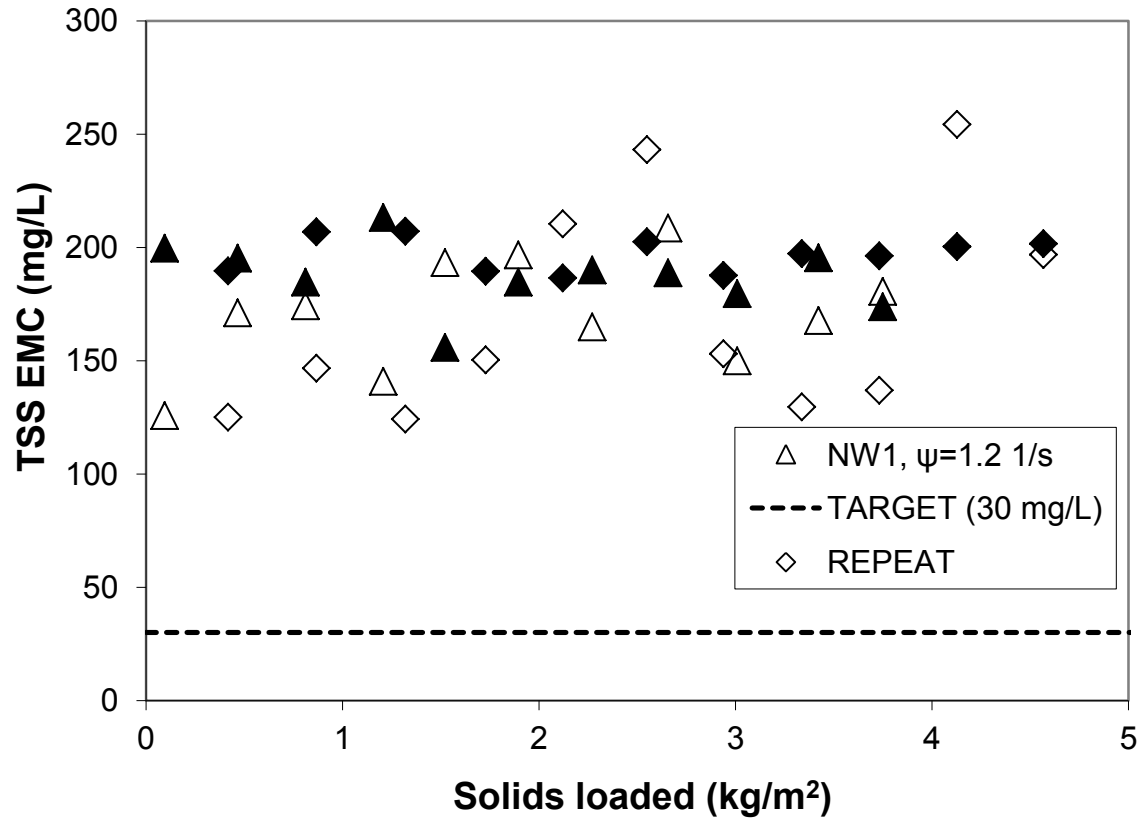
Figure 8. Effect of total solids loaded to NW1 filter on TSS concentration for particle

size distribution P2. Closed symbols indicate influent values. Open symbols indicate

effluent values. Initial permittivity values are given in the legend for each geotextile.

Dashed line indicates the target concentration of 30 mg/L.
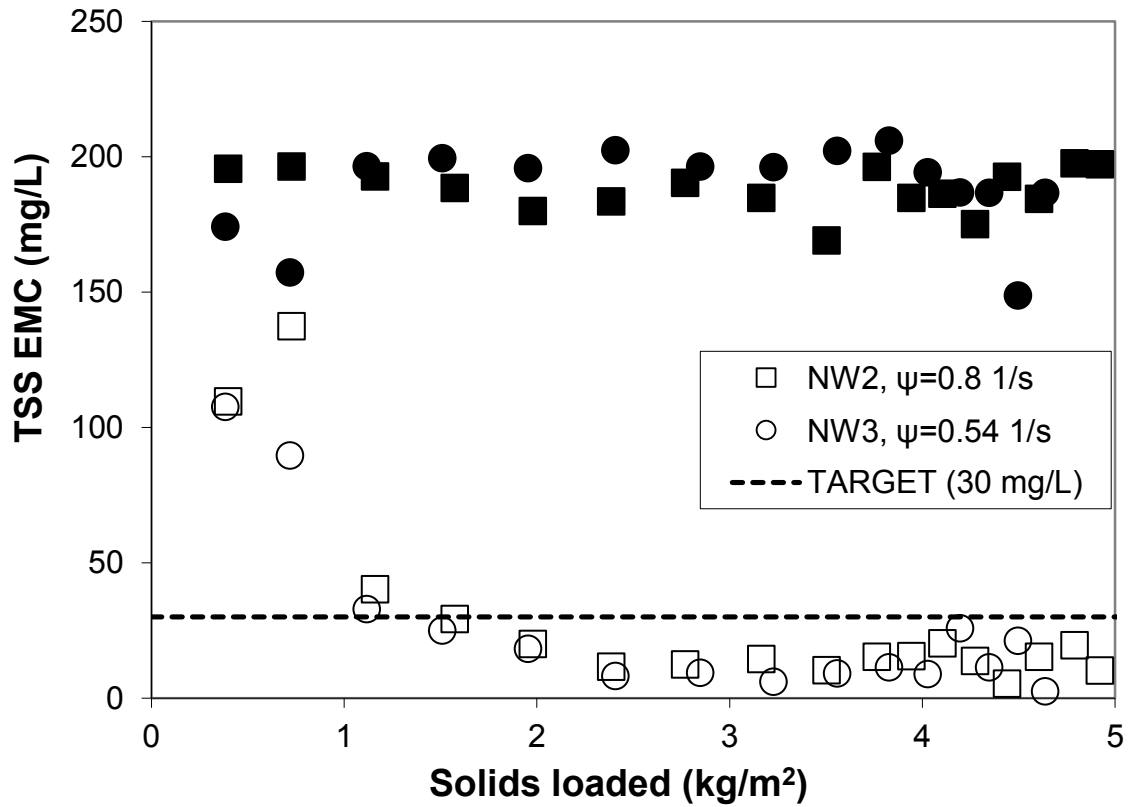
Figure 9. Effect of total solids loaded to filters NW2 and NW3 on TSS concentration for particle size distribution P3. Closed symbols indicate influent values. Open symbols indicate effluent values. Initial permittivity values are given in the legend for each geotextile. Dashed line indicates the target concentration of 30 mg/L.

TOTAL SOLIDS CAPTURED

Analysis of the regression lines of the total cumulative solids captured in and on each

filter as a function of the total solids loaded for tests 1.P1, 2.P1, and 3.P1 (Figure 10)

gives a direct comparison of the behavior of each filter when loaded with particle size

distribution P1. Statistical analysis (as described in METHODOLOGY AND

MATERIALS) indicates that the slopes for Tests 2.P1 and 3.P1 regression lines (shown

in Fig. 10) are equal to each other at the 5% level of significance (Tables 4 and 5). Thus,

mass capture of suspended solids loaded to the filters is statistically the same. As seen in

Figure 5, for P1 tests, NW1 greatly reduces the TSS concentration, but does not reduce

the concentration to the target value. When comparing the regression line for NW1 in

Figure 10 with those for NW2 and NW3, the slopes are significantly different (0.79 for

NW1, 0.94 for NW2 and NW3) using a 1% level of significance (Table 5), indicating that

the mass of solids captured per solids loaded for NW1 is significantly different than that

of NW2 and NW3.

Similar to P1 results, NW2 and NW3 behaved similarly in terms of total solids

captured for particle size distribution P2. Statistical analysis indicates that the slopes of

the regression lines of the P2 tests, 2.P2 and 3.P2, for total solids captured in and on each

filter as a function of total solids loaded are statistically equal to each other for the 1%

level of significance (Figure 11). The y-intercept values (b_0 values; Table 4, Fig. 11) for

the regression lines for tests 2.P2 and 3.P2 are equal for the 5% level of significance

(Table 5). This indicates that the amount of solids required to reach ripening is equal

(approximately 0.5 kg/m^2 solids loading) for both the NW2 and NW3 filters because the

x-intercepts of the regression lines correspond to total masses of solids loaded (per area) before any solids are captured by the filters.

NW2 and NW3 behaved similarly in terms of total solids captured as a function of total solids loaded for particle size distribution P3. Just as in the statistical analysis of the P2 tests, the slopes of the regression lines of the P3 tests, 2.P3 and 3.P3, for total solids captured in and on each filter as a function of total solids loaded are statistically equal to each other for the 1% level of significance (Figure 12). The y-intercept values (b_0 values; Table 4, Fig. 12) for the regression lines for tests 2.P3 and 3.P3 are equal for the 5% level of significance (Table 5). This indicates that the amount of solids required to reach ripening is equal (approximately 0.4 kg/m^2 solids loading) for both the NW2 and NW3 filters because the x-intercepts of the regression lines correspond to total masses of solids loaded (per area) before any solids are captured by the filters.

Since NW1 produced no significant reduction in P2 TSS concentration, both the slope and y-intercept values for the NW1 regression line are significantly different from those for NW2 and NW3 for all practical levels of significance, i.e., 0.1 – 99% (Fig. 11, Table 5). NW1 has a higher permittivity, AOS, and porosity than both NW2 and NW3. As a result, NW1 is unable to reduce the TSS concentration in the effluent to the target concentration for either PSD.
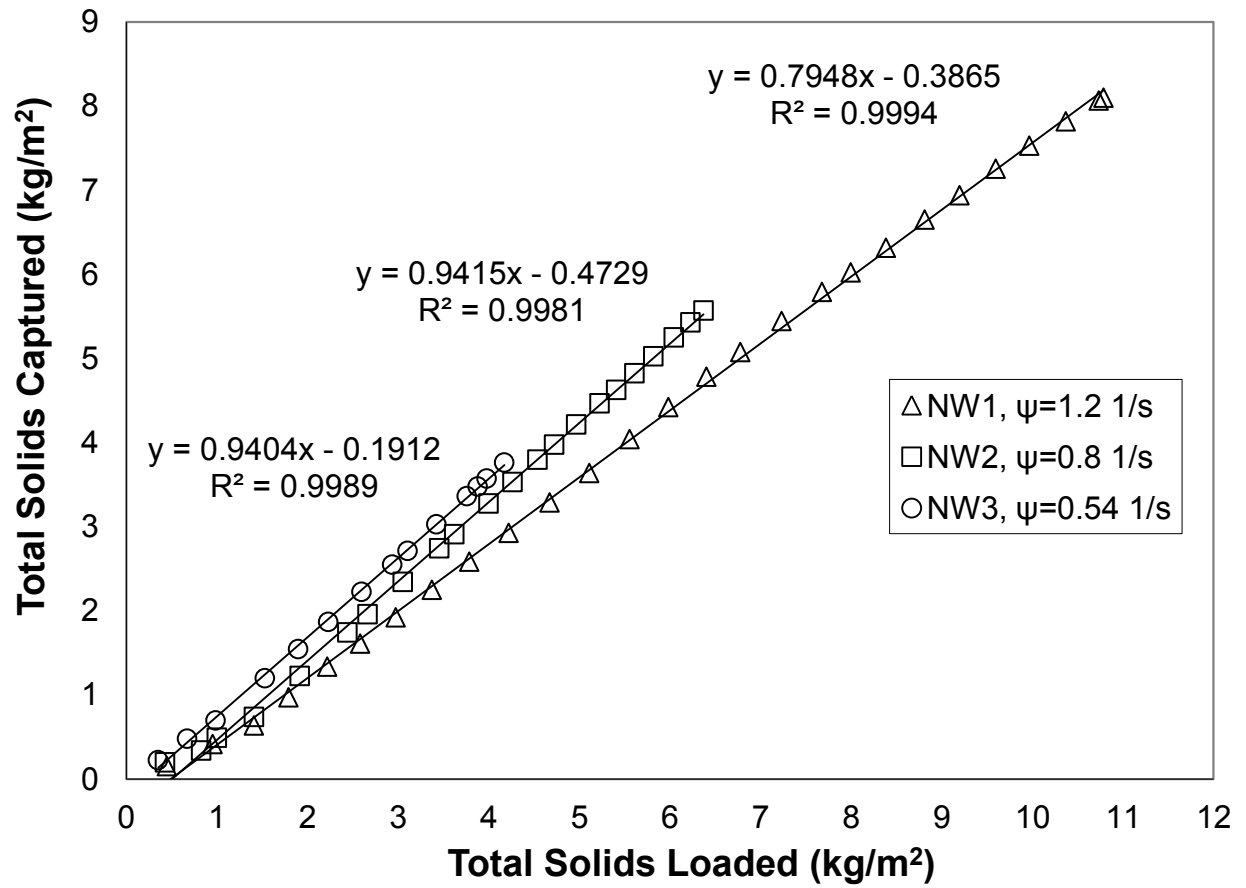
Figure 10. Total solids captured by the filters as a function of the solids loaded to each filter for TSS concentration of 200 mg/L and particle size distribution P1.
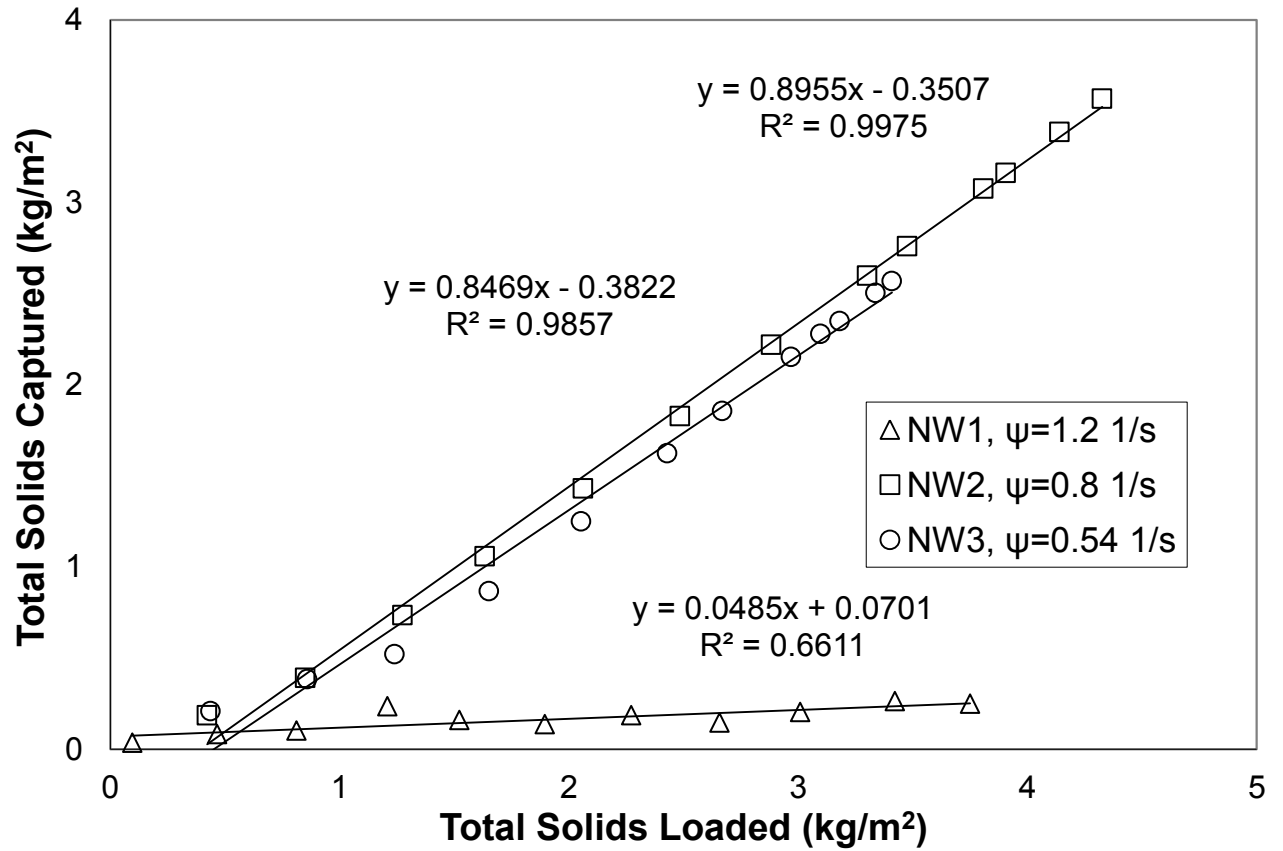
Figure 11. Total solids captured by the filters as a function of the solids loaded to each filter for TSS concentration of 200 mg/L and particle size distribution P2.
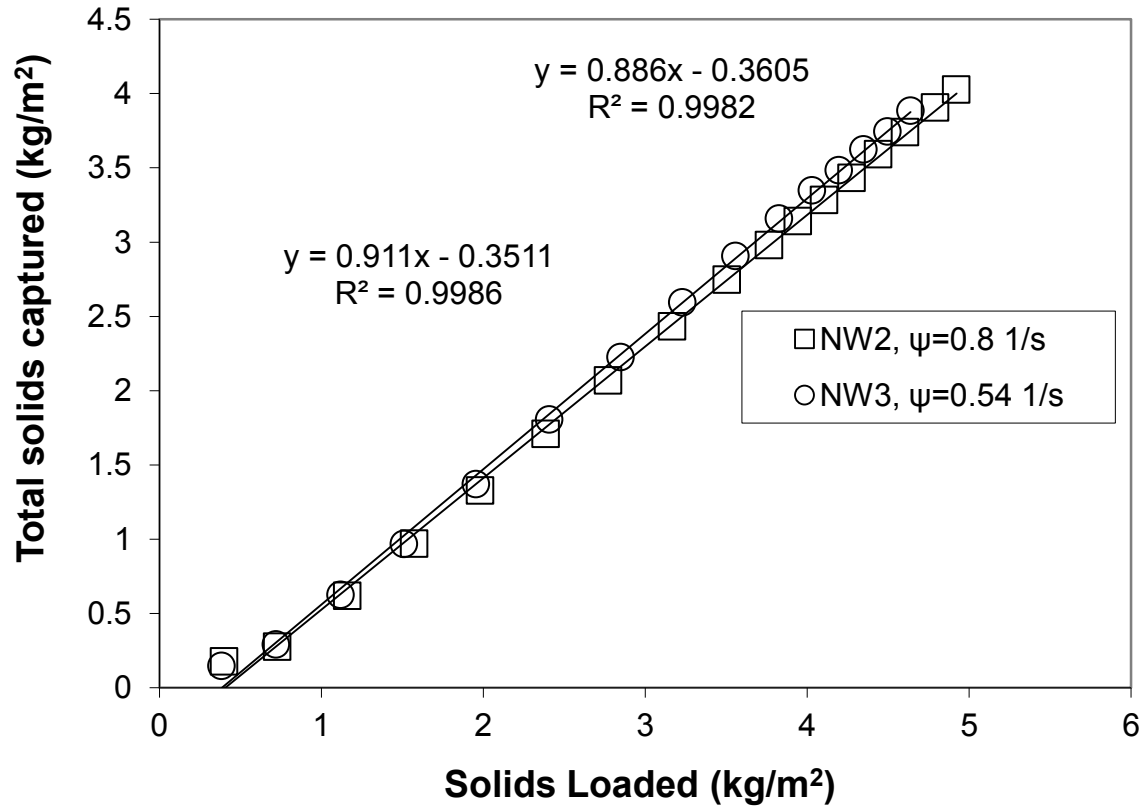
Figure 12. Total solids captured by the NW2 and NW3 filters as a function of the solids

loaded to each filter for TSS concentration of 200 mg/L and particle size distribution P3.

Table 4. Slope and y-intercept values (b_1 and b_0 respectively) and their corresponding standard error values for the solids captured as a function of solids loaded regression lines shown in Figures 10-14.

PSD	Filter type	b_1	Se (b_1)	b_0	Se (b_0)
	1	0.79	0.004	-0.39	0.027
P1	2	0.94	0.009	-0.47	0.038
	3	0.94	0.009	-0.19	0.025
	1	0.05	0.012	0.07	0.026
P2	2	0.90	0.013	-0.35	0.040
	3	0.85	0.032	-0.38	0.080
P3	2	0.89	0.010	-0.36	0.033
	3	0.91	0.010	-0.35	0.031

Table 5. Critical levels of significance for two-tailed t-tests setting either b_1 or b_0 (given in Table 4) for the each test listed at the top of the chart equal to the corresponding b_1 or b_0 for each test listed at the left side of the chart. Bold indicates those meeting the standard significance level of 0.01 (1%). Values italicized indicate those meeting both standard significance levels of 0.01 (1%) and 0.05 (5%).

Parameter in linear regression	Particle size distribution (PSD)	Filter type	P1			P2			P3	
			1	2	3	1	2	3	2	3
b_1	P1	1	1	<0.0001	<0.0001	<0.0001	<0.0001	*0.1436*	<0.0001	<0.0001
		2	<0.0001	1	***0.4949***	<0.0001	0.0053	**0.0158**	<0.0001	0.0075
		3	<0.0001	*0.4997*	1	<0.0001	0.0072	**0.0166**	<0.0001	0.0092
	P2	1	<0.0001	<0.0001	<0.0001	1	<0.0001	<0.0001	<0.0001	<0.0001
		2	<0.0001	<0.0001	0.0004	<0.0001	1	0.1621	0.3691	0.1333
		3	<0.0001	<0.0001	<0.0001	<0.0001	**0.0128**	1	0.0014	<0.0001
	P3	2	<0.0001	<0.0001	<0.0001	<0.0001	*0.4960*	*0.2715*	1	**0.0214**
		3	<0.0001	0.0038	0.0069	<0.0001	*0.2946*	**0.0786**	**0.0220**	1
b_0	P1	1	*1*	**0.0367**	<0.0001	<0.0001	*0.4076*	*0.7889*	*0.4579*	*0.2887*
		2	**0.0446**	1	<0.0001	<0.0001	**0.0103**	*0.3057*	0.0045	0.0021
		3	<0.0001	<0.0001	1	<0.0001	0.0028	**0.0408**	0.0002	0.0002
	P2	1	<0.0001	<0.0001	<0.0001	1	<0.0001	0.0003	<0.0001	<0.0001
		2	*0.1995*	0.0049	<0.0001	<0.0001	1	*0.6364*	*0.6837*	*0.8124*
		3	*0.7492*	**0.0315**	<0.0001	<0.0001	*0.4561*	1	*0.5165*	*0.3517*
	P3	2	*0.3795*	**0.0087**	<0.0001	<0.0001	*0.7021*	*0.6908*	1	*0.6770*
		3	*0.2050*	0.0049	<0.0001	<0.0001	*0.8083*	*0.6382*	*0.6884*	1

ROLE OF PARTICLE SIZE DISTRIBUTION

As seen in Figures 5 and 7, P2 was more difficult to retain than P1 due to the smaller range of particle sizes. These smaller particles of P2 are not easily captured by the filters and in particular with NW1, the geotextile with the largest permittivity. This follows the retention criteria developed for geotextiles in filtration which imply that a larger ratio between a specific opening size and a specific particle diameter is less likely to perform adequate retention of particles (Aydilek 2011). As shown in Table 3, the opening diameter-to-particle diameter (O/D) ratios for NW1 with P2 are the largest in all but one of the permutations of a specific filter with a particular particle size distribution included in this study, indicating that this combination is the least likely to retain suspended solids.

Particle size distribution plays a role in the test results for NW2 and NW3 as well. As particles accumulate on the surface of a filter, a layer of particles or cake is formed. This cake affects the further retention of particles and the hydraulic conductivity of the filter-filter cake system. Figure 13 compares the solids captured as a function of solids loading for P1, P2, and P3 tests performed on filter NW2. Statistical analysis indicates that the slopes of the regression lines for 2.P1 and 2.P2 in Figure 13 are only statistically equal to each other for a hypothesis test setting b_1 of 2.P2 equal to b_1 of 2.P1 (and not vice versa) using a level of significance of 0.5%. This indicates that the total percentage of solids captured by the NW2 filter is different for the two particle size distributions, P1 and P2, and therefore, dependent upon the particle size distribution. The y-intercept values for the 2.P1 and 2.P2 regression lines are statistically equal only for levels of significance less than 0.01. The regression lines for 2.P1 and 2.P3 (Figure 13) are not statistically equal to each other. The slopes, or b_1 values, are not equal to each other at

any level of significance, and the y-intercepts, or b_0 values, are only equal to each other using a level of significance of 0.4%. The regression lines for 2.P2 and 2.P3 in Figure 13 are statistically equal to each other in that both the b_1 and b_0 values are statistically equal at a 5% level of significance. Because the range of particles in particle size distributions P2 and P3 is the same, but different from the range in P1, this analysis indicates that the behavior of the filter-filter cake systems (in terms of mass of solids captured per mass of solids loaded) for different particle size distributions is different if the range of particle sizes differs.

A greater difference in behavior of the filter-filter cake systems can be seen in Figure 14 which compares the solids captured as a function of solids loading for P1, P2, and P3 tests performed on filter NW3. Statistical analysis indicates that the slopes of the regression lines for 3.P1 and 3.P2 are not statistically equal to each other for the 1% level of significance. Neither the slope nor the y-intercept of the regression line for 3.P1 is statistically equal to those of 3.P3 (Figure 14) for the 1% level of significance. The slopes of the regression lines for 2.P3 and 3.P3 in Figure 14 are only statistically equal to each other for a hypothesis test setting b_1 of 2.P3 equal to b_1 of 3.P3 (and not vice versa) using a level of significance of 5%. The differing slopes indicate that the mass of solids captured in and on the filter depends on particle size distribution. P1 tests have larger slopes than P2 and P3 tests for both NW2 and NW3, indicating that more solids are captured for the same solids loading for P1 than P2 or P3. Larger particles are more likely to cause blocking or clogging of the filter, preventing smaller particles from passing through (Aydilek 2011).

The difference in filter performance in retaining the three PSDs can also be seen in the lifespans of the filter systems. For the NW2 filter, the cumulative solids loading attained at the failure point of the test was larger for P1 than for P2 or P3. For the NW3 filter, the cumulative solids loading attained at the failure point of the test is larger for P1 than for P2. This is shown in Figure 13 where P1 testing ended at about 6.4 kg/m^2 solids loading and 5.6 kg/m^2 solids captured while P2 testing on the same type of filter ended at about 4.3 kg/m^2 loading and 3.6 kg/m^2 captured and P3 testing ended at about 4.9 kg/m^2 loading and 4.0 kg/m^2 captured. Similar results are noted for NW3 in Figure 14. However, as seen in Figure 14, the 3.P3 test ended at a higher total solids loading than 3.P1. Since the slope of the regression line for 3.P3 is smaller than the slope of 3.P1, test 3.P1 still had a higher total solids captured than test 3.P3. The phenomenon is likely a result of the more open and porous filter cake established by P1. P1 includes a larger range of particle sizes than P2 and P3, and the largest particles in P1 (180 μm) are larger than the largest particles in P2 (106 μm). As shown in Figure 15, the larger particles are expected to form a more porous graded filter zone in the cake above the filter (Aydilek 2011). Since P1 has larger particles than P2 and P3, the filter cake that forms is likely more porous, and a P1 cake with the same mass of solids as a P2 cake allows a greater amount of water to pass through. The result is a longer lifespan overall because at the point where each geotextile-filter cake system reaches the same hydraulic conductivity, the P1 cake will have a larger collected mass than the P2 or P3 cake, meaning that the filter had reached a higher cumulative solids loading before it reached its final failure hydraulic conductivity. The cakes formed by P2 and P3 likely had a greater

accumulation of fines at the filter-cake interface which often promotes clogging of the

geotextile by forming a blinding zone at the interface (Kutay and Aydilek 2005).
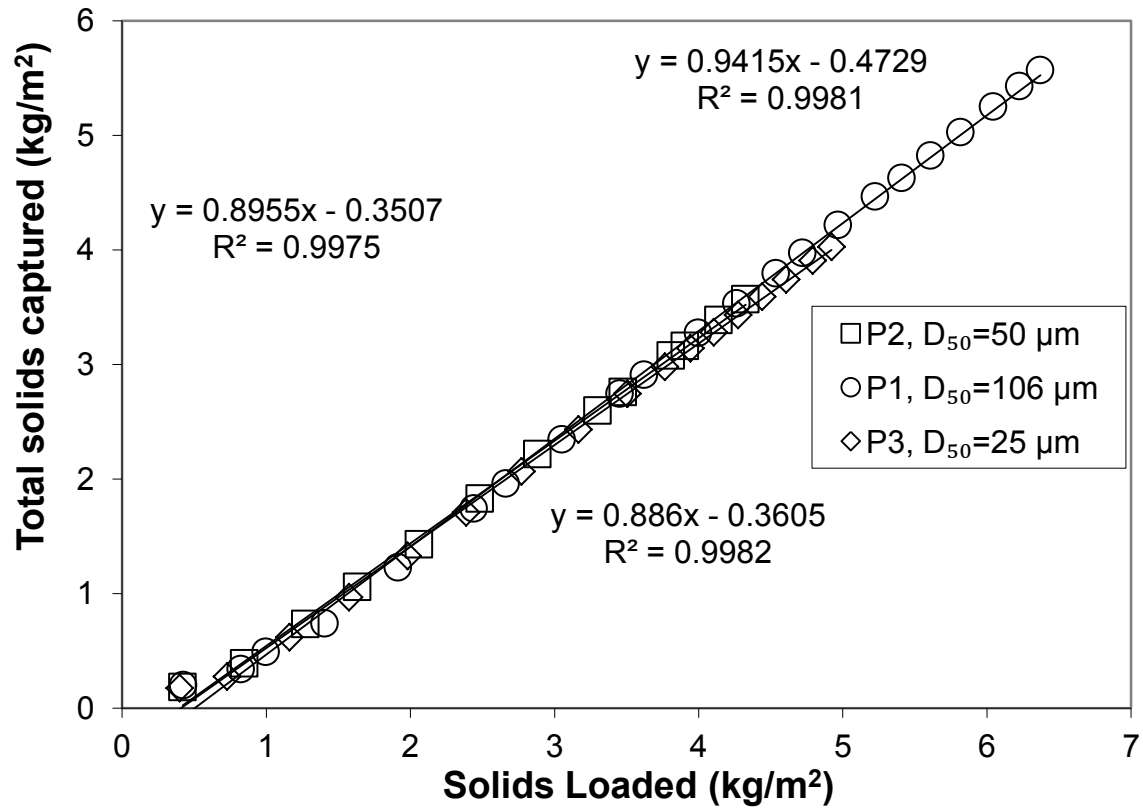
Figure 13. Total solids captured by the NW2 filter as a function of the solids loaded to

the filter for TSS concentration of 200 mg/L.
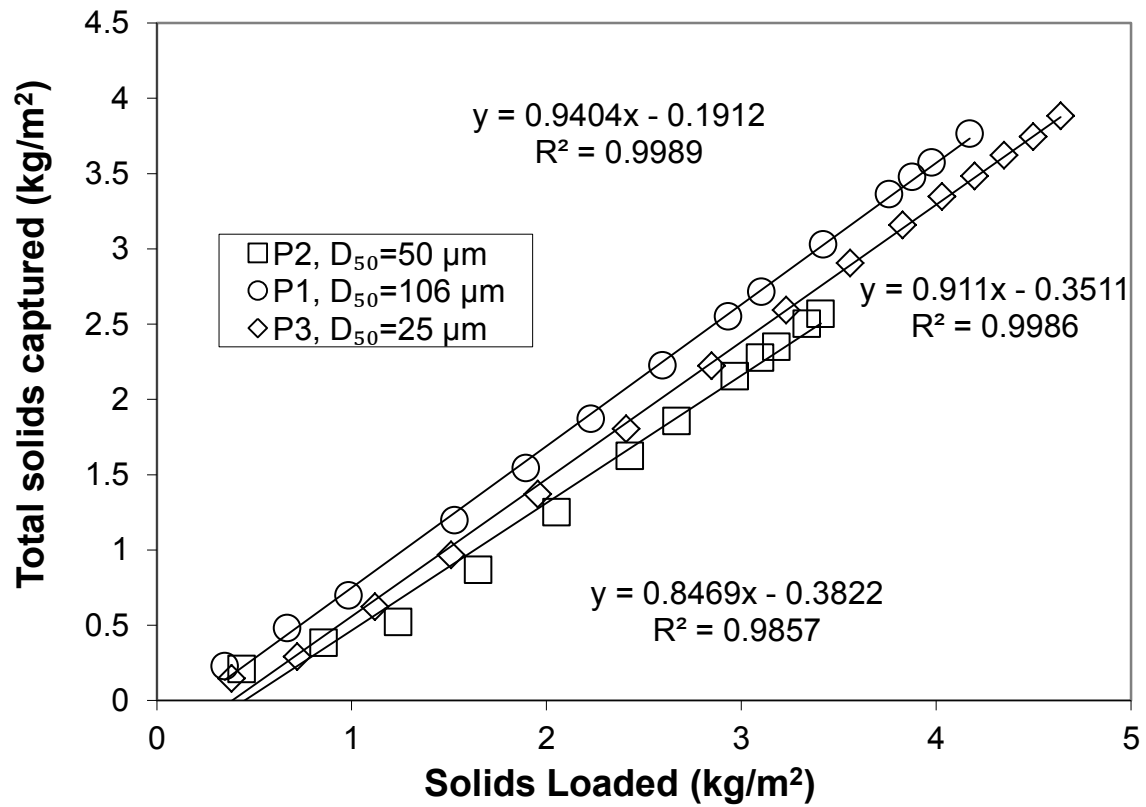
Figure 14. Total solids captured by the NW3 filter as a function of the solids loaded to the filter for TSS concentration of 200 mg/L.
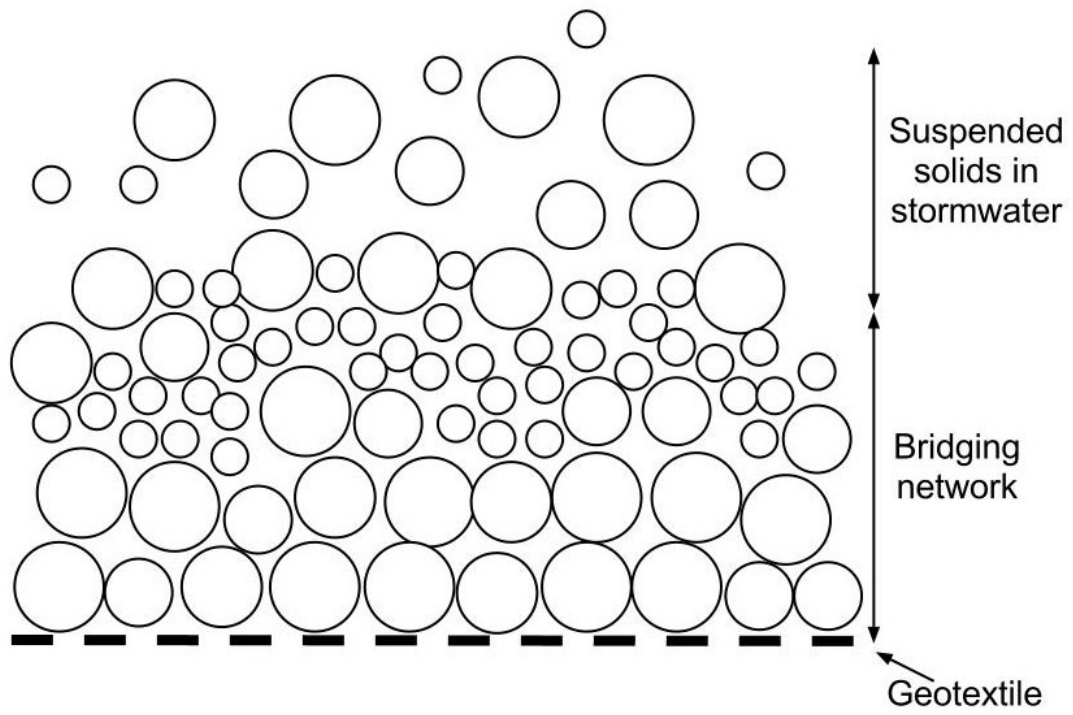
Figure 15. Graded filter zone (bridging network) (adapted from: Aydilek 2011).

ROLE OF INFLUENT TSS CONCENTRATION

Several tests were performed on geotextile filters using a lower TSS concentration of 100

mg/L, which is slightly lower than the average event mean concentration (EMC) for TSS

in stormwater runoff events occurring in urban areas (Sansalone et al. 1998; Furumai et al.

2002; Taebi and Droste 2004; Sansalone et al. 2005; Barrett et al. 2006; Flint and Davis

2007; Hallberg and Renman 2008; Kim and Sansalone 2008; Li and Davis 2008). Figure

16 shows an example of the influent and effluent TSS concentrations found for one 75

minute test (from Test 3.P1(100)). Just as in the tests with 200 mg/L solids loading

(Figure 4), the first effluent concentration measured at 3 minutes was above the target

concentration of 30 mg/L, while all others were below the 30 mg/L limit. Again, this

phenomenon, i.e., the highest concentration observed in the earliest effluent sample and

then a decrease in effluent concentration with time, was observed in most of the 75

minute tests because the filter cake was disturbed by the initial influent flow and with

time, the soil particles settled back onto the filter.

Similar to the 200 mg/L tests described earlier, effluent concentrations decreased

as the total solids loading increased for the 100 mg/L tests. Figure 17 shows both

influent and effluent TSS EMCs as a function of total cumulative solids loading for tests

2.P1(100), 3.P1(100), and 2 repeated tests, one for each type of filter. For both NW2 and

NW3 filters, the effluent EMCs dropped below the target concentration (30 mg/L)

between a solids loading of 0.5 and 1 kg/m^2, and beyond this loading, the effluent TSS

EMCs remained below the target value, at about 8 mg/L, except for a few points around

the final solids loading. The three points at or exceeding the target concentration after the

ripening period occurred in Figure 17 can be explained by the shortened timespan of

those tests. Because the water head reached the top of the Plexiglass column during testing in less than 75 minutes, the TSS EMC was higher than the others due to testing ending before the filter cake could completely re-settle after its initial disturbance at the onset of testing and fully contribute to the reduction of TSS.

One difference between the two filters tested at 100 mg/L loading was the total solids loaded at the end of the test set, i.e., at the final clogging point (as defined in the METHODOLOGY AND MATERIALS section). In general, clogging occurred at a lower total solids loading for NW3 (4.5 and 5.6 kg/m^2), than for NW2 (5.0 and 6.8 kg/m^2). (Figure 17). These results are similar to the results for the 200 mg/L tests and they correlate directly with the permittivities of the filters; NW2 and NW3 had permittivities of 0.8 s^{-1} and 0.54 s^{-1} respectively. Therefore, a higher permittivity indicates that a greater mass of solids can be loaded to the filter before clogging occurs.

Figure 18 shows the TSS concentrations in the influent and effluent suspensions as a function of the total solids loaded for the NW2 and NW3 geotextiles using particle size distribution, P2. Similar to the results in Figure 17, for both NW2 and NW3 filters, the effluent concentrations dropped below the target concentration (30 mg/L) around a solids loading of 0.5 kg/m^2, and beyond this loading, the effluent TSS concentrations remained below the target value, except for one value in the NW2 test which can be attributed to an extremely large TSS concentration (>400 mg/L) measured within the first 5 minutes of testing. Before the concentration drop, a ripening process occurred for both filters. Unlike the results of the P1 tests and the previously discussed tests with influent TSS concentration of 200 mg/L, NW3 reached a greater solids loading than NW2 at its clogging point when loaded with soil particles of particle size distribution P2 at an

influent TSS concentration of 100 mg/L. A reason for this difference is the greater

thickness of the NW3 filter. If the filter was able to retain more solids within the

thickness of the material before a filter cake formed and caused clogging, then the total

mass of solids captured by the filter and also total mass of solids loaded the filter would

be larger for a thicker geotextile.

Analysis of the regression lines of the total cumulative solids captured in and on

each filter as a function of the total solids loaded for tests 2.P1(100), and 3.P1(100)

(Figure 19) gives a direct comparison of the behavior of each filter when loaded with

particle size distribution P1. Statistical analysis (as described in METHODOLOGY

AND MATERIALS) indicates that the slope and y-intercept of the Test 2.P1(100)

regression line are not equal to those of the repeated Test 2.P1(100) regression line at any

level of significance (Fig. 19). Likewise, the slope and y-intercept of the Test 3.P1(100)

regression line are not equal to those of the repeated Test 3.P1(100) regression line at any

level of significance. The slope of the Test 2.P1(100) regression line is however, equal to

the slope of the repeated Test 3.P1(100) regression line (at 0.4% level of significance)

(Tables 6 and 7), and the slope of the repeated Test 2.P1(100) is equal to the slope of the

Test 3.P1(100) regression line (at 5% level of significance). These results indicate that

the behavior of NW2 and NW3 filters, in terms of mass capture of suspended solids

loaded to the filters, is nearly equal.

Unlike the P1 results, NW2 and NW3 did not behave similarly in terms of total

solids captured for particle size distribution P2 with an influent TSS concentration of 100

mg/L (Figure 20). Statistical analysis indicates that the slopes of the regression lines of

the P2 tests, 2.P2(100) and 3.P2(100), for total solids captured in and on each filter as a

function of total solids loaded are not statistically equal to each other for either the 1% or 5% level of significance (Table 7). As discussed earlier, the ability of the NW3 filter to retain more solids overall is likely a result of the thickness of the filter. The greater thickness of NW3 allowed more solids to be retained within the thickness before a filter cake formed on the surface.

The results for the 100 mg/L tests have been very similar to the results from the 200 mg/L tests. In general, the behaviors of the NW2 and NW3 filters in terms of mass capture of suspended solids per solids loaded have been the same. Also, the NW2 filters typically last longer than the NW3 filters in terms of total solids loaded to the filters at the final clogging point. These results were observed for both types of tests (100 and 200 mg/L). Additionally, statistical analysis shows that the parameters, b_1 and b_0, the slope and y-intercept for a regression line, of one set of data are often equal to the b_1 and b_0 (respectively) of another set of data with the only parameter changing between the two sets being the influent TSS concentration. For example, the slope of the Test 2.P1 regression line is nearly identical to the slope of the Test 2.P1(100) regression line (Fig. 21, Table 7), indicating very similar behavior by the NW2 filter in terms of mass of solids captured per solids loaded regardless of the influent TSS concentration. The only significant difference between the 100 mg/L tests and the 200 mg/L tests is the mass of solids loaded to the filter at the end of the ripening period, or the point at which the effluent TSS concentrations drop below the target concentration. For the 200 mg/L tests, the ripening period typically ended at a solids loading of 1-2 kg/m^2; the ripening period typically ended at a solids loading of 0.5-1 kg/m^2 for the 100 mg/L tests. The mass of solids loading at the end of the ripening period halves as the influent TSS concentration

halves, or more likely, the mass of solids loaded at the end of the ripening period is dependent upon the mass of solids loaded to the filter per 75 minute test. This phenomenon will be addressed again later in Chapter V.
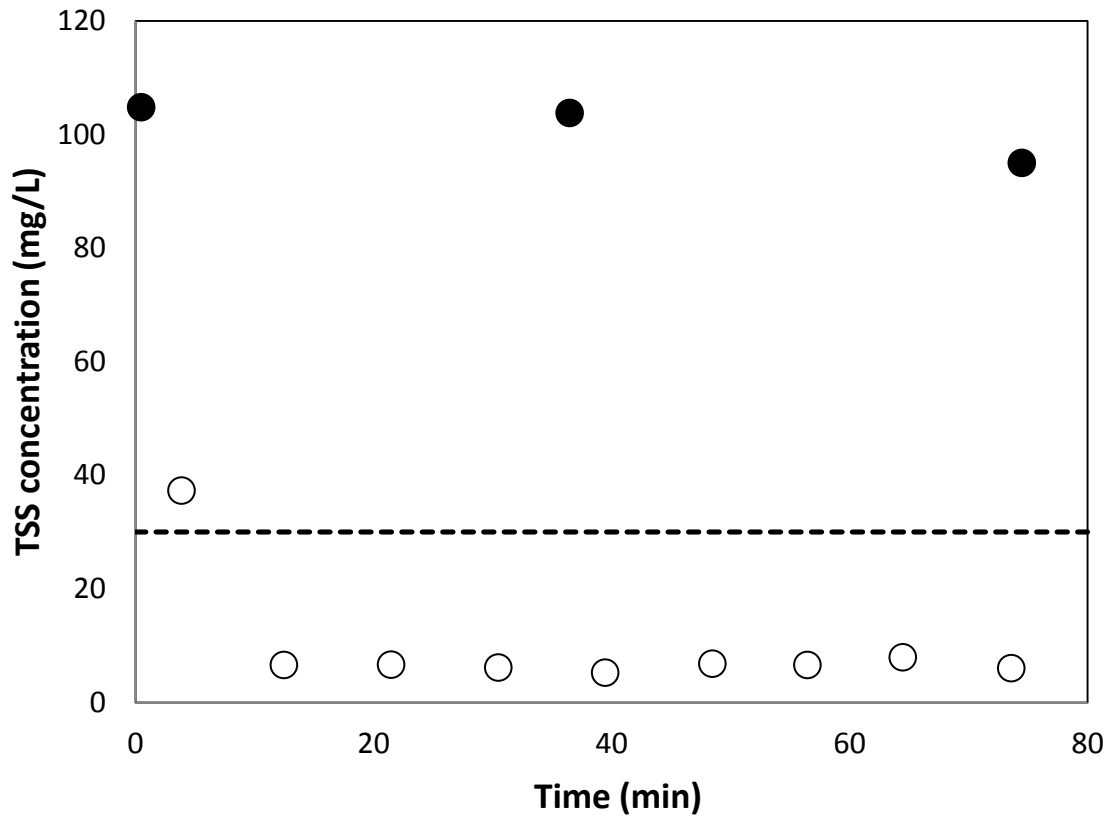
Figure 16. TSS concentration as a function of time during the fifth test of Test 3.P1(100). Closed symbols indicate influent values. Open symbols indicate effluent values. Dashed line indicates the target concentration of 30 mg/L.
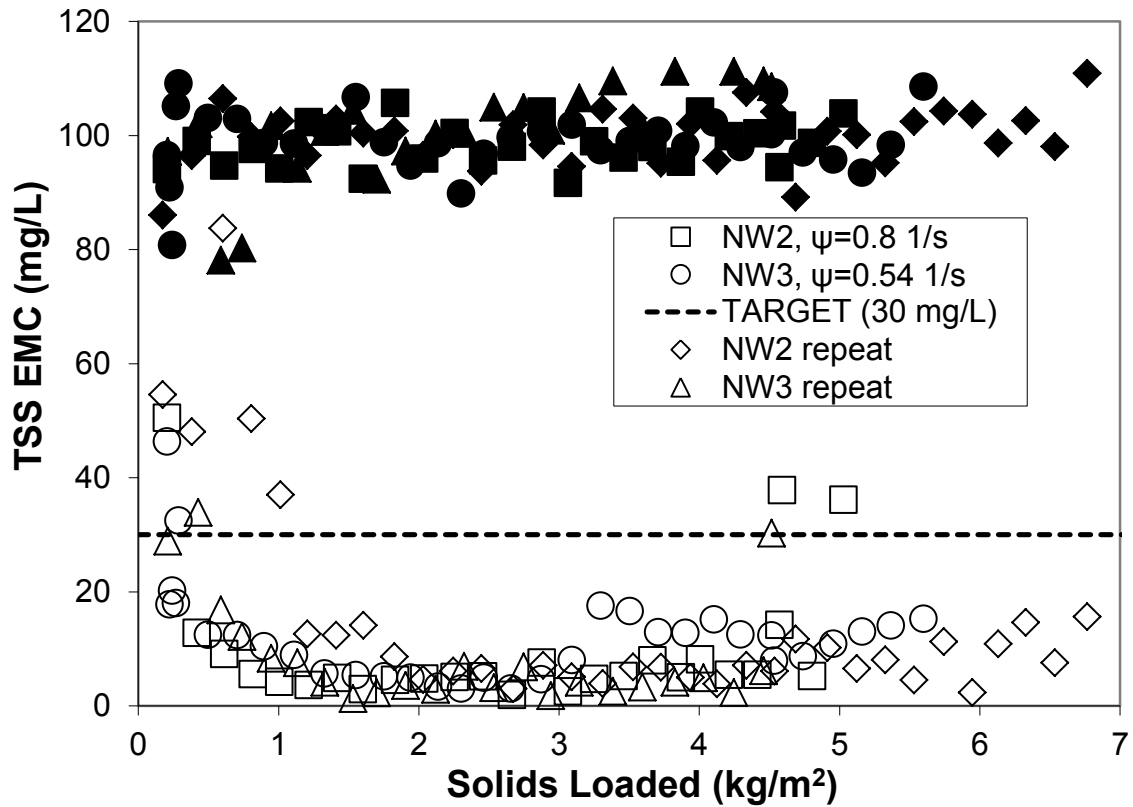
Figure 17. Effect of total solids loaded to NW2 and NW3 filters on TSS concentration for particle size distribution P1. Closed symbols indicate influent values. Open symbols indicate effluent values. Initial permittivity values are given in the legend for each geotextile. Dashed line indicates the target concentration of 30 mg/L.
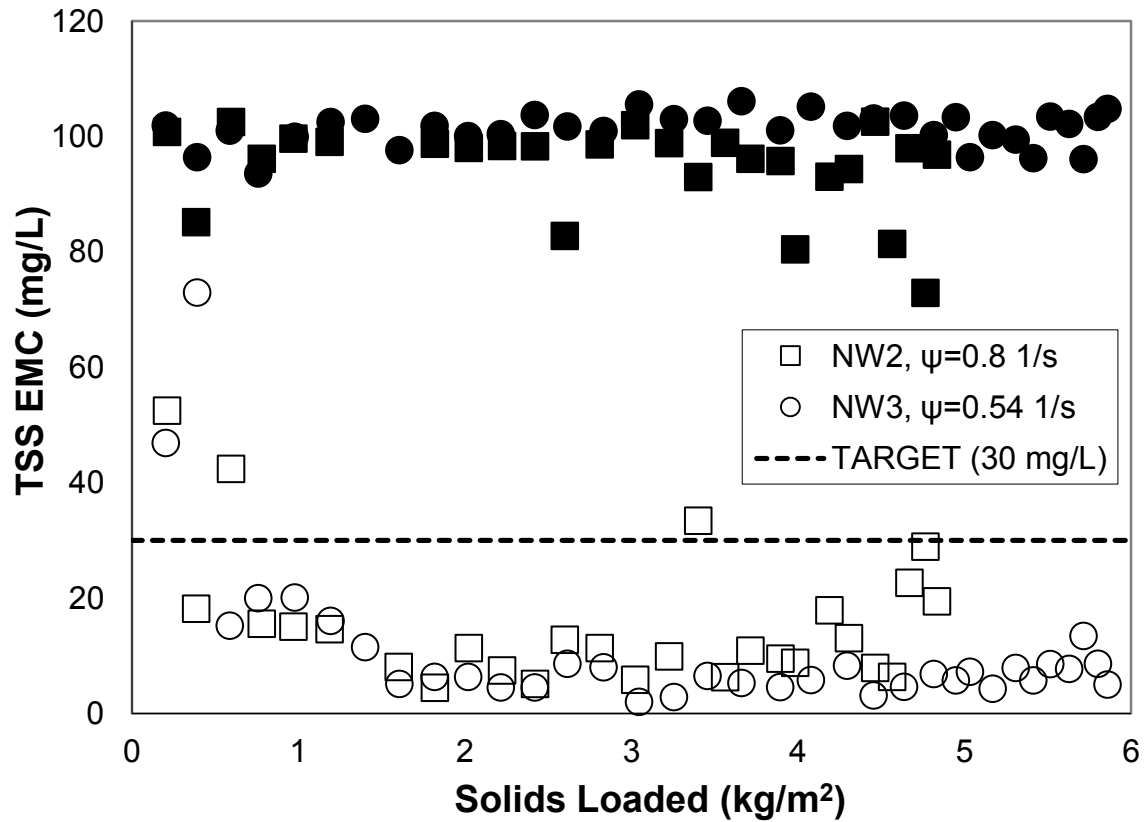
Figure 18. Effect of total solids loaded to NW2 and NW3 filters on TSS concentration for particle size distribution P2. Closed symbols indicate influent values. Open symbols indicate effluent values. Initial permittivity values are given in the legend for each geotextile. Dashed line indicates the target concentration of 30 mg/L.
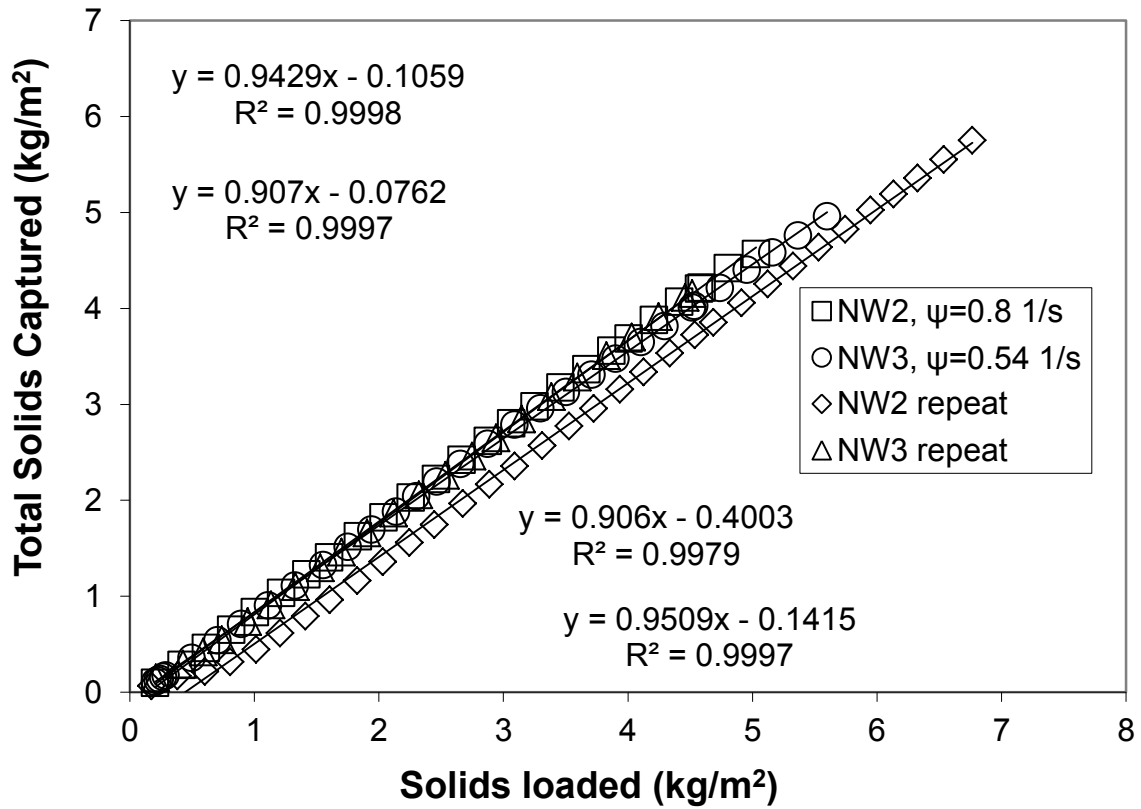
Figure 19. Total solids captured by the NW2 and NW3 filters as a function of the solids

loaded to each filter for TSS concentration of 100 mg/L and particle size distribution P1.
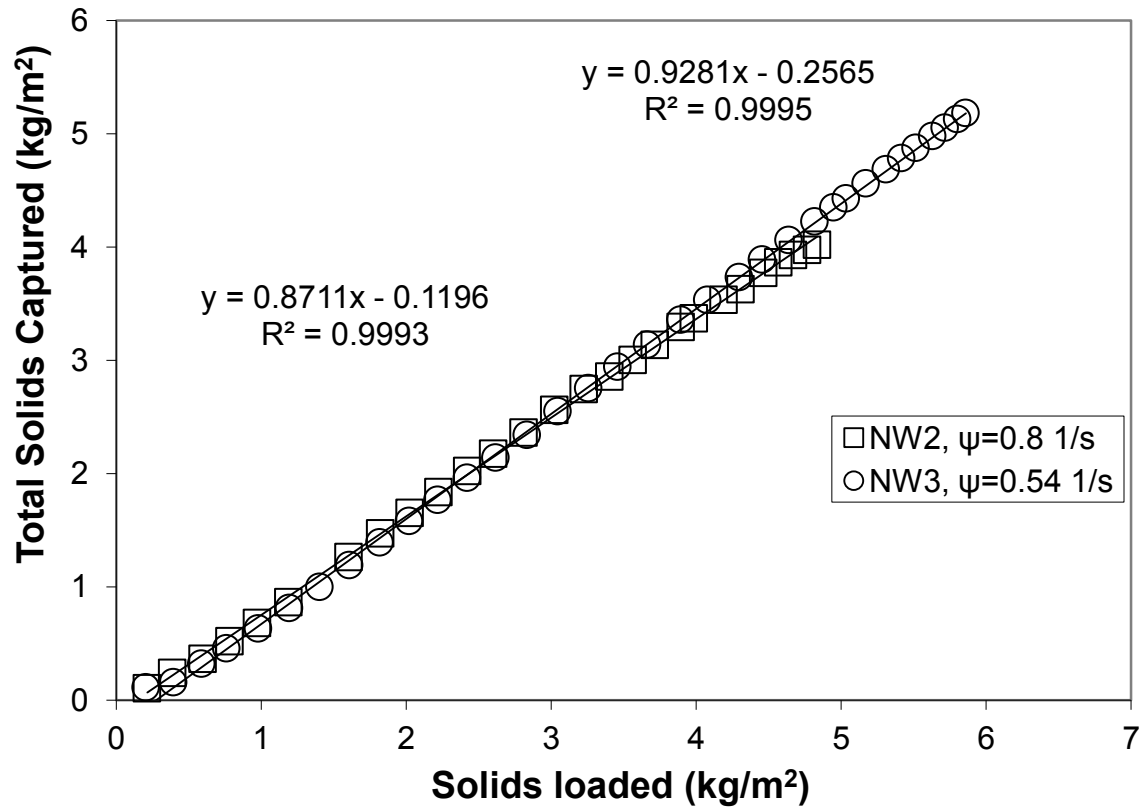
Figure 20. Total solids captured by the NW2 and NW3 filters as a function of the solids

loaded to each filter for TSS concentration of 100 mg/L and particle size distribution P2.
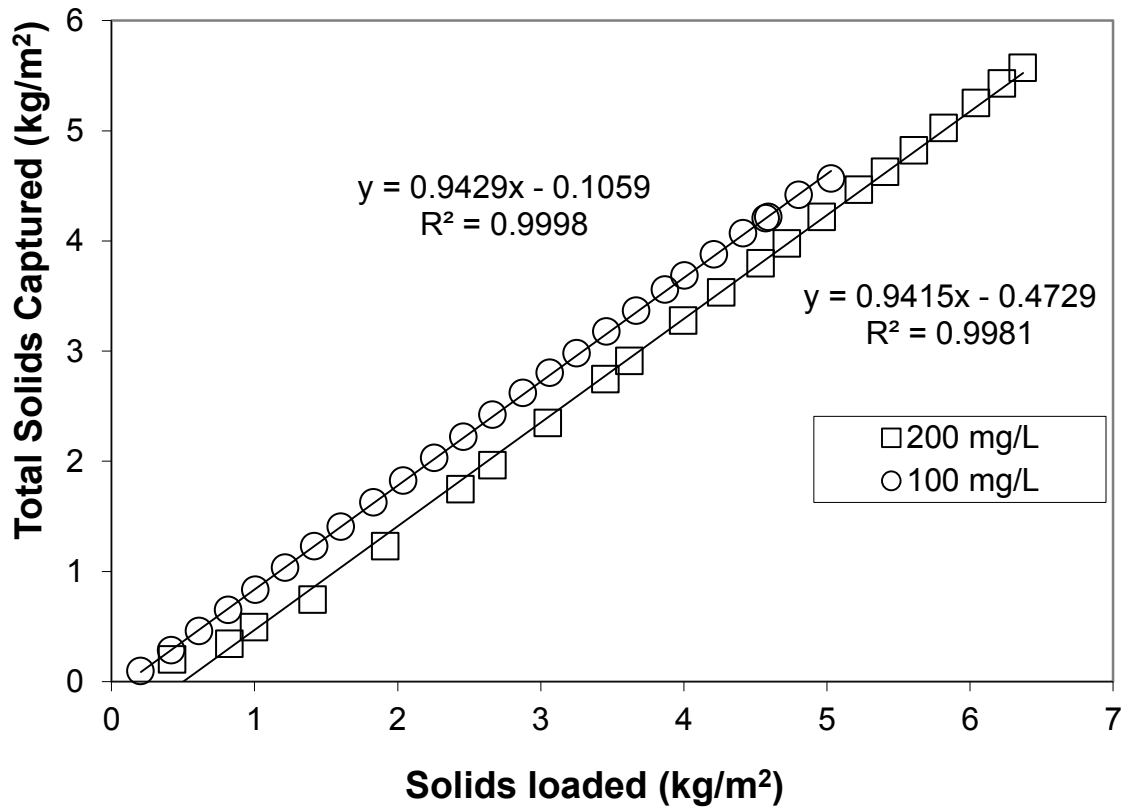
Figure 21. Total solids captured by NW2 filters as a function of the solids loaded to each filter for particle size distribution P1.

Table 6. Slope and y-intercept values (b_1 and b_0 respectively) and their corresponding

standard error values for the solids captured as a function of solids loaded regression lines

shown in Figures 19 and 20.

PSD	Filter type	b_1	Se (b_1)	b_0	Se (b_0)
	2	0.94	0.002	-0.11	0.008
P1	3	0.91	0.007	-0.40	0.030
	2	0.91	0.003	-0.08	0.009
	3	0.95	0.004	-0.14	0.010
P2	2	0.87	0.005	-0.12	0.014
	3	0.93	0.004	-0.26	0.015

Table 7. Critical levels of significance for two-tailed t-tests setting either b_1 or b_0 (given in Table 6) for the each test listed at the top of the chart equal to the corresponding b_1 or b_0 for each test listed at the left side of the chart. Bold indicates those meeting the standard significance level of 0.01 (1%). Values italicized indicate those meeting both standard significance levels of 0.01 (1%) and 0.05 (5%). Blank cells represent values given in Table 5.

Parameter in linear regression	Influent TSS conc.	Particle size distribution (PSD)	Filter type	200 mg/L P1 — 2	P1 — 3	P2 — 2	P2 — 3	100 mg/L P1 — 2	P1 — 2	P1 — 3	P1 — 3	P2 — 2	P2 — 3
b_1	200 mg/L	P1	2					***0.5600***	<0.0001	<0.0001	**0.0264**	<0.0001	0.0016
		P1	3					***0.3345***	<0.0001	<0.0001	**0.0132**	<0.0001	0.0038
		P2	2					<0.0001	***0.1738***	0.0003	<0.0001	<0.0001	<0.0001
		P2	3					<0.0001	<0.0001	<0.0001	<0.0001	<0.0001	<0.0001
	100 mg/L	P1	2	***0.7514***	***0.6851***	0.0049	**0.0147**	1	<0.0001	<0.0001	***0.0522***	<0.0001	0.0006
		P1	2	0.0009	0.0031	***0.4636***	***0.0976***	<0.0001	1	***0.6538***	<0.0001	<0.0001	<0.0001
		P1	3	0.0012	0.0036	***0.4300***	***0.0938***	<0.0001	***0.7620***	1	<0.0001	<0.0001	<0.0001
		P1	3	***0.3406***	***0.2815***	0.0024	0.0093	0.0043	<0.0001	<0.0001	1	<0.0001	<0.0001
		P2	2	<0.0001	<0.0001	***0.0985***	***0.4776***	<0.0001	<0.0001	<0.0001	<0.0001	1	<0.0001
		P2	3	***0.1614***	***0.1959***	**0.0371**	**0.0337**	<0.0001	0.0058	<0.0001	<0.0001	<0.0001	1
b_0	200 mg/L	P1	2					<0.0001	**0.0207**	<0.0001	<0.0001	<0.0001	<0.0001
		P1	3					<0.0001	<0.0001	<0.0001	0.0001	<0.0001	0.0001
		P2	2					<0.0001	***0.1067***	<0.0001	<0.0001	<0.0001	<0.0001
		P2	3					<0.0001	***0.5355***	<0.0001	<0.0001	<0.0001	<0.0001
	100 mg/L	P1	2	<0.0001	0.0055	<0.0001	0.0065	1	<0.0001	0.0027	0.0034	***0.3710***	<0.0001
		P1	2	***0.0772***	<0.0001	***0.2506***	***0.7116***	<0.0001	1	<0.0001	<0.0001	<0.0001	<0.0001
		P1	3	<0.0001	0.0007	<0.0001	0.0040	0.0007	<0.0001	1	<0.0001	0.0060	<0.0001
		P1	3	<0.0001	***0.0756***	0.0003	**0.0138**	<0.0001	<0.0001	<0.0001	1	***0.1469***	<0.0001
		P2	2	<0.0001	**0.0156**	0.0001	**0.0085**	***0.0870***	<0.0001	<0.0001	**0.0487**	1	<0.0001
		P2	3	<0.0001	**0.0253**	***0.0397***	***0.1539***	<0.0001	<0.0001	<0.0001	<0.0001	<0.0001	1

ROLE OF INFLUENT FLOW RATE

Two tests were completed on geotextile filters using a lower influent flow rate of 3 mL/s because this flow rate corresponds to a more realistic hydraulic loading rate (HLR) than the previous flow rate (1.8 cm/hr versus 3.6 cm/hr) assuming a runoff area-to-drainage area ratio of 50 (0-0.254 cm, 1 hr; Kreeb 2003). Figure 22 shows an example of the influent and effluent TSS concentrations found for one 150 minute test (from Test 2.P1(3)). The influent concentrations were constant at approximately 200 mg/L. The first effluent concentration measured at 6 minutes was above the target concentration of 30 mg/L, while all others were below the 30 mg/L limit. This phenomenon, i.e., the highest concentration observed in the earliest effluent sample and then a decrease in effluent concentration with time, was observed in the 75 minute tests previously discussed and is a result of the filter cake being disturbed by the initial influent flow.

As in all the tests previously discussed, effluent concentrations were determined to decrease as the total solids loading increased. Figure 23 shows both influent and effluent TSS EMCs as a function of total cumulative solids loading for Tests 1.P1(3) and 2.P1(3). Each point represents an EMC for each 150 min test. For both filters, the effluent EMCs dropped below the target concentration (30 mg/L) between a solids loading of 1 and 2 kg/m^2, and beyond this loading, the effluent TSS EMCs remained below the target value, at about 6 mg/L for all but one of the points. The EMC point larger than the target concentration can be attributed to the shortened timespan of that test, similar to the results of Test 2.P1(100) (Figure 17). As shown in Figure 23, a ripening period occurred for both filters. While TSS removal was good, the effluent EMC for NW1 did not fall below the target concentration for the entire series of 150 min tests.

The differing result for NW1 as compared with NW2, which was observed for tests at the 6 mL/s influent flow rate as well, can be attributed to the larger AOS and the larger permittivity of the filter (Table 2).

Another difference between the two filters was the total solids loaded at the end of the test set, i.e., at the final clogging point (as defined in METHODOLOGY AND MATERIALS). Clogging occurred at a lower total solids loading for NW2 than for NW1 (6.7 kg/m^2 vis-a-vis 8.8 kg/m^2, respectively) (Figure 23). These results correlate directly with the permittivities of the filters. Therefore, like previous test results, a higher permittivity indicates that a greater mass of solids can be loaded to the filter before clogging occurs.

Analysis of the regression lines of the total cumulative solids captured in and on each filter as a function of the total solids loaded for Tests 1.P1(3) and 2.P1(3) (Figure 24) gives a direct comparison of the behavior of the NW1 and NW2 filters when loaded with particle size distribution P1 and an influent flow rate of 3 mL/s. The test results were similar to the results of tests performed with a higher influent flow rate. Statistical analysis (as described in METHODOLOGY AND MATERIALS) indicates that the slopes for Tests 1.P1(3) and 2.P1(3) regression lines (shown in Fig. 24) are significantly different (0.90 for NW1, 0.97 for NW2) using a 1% level of significance, indicating that the mass of solids captured per solids loaded for NW1 is significantly different than that of NW2.

Statistical analysis of the low flow rate test (Tests 1.P1(3) and 2.P1(3)) regression lines and the regression lines for the higher flow rate tests discussed previously (1.P1, 2.P1, 2.P1(100)) for total solids captured as a function of total solids loaded to the filter

shows how the total solids captured is affected by flow rate. The slopes and y-intercepts of the 3 mL/s test regression lines were significantly different from those of the 6 mL/s-test regression lines at the 1% level of significance (Figure 24 versus Figure 10). Also, the slope and y-intercept of the 2.P1(3) regression line are not statistically equal to those parameters of the 2.P1(100) regression lines at the 1% level of significance (Figure 25). However, the b_1 values for the lower flow rate tests are within the range of b_1 values calculated for the other particle size distribution P1 tests (Table 8), and the regression lines of all P1 tests on the NW2 filter in Figure 25 appear to be very similar to each other. This indicates that while the slopes are not statistically equal to each other, the mass of solids captured per solids loaded for the low flow rate tests is very similar to the mass of solids captured per solids loaded for the higher flow rate tests when testing the filters with particle size distribution P1 at either influent TSS concentration, 100 or 200 mg/L, indicating that results are based on total mass of influent solids, not the solids concentration.
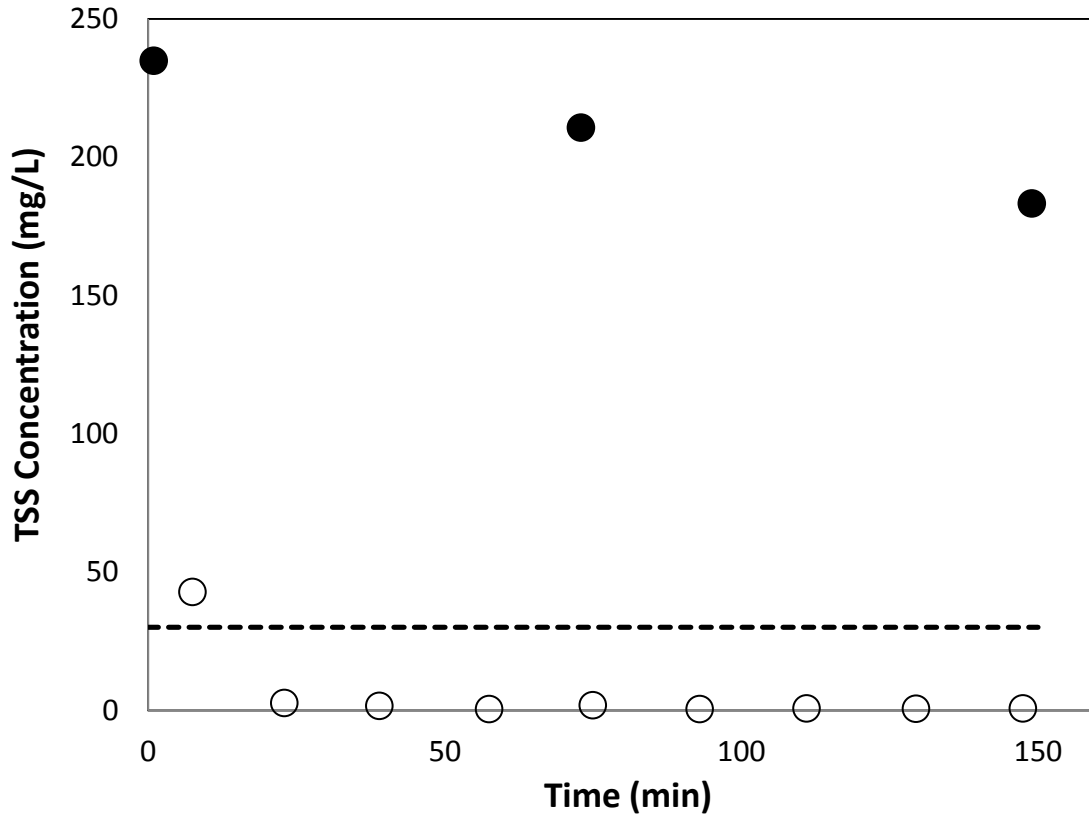
Figure 22. TSS concentration as a function of time during the fifth test of Test 2.P1(3). Closed symbols indicate influent values. Open symbols indicate effluent values. Dashed line indicates the target concentration of 30 mg/L.
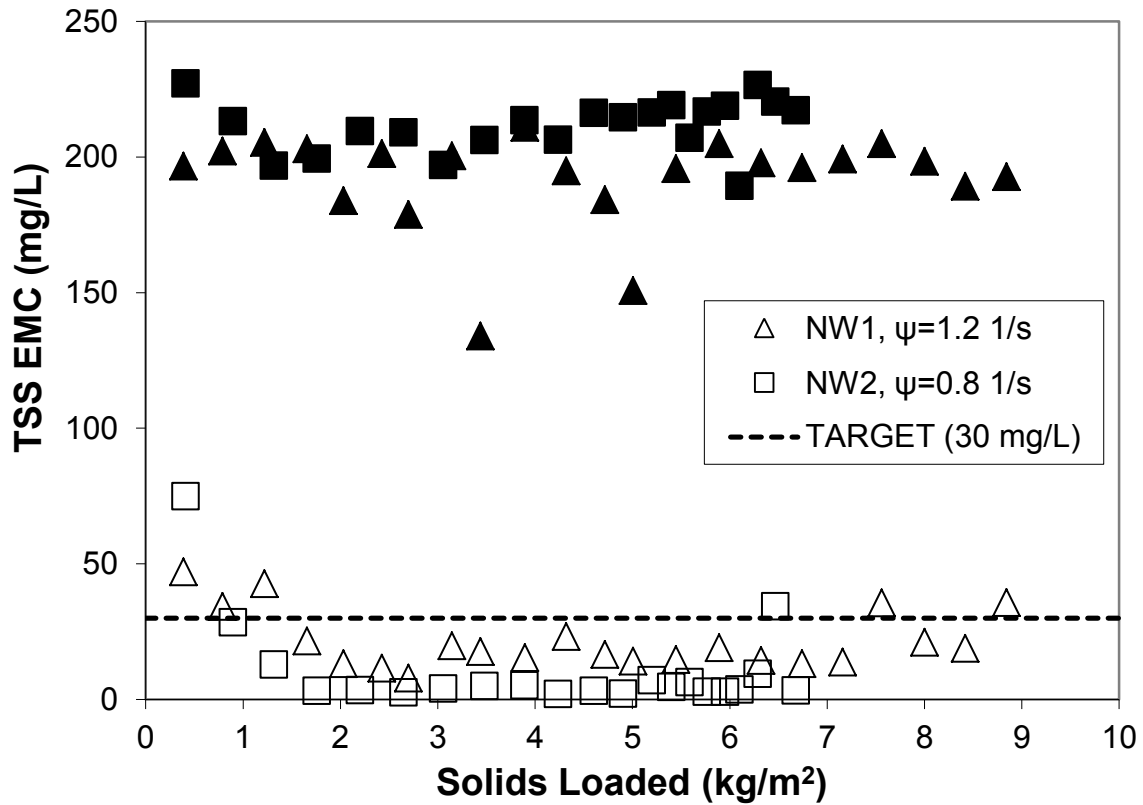
Figure 23. Effect of total solids loaded to NW1 and NW2 filters on TSS concentration for particle size distribution P1 at an influent flow rate of 3 mL/s. Closed symbols indicate influent values. Open symbols indicate effluent values. Initial permittivity values are given in the legend for each geotextile. Dashed line indicates the target concentration of 30 mg/L.
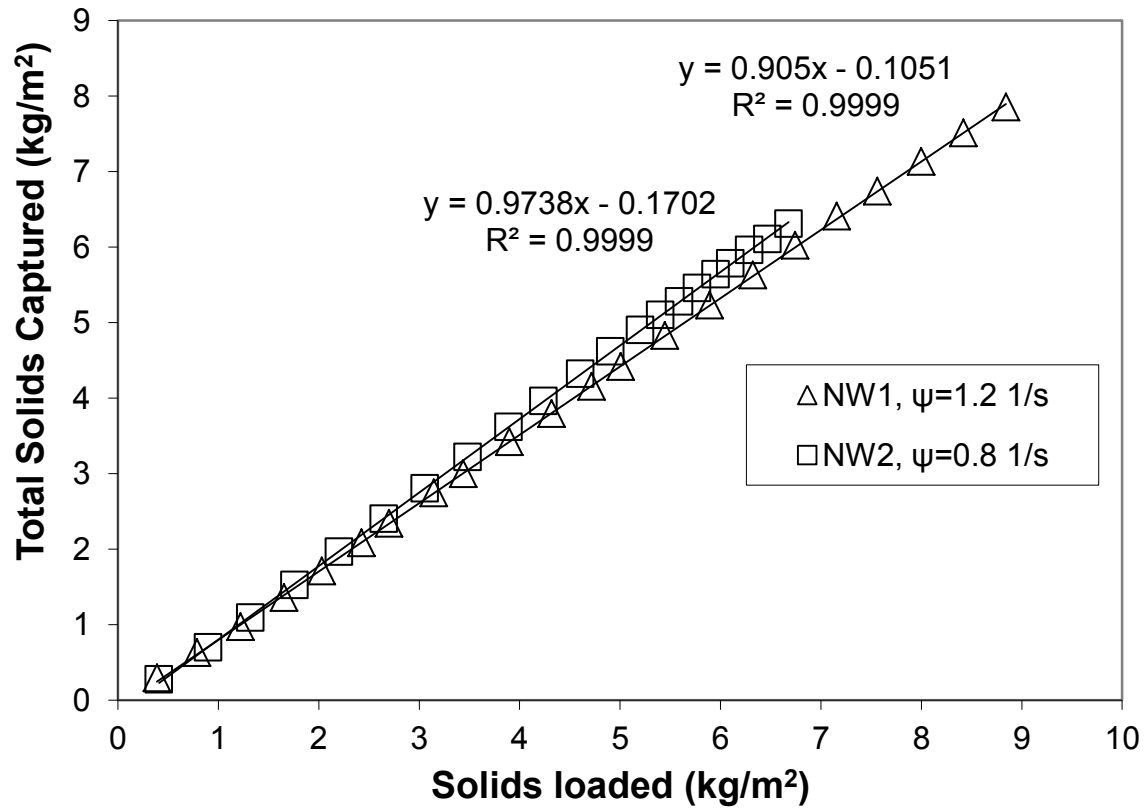
Figure 24. Total solids captured by the NW1 and NW2 filters as a function of the solids loaded to each filter for TSS concentration of 200 mg/L, particle size distribution P1, and influent flow rate of 3 mL/s.

Table 8. Slope and y-intercept values (b_1 and b_0 respectively) and their corresponding standard error values for the solids captured as a function of solids loaded regression lines shown in Figures 10, 19, and 24. Values listed are from tests with particle size distribution P1.

TSS C_0 (mg/L)	Influent flow rate (mL/s)	Filter type	b_1	Se (b_1)	b_0	Se (b_0)
200	6	1	0.79	0.004	-0.39	0.027
		2	0.94	0.009	-0.47	0.038
	3	1	0.90	0.002	-0.11	0.010
		2	0.97	0.002	-0.17	0.009
100	6	2	0.94	0.002	-0.11	0.008
		2	0.91	0.007	-0.40	0.030
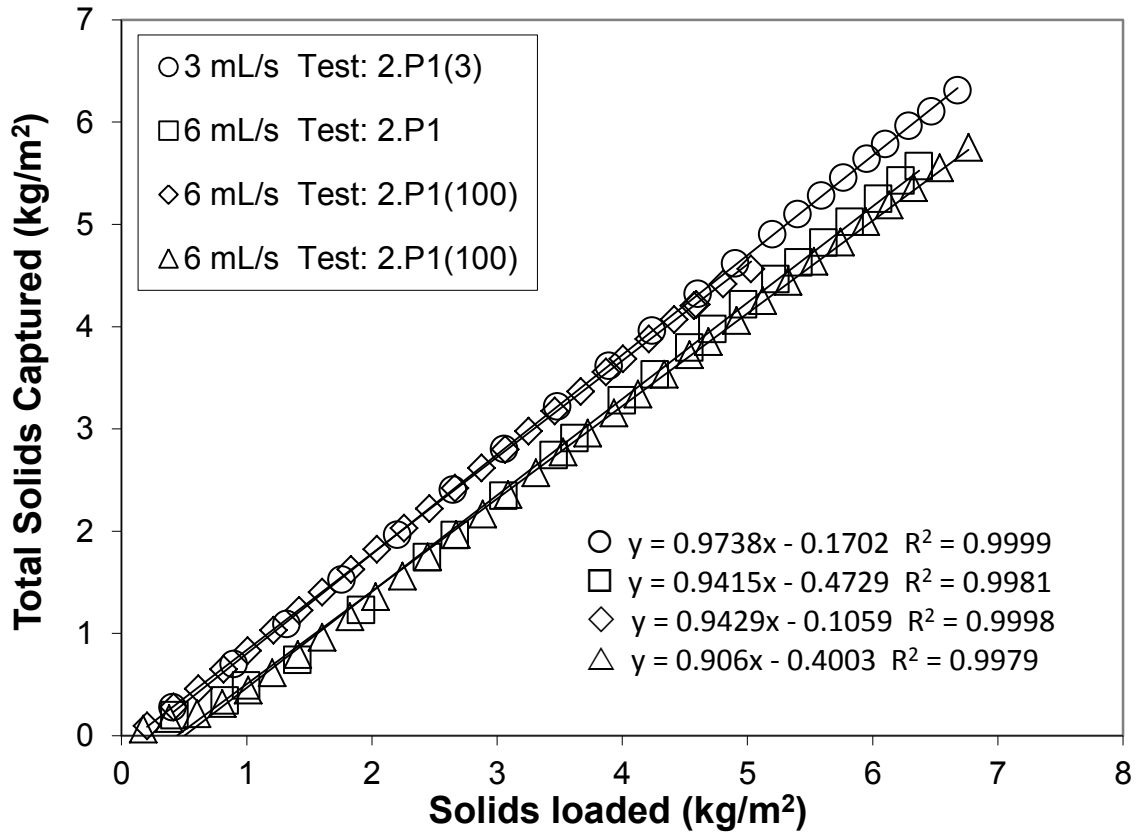
Figure 25. Total solids captured by the NW2 filter as a function of the solids loaded to the filter for TSS concentrations of 100 and 200 mg/L, particle size distribution P1, and influent flow rate of 3 and 6 mL/s.

COMPARISON WITH THEORY

Because the thicker and less porous filters reduced the TSS concentrations to the greatest extent, the results of this study follow theory for porous media capture. The steady state expression for porous media capture shows that as the porosity, ε, of a filter decreases, the effluent concentration of particles should decrease (AWWA 1999):

$$\frac{C}{C_0} = \exp\left(-\frac{3}{2}\frac{(1-\varepsilon)}{D_C}\alpha_s\eta L\right) \qquad (4)$$

where C is the concentration of particles leaving the filter, C_0 is the concentration of particles in the incoming suspension, L is the media depth, ε is the filter bed porosity, D_C is the collector particle diameter, α_s is the sticking coefficient (usually determined from column tests), and η is the single collector collision efficiency. This equation also shows that as the media depth increases, the effluent particle concentration decreases (AWWA 1999). Although testing performed for this study was not set at steady-state conditions as required by Equation 4, the assumption of steady-state was made for simplicity in comparison of the results of this study with granular bed filtration theory. The results were assessed by Equation 4 given that only the results of each test run on a clean filter (the first 75 min test in each set) were used because Equation 4 is only valid for clean-bed porous media capture. The results of this analysis show that the reduction in TSS concentrations (C) is directly correlated with the filter thickness (L) for NW1, NW2, and NW3, as predicted by Equation 4. Additionally, Equation 4 shows that as porosity of the filter increases, the effluent concentration increases. NW1 has a slightly higher porosity than the other filters and exhibited larger effluent concentrations overall, thus, following the granular bed theory.

In order to address the other variables in Equation (4), α_s, η and D_C are lumped into a single constant, X, in the following equation:

$$\frac{C}{C_0} = \exp\left(-\frac{3}{2}X(1-\varepsilon)L\right) \qquad (5)$$

The X values for the results of the tests in this study, using the effluent concentration C from the first test run (i.e., first 75 minutes of testing) on each filter are given in Table 9. In general, the values given in Table 9 follow a trend demonstrating that as permittivity of the filter decreases while all other parameters are kept constant, X increases. One exception is 1.P2, in which a ripening period never occurred and the effluent TSS concentrations did not consistently drop below the influent concentration. Another exception is 1.P1(3), the test on NW1 with PSD P1 using a lower flow rate, 3 mL/s. During this test, the ripening period was more subdued than in previous tests; the filter reduced the TSS concentration to nearly the target concentration during the initial test. The final test that does not follow the trend described above is 3.P3, and this is likely a result of the lower influent TSS concentration during the first test run (175 mg/L). If the influent concentration had been closer to 200 mg/L and the effluent concentration remained the same, the X value would follow the trend of decreasing permittivity resulting in increasing X.

Assuming that the sticking coefficient, α_s, and single collector collision efficiency, η, remain constant for all three filters at a given particle size distribution, then, an increase in X indicates a decrease in the collector diameter, D_C. Therefore, permittivity of the filters behaves similarly to the collector diameter of a granular filter (Table 9). This result is rational because as the collector particles in a granular filter decrease in diameter, the pore spaces between the particles decrease and the media becomes less permeable.

A trend in the X values is also apparent as the PSD changes (Table 9). X values are largest for P1, followed by values for P2 and P3 because P1 includes larger particles than P2 and P3. For tests performed with 200 mg/L influent TSS concentration, the average X values for P1, P2 and P3 tests are 1565, 963, and 818, respectively, and for the tests performed with 100 mg/L influent TSS concentration, the average X values for P1 and P2 are 1156 and 1095, respectively. Assuming that α_s and D_C are constant for the same filter, these observations demonstrate that collector collision efficiency, η, depends on particle size following the granular filtration theory that larger particles are more likely to collide with a collector via sedimentation and interception mechanisms.

Table 9. X values from Equation 5 computed using initial concentration reductions C, for
each test.

TSS Conc. (mg/L)	PSD	Flow rate (mL/s)	Filter type	ψ (s^{-1})	C_0 (mg/L)	C (mg/L)	ε	t (m)	X (m^{-1})
200	P1	6	1	1.2	197	132	0.87	0.0023	929
			1	1.2	199	131	0.87	0.0023	934
			2	0.8	194	103	0.86	0.003	1001
			3	0.54	185	65	0.86	0.0032	1553
		3	1	1.2	197	47	0.87	0.0023	3208
			2	0.8	227	75	0.86	0.003	1765
	P2	6	1	1.2	200	126	0.87	0.0023	1032
			1	1.2	190	125	0.87	0.0023	936
			2	0.8	201	113	0.86	0.003	917
			3	0.54	198	103	0.86	0.0032	968
	P3	6	2	0.8	195	110	0.86	0.003	920
			3	0.54	174	108	0.86	0.0032	716
100	P1	6	2	0.8	94	50	0.86	0.003	1003
			2	0.8	86	54	0.86	0.003	727
			3	0.54	97	46	0.86	0.0032	1089
			3	0.54	97	29	0.86	0.0032	1806
	P2	6	2	0.8	101	53	0.86	0.003	1030
			3	0.54	102	47	0.86	0.0032	1161

HYDRAULIC CONDUCTIVITY

Several hydraulic conductivity values were calculated for each test and compiled into one value per test by taking an average of the stabilized measures (with standard deviation of 25% or less). Figure 26 shows each stabilized value of hydraulic conductivity as a function of the total solids captured by each filter using particle size distribution P1. For all three filters, the hydraulic conductivity values decrease with increasing solids captured after the brief ripening period occurs. Each data set in Figure 26 was fitted by a power model after the ripening period ended. The R^2 values, which are given in the plot, indicate that the power model fits NW3 data best, followed by NW2 data, then NW1. The hydraulic conductivity values are generally highest for the filter with the largest permittivity, NW1 and lowest for the filter with the smallest permittivity, NW3.

Similar to P1 results, the hydraulic conductivity values for NW2 and NW3 filters loaded with particles from particle size distributions P2 and P3 could also be fitted by a power model (Figures 27 and 28). The NW1 filter never passed a priming period and therefore, the hydraulic conductivity values never dropped significantly below the clean filter value for PSD P2. The R^2 values indicate that the power model fits NW3 data best for P2, but NW2 best for P3. Once again, the hydraulic conductivity values are consistently higher for the filter with the larger permittivity (NW2) and lower for the filter with the smaller permittivity (NW3) for P2. The hydraulic conductivity values appear to be higher for NW3 than NW2 when loaded with P3 particles. However, from Figure 28, one can see that the hydraulic conductivity values are very similar. Statistical analysis proves that the stabilized hydraulic conductivity values for NW2 are equal to the stabilized hydraulic conductivity values for NW3 using a 2-tailed t-test on the values for

72

either 1% or 5% level of significance. Additionally, the total solids captured by the filters at the clogging point differ by less than 4% (3.883 kg/m^2 for NW2, 4.025 kg/m^2 for NW3). Therefore, the hydraulic conductivity values of NW3 are equal to the hydraulic conductivity values of NW2 when loaded with P3 particles.

The hydraulic conductivity values calculated for column tests performed with a lower influent flow rate (3 mL/s) exhibited similar behavior as previous tests when plotted as a function of solids captured in and on the filters (Figure 29). Each set of values could be fitted by a power model with coefficients of determination of 0.57 and 0.98 for NW1 and NW2, respectively. Once again, the filter with the larger permittivity, NW1, had larger hydraulic conductivity values throughout testing, as seen in Figure 29.

Hydraulic conductivity values calculated for column tests performed with lower influent TSS concentration (100 mg/L) and particle size distribution P1 also exhibited the same behavior as previous tests when plotted as a function of total solids captured by the filters (Figure 30). Three of the four sets of data in Figure 30 could be fitted well by a power function. The one NW3 values which were not fitted well by a power function (R^2 equal to 0.35) were likely inaccurate values due to a laboratory accident involving the filter test column. The accident likely caused the filter cake to break up completely, and the higher than expected hydraulic conductivity values for this test set were likely a result of the inability of the cake to reform properly. The other three sets of data in Figure 30 follow the same trends as previous tests, where the filter with the lower permittivity, NW2 in this case, had higher hydraulic conductivity values than the other filter, NW3, and the hydraulic conductivity values could be fitted well by a power function with R^2 values of 0.62 and 0.78 for the NW2 data sets and 0.73 for the successful NW3 data set.

73

Figure 31 shows the hydraulic conductivity values for the tests performed with a lower influent TSS concentration (100 mg/L) and particle size distribution P2. For these test conditions, the hydraulic conductivity values appear to be higher for NW3 than NW2. From Figure 31, one can observe that the final hydraulic conductivity values for the filters appear to be very similar, and statistical analysis proves that the stabilized hydraulic conductivity values for NW2 are equal to the stabilized hydraulic conductivity values for NW3 using a 2-tailed t-test on the values for either 1% or 5% level of significance. However, unlike in the earlier tests with PSD P3, the total solids captured by the filters at the clogging point differ by more than 20% (4.019 kg/m^2 for NW2, 5.183 kg/m^2 for NW3). As discussed in the TOTAL SOLIDS CAPTURED section, this result may be an indication that permittivity is not the only important geotextile parameter affecting hydraulic conductivity and particle capture. The thickness of geotextile may play a large role as well. The greater thickness of NW3 would allow more particles to build up within the thickness before forming a filter cake which causes clogging to occur, thus contributing to a larger total mass of solids captured at the clogging point.

Figure 32 shows the final hydraulic conductivity of the filters as a function of their initial permittivity. From this figure, it can be concluded that as the permittivity of a geotextile increases, the hydraulic conductivity of the filter throughout its lifespan increases.

The behavior of hydraulic capacity as a function of solids loading noted here for the geosynthetic filters has been similarly observed in other media-based stormwater filtration systems. Urbonas (1999) stated that the flow velocity through a natural media, such as a sand filter, is directly impacted by the amount of sediment accumulated on the

74

filter's surface. This relationship was described in the INTRODUCTION /

BACKGROUND section by Equation 3.

Comparing the flow velocities of this study with those of mixed-media filters is useful for determining whether or not a geotextile filter could perform as well as current stormwater treatment systems such as sand filters and mixed-media filters, which consist of combinations of sand, peat moss, activated carbon, compost, etc. (Clark and Pitt 2009). However, the effluent flow velocities from the six tests discussed in this study cannot be fitted by a power model because they were not run as constant-head tests like those performed in the Clark and Pitt (2009) study. Instead, for simplicity, the current study focus is on the behavior of hydraulic conductivity throughout the lifespan of a filter. As noted, power equations for hydraulic conductivity similar to Equation 3 are given in Figures 26-31. Table 10 gives the r and x values for mixed-media filters in Clark and Pitt (2009) and for the hydraulic conductivity equations in this study. While both sets of r values vary widely (1550-6.3×10^{13}, Clark and Pitt 2009; 5.7-2.0×10^{7}, this study), the values of r and x for this study are generally within the range of values from the previous studies. Although effluent flow rate and hydraulic conductivity are different parameters (and a geotextile filter is not a mixed-media filter), the similarity in r and x values in Table 10 could be an indicator of similar hydraulic behavior between geotextile filters and mixed-media filters. Additionally, there is a clear trend in r and x values for the geotextile filters for the 0.2 g/L tests; as AOS and permittivity decrease, both r and x increase. This indicates that AOS and permittivity could be important parameters for modeling hydraulic conductivity of geotextile filters as they are loaded with suspended solids.

Le Coq (1996) developed a power model that described the increase of head loss through a mineral fiber filter as a function of clogging by oil. Faure et al. (2005) applied this model, a power model describing the pressure head of a filter as a function of cumulative solids loading, to empirical laboratory data on loading a nonwoven geotextile with suspended solids. Empirical and theoretical development of a model describing the hydraulic conductivity of a geotextile filter as a function of solids loading allows assessment of the lifespan of a filter with knowledge of only the approximate influent TSS concentrations to the system. Further discussion on modeling hydraulic conductivity can be found in Chapter V.

Table 10. Power model parameters for flow through granular and geotextile filters where m_c is the cumulative mass of solids loaded to the filter and m is the cumulative mass of solids captured by the filter. Units of m/A are g/m^2. Units of v and K are m/day.

Influent soil concentration	Media/filter type	r	x
		From Clark and Pitt (2009) for $v = r (m_c/A)^{-x}$	
4 g/L	Sand	44500	1.02
	Carbon sand	14800	0.77
	Peat sand	2000	0.71
	Compost sand	1.6×10^{13}	4.09
1.5 g/L	Sand	1550	0.227
	Carbon sand	6.3×10^{13}	5.17
	Peat sand	5100	0.405
	Compost sand	1.6×10^{13}	4.09
		From this study for $K = r (m/A)^{-x}$	
0.2 g/L	1.P1	311	0.603
		21	0.368
	2.P1	10237	1.22
	3.P1	748768	1.83
	1.P2	-	-
	2.P2	2×10^7	2.23
	3.P2	2×10^7	2.49
	2.P3	1653	1.065
	3.P3	3094	1.124
	1.P1 (3)	377	0.779
	2.P1 (3)	1003	1.022
0.1 g/L	2.P1	7.6	0.27
		126	0.612
	3.P1	5.7	0.146
		79	0.589
	2.P2	3135	1.11
	3.P2	2787	1.066
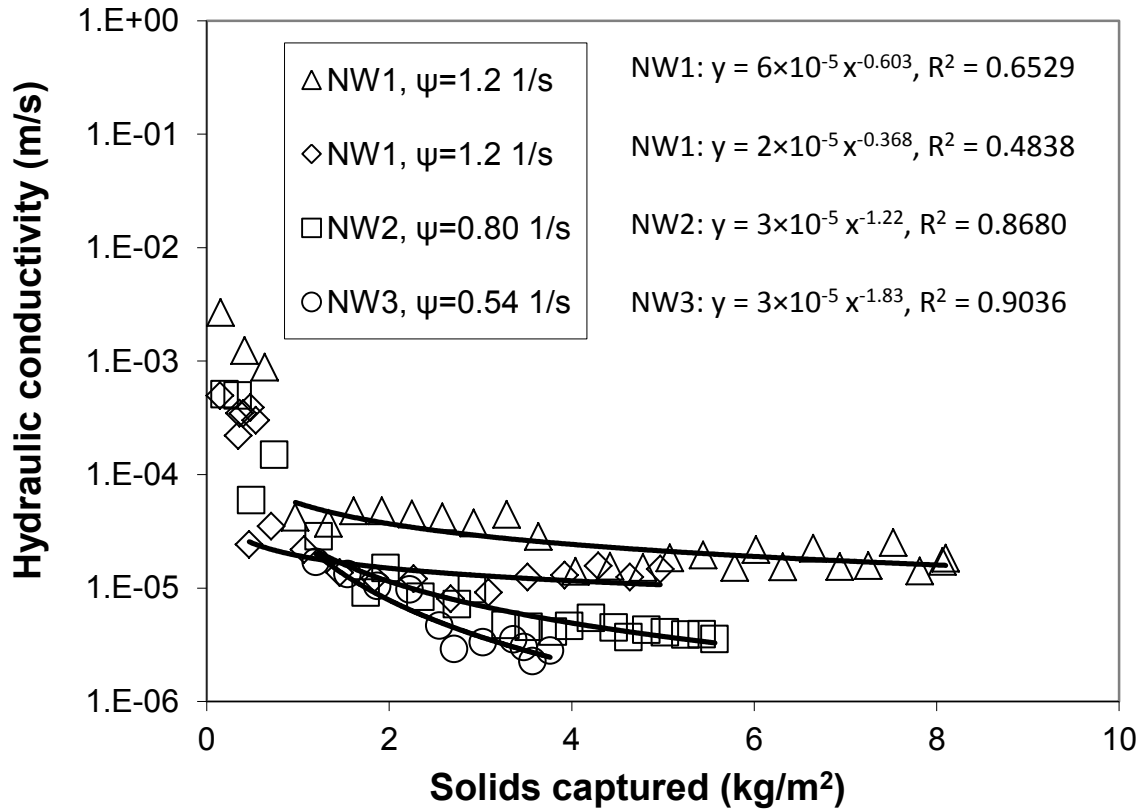
Figure 26. Hydraulic conductivity of geotextile and captured soil system as a function of the cumulative solids captured in and on the filter for tests conducted with PSD P1 at 200 mg/L influent TSS concentration and 6 mL/s influent flow rate.
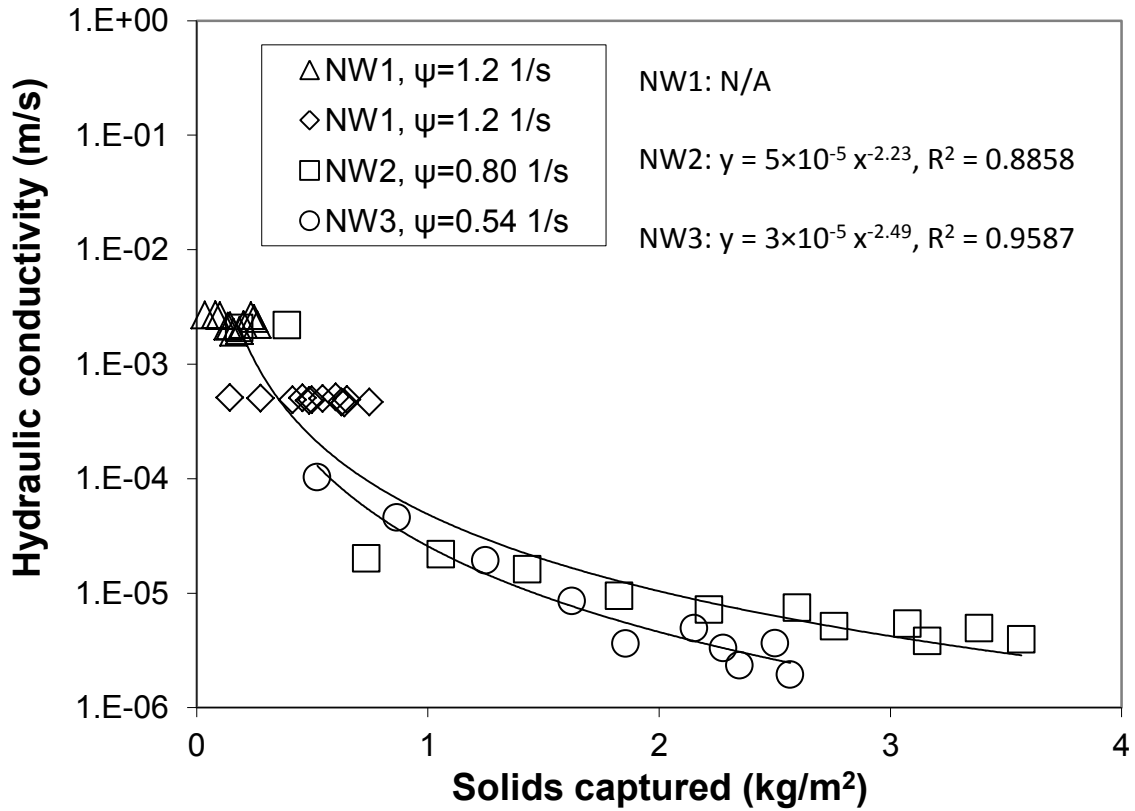
Figure 27. Hydraulic conductivity of geotextile and captured soil system as a function of the cumulative solids captured in and on the filter for tests conducted with PSD P2 at 200 mg/L influent TSS concentration and 6 mL/s influent flow rate.
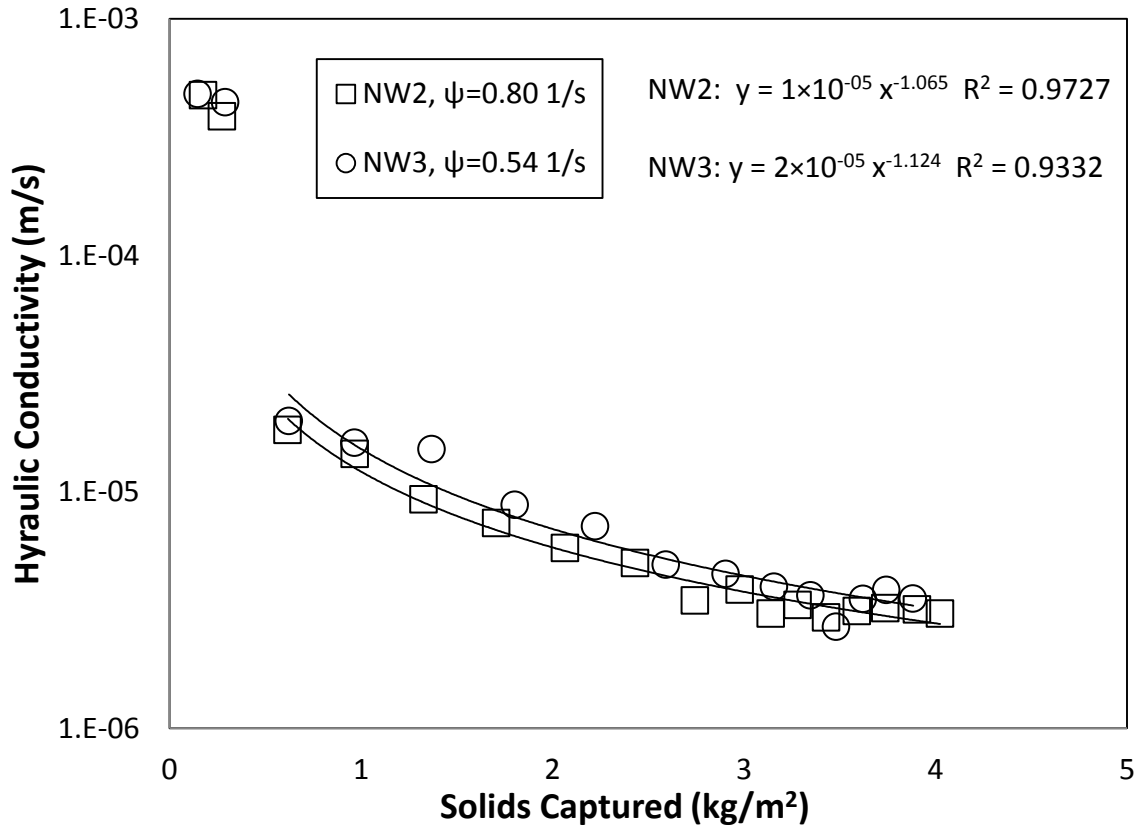
Figure 28. Hydraulic conductivity of geotextile and captured soil system as a function of the cumulative solids captured in and on the filter for tests conducted with PSD P3 at 200 mg/L influent TSS concentration and 6 mL/s influent flow rate.
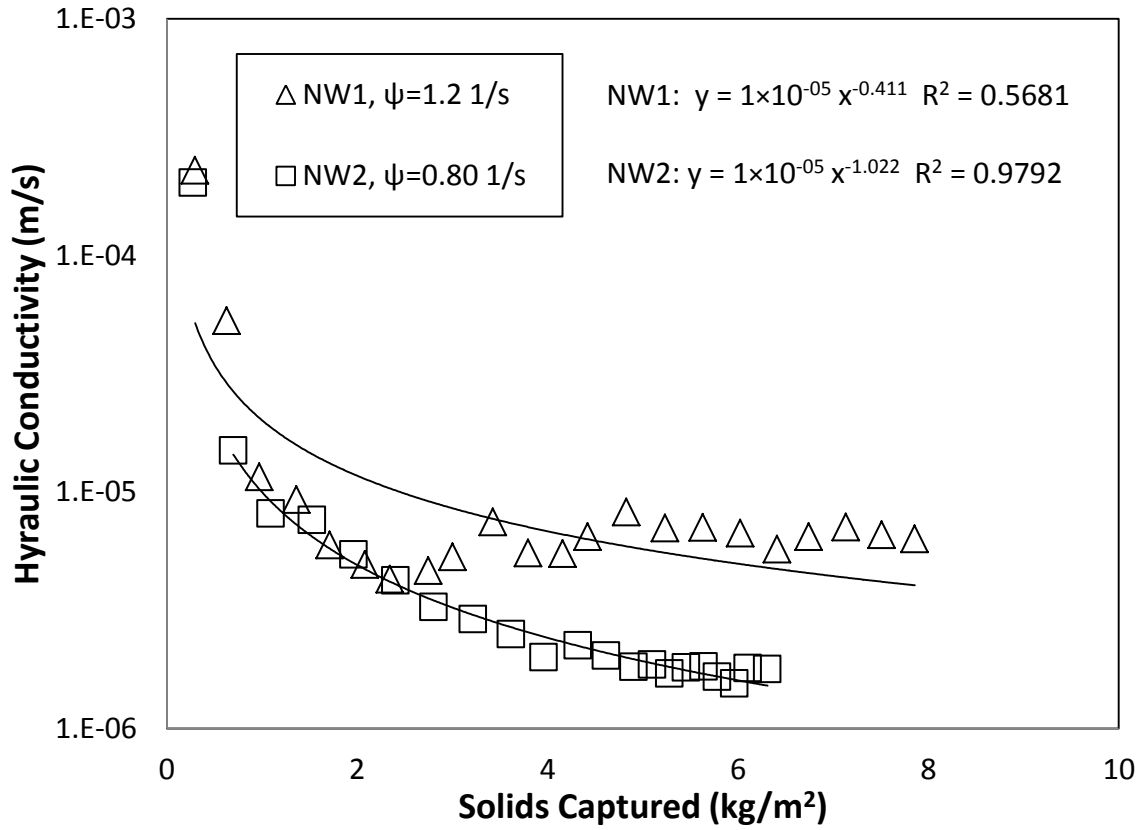
Figure 29. Hydraulic conductivity of geotextile and captured soil system as a function of the cumulative solids captured in and on the filter for tests conducted with PSD P1 at 200 mg/L influent TSS concentration and 3 mL/s influent flow rate.
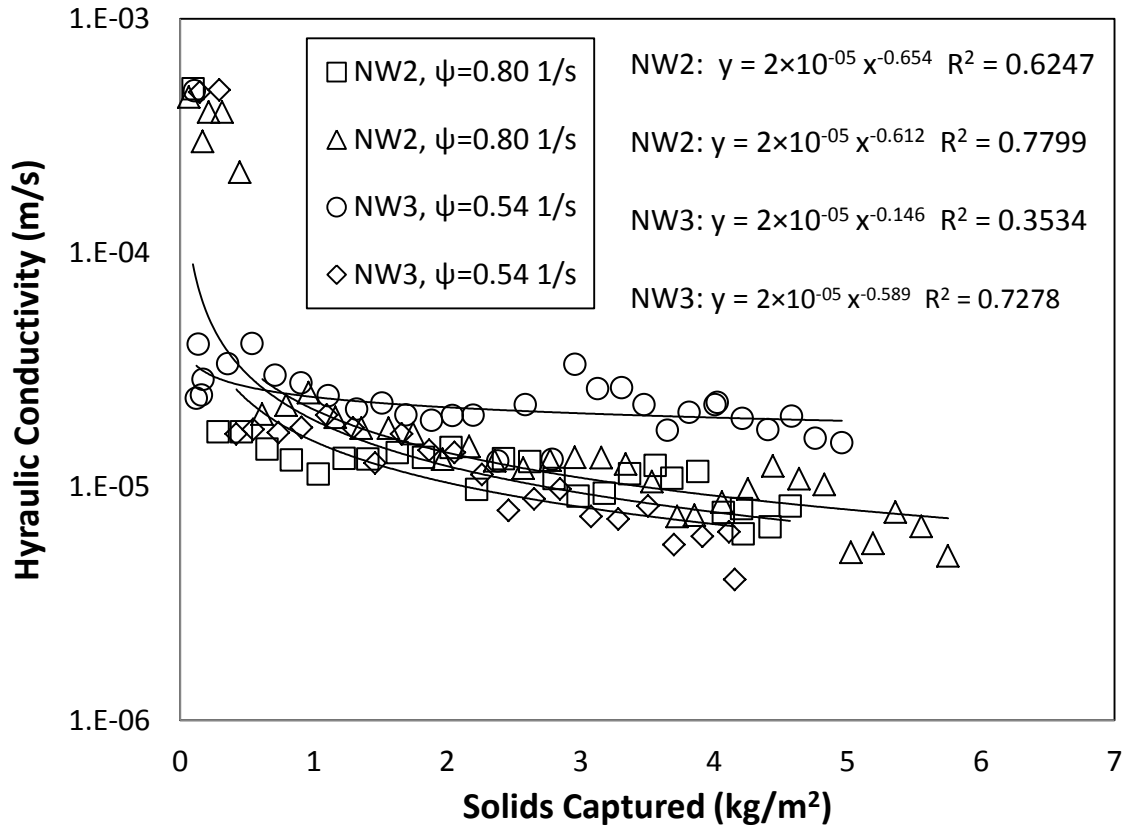
Figure 30. Hydraulic conductivity of geotextile and captured soil system as a function of the cumulative solids captured in and on the filter for tests conducted with PSD P1 at 100 mg/L influent TSS concentration and 6 mL/s influent flow rate.
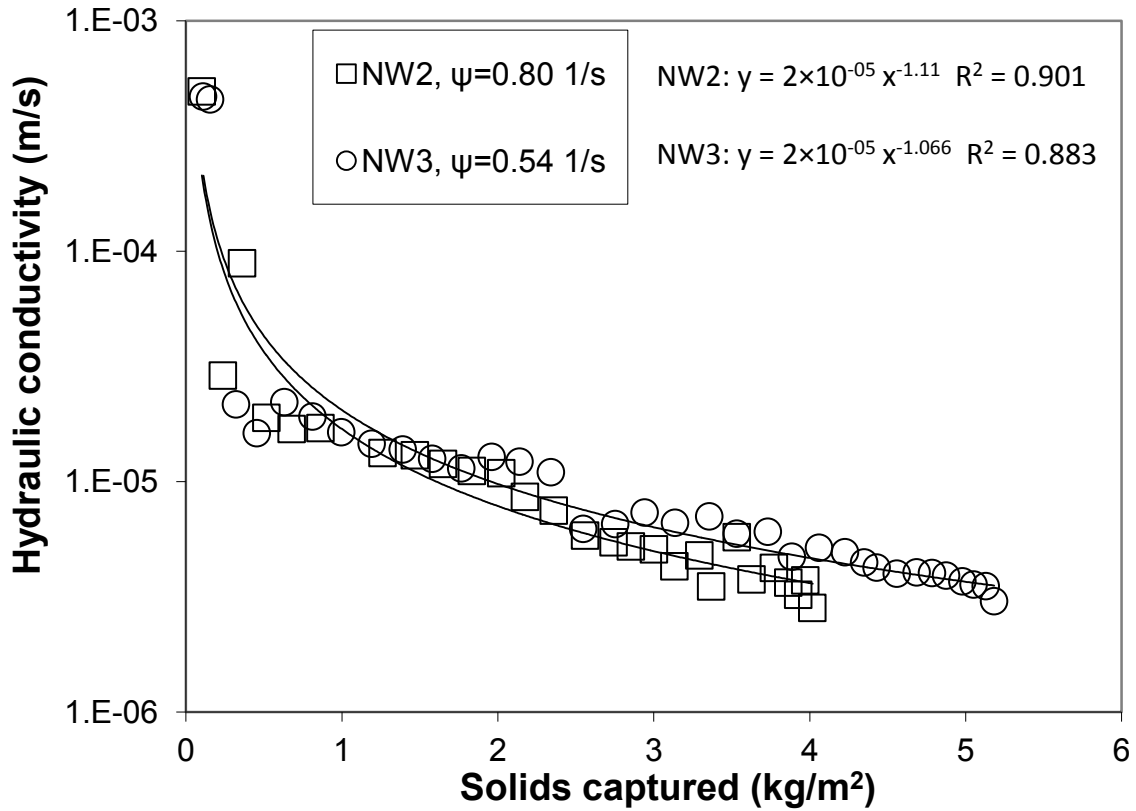
Figure 31. Hydraulic conductivity of geotextile and captured soil system as a function of

the cumulative solids captured in and on the filter for tests conducted with PSD P2 at 100

mg/L influent TSS concentration and 6 mL/s influent flow rate.
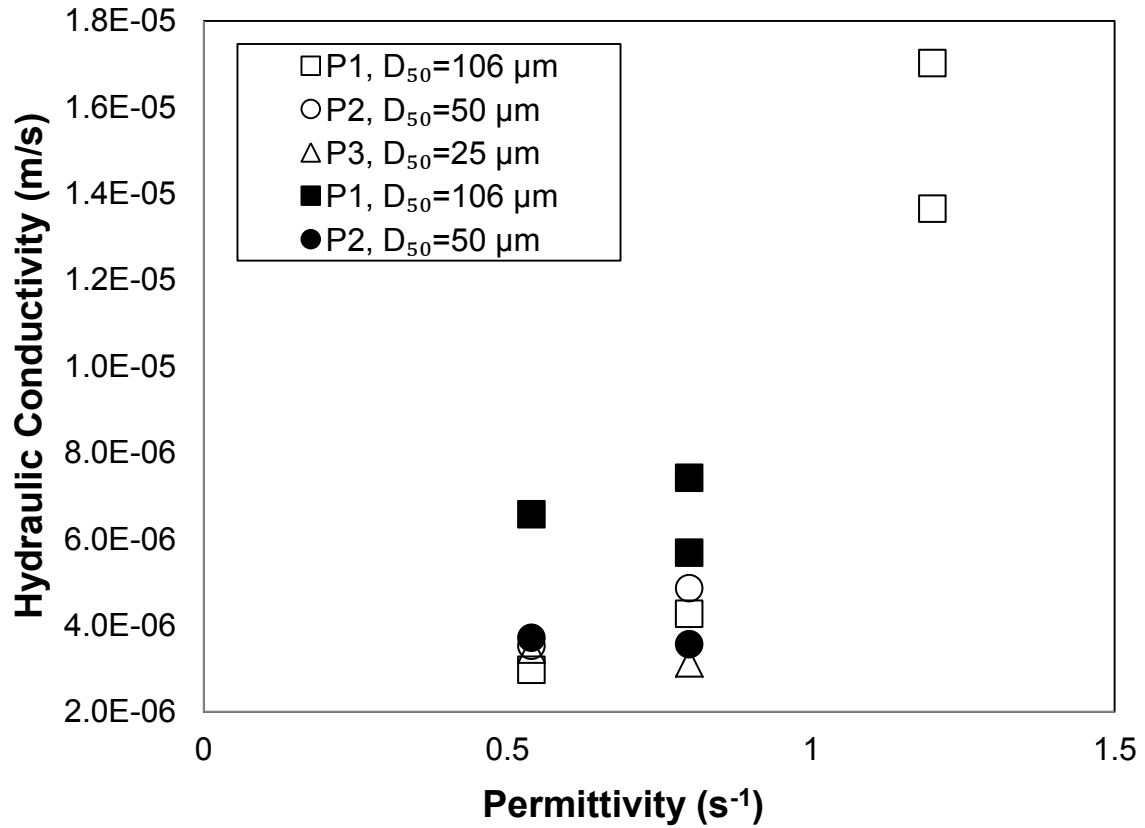
Figure 32. Stabilized hydraulic conductivity values for tests nearing the clogging point of filters as a function of initial permittivity values of the filters. Open symbols indicate tests run with influent TSS concentration of 200 mg/L. Closed symbols indicate tests run with influent TSS concentration of 100 mg/L.

CONCLUSIONS

Design parameters for geotextile filtration of urban stormwater runoff must address the phenomena discussed in the TSS removal results of this study. First, the permittivity played a greater role in affecting TSS removal than the AOS because NW2 and NW3 had the same AOS, different permittivities, and different TSS removal. This indicates that knowing one pore size (such as AOS) is not enough to determine the capability of a geotextile to retain TSS. Using permittivity or more than one geotextile pore size should provide greater accuracy in predicting the right geotextile for the need. Also, the particle size distribution played a large role in affecting TSS removal. In general, the coarser distribution provided a more open and porous cake, allowing more solids to be captured while allowing water to pass through the filter. This indicates that knowing one particle size, like D_{50}, of a soil is not to enough in order to choose the appropriate geotextile to retain that soil. A range of particle sizes or at least more than one size, would enhance the design parameter selection for geotextiles in stormwater treatment. These parameters will be discussed in greater detail in a later section.

In the laboratory tests performed for this study, NW2 (0.8 s^{-1}) was the most successful. Both NW2 and NW3 reduced TSS concentrations to below the target concentration of 30 mg/L and had large removal efficiencies. However, NW2 experienced larger total solids loadings at clogging and maintained larger hydraulic conductivity values overall than NW3. Therefore, NW2 is more successful than NW3 at TSS removal from stormwater runoff because the laboratory column studies predict that it will last for a longer period of time (i.e., larger mass of solids loading) than NW3.

Neither influent TSS concentration nor influent flow rate was determined to greatly affect the amount of suspended solids captured by the filter per solids loading. One effect of influent TSS concentration was noted. The mass of solids loaded to the filter for the lower concentration tests at the end of the ripening period was about half that of the higher concentration tests. While this did not significantly impact the total amount of solids captured by the filters, it will play a role in modeling the hydraulic conductivity of the filter throughout the lifespan of the filter, which will be discussed later in this study.

Hydraulic conductivity of the geotextile filters decreased for increasing solids capture by the filter. In general, the filters with larger permittivity values maintained higher hydraulic conductivity values for equivalent cumulative solids captured and thus had longer lifespans before clogging occurred. The hydraulic conductivity values could be fitted well by a power model for nearly all filter tests in which a ripening period occurred. Additionally the hydraulic conductivity values were consistently larger for the tests with the larger distribution of particle sizes, P1, due to the expected formation of a more permeable graded filter zone.

The successful retention of suspended solids and maintenance of adequate drainage of the geotextile filters indicates that a geotextile filter may be an effective new best management practice (BMP). A BMP is defined as "a device, practice, or method for removing, reducing, retarding, or preventing targeted storm water runoff quantity, constituents, pollutants, and contaminants from reaching receiving waters" (Strecker et al., 2001). Development of new BMPs and continued analysis and improvement of current BMPs is very important because the US Environmental Protection Agency (EPA) continues to make regulatory improvements to strengthen its stormwater program. A

new rule to strengthen the national stormwater program should be proposed by the EPA by June 10, 2013 and a final action regarding the rule should be completed by December 10, 2014. New BMPs may be needed to meet the higher regulatory standards set by the EPA (EPA, 2012).

Several items should be addressed in considering practical implications of this study. First, particle sizes in urban highway runoff can vary widely, from a diameter of 1 μm to over 1 cm (Sansalone et al. 1998). The particle size distribution in runoff depends on the characteristics of the runoff surface and its surroundings. The particle size distributions in this study were chosen not only to resemble those from urban highway runoff (as seen in literature), but also to mimic the distribution of particles that a typical underground sand filter would experience after the runoff passes through an underground detention basin. This study focused on particles with a diameter of 180 μm or less because larger particles are easily removed via sedimentation in a detention basin (Li et al. 2006). Second, the TSS concentrations in urban highway runoff can vary greatly depending on location, season, and amount of traffic. For simplicity, two influent TSS concentrations for this study were chosen by averaging typical EMCs of urban highway runoff discussed in literature. Third, influent flow rates will not remain constant in practical applications. The influent flow rates were chosen based on average flow rates per area of filter for typical rainfall events in the eastern United States. Finally, the laboratory tests of this study do not address the potential for biological growth on the filter. While nonwoven polypropylene geotextiles are inert to biological degradation, biological growth can occur in and on the material, particularly when the geotextile is exposed to liquids with high organic content. Korkut et al. (2006) exposed nonwoven

geotextile baffles to wastewater from a combined sewer system and demonstrated that geotextiles with attached biomass not only capture TSS, but also reduce the biochemical oxygen demand (BOD) and ammonia concentration of the influent. Additionally, biological growth reduced the hydraulic conductivity of the geotextile.

Any biofilm growth on the stormwater geotextile could result in increased pollutant retention and reduction and decreased hydraulic conductivity. Maintenance schedules would need to consider any growth of biomass on the geotextile.

Chapter III: FILTRATION CRITERIA FOR GEOTEXTILES

INTRODUCTION / BACKGROUND

Several existing criteria have been proposed for selecting a geotextile filter in geotechnical applications. These criteria typically are expressed in terms of ratios of a characteristic geotextile pore size to a characteristic soil grain size. They give limiting values for such a ratio so that the filter is not clogged and also the filtered materials are retained. This chapter intends to evaluate the applicability of current filter criteria to stormwater treatment and establish new criteria that can be used to choose the appropriate geotextile for capture of suspended solids in urban stormwater runoff.

PROPERTIES OF GEOTEXTILES

Geosynthetics are polymeric man-made materials used to facilitate infrastructure and environmental projects. These materials are currently used in a variety of applications for reinforcement, separation, filtration, and drainage of soils, and containment of liquids and gases. The most commonly used form of geosynthetic is geotextile, a material of synthetic fibers either woven or matted together. Geotextiles are porous to liquid flow not only across their plane, but also within their thickness. This porosity can vary greatly among different types of geotextiles (Koerner 2005).

Permeability is an important characteristic of geotextiles. Cross-plane permeability refers to liquid flow perpendicular to the plane of the material. Because the thickness varies widely between different types of geotextiles, permittivity is often used instead of permeability. Permittivity, ψ, is defined as,

89

$$\psi = \frac{k}{t} \tag{6}$$

where k is the cross-plane permeability and t is the thickness of the material (Koerner 2005).

In the case of in-plane flow through geosynthetics, often referred to as drainage, the most essential property that affects the in-plane flow is transmissivity. Transmissivity is the amount of water flow within the plane of a geotextile under a certain hydraulic gradient.

$$\theta = k_{in}t \tag{7}$$

where θ is defined as the transmissivity, and k_{in} is the in-plane permeability coefficient (Koerner 2005).

Another important characteristic of geotextiles is apparent opening size (AOS), which corresponds to the pore diameter that 95% of the pores in the geotextile have diameters smaller than this particular size (i.e., O_{95}). In the United States, AOS (or O_{95}) is obtained using two dry-sieving tests whereas this parameter is obtained by wet or hydrodynamic sieving test in Europe and Canada, and is referred to as filtration opening size (FOS) (Koerner 2005).

The minimum porosity of nonwoven geotextiles is also important to determine their clogging potential in filtration applications. Porosity is the ratio of void volume to total volume and is related to the ability of liquid to flow through the geotextile, but is rarely measured directly. Therefore, the porosity is calculated from geotextile properties using the following formula:

$$\varepsilon = 1 - \frac{w}{\rho_f t} \tag{8}$$

where ε is porosity, w is mass per unit area, and ρ_f is the density of the fibers. Previous research supported the use of Eq. 8 and indicated that geotextile porosity decreases with increasing mass per unit area (Koerner 2005).

RETENTION AND CLOGGING CRITERIA

Three criteria have been established for proper selection of a geotextile filter: 1) retention criterion, 2) clogging criterion, and 3) hydraulic conductivity criterion. The geotextile is also expected to meet the durability and survivability requirements, meaning that the material must be able to perform properly throughout the entire lifetime of the designated project. The hydraulic conductivity criterion requires that the geotextile and bridging network formed on the geotextile surface must have a hydraulic conductivity that is greater than or equal to the hydraulic conductivity of the surrounding soil.

Geotextile filter criteria typically are expressed in terms of ratios of a characteristic geotextile pore size to a characteristic soil grain size. They basically give limiting values for such a ratio so that the filter is not clogged and also the filtered materials are retained. These ratios were proposed based on analogies with earthen (granular) filters in early days of geotextiles. Later on, they were based on laboratory filtration performance tests, i.e., column tests. Some of the existing criteria have also been verified by field observations and usually include certain safety factors incorporated to account for material variability. In summary, they all are empirical criteria based on tests of various soils with various geotextiles. The existing retention and clogging criteria use ratios of a characteristic geotextile pore size to a characteristic soil grain size. The general formula of the criteria can be written as follows:

$$\frac{O_x}{D_x} < B_R$$

$$\frac{O_y}{D_y} > B_C \tag{9}$$

where B_R and B_C are constants, O_x and O_y are the characteristic retention and clogging pore sizes, and D_x and D_y are the characteristic retention and clogging soil grain sizes, respectively (Aydilek 2011).

A good filter is expected to retain a significant portion of solid particles and therefore, the largest pore size of the geotextile filter is expected to be smaller than the largest soil grains. Despite the fact that few researchers promote O_{100} as the largest pore size, accurate determination of this size is not possible. Therefore, sizes between O_{85} to O_{95} are generally used for this purpose. This is logical; however, selection of this size is arbitrary in most cases. Most of the researchers prefer to include O_{95} (AOS) in their criteria since it is readily available from the manufacturers' reports. As larger particles are captured at the surface of the filter, they aid in the filtration of smaller particles by forming smaller openings than the geotextile pores, which is referred to as bridging. Thus, existing studies showed that relatively larger grain sizes control retention; D_x ranges from D_{50} to D_{85} for geotextiles, and a conservative grain size of D_{85} has been used in several criteria. The term B_R in Equation 9 is referred to as the retention ratio and is usually multiplied by a factor of safety, ranging typically from 1.5 to 7.5 in various criteria proposed in the literature (Koerner 2005).

The opening size of a geotextile filter is important for the retention criterion because characteristic retention pore sizes must be large enough to allow water to pass freely, but small enough to retain most particles in the soil. If the larger opening sizes of

the material are larger than the smaller particles present, then the loss of fine particles, known as piping, may occur (Kutay and Aydilek 2005). A piping rate of 2,500 g/m^2 or less has been widely employed as the rate at which the stability of soil is unaffected for both granular and geotextile filters (Lafleur et al. 1989; Fischer 1994). It should be noted that it is imperative to allow some of soil fines pass through the geotextile for a bridging formation to occur and the geotextile to not get clogged, although this may be problematic from a water quality perspective.

The second important function expected from a good filter is that it has pore sizes large enough so it does not clog during filtration. In order for the geotextile to fulfill the clogging criteria the largest pore openings of the geotextile must not be smaller than the smallest particles in the soil. If this is the case, blinding, blocking or clogging of the geotextile can occur. Blinding occurs when fine soil particles accumulate on the side of the nonwoven geotextile facing the incoming flow. This occurs when all of the soil particles are larger than the largest pore opening in the geotextile (Aydilek 2011). Blocking happens in woven geotextiles when large particles locate themselves at the pore openings on the side of the geotextile nearest the incoming flow. It is typically a result of low-concentration suspensions or little contact between the soil and the geotextile (Rollin and Lombard 1988). Clogging occurs when particles lodge themselves between the fibers of nonwoven geotextiles, resulting in a majority of the pores becoming closed. In geotechnical applications, blinding, blocking or clogging must be avoided by choosing a geotextile with the largest pore sizes being larger than the smallest particles. However, since it is unknown whether the geotechnical clogging criteria are applicable to stormwater filtration, this caveat may not be applicable to this study.

Despite some laboratory tests demonstrating that smaller pore sizes (i.e., O_{40} - O_{50}) can be the controlling size for clogging, existing clogging criteria typically use the largest pore opening size of the geotextile (O_{95}) due to its availability. Hydraulic conductivity of soils is controlled by the size of its fine particles, i.e., D_{10} or D_{15} (Cedergren 1989). Therefore, smaller soil particle sizes have a significant effect on the clogging performance, and are included in the existing clogging criteria. The term B_C in Equation 9 is referred to as the clogging ratio and is occasionally multiplied by a factor of safety ranging from 0.2 to 3.

Many specific retention and clogging criteria have been developed for geotextile filtration. These criteria are similar to the granular soil filter criteria and have been established by either converting the grain size in a granular filter to the opening size of a geotextile or developing them from laboratory methods. A few of the geotextile clogging criteria use geotextile porosity as percent open area instead of pore size-to-grain size ratios. Table 3 lists several existing geotextile filter selection criteria chosen for use in selecting geotextiles in this research.

Table 3. Applicability of the existing geotextile filter selection criteria for stormwater filtration (Fischer et al. 1990). C_U (D_{60}/D_{10}) is approximately 12 and 35 for P1 and P2, respectively. Bold indicates those exceeding the minimum limit. Italic indicates values from a test which did not complete a ripening period during this study. O_{small} = AVERAGE(O_{10}, O_{20}, O_{30}). O_{large} = AVERAGE(O_{95}, O_{100}).

Criteria Type	Criteria	Reference	PSD1			PSD2			PSD3		
			NW1	NW2	NW3	NW1	NW2	NW3	NW1	NW2	NW3
Existing retention criteria	O_{50}/D_{50} <25-37	Rankilor, 1981	0.81	0.51	0.77	*1.71*	1.08	1.64	*3.43*	2.16	3.28
	O_{90}/D_{90} <1.8	Ogink (1975)	0.71	0.49	0.83	*1.27*	0.87	1.47	*1.31*	0.90	1.52
	O_{90}/D_{50} <2.5-4.5	Schober and Teindl (1979)	1.09	0.75	1.26	*2.31*	1.58	**2.68**	***4.62***	**3.16**	**5.36**
	O_{50}/D_{85} <1	Millar et al. (1980)	0.57	0.36	0.55	*0.98*	0.62	0.94	***1.04***	0.66	**1.00**
	O_{95}/D_{50} <(9-18)C_U	Giroud (1982)	1.15	0.83	1.37	*2.45*	1.76	2.90	*4.90*	3.52	5.80
	O_{95}/D_{85} <1-2	Holtz et al. (1998)	0.82	0.59	0.97	***1.40***	**1.01**	**1.66**	***1.49***	**1.07**	**1.77**
Existing clogging criteria	O_{95}/D_{15} >3	Holtz et al. (1998)	6.12	4.40	7.25	*15.3*	11.0	18.1	*31.0*	22.3	36.8
	Porosity >30-40%	Koerner (2005)	87	86	86	*87*	86	86	*87*	86	86
New Retention criteria	$(O_{95}/D_{95})/(O_{30}/D_{30})$ > 0.48	This study	0.53	0.60	0.68	***0.48***	0.54	0.62	***0.23***	**0.27**	**0.30**
	$(O_{95}/D_{60})/(O_{30}/D_{10})$ > 0.05	This study	0.15	0.17	0.20	***0.05***	0.06	0.07	***0.05***	0.06	0.07
	$(O_{large}/D_{60})/(O_{small}/D_{10})$ > 0.076	This study	0.219	0.237	0.285	***0.072***	0.078	0.094	***0.076***	0.083	0.099
	$(O_{large}/D_{95})/(O_{small}/D_{30})$ > 0.68	This study	0.75	0.81	0.98	***0.68***	0.73	0.88	***0.33***	**0.36**	**0.43**

APPLICABILITY OF EXISTING AND NEW CRITERIA

Generally the stormwater filtration ratios determined in this study are less than the given values set by the existing geotechnical filter selection criteria. The calculated ratios for the tests performed in this study are listed in Table 3. For the particle size distributions P1 and P2, 4 out of 48 values are not below the minimum value in the criteria range, but these values are within the range, indicating that the chosen geotextile can be an adequate choice for stormwater filtration. For example, the retention criterion set by Holtz et al. (1998) requires the O_{95}/D_{85} ratio to be less than 1-2 and the value for the 1.P2 test is 1.40. Therefore, this combination of geotextile and particle size distribution would either fail or meet the criterion depending on what specific value between 1 and 2 is chosen.

For the particle size distribution P3, 4 out of 24 values exceed the maximum value in the criteria range and another 4 exceed the minimum value in the criteria range. Additionally, the three tests with NW1 are within the retention criteria ranges set by geotextile literature for all of the PSD1 and PSD2 ratios and most of the PSD3 ratios, yet the results in this study indicate that this filter does not retain enough solids to reduce the effluent TSS concentration to the target concentration (as seen in Figures 5 and 7 and Table 11 in Chapter IV. Because the existing filtration criteria indicate success for a filter while the filter does not meet the target set for stormwater filtration, new criteria ratios may be more effective at selecting the appropriate geotextile for stormwater filtration.

The established criteria may not be appropriate for stormwater data because each ratio only incorporates one opening size and one particle diameter. A more effective criterion will compare a range of opening sizes with a range of particle sizes to better capture the distributions of both. For example, a ratio of O_{95}/D_{95} to O_{30}/D_{30} gives information about the larger as well as

smaller filter opening and particle sizes. This ratio ($\frac{O_{95}/D_{60}}{O_{30}/D_{10}}$), along with 3 other $\frac{O_x/D_y}{O_a/D_b}$

ratios, was selected (after several trials with various ratios) to accurately predict success for

stormwater filtration by geotextiles based on the results of this study.

The first criterion ratio determined by this study is $\frac{O_{95}/D_{60}}{O_{30}/D_{10}}$. Figure 33 shows the

percentage of solids captured as a function of the ratio $\frac{O_{95}/D_{60}}{O_{30}/D_{10}}$ calculated for all geotextile

column tests in this study. The ratio is appropriate for use in choosing a successful geotextile for

capturing suspended solids because at a ratio of 0.05 or lower, the filter did not complete a

ripening period and retained only 7-12% of the total solids loaded to the filter. Above a ratio of

0.05, all tests removed 64-94% of the total solids, with an average removal rate of 84%, which is

comparable to retention by a sand filter system (Barrett 2003).

The second criterion ratio determined by this study is $\frac{O_{large}/D_{60}}{O_{small}/D_{10}}$. Figure 34 shows the

percentage of solids captured as a function of the ratio $\frac{O_{large}/D_{60}}{O_{small}/D_{10}}$ calculated for all geotextile

column tests in this study. This ratio is also appropriate for use in choosing a successful

geotextile for capturing suspended solids because at a ratio of 0.076 or lower, the filter did not

complete a ripening period and retained only 7-12% of the total solids loaded to the filter.

Above a ratio of 0.076, all tests removed 64-94% of the total solids, with an average removal rate

of 84%.

The third criterion ratio determined by this study is $\dfrac{O_{95}/D_{95}}{O_{30}/D_{30}}$. Figure 35 shows the

percentage of solids captured as a function of the ratio $\dfrac{O_{95}/D_{95}}{O_{30}/D_{30}}$ calculated for the PSD P1 and

P2 tests in this study. This ratio is appropriate for these data sets because at a ratio of 0.48 or

lower, the filter did not complete a ripening period and was unsuccessful at retaining suspended

solids. At a ratio above 0.48, the filter did complete a ripening period and was able to retain a

large percentage of the total solids loaded (85% average).

The fourth and final criterion ratio determined by this study is $\dfrac{O_{l\arg e}/D_{95}}{O_{small}/D_{30}}$. Figure 36

shows the percentage of solids captured as a function of the ratio $\dfrac{O_{l\arg e}/D_{95}}{O_{small}/D_{30}}$ calculated for the

PSD P1 and P2 tests in this study. This ratio is appropriate for these data sets because at a ratio

of 0.68 or lower, the filter did not complete a ripening period and was unsuccessful at retaining

suspended solids. At a ratio above 0.68, the filter did complete a ripening period and was able to

retain a large percentage of the total solids loaded (85% average).

The third and fourth ratios, $\dfrac{O_{95}/D_{95}}{O_{30}/D_{30}}$ and $\dfrac{O_{l\arg e}/D_{95}}{O_{small}/D_{30}}$, have different critical values, less

than 0.48 and 0.68, respectively, for geotextile tests with particle size distribution P3. As seen in

Table 3, these ratios accurately predict filters that are successful at capturing suspended solids

for particle size distributions P1 and P2. However, these ratios inaccurately predict that NW2

and NW3 would not be successful at retaining suspended solids of particle size distribution P3,

when NW2 and NW3 were successful at retaining over 80% of the total solids loaded to them for

P3 (Figures 37 and 38; Table 11 in Chapter V). Despite the slight inaccuracy, these two ratios

are acceptable for use in stormwater management because they do not predict that a filter will be

successful at retaining solids when it is not; they may predict that a filter is unsuccessful at retaining solids when it actually is able to retain a large percentage of suspended solids. Therefore, the consequence is merely the possibility of excluding viable geotextiles in consideration of a geotextile filter for stormwater treatment. To eliminate the risk of excluding these geotextiles from consideration, a stipulation could be included that for particle size distributions with D_{50} of 25 μm or less, the criteria become $\frac{O_{95}/D_{95}}{O_{30}/D_{30}} > 0.23$ and $\frac{O_{large}/D_{95}}{O_{small}/D_{30}} > 0.33$.

In addition to using two particle sizes and two opening sizes in the new retention criteria, it may be beneficial to employ the complete particle size distribution in comparison with the entire opening size distribution of each filter (found using bubble point testing outlined in detail in Aydilek et al. (2007)). Figure 39 shows these distributions for each of the tests performed with all particle size distributions for this study. One significant conclusion drawn from Figure 39 is that the only test that did not capture at least 75% of the total suspended solids was 1.P2 in which the particle size was smaller than the opening size for the entire distributions. While no tests were performed with NW1 and PSD P3, it is assumed that NW1 would not capture at least 75% of the total suspended solids because P3 had the same range of particle sizes as P2, and like 1.P2, all particle sizes were smaller than the corresponding opening sizes for the entire distribution. However, NW3 had a similar distribution, but demonstrated good removal with P2 and P3. A relatively higher permittivity of NW1 ($\psi=1.2$ s^{-1}) must have contributed to the poor performance of this combination. The results suggest that while opening size distribution is important when determining how effective a filter will be at retaining solids, the filter permittivity plays a significant role in the performance as well. Using the laboratory results in this study, the two criteria could be changed to improve accuracy and incorporate permittivity. If

permittivity of the filter is 0.8 s^{-1} or less, the criteria become $\dfrac{O_{95}/D_{95}}{O_{30}/D_{30}} > 0.26$ and $\dfrac{O_{l\arg e}/D_{95}}{O_{small}/D_{30}} >$

0.35, but for permittivity greater than 0.8 s^{-1}, the criteria remain $\dfrac{O_{95}/D_{95}}{O_{30}/D_{30}} > 0.48$ and

$\dfrac{O_{l\arg e}/D_{95}}{O_{small}/D_{30}} > 0.68$. However, it is important to note that neither of the filters with permittivity

less than or equal to 0.8 s^{-1} were unable to retain a large percentage (i.e., greater than 75%) of

total suspended solids for any of the tests performed in this study.
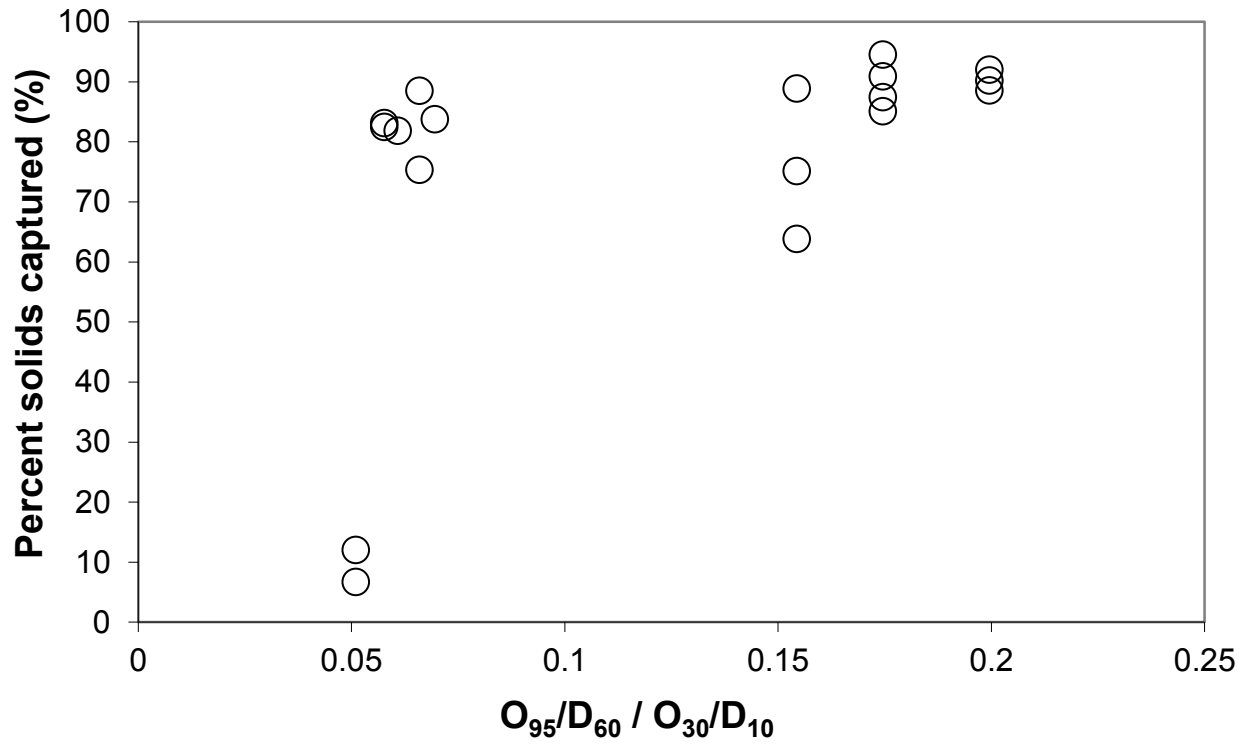
Figure 33. Plot of solids captured in and on the geotextile filter as a function of the ratio O_{95}/D_{60} to O_{30}/D_{10} for all tests.
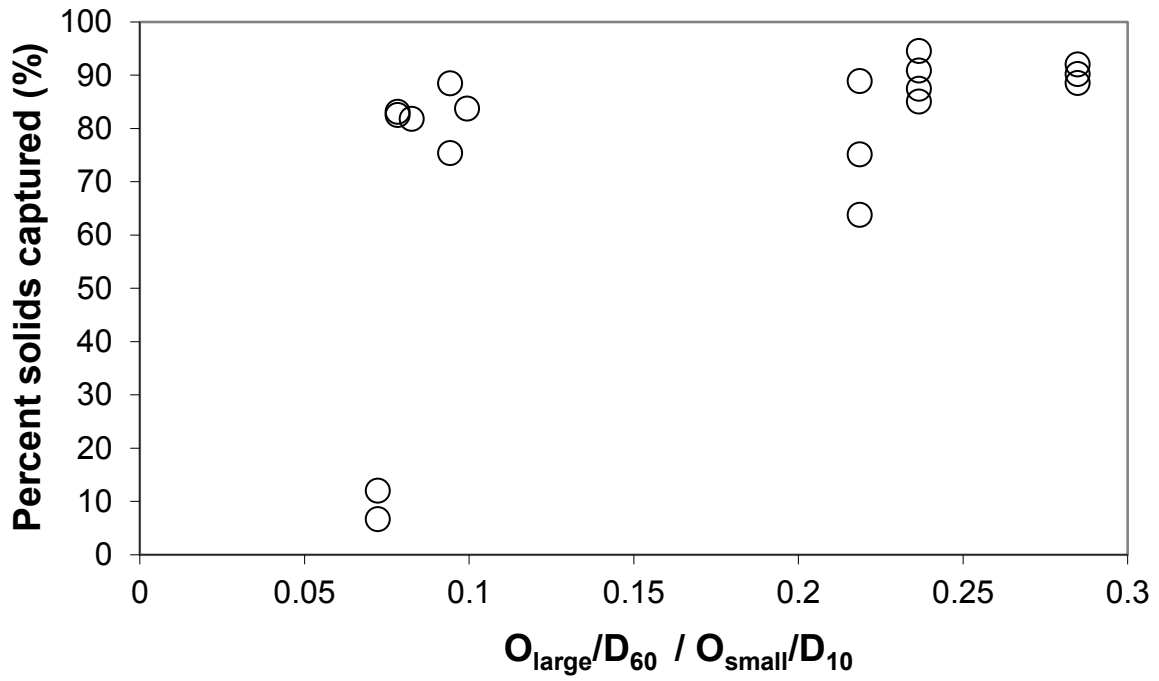
Figure 34. Plot of solids captured in and on the geotextile filter as a function of the ratio

O_{large}/D_{60} to O_{small}/D_{10} for all tests. $O_{small} = \text{AVERAGE}(O_{10}, O_{20}, O_{30})$. $O_{large} = \text{AVERAGE}(O_{95}, O_{100})$.
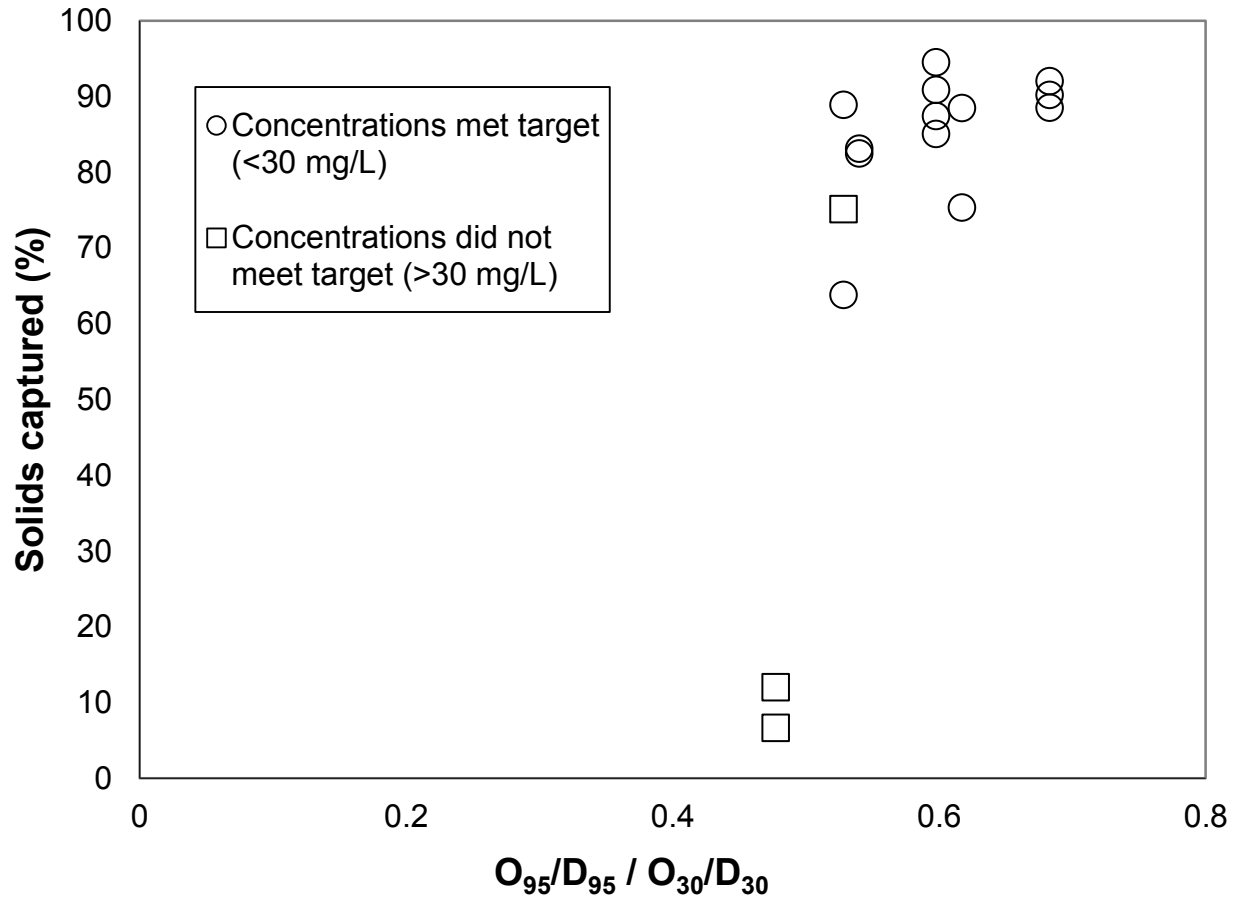
Figure 35. Plot of solids captured in and on the geotextile filter as a function of the ratio O_{95}/D_{95} to O_{30}/D_{30} for P1 and P2 tests.
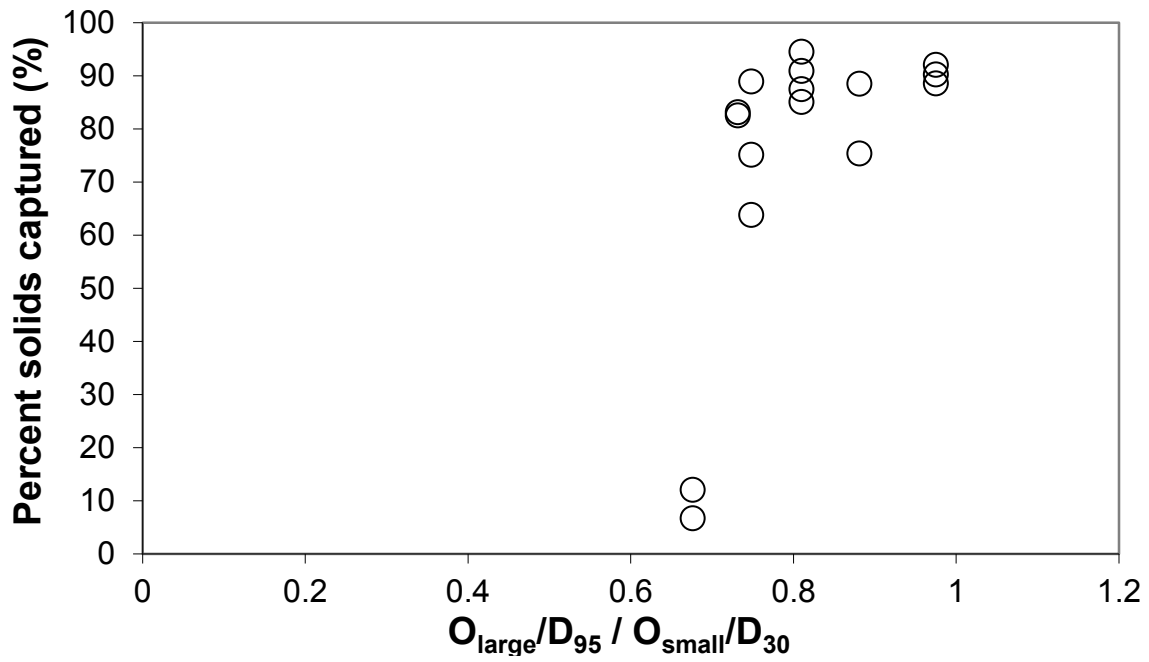
Figure 36. Plot of solids captured in and on the geotextile filter as a function of the ratio O_{large}/D_{95} to O_{small}/D_{30} for P1 and P2 tests. O_{small} = AVERAGE(O_{10}, O_{20}, O_{30}). O_{large} = AVERAGE(O_{95}, O_{100}).
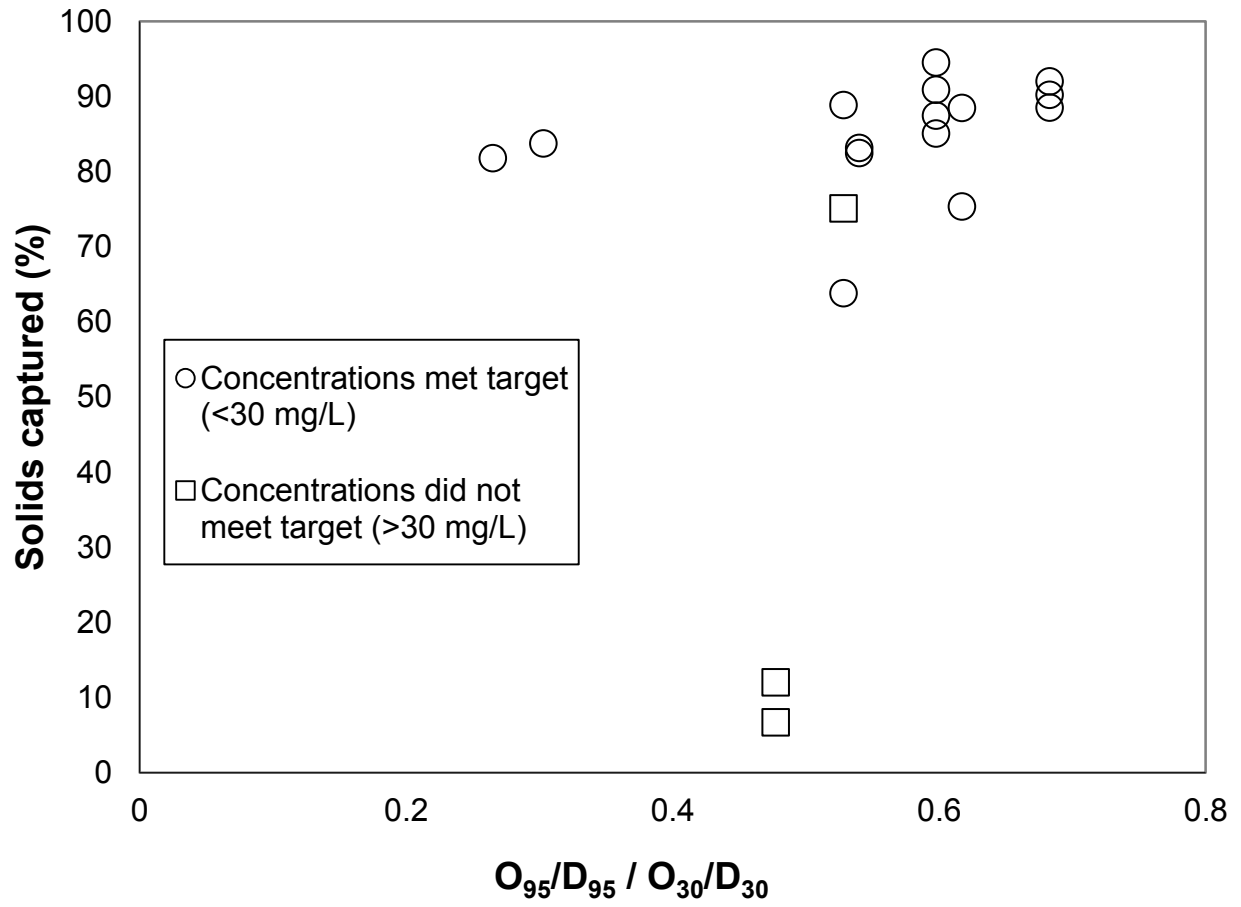
Figure 37. Plot of solids captured in and on the geotextile filter as a function of the ratio O_{95}/D_{95} to O_{30}/D_{30} for all tests.
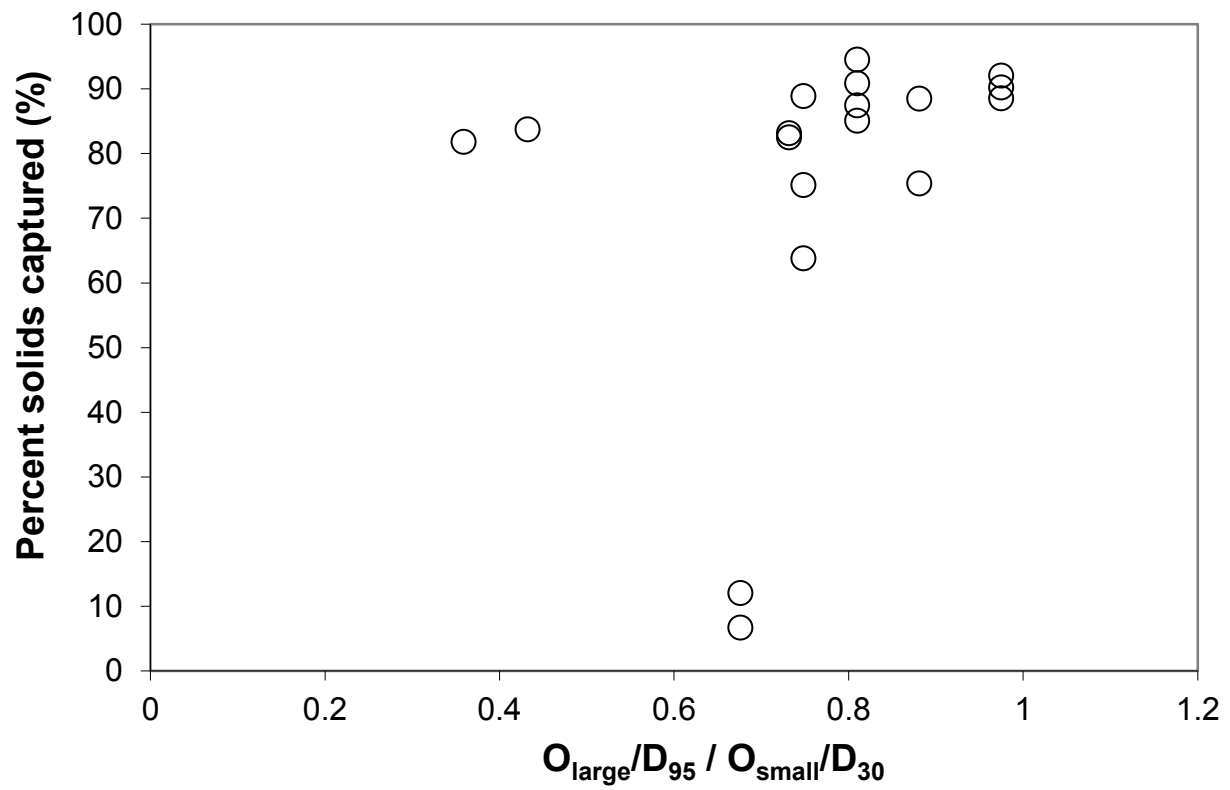
Figure 38. Plot of solids captured in and on the geotextile filter as a function of the ratio O_{large}/D_{95} to O_{small}/D_{30} for all tests. O_{small} = AVERAGE(O_{10}, O_{20}, O_{30}). O_{large} = AVERAGE(O_{95}, O_{100}).
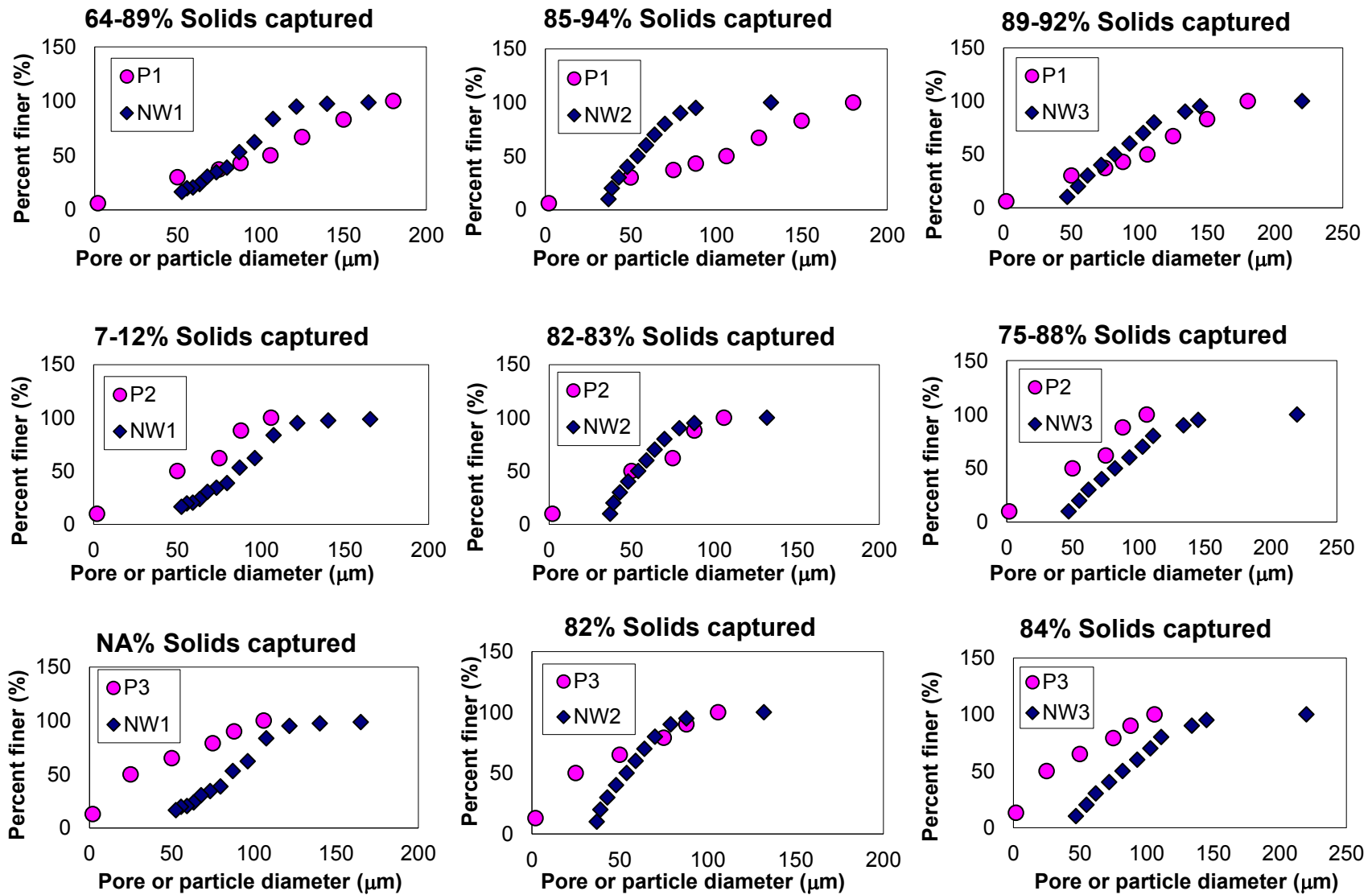
Figure 39. Size distributions for both particles and geotextile openings for the tests performed for this study with particle size distributions P1, P2, and P3, with the percentage ranges of total solids captured in and on the filter indicated for the tests performed under those conditions.

CONCLUSIONS

New retention criteria were developed to accurately predict success of a geotextile filter at retaining suspended solids in stormwater runoff. Established criteria for geotextiles in geotechnical applications were not adequate for this use of geotextile because they incorporate only one filter opening size and one particle diameter in each criterion ratio. The criteria developed in this study utilize at least two filter opening sizes and two particle diameters in each criterion ratio. Two of the new criteria, $\frac{O_{95}/D_{60}}{O_{30}/D_{10}} > 0.05$ and

$\frac{O_{l\arg e}/D_{60}}{O_{small}/D_{10}} > 0.076$, are accurate when predicting success or failure of a geotextile for any of the three particle size distributions in this study. The other two criteria, $\frac{O_{95}/D_{95}}{O_{30}/D_{30}} >$

0.48 and $\frac{O_{l\arg e}/D_{95}}{O_{small}/D_{30}} > 0.68$, are accurate for use in choosing a successful geotextile filter

for particle capture. However, to increase accuracy of these two final criteria, a stipulation could be added that for filters with permittivity of 0.8 s^{-1} or less, or for particle size distributions with D_{50} of 25 μm or less, the values in the ratios are lower ($\frac{O_{95}/D_{95}}{O_{30}/D_{30}} >$

0.23 and $\frac{O_{l\arg e}/D_{95}}{O_{small}/D_{30}} > 0.33$).

Chapter IV: COMPARISON BETWEEN SAND FILTER AND GEOTEXTILE

FILTRATION

INTRODUCTION / BACKGROUND

Low Impact Development (LID) and related natural technologies are being utilized to address urban stormwater challenges. These technologies can however, require more land for implementation than is available in highly urbanized areas. One current stormwater runoff treatment system used in urban areas is a sand filter, as shown in Figure 1 (Chapter I). Sand filters effectively capture the particulate pollutants in stormwater runoff; however, as sand filters clog, highly labor-intensive maintenance is required to ensure adequate drainage through the treatment system.

This research intended to address the hypothesis that a geotextile filter could effectively capture suspended solids in stormwater comparable to a sand filter and maintain adequate drainage for a greater amount of solids loading by comparing results of laboratory tests on geotextile filters with similar laboratory tests on sand filters. This study also includes a comparison of laboratory geotextile test results with results of in-field stormwater treatment by sand filters.

METHODOLOGY

A laboratory column set-up was assembled to test the efficiency of filtration of synthetic stormwater runoff by a sand filter. Similar to the geotextile column tests, the set-up included a pump, a mixer, a 40-L plastic tub, tubing, 500-mL plastic sampling containers, a metal screen for material support, and a Plexiglas column with clean AASHTO-M-43

gravel and ASTM-C-33 concrete sand. Figure 40 shows the Plexiglas column during

testing. A simulated stormwater suspension was pumped into the top of the Plexiglas

column and effluent samples were collected at the bottom of the column.

The specifications for the sand and underdrain gravel were given by a Low

Impact Development Manual for the state of Michigan (SEMCOG 2008). The concrete

sand was sieved to contain only sizes 0.05-0.10 cm (0.02 - 0.04 in) and rinsed thoroughly

with tap water to remove fines. The gravel was between 0.953 cm (0.375 in) and 1.905

cm (0.75 in) and was also washed with tap water before use. No geotextile was used for

separation or support to ensure that all filtration measured was done by the sand.

The silt soil used to produce the simulated stormwater was the same as that used

for the geotextile column tests (described in the Chapter II). The soil was sieved to

produce particle size distributions P1 and P2 (as described in the Chapter II). Two tests

were performed, one with P1 and one with P2, at 200 mg/L solids loading and 6 mL/s

influent flow rate, a hydraulic loading rate of 0.49 mm/s.

Several measurements were taken during testing. Head losses were measured as

water levels rose above the surface of the sand in the column. Outlet flow rates were

calculated by measuring the volume of water exiting the column in a given amount of

time. After the suspension passed through the sand filter, samples of effluent were

collected in plastic containers every 8 minutes, and TSS concentration measurements

were conducted using Standard Method 2540 B (Eaton et al. 1995). Just as in geotextile

column testing, each test was run for 75 minutes because rainfall events between 0 and 2

hours occur at a higher frequency than all other rainfall events in the state of Maryland

(Kreeb 2003). Nine effluent samples were collected during each test, and the TSS

110

concentrations of all nine samples were used to calculate an effluent TSS EMC value for each test.

After 75 minutes of treatment, the test was stopped and the filter was allowed to dry by exposing the surface to the atmosphere for 2 or more days. Subsequently, the suspension loading was continued for another 75 minutes, and effluent samples were collected. The process was repeated for 13-14 tests stopping at 75 minutes or whenever the ponded water level reached the top of the column, until the filter clogged. Clogging was defined to occur when the height of standing water on the filter reached the top of the column within 15 minutes of testing. This length of time was chosen instead of 20-25 minutes (the time used in the geotextile column tests) because the height of the sand column above the surface of the sand (about 18 cm) was shorter than the height of column above the geotextile (around 30 cm). Assuming a linear increase in head loss, reaching the top of the 18 cm clearance within 15 minutes is approximately equivalent to reaching the typical vertical clearance (1 m) in an underground sand column system within the average duration of a rainfall event (1 hr) (Barrett 2003; Kreeb 2003). Each complete set of tests addressed in this work is labeled as Test 1S or Test 2S, where 1 or 2 indicates the particle size distribution of the solids in the influent solution. Between Tests 1 and 2, the top 15 cm (6 in) of sand in the column were removed and replaced with clean sand.

Figure 40. Sand column used for testing a simulated sand filter system.

SAND FILTER PERFORMANCE IN LITERATURE

A few studies have been performed on the effectiveness of sand filtration systems on the water quality of stormwater runoff. One study performed in Sydney, Australia by Kandasamy et al. (2008) compared the performances of two types of sand filters. One filter contained fine sand; the other contained coarse sand. Both were free from organic material and clay. Initially, the coarse sand filter performed significantly better than the fine sand filter in removal of suspended solids because there was an initial flushing of pollutant fines due to high loads of suspended solids in the early events. Later, the fine sand filter behaved more like the coarse sand filter removing approximately 75% of the suspended solids, while the inlet suspended solids concentration was around 14.4 mg/L.

Barrett (2003) examined the performance of five sand filter systems in California. The results showed that all filter sites had excellent TSS removal regardless of the influent concentrations (average influent TSS: 90 mg/L); the average effluent TSS for all sites was 7.8 mg/L (i.e., 91% removal). The 3 Los Angeles sites required filter bed rejuvenation after 3 years and a solids loading to the system of 5 to 7.5 kg/m^2. Assuming a 50% reduction in sediments by the detention basins, the sand filters reached a point of failure flow rate (when drain times exceeded 72 hours) at 25 to 50 mm/hour, when the cumulative solids loading was between 2.5 and 3.75 kg/m^2. The 2 San Diego sites did not reach a failure point after 3 years of operation and 2 kg/m^2 loading. It was assumed that these filters would last for a total of 8 years, reaching a failure flow rate of 20 mm/hr once 5 kg/m^2 solids had been loaded (Barrett 2003).

According to CASQA (2003), sand filter removal efficiencies of TSS range from 83% to 98% with an average around 89%. This study not only included a standard sand

filter, but also compost filter systems and multi-chamber treatment systems (CASQA 2003)

Another type of stormwater treatment is bioretention, a mixture of soil, sand, and mulch. In Li and Davis (2008), the total solids needed to clog laboratory bioretention column tests was $0.9 - 14.5$ kg/m^2, with an average of 3.08 kg/m^2.

COMPARISON OF GEOTEXTILE FILTRATION WITH SAND FILTER PERFORMANCE IN LITERATURE

The three geotextile filters in the current study (discussed in Chapter II) were loaded at higher TSS concentrations than the sand filters (100-200 mg/L vis-a-vis 90 mg/L). Removal rates of total suspended solids for the geotextile filters which experienced a ripening period, ranged from 64 - 94%, with an average of 84%. As stated earlier, the average removal rate of TSS for sand filters in California was 91%. Although the total removal rate for California sand filters was larger than that of geotextiles, the average effluent TSS concentrations for geotextiles were comparable to those of the sand filters. In 15 out of the 16 geotextile tests in which a ripening period occurred, effluent TSS concentrations dropped below that target of 30 mg/L. After the ripening period, all effluent EMC values were below the target concentration of 30 mg/L at average concentrations of 5.2, 6.5, 16, 12, 15, and 13 mg/L for Tests 2.P1, 3.P1, 2.P2, 3.P2, 2.P3, and 3.P3, respectively. Tests run with an influent TSS concentration of 100 mg/L also saw effluent EMC values below the target concentration after a ripening period at average concentrations of 8.0-8.4, 6.4-11, 13, and 7.8 mg/L for Tests 2.P1(100), 3.P1(100), 2.P2(100), and 3.P2(100), respectively. Effluent EMC values were below the

target for tests run at a lower flow rate (3 mL/s) as well; average concentrations after the ripening period were 16 and 5.8 for Tests 1.P1(3) and 2.P1(3), respectively. These average effluent TSS concentrations for the geotextile tests are comparable to the average effluent TSS concentration of 7.8 mg/L for the California sand filters (Barrett 2003).

The geotextile laboratory tests ended when maximum head loss in the 0.30 m (1 ft) column restricted continuation of tests, occurring at a solids loading of 3.4 – 10.8 kg/m^2, which is either comparable to or more than the solids loading at failure for the California sand filters (2.5 – 5 kg/m^2) (Barrett 2003). A greater solids loading at failure indicates that the geotextile filters would have a longer lifespan (in terms of total solids loaded to the filter) than a sand filter. Additionally, the effluent unit flow rates (flow rates normalized by filter surface area) of the NW1, NW2, and NW3 filters never dropped below 100 mm/hr (compared to 25 to 50 mm/hr for the California sand filters) which indicates that the geotextile filters could be loaded significantly more before reaching a flow rate failure point equivalent to the sand filter flow rates (Barrett 2003).

RESULTS FROM SAND FILTER LABORATORY TESTS

TSS REMOVAL

Two tests, Tests 1S and 2S, were performed on a clean sand filter using particle size distribution P1 and PSD P2, respectively. For both tests, approximately 100% of the suspended solids loaded to the filter were retained. Therefore, effluent TSS concentrations for both tests were minimal; the average effluent TSS concentrations were

0.55 and 1.0 mg/L for 1S and 2S, respectively, which are considered below the detection limit by the Quality Control and Quality Assurance manual established for this laboratory. Figures 41 and 42 show the TSS EMCs and the amount of solids captured by the filter as a function of the solids loaded to the filter, respectively, for tests 1S and 2S. Unlike the geotextile column studies, there was no ripening period for retaining suspended solids for either of the sand filter tests. The sand filter was able to retain nearly 100% of the suspended solids from during every 75 min test. This result can be attributed to the very large thickness of the sand filter compared with the geotextile filters (61 cm versus 0.23-0.32 cm).

Similar to the results produced by geotextile column studies, the total solids loading at the final clogging point (as defined in Methodology) was larger for Test 1S, the sand filter test with particle size distribution P1 (4.1 kg/m^2) than for Test 2S, the sand filter test with particle size distribution P2 (3.5 kg/m^2). The phenomenon is likely, once again, a result of the more open and porous filter cake established by P1. P1 included a larger range of particle sizes than P2, and the largest particles in P1 (180 μm) were larger than the largest particles in P2 (106 μm). Figure 15 in Chapter II shows how the larger particles can form a more porous graded filter zone in the cake above the filter (Aydilek 2011). Since P1 had larger particles than P2, the filter cake that formed is likely more porous, and a P1 cake with the same mass of solids as a P2 cake allows a greater amount of water to pass through. The result is a longer lifespan overall because at the point where the sand-filter cake system reaches the same hydraulic conductivity, the P1 cake will have a larger collected mass than the P2 cake, meaning that the filter had reached a higher cumulative solids loading before it reached its final failure hydraulic conductivity.

116

The cake formed by P2 likely had a greater accumulation of fines due to the smaller particles within the P2 distribution which often promotes clogging (Kutay and Aydilek 2005).

Upon visual inspection, suspended solids accumulated primarily in approximately the top 2.5 cm (1 in) out of around 61 cm (24 in) of sand in the column. Figures 43 and 44 show the top 8 cm of the sand in the sand column during Tests 1S and 2S, respectively. The pattern produced by the particles within the top 3 cm of sand, most visible in Figure 44, is a result of varying the position of the influent water flow. The influent flow position was changed every 5 minutes in order to subject the sand filter to particles evenly. In each position, the force of the water flow pushed the grains of sand out of place, allowing particles to settle in place of the sand. This demonstrated how the depth of clogging in a sand filter is reliant upon the influent flow rate. Because the hydraulic loading rate chosen for testing (0.49 mm/s) corresponds to a rainfall rate (3.6 cm/hr or 1.4 in/hr assuming a runoff area-to-drainage area ratio of 50) approximately 10 times greater than the rainfall rate for the highest frequency of rainfall events for the state of Maryland, it is unlikely that particles would ever settle far beyond 2.5 cm (1 in) within the sand (0-0.254 cm, 1 hr; Kreeb 2003).

The results of the laboratory sand filter tests were similar to the results of the Barrett 2003 study of California sand filters. The removal rate of total suspended solids for the two laboratory column tests was 99.6-99.7%. The removal rate for the California sand filters was also over 90% (91%). Also, the total solids loading for the column tests was 3.5-4.1 kg/m^2, which is within the same range of total solids loading at which failure occurred (or was presumed to occur) for the California sand filters (2.5-5 kg/m^2) (Barrett

2003). These results indicate that the sand filter in the laboratory column studies performed similarly to a sand filter in use in field practice.

The sand filters captured a greater total percentage of loaded suspended solids (99.6 - 99.7%) than the geotextile filters (63.8 – 94.5%) as seen in Figure 42. However, generally, the sand filters clogged at a smaller mass of solids loaded than the geotextile filters. The sand filters clogged at 3.5-4.1 kg/m^2 solids loading with an average of 3.8 kg/m^2, while the geotextiles clogged at 3.4-10.8 kg/m^2 with an average of 5.9 kg/m^2 (Table 11). Only one of the 16 successful geotextile tests clogged at a lower solids loading than the sand filter (3.4 kg/m^2). This result indicates that a geotextile filter will last longer during stormwater treatment before maintenance is necessary compared to a sand filter. This phenomenon is likely a result of the much larger thickness of the sand filter compared with a geotextile. When a geotextile filter was exposed to the influent stream of simulated stormwater, the cake on the surface of the geotextile broke up in the location of the influent stream. This break-up allowed some particles to pass through the filter, but it also allowed a greater flow of water through the filter in the location of the break-up until the filter cake re-settled on to the surface in that location. The thickness of the sand filter was so large (61 cm) that a break-up in filter cake had little effect on the flow rate of water through the system. The larger flow rate occurring at the beginning of each geotextile test allowed more water and thus, more suspended solids, to be loaded to the filter before the head loss above the filter reached its maximum height.

Additionally, the maximum head loss within the sand column is over two times greater than that of the geotextile column (78 cm versus 30 cm). If head loss within the

118

geotextile columns was allowed to reach the same maximum height as within the sand column, the geotextile could have been loaded much further before clogging.

As stated earlier, the sand filters clogged at 3.5-4.1 kg/m^2 solids loading with an average of 3.8 kg/m^2, while the geotextiles clogged at 3.4-10.8 kg/m^2 with an average of 5.9 kg/m^2 (Table 11). Scaling up by 50 (the typical runoff-area-to-drainage area ratio) and assuming an influent TSS concentration of 200 mg/L and a runoff coefficient of 0.9, the sand filters would clog at 0.39 – 0.46 m (15.3 – 17.9 in) of total rainfall, and the geotextile filters would clog at 0.38 – 1.2 m (14.9 – 47.2 in) of total rainfall. The average total rainfall amounts at the point of clogging for the sand and geotextile filters are 0.42 m (16.5 in) and 0.66 m (26.0 in), respectively. Assuming an influent TSS concentration of 100 mg/L, the average rainfall amounts are 0.84 m (33.1 in) and 1.31 m (51.6 in) for the sand and geotextile filters, respectively. The average rainfall for the state of Maryland is 1.04 m (40.8 in) (MSA 2012). Therefore, the sand filters would need maintenance after approximately 147 days, and the geotextile filters would need maintenance after approximately 231 days, assuming an average influent TSS concentration of 200 mg/L. The possible lifespans of the sand and geotextile filters in terms of total rainfall and days are given in Table 12 for various assumed parameters, i.e., TSS concentration, runoff coefficient, and runoff area-to-drainage area ratio. The cumulative solids loaded values, 5.91 and 3.77 kg/m^2, are the average values of total mass of solids loaded at failure determined by laboratory testing, and 1.04 m (40.8 in) annual rainfall is assumed.

HYDRAULIC CONDUCTIVITY

Unlike the hydraulic conductivities of the geotextile tests, the hydraulic conductivity values of Tests 1S and 2S could not be fitted by a power function. Figure 45 shows the hydraulic conductivities of both tests as a function of total solids captured in and on the sand filter. The data points in Figure 45 can be fitted by linear regression lines with coefficients of determination (R^2) equal to 0.88 and 0.94 for Tests 1S and 2S, respectively.

The hydraulic conductivities measured for the sand filter were much larger than the hydraulic conductivities measured for the geotextile filter (2.1-2.2×10^{-4} m/s versus 1.7×10^{-6} - 1.8×10^{-5} m/s) (Table 11). The reason for this is largely due to the column testing set-up and the manner in which hydraulic conductivity was calculated. The ratio between the length of the sample (i.e., filter thickness) and hydraulic head, which is used to calculate hydraulic conductivity (Equation 4), is much greater at the maximum head loss for the sand filter than for the geotextile filter. Because the sand filter was approximately 61 cm in height with about 17 cm above the surface of the filter for standing water, the ratio of length of the filter to maximum hydraulic head was 0.8. The geotextile filter was only 2.3 – 3.2 mm in height with about 30 cm above the surface of the filter for standing water. Therefore, the average ratio between length of the filter and maximum hydraulic head was 0.009. Because that ratio for the sand filters was about 2 orders of magnitude greater than that ratio for the geotextiles, the average of the stabilized final hydraulic conductivities of the sand filters was approximately 2 orders of magnitude larger than that of the geotextile filters (2.2×10^{-4} m/s versus 6.4×10^{-6} m/s).

Similar to the geotextile column test results, the hydraulic conductivities for the smaller particle size distribution, P2, are smaller than the hydraulic conductivities for the larger PSD, P1, for the same mass of solids captured (Figure 45). This result enforces the argument made earlier that larger particles form a more porous and open filter cake which allows water to pass more easily than a cake formed by smaller particles.

Due to the large difference in hydraulic conductivity values resulting from the larger thickness of the sand filters, permeability and flow rates between the sand filters and the geotextiles filters were evaluated as well. The initial permeability of the sand filter was likely around 1.2×10^{-5} m/s (CASQA 2003). The permeability of the clean geotextile filters was much larger than the sand filter permeability at $1.73 - 2.76 \times 10^{-3}$ m/s (Table 2). The values indicate that the geotextile will allow water to flow through much more easily throughout testing than the sand.

The effluent flow rates from the sand filter at the clogging point were very similar to those for the geotextile filter. The average final effluent velocities were 2.84×10^{-4} m/s and 3.50×10^{-4} m/s for the sand filters and geotextile filters, respectively (for the tests with an influent flow rate of 6 mL/s). This result is expected because the meaning of the clogging or failure point established in Chapter II implies similar failure flow rates for similar influent flow rates.

CONCLUSIONS

Sand filters perform very well at total suspended solids removal (91-100% of total solids), both in field studies from literature and in the laboratory studies of the current study. However, sand filters clog faster in terms of solids loaded to the system than geotextile filters, and thus, would require more frequent replacement than a geotextile filter.
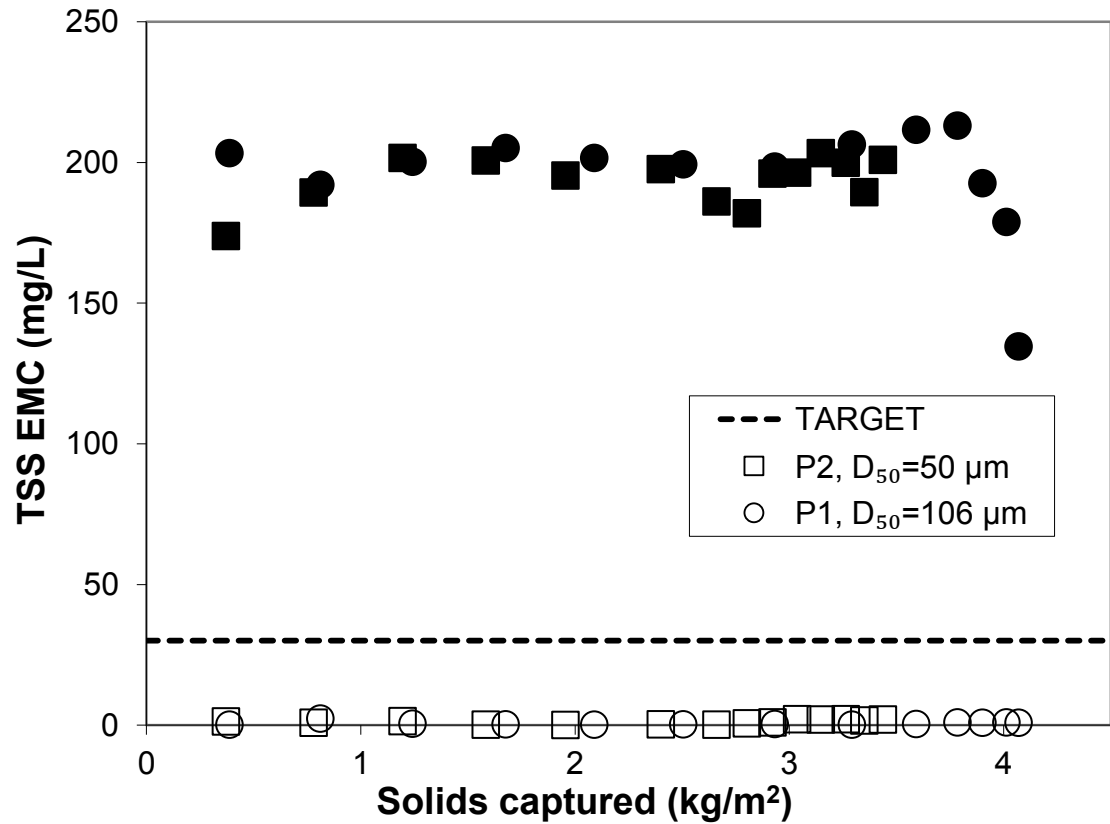
Figure 41. Effect of total solids captured by the sand filter on TSS concentration for particle size distributions P1 and P2. Closed symbols indicate influent values. Open symbols indicate effluent values. Dashed line indicates the target concentration of 30 mg/L.
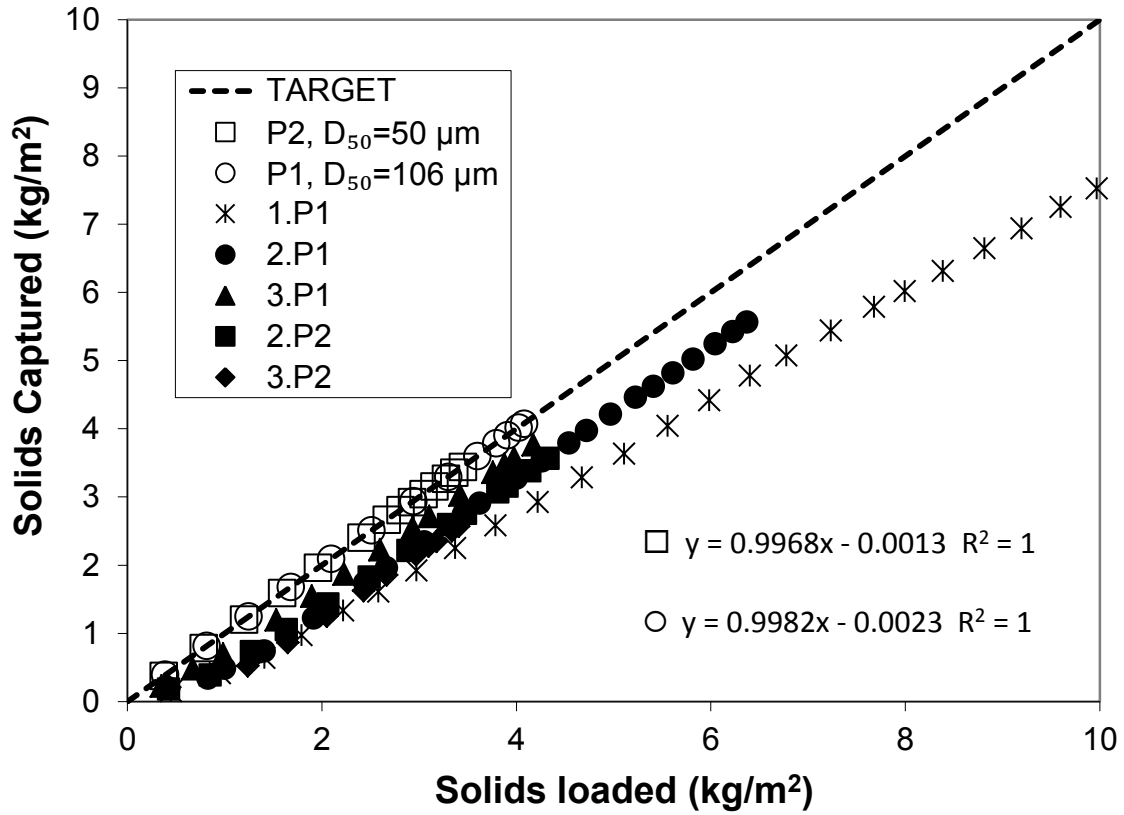
Figure 42. Total solids captured by the sand filter as a function of the solids loaded to the

sand filter and the geotextile filters for TSS concentration of 200 mg/L and influent flow

rate of 6 mL/s. Dashed line indicates the target removal rate of 100%.
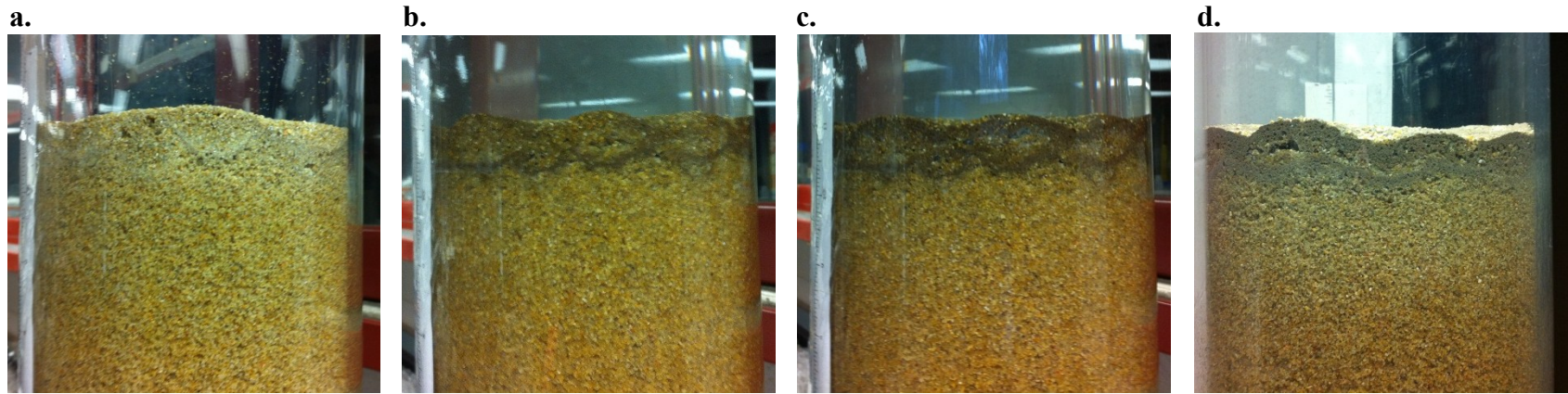
Figure 43. Build-up of solids in top 8 cm of sand in the sand column throughout Test 1S **a**. After 1 (75-min) test (dry), **b**. During 5th (75-min) test (wet), **c**. During 9th test (wet), **d**. After 13 tests (dry).
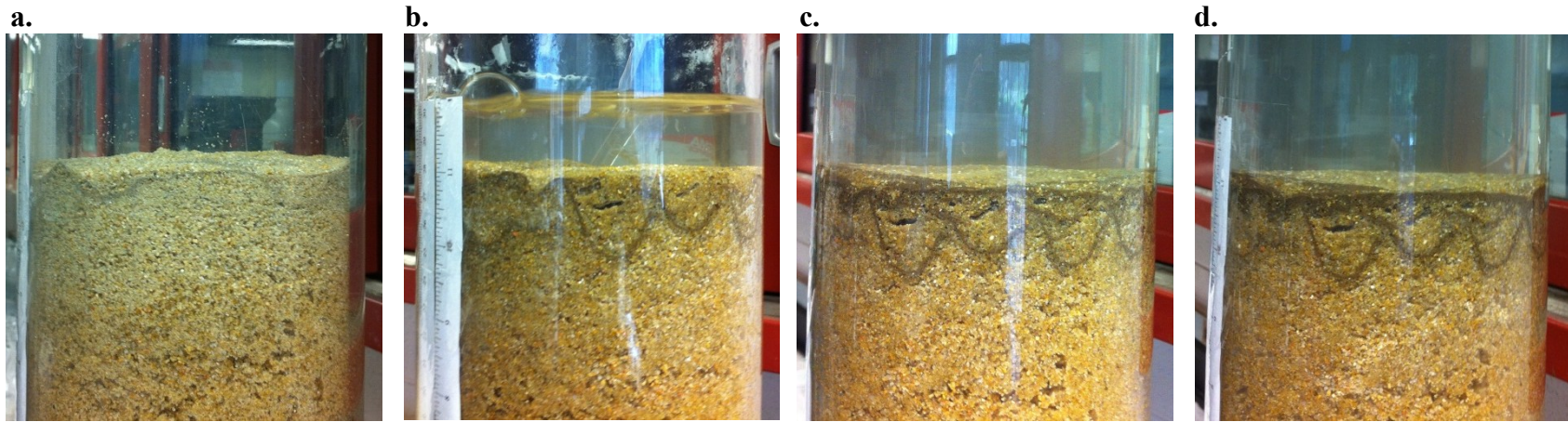
Figure 44. Build-up of solids in top 8 cm of sand in the sand column throughout Test 2S **a**. After 2 (75-min) tests (dry), **b**. During 5th (75-min) test (wet), **c**. During 9th test (wet), **d**. During 14th and final test (wet).

Table 11. Summary of test results.

Test Parameters				Test Results			
Influent TSS Conc. (mg/L)	PSD	Flow rate (mL/s)	Filter type	Solids loaded at end (kg/m^2)	Solids retained at end (kg/m^2)	Total solids retained (%)	Hydraulic Conductivity at end (m/s)
200	P1	6	1	10.8	8.10	75.1	1.64×10^{-5}
			1	7.79	4.97	63.8	1.36×10^{-5}
			2	6.37	5.57	87.4	4.16×10^{-6}
			3	4.17	3.76	90.2	3.05×10^{-6}
			sand	4.08	4.07	99.7	2.22×10^{-4}
		3	1	8.84	7.86	88.9	6.62×10^{-6}
			2	6.68	6.31	94.5	1.74×10^{-6}
	P2	6	1	3.75	0.25	6.64	3.76×10^{-4}
			1	5.02	0.60	12.0	4.89×10^{-4}
			2	4.33	3.57	82.5	4.85×10^{-6}
			3	3.41	2.57	75.3	3.48×10^{-6}
			sand	3.45	3.43	99.6	2.10×10^{-4}
	P3	6	2	4.92	4.02	81.8	3.04×10^{-6}
			3	4.64	3.88	83.7	3.50×10^{-6}
100	P1	6	2	5.03	4.57	90.9	7.47×10^{-6}
			2	6.77	5.75	85.0	5.64×10^{-6}
			3	5.60	4.96	88.5	1.75×10^{-5}
			3	4.52	4.15	92.0	5.95×10^{-6}
	P2	6	2	4.84	4.02	83.1	3.47×10^{-6}
			3	5.86	5.18	88.5	3.48×10^{-6}

Table 12. Durations of filter use (in rainfall depth and days) before maintenance needed using the cumulative TSS loaded values determined in laboratory testing and assumptions of constant TSS concentrations, runoff coefficients, and runoff area-to-drainage area ratios given. The number of days assumes 1.04 m (40.8 in) rainfall per year, evenly distributed among each day of the year.

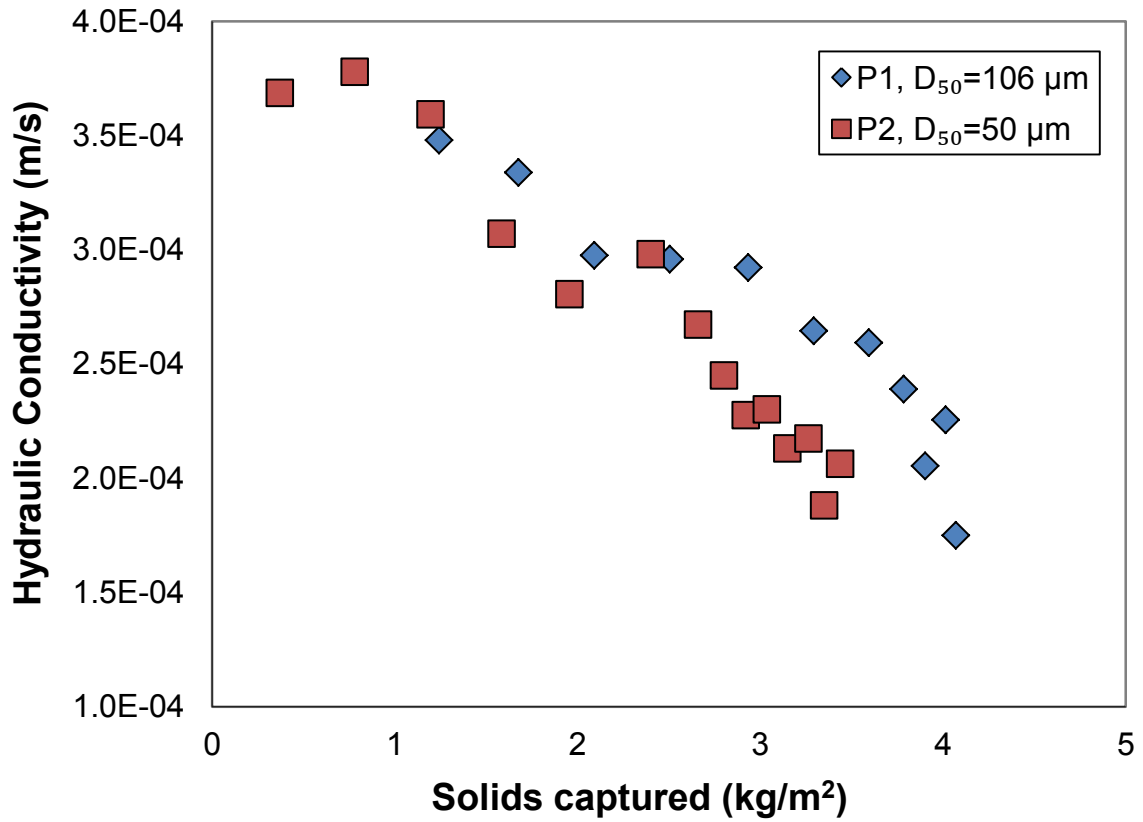| Filter type	Cumulative TSS loaded (kg/m²)	TSS Conc (mg/L)	Runoff coefficient	Runoff area-to-drainage area ratio	Without retention basin		With retention basin (50% reduction of TSS)	
					Rainfall (m)	Days	Rainfall (m)	Days
Geotextile	5.91	200	0.9	25	1.31	462	2.63	925
				50	0.66	231	1.31	462
				100	0.33	116	0.66	231
			0.5	25	2.36	832	4.73	1665
				50	1.18	416	2.36	832
				100	0.59	208	1.18	416
		100	0.9	25	2.63	925	5.25	1850
				50	1.31	462	2.63	925
				100	0.66	231	1.31	462
			0.5	25	4.73	1665	9.45	3330
				50	2.36	832	4.73	1665
				100	1.18	416	2.36	832
Sand	3.77	200	0.9	25	0.84	295	1.67	590
				50	0.42	147	0.84	295
				100	0.21	74	0.42	147
			0.5	25	1.51	531	3.01	1061
				50	0.75	265	1.51	531
				100	0.38	133	0.75	265
		100	0.9	25	1.67	590	3.35	1179
				50	0.84	295	1.67	590
				100	0.42	147	0.84	295
			0.5	25	3.01	1061	6.03	2123
				50	1.51	531	3.01	1061
				100	0.75	265	1.51	531

Figure 45. Hydraulic conductivity of the sand and captured soil system as a function of

the cumulative solids captured in and on the sand filter for tests conducted with PSD P1

and P2.

Chapter V: MODELING HYDRAULIC CONDUCTIVITY OF A GEOTEXTILE FILTER

INTRODUCTION / BACKGROUND

As discussed in the Chapter II, the hydraulic conductivity of the geotextile filter system can be described as a power model as a function of solids captured by the filter. Using solids loaded onto the system instead of solids captured will provide a simpler way to estimate when the filter will reach a maintenance-trigger point in actual practice (Clark and Pitt 2009). However, for the model development in this study, solids captured will be used instead of solids loaded in order to ensure the greatest amount of accuracy.

Le Coq and Silvy (1999) developed a power model for filtration through fibrous media based on the pore theory approach, which incorporates structural properties of the filter such as pore size distribution and porosity gradient, but does not account for tortuosity of flow. The model assumes a homogeneous fibers/pollutants network build-up and takes into account the plugging/compression of the filter structure. Relationships between the model parameters and structural properties of the filter were determined empirically (Le Coq and Silvy 1999). Le Coq (1996) used the model to describe the increase of head loss through a mineral fiber filter due to clogging of oil.

The Le Coq (1996) model was developed considering two different types of particle accumulation: parallel and series. A filter consists of pore openings which make up a series of pipes where water and particles flow vertically through the material. As particles gradually settle and accumulate in each pipe, the accumulation is in parallel (Faure et al. 2006). Since the pipes could be various sizes due to the varying pore sizes,

the velocity of the accumulation of particles differs between pipes. This causes some pipes to become clogged before others, and this is referred to as accumulation in series. While both types of accumulation occur simultaneously, accumulation in series is more predominant than parallel (Faure et al. 2006). Particles can fill up some pipes in the material and accumulate on the surface of the filter, forming cakes, before all of the pipes have become clogged. This causes head loss to increase; therefore, when accumulation in series is the leading accumulation mechanism, the filter is more likely to become clogged than when parallel accumulation is the leading mechanism (Faure et al. 2006).

The goal of this research is to transform the Le Coq (1996) model to describe hydraulic conductivity as a function of the mass of solids captured by a geotextile filter and show that this model is a good fit for the data in this study. In doing so, the model will be able to provide a method for predicting the clogging point of a geotextile filter in stormwater filtration with knowledge of only a few filter and runoff parameters. Additionally, this study intends to define the fitted parameters of the Le Coq (1996) model as functions of some of the important filter and runoff parameters.

THEORY

The Le Coq model is given in Equation (10) and derived in the Appendix.

$$\delta p = \Delta p_0 \left[(1 - N) \exp \frac{m}{m_1} + N \left(\frac{m}{m_1} \right)^a - 1 \right] \qquad N = \tanh \left(b \frac{m}{m_1} \right) \tag{10}$$

Δp_0 is the initial pressure loss in the filter, δp is the excess pressure or the difference between p, the pressure recorded as the filter encounters the concentrated flow mass of accumulated particles and p_0, the pressure is measured at a specific height above a

131

geotextile filter when a pump imposes a flow rate of clear water onto it, m is the mass of accumulated particles in the filter, m_1 is the critical value of mass of accumulated particles, and a and b are fitted parameters (Le Coq 1996).

In order to use the Le Coq model in Equation 10 for this study, the equation must be developed for hydraulic conductivity instead of pressure drop as a function of solids captured by the filter media. Dullien (1975) developed a permeability model for porous media. The derivation of this permeability model incorporated the effects of parallel and series nonuniformities in the media. Nilsson and Stenstrom (1996) describe parallel-type pore nonuniformities in porous media as a distribution of pore sizes and series-type nonuniformities as connected segments of different pore diameters. Both are diagrammed in Figure 46.

For the development of a permeability model, Dullien (1975) defined the media as cubic networks of capillaries, where each network is made up of identical capillary elements. Each element has identical length, pore size distribution, and hydraulic conductivity. However, elements in different networks have different lengths, pore size distributions, and hydraulic conductivities. Each network of capillaries is isotropic; it has the same permeability in any arbitrary direction as the permeability measured in a principal direction. Additionally, the model developed to predict permeability in porous media "implies that the permeability of a cubic network of capillaries is independent of the macroscopic flow direction through the network" (Dullien 1975). Therefore, the total permeability of the media is calculated by adding the permeabilities of each network in the media (Dullien 1975).

132

Permeability can be converted to hydraulic conductivity by multiplying by fluid

parameters, using Darcy's Law:

$$K = \frac{k \rho g}{\mu} \qquad (11)$$

where K is hydraulic conductivity, k is permeability, ρ is density of water, g is

gravitational acceleration and μ is dynamic viscosity of water. Because permeability is

directly proportional to hydraulic conductivity, the calculation of hydraulic conductivity

for a system of networks in a media can be treated as the calculation of permeability for a

system of networks in a media. Therefore, since permeability is calculated for each

individual network and then, the network permeabilities are summed to get the total

permeability, hydraulic conductivity can be calculated for each network, and then

summed to get total hydraulic conductivity of the media (Dullien 1975).

The version of Darcy's Law used by Dullien (1975) to calculate permeability is as

follows:

$$k_i = \frac{q_i \mu}{A_i \left(\Delta P \big/ L_i \right)} \ or \ \frac{v_i \mu L}{\Delta P} \qquad (12)$$

where q is volumetric flow rate, A is cross-sectional area perpendicular to the

macroscopic flow, v is velocity of the flow (q/A), ΔP is the pressure drop across the

media, and L is the length of the macroscopic flow (or the thickness of the filter).

Combining equations 11 and 12 gives:

$$K = \frac{\rho g v L}{\Delta P} \qquad (13)$$

Assuming that each section (or network) of filter is of length L, and is either dominated

by parallel accumulation/nonuniformities or series accumulation/nonuniformities, then

the total hydraulic conductivity of the filter is equal to the sum of the hydraulic

conductivities of each network.

$$K_{total} = (1 - N)K_{parallel} + (N)K_{series} \qquad (14)$$

where N is a weighting function that represents the excess pressure (or hydraulic

conductivity) due to accumulation in series and is as follows for particle filtration by

geotextile filter (Faure et al. 2006):

$$N = \tanh\left(b\frac{m}{m_1}\right) = \frac{e^{2b\frac{m}{m_1}} - 1}{e^{2b\frac{m}{m_1}} + 1} \qquad (15)$$

where b is a fitted parameter which changes the gradient of N, m is the mass of solids

accumulated in and on the filter, and m_1 is the critical value of mass of accumulated

particles, i.e., the mass of particles which produces a significant drop in hydraulic

conductivity (Faure et al. 2006).

$$K_{parallel} = \frac{\rho g v L}{\Delta P_{parallel}} \qquad (16a)$$

$$K_{series} = \frac{\rho g v L}{\Delta P_{series}} \qquad (16b)$$

Based on the Hermans and Bredee law and confirmed by Faure et al. (2006), the pressure

drops across a geotextile as a function of solids accumulated in and on the filter are:

$$\Delta P_{parallel} = \Delta P_0 \exp\left(\frac{m}{m_1}\right) \qquad (17a)$$

$$\Delta P_{series} = \Delta P_0 \left(\frac{m}{m_1}\right)^a \qquad (17b)$$

134

where a is a fitted parameter (determined empirically) and ΔP_0 is the initial pressure drop across the filter before solids loading occurs (Le Coq and Silvy 1999). Using Equation 13 to determine the initial pressure drop:

$$\Delta P_0 = \frac{\rho g v_{in} L}{K_0} \tag{18}$$

where effluent flow rate per unit area, v, is equal to the influent flow per unit area, v_{in}, because before any solids build up in a geotextile, the flow out is equal to the flow in, i.e., there is no head loss and hydraulic conductivity, K, is equal to the initial hydraulic conductivity of the clean filter, K_0. Combining equations 14, 16a-18:

$$K_{total} = K_0 \frac{v}{v_{in}} \left(\frac{1-N}{\exp\left(m/m_1\right)} + \frac{N}{\left(m/m_1\right)^a} \right) \text{ with } N = \tanh\left(b \frac{m}{m_1} \right) \tag{19}$$
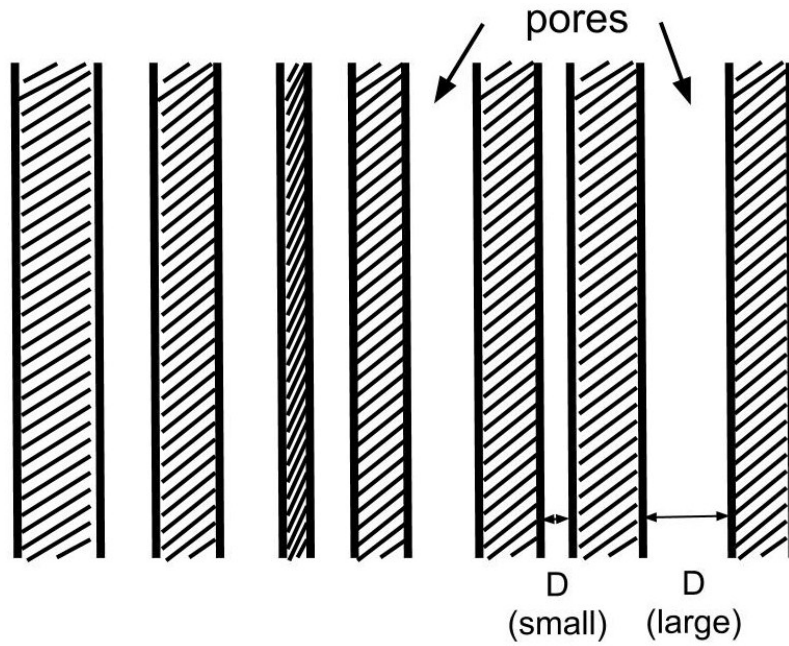
a. Structure involving parallel-type pore nonuniformities
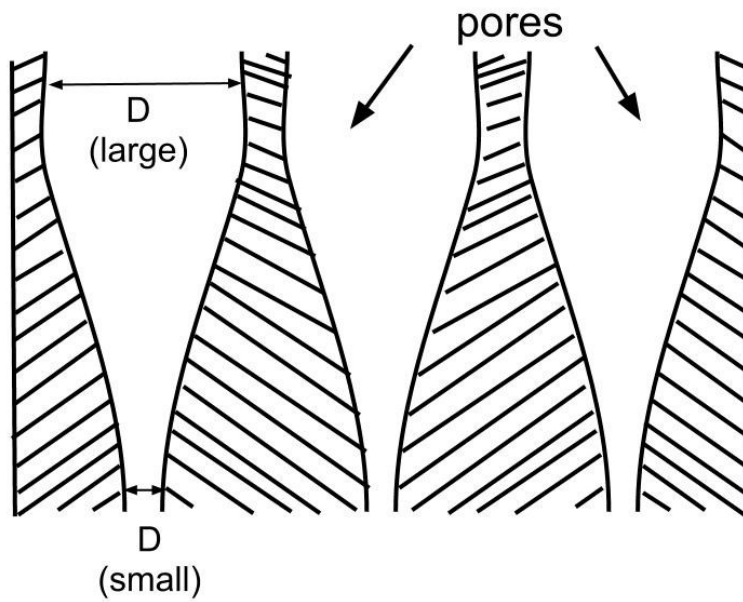
b. Structure with series-type pore nonuniformities

Figure 46. Cross-sections of porous media with varying diameters D **a**. Parallel-type nonuniformities **b**. Series-type nonuniformities

DATA USED IN MODEL DEVELOPMENT

For every data set in which a ripening period occurred, m values, K values, m_1, K_0, and v/v_{in} values were input into Equation 19. The m values were the total solids captured in and on the filter at the end of each 75 minute (or less if water in the column reached the top of the column in less than 75 minutes) test per unit area of geotextile filter, and they were calculated using the influent and effluent TSS EMCs of that test.

$$m_n = \sum_{i=1}^{n} V_i \left(EMC_{INi} - EMC_{OUTi} \right) / A \tag{20}$$

m_n is the m value for the 75 min (or less) test n, V is volume of water treated per test, equal to the average influent flow rate multiplied by 75 min, EMC_{IN} is the influent TSS EMC, EMC_{OUT} is the effluent TSS EMC, and A in the area of the geotextile filter. Each data set included n number of m values.

The K values were the stabilized hydraulic conductivity values for each 75 min (or less) test. They were calculated using Equation 2 in the Chapter II, and a stabilized value meant that the average of hydraulic conductivities which were within 25% of that average was used.

The parameter m_1 is defined as Le Coq's model parameter representing mass of injected particles which leads to geotextile clogging (Faure et al., 2006). It represents a critical value of mass captured by the filter at which the leading mechanism for accumulation transitions from parallel to series. For Faure et al. (2006), a very fast increase in Δp was observed at the point at which m is equal to m_1 (i.e. where pressure increased suddenly until a safety valve was triggered). For this study, the m_1 value for each data set was chosen as the mass of solids captured by the filter (per unit area) at the point of a significant drop (at least one order of magnitude) between the stabilized

hydraulic conductivity values of two consecutive test sets. Because there was often a small range of values that m_1 could be, several values of m_1 within that range were used when determining the a and b values with Microsoft Excel Solver, and the m_1 which produced the smallest S_e/S_y ratio was chosen.

The initial hydraulic conductivity, K_0, is the hydraulic conductivity of a geotextile filter before any solids loading. For checking the validity of the model to the data in this study, it was an estimate based on the initial values of K before the drop at m_1. The K_0 value can also be calculated using Equation 2, assuming head loss is equal to the thickness of the filter, if an approximate value of flow rate is known.

The v/v_{in} values are ratios between the effluent flow velocity v and influent flow velocity v_{in}, and they are equal to ratios between effluent flow rate q and influent flow rate q_{in}. Flow rates were measured throughout tests by measuring the volume of water entering or exiting the column in a given amount of time.

APPLICABILITY OF MODEL TO LABORATORY DATA

For every data set in which a ripening period occurred, m_1, K_0, m values, K values, and v/v_{in} values were entered into Matlab. The nonlinear model parameter fit function nlinfit was used to determine a and b for each data set. The nlinfit function used the Levenberg-Marquardt algorithm for nonlinear least squares to compute non-robust fits. For robust fits, the function used an algorithm that iteratively refitted a weighted nonlinear regression where the weight at each iteration was based on the residual of the previous iteration (Mathworks 2012). This method usually provided a and b values which could predict a relatively accurate hydraulic conductivity for a given mass of solids captured (as

defined by the standard error of estimate divided by the standard deviation of the actual hydraulic conductivity values). The coefficient of determination (R^2) and correlation coefficient (R) for the predicted estimates versus actual hydraulic conductivities were also in the good to excellent range ($R^2 > 0.5$, $R > 0.7$) for every data set (Ayyub and McCuen 2003). However, due to the much smaller (typically by several orders of magnitude) values of hydraulic conductivity during the duration of particle accumulation in series versus accumulation in parallel, the model would sometimes predict values of hydraulic conductivity that were one or more orders of magnitude away from the actual values during the duration of series accumulation. Although the predicted values were orders of magnitude away from the actual values, the residuals of the predictions of hydraulic conductivity during series accumulation were approximately equal to the residuals of the more accurate predictions of hydraulic conductivity during parallel accumulation. Also, the hydraulic conductivities during series accumulation are most important because it is during series accumulation in which the final clogging point occurs, and if the model is to predict when this will occur, then, the hydraulic conductivities predicted during series accumulation must be the most accurate. Therefore, an additional method was needed to determine *a* and *b* values for each data set.

More importance was placed on the hydraulic conductivities during series accumulation by taking the natural logarithm of *K* before inputting those values into Matlab, and the model was altered to incorporate that change. However, the new model became too complex for the number of iterations that Matlab could perform using nlinfit, and the values given for *a* and *b* did not produce reasonable predictions of hydraulic

139

conductivities. Therefore, another method was needed to find the appropriate a and b values for each data set.

In Microsoft Excel, the Solver tool was used to determine a and b for each data set by minimizing the standard error of estimate divided by standard error ratio, S_e/S_y, using the generalized reduced gradient algorithm for nonlinear regression models. This method also utilized the natural logarithms of K and the natural logarithm of the model in order to place importance on the hydraulic conductivities during series accumulation. The hydraulic conductivity values predicted by the model for this method of finding a and b values and the method of using nlinfit in Matlab along with the actual hydraulic conductivity values are plotted in figures 47 and 48 and in Figures 85-98 the Appendix. Figures 47 and 48 display the data for Tests 2.P1 and 2.P1(3), respectively, in two different ways. Plots in logarithmic scale show that while the predicted hydraulic conductivities from the Matlab-produced model parameters are very accurate at low values of solids captured, the values are sometimes incorrect by several orders of magnitude at higher values of solids captured (Figure 48b).

One of the goodness of fit parameters used to evaluate the $\ln(K)$ values versus the predicted $\ln(K)$ values (i.e., $\ln(K_{model})$) is model bias, $\bar{e}$,

$$\bar{e} = \frac{1}{n}\sum_{i=1}^{n}(\hat{y} - y) \tag{21}$$

divided by $\bar{y}$, the mean of y, where y is the measured value ($\ln(K)$ in this case), $\hat{y}$ is the predicted value ($\ln(K_{model})$), and n is the number of data points in the set. All data sets had minimal values of the bias ratio (<5%), indicating low systematic error in the predicted values (Table 13).

Another goodness of fit parameter used to evaluate the applicability of the model to the hydraulic conductivity data was the coefficient of determination, R^2, where R^2 is equal to the explained variance (EV) divided by the total variance (TV). TV is equal to the sum of EV and the unexplained variance (UV).

$$R^2 = \frac{EV}{TV} = \frac{TV - UV}{TV} = 1 - \frac{UV}{TV} = 1 - \frac{\sum(\hat{y} - y)^2}{\sum(y - \bar{y})^2} \tag{22}$$

R^2 values for all data sets showed excellent correlation between the predicted and actual values ($R^2 > 0.7$) and are given in Table 13.

The final goodness of fit parameter used to assess the validity of the model was the standard error ratio, S_e/S_y, which was minimized by the Excel Solver to choose the best a and b values.

$$S_e = \left[\frac{1}{n - m} \sum_{i=1}^{n} (\hat{y} - y)^2 \right]^{\frac{1}{2}} \tag{23}$$

$$S_y = \left(\frac{TV}{n - m} \right)^{\frac{1}{2}} = \left(\frac{\sum(y - \bar{y})^2}{n - m} \right)^{\frac{1}{2}} \tag{24}$$

Although the ratio was minimized by the solver, only half of the values were in the good relative accuracy range ($S_e/S_y < 0.3$). However, the other half were not in poor relative accuracy range either ($0.3 < S_e/S_y < 0.5$; poor accuracy means $S_e/S_y > 0.7$) (Ayyub and McCuen 2003). The standard error ratios for all data sets are given in Table 13.
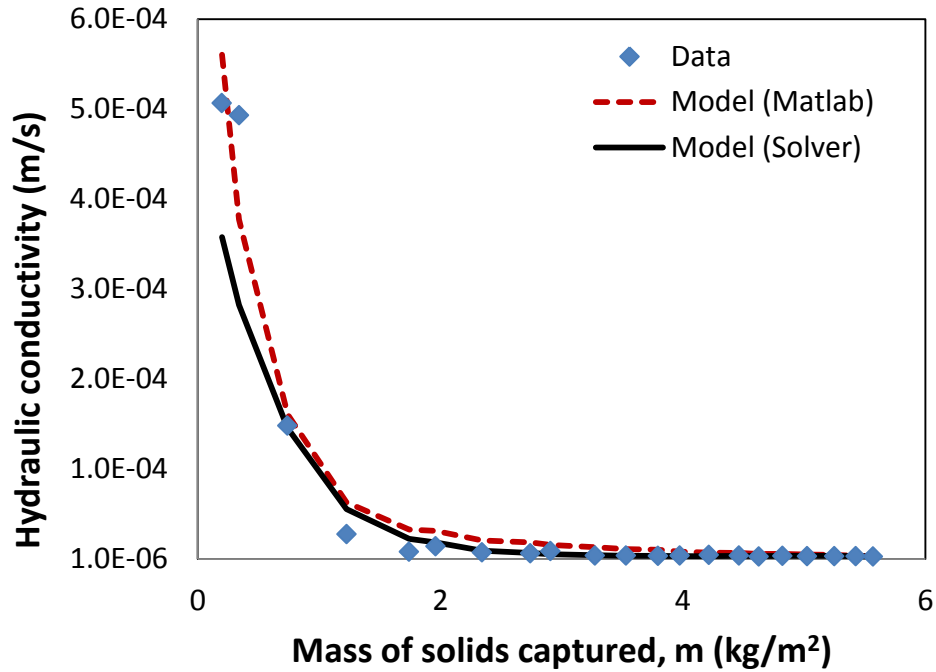
a. Linear scale
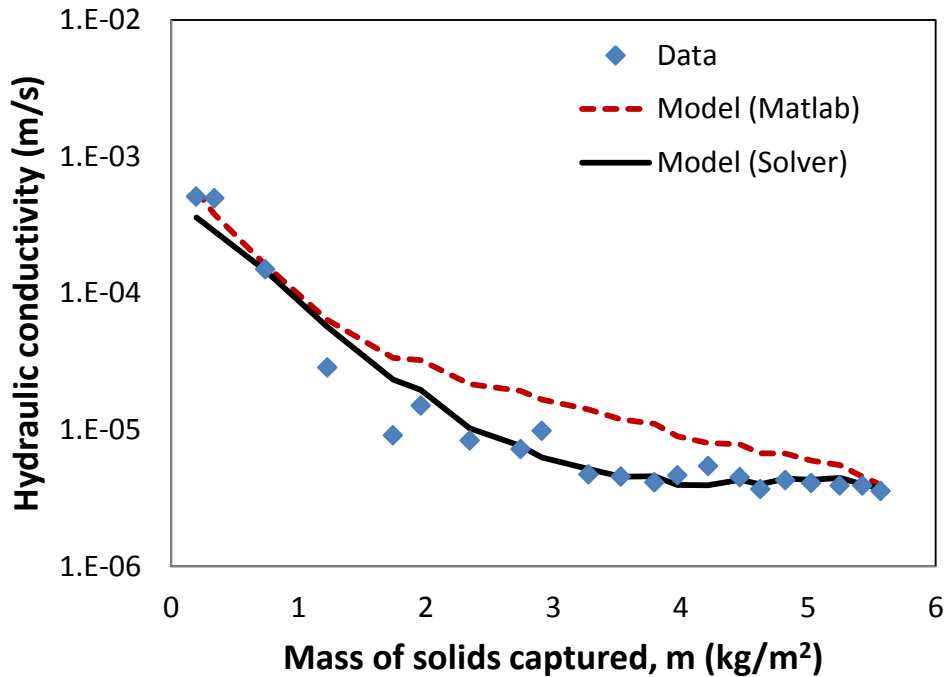
b. Logarithmic scale

Figure 47. Hydraulic conductivity values measured during laboratory testing and hydraulic conductivities predicted by the theoretical model (Equation 19) as a function of the mass of solids captured by the filter for Test 2.P1. **a**. Linear scale **b**. Logarithmic scale (Note: The same values are plotted in parts **a** and **b**.)
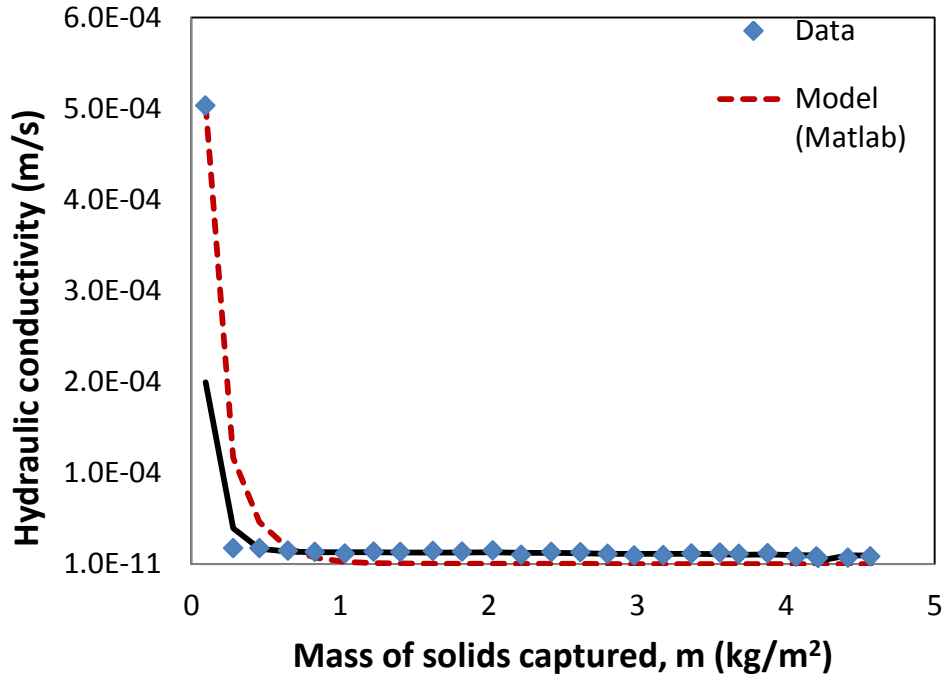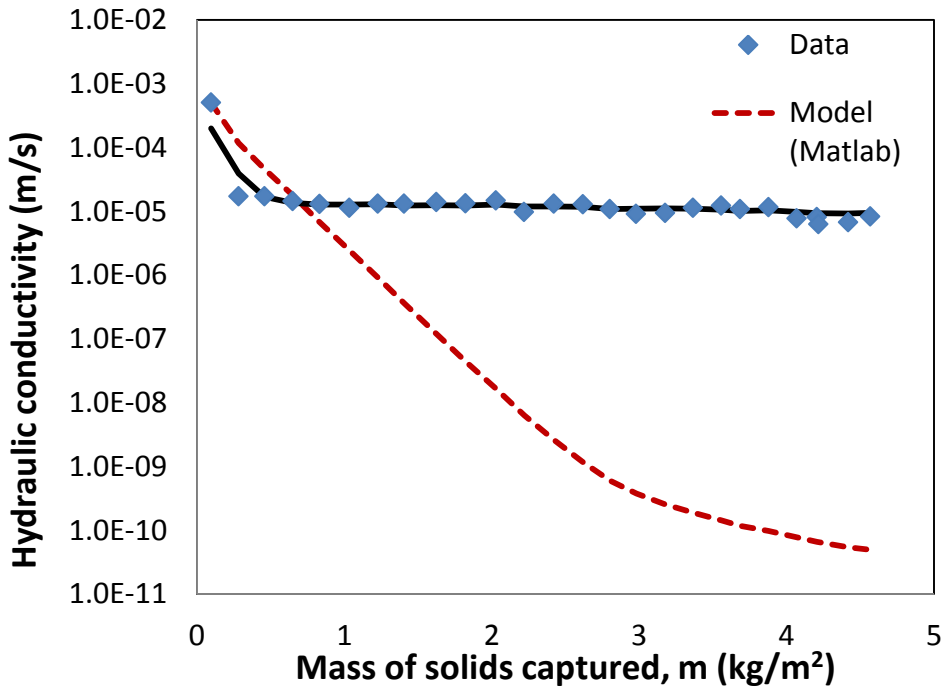
a. Linear scale

b. Logarithmic scale

Figure 48. Hydraulic conductivity values measured during laboratory testing and hydraulic conductivities predicted by the theoretical model (Equation 19) as a function of the mass of solids captured by the filter for Test 2.P1(3). **a**. Linear scale **b**. Logarithmic scale (Note: The same values are plotted in parts **a** and **b**.)

Table 13. Model parameters and measurements of goodness of fit for each data set.

Test parameters					Model parameters (from Excel Solver tool)			Goodness of fit parameters (for $\ln(K_{model})$ vs. $\ln(K)$)		
Test	C_0 (mg/L)	Flow rate (mL/s)	PSD	Filter type	a	b	m_1 (kg/m^2)	e/y (%)	S_e/S_y	R^2
1.P1	200	6	1	1	1.15	0.0595	0.60	0.205	0.363	0.868
					0.231	0.00561	0.40	0.997	0.419	0.824
2.P1				2	0.0898	0.00163	0.60	0.347	0.217	0.953
3.P1				3	0.984	0.0255	0.50	0.0792	0.322	0.896
2.P2			2	2	1.08	0.0170	0.35	0.263	0.311	0.903
3.P2				3	2.90	0.239	0.50	1.54	0.256	0.935
2.P3			3	2	1.39	0.0279	0.25	0.231	0.228	0.948
3.P3				3	1.64	0.0674	0.25	0.276	0.244	0.940
1.P1(3)		3	1	1	0.771	0.145	0.30	0.475	0.286	0.918
2.P1(3)				2	1.35	0.0349	0.30	0.0276	0.225	0.949
2.P1(100)	100	6	1	2	0.996	0.0251	0.10	0.0891	0.386	0.851
2.P1(100)					1.21	0.0320	0.40	0.887	0.364	0.867
3.P1(100)				3	0.905	0.0380	0.15	0.109	0.403	0.837
3.P1(100)					1.32	0.0439	0.25	0.732	0.498	0.752
2.P2(100)			2	2	1.28	0.0777	0.10	0.173	0.280	0.921
3.P2(100)				3	1.29	0.0529	0.15	0.0404	0.290	0.916

SENSITIVITY OF MODEL TO PARAMETERS a, b, AND m_1

In order to assess the sensitivity of the model to the parameters, a, b, and m_1, each parameter value was altered by 1%, 5%, 10%, -5%, and -10% and the hydraulic conductivity values were recalculated for each case. The new hydraulic conductivity values were plotted as a function of the mass of solids captured, m, using a linear equation of v/v_{in} as a function of m for each set of data. The mass of solids captured at the failure or clogging point for each new case was determined as m when the new hydraulic conductivity equaled the measured stabilized hydraulic conductivity from the corresponding laboratory test. The mass of solids loaded to the filter at failure was then determined by dividing the mass of solids captured by the total percentage of solids captured for that laboratory test. Assuming a runoff area-to-drainage area ratio of 50, a runoff coefficient of 0.9, and an average influent TSS concentration of 200 mg/L, the mass of solids loaded to the filter was used to determine the total rainfall depth at filter failure. Finally, assuming an annual rainfall of 1.04 m (40.8 in), the rainfall depth was converted to a number of days that the filter would operate before maintenance was needed, as predicted by the model.

Altering a had various effects on hydraulic conductivity values among the data sets. Figure 49 shows an example of how changing a had very little effect on hydraulic conductivity values, and Figure 50 shows the results of one of the data sets in which changing a had a larger effect on hydraulic conductivity values. On average, altering a did have a significant effect on the number of days that the filter could function before clogging and needing maintenance, which will be referred to as maintenance days, as predicted by the model. The average differences between the original model predicted

number of maintenance days and the altered *a* predicted maintenance days as a

percentage of total maintenance days for all data sets were 3%, 16%, 29%, -18%, and -38%

for the corresponding percentage changes in *a*, 1%, 5%, 10%, -5%, and -10%. A -38%

difference in maintenance days means that, for an *a* value with -10% error, the model

could determine a cleaning or replacement date which is months after the filter has

clogged. This indicates that *a* is a sensitive parameter, and fluctuations caused by errors

or other factors could have large impacts on the model outputs.

Altering *b* had less effect on hydraulic conductivity values than altering *a*. Figure

50 includes the same laboratory data as Figure 50, however, the changes in hydraulic

conductivity are much less in Figure 51, when altering *b* values than in Figure 50, when

altering *a* values. On average, altering *b* did not have a significant effect on the number

of maintenance days predicted by the model. The average differences between the

original model predicted number of maintenance days and the altered *b* predicted

maintenance days as a percentage of total maintenance days for all data sets were -1%, -

3%, -5%, 3%, and 7% for the corresponding percentage changes in *b*, 1%, 5%, 10%, -5%,

and -10%. Therefore, if *b* is altered by up to 10%, the number of maintenance days

predicted changes by less than 10%. This indicates that *b* is not a sensitive parameter,

and fluctuations caused by errors or other factors are not likely to have large impacts on

the model outputs.

Altering m_1 had little effect on hydraulic conductivity values similar to altering *b*.

Figure 52 includes the same laboratory data as Figures 50 and 51. The changes in

hydraulic conductivity are much less in Figure 52, when altering m_1 values than in Figure

50, when altering *a* values, and even less than the changes in Figure 51, when altering *b*

146

values. On average, altering m_1 did not have a significant effect on the number of

maintenance days predicted by the model. The average differences between the original

model predicted number of maintenance days and the altered m_1 predicted maintenance

days as a percentage of total maintenance days for all data sets were -1%, -3%, -7%, 4%,

and 7% for the corresponding percentage changes in m_1, 1%, 5%, 10%, -5%, and -10%.

Therefore, if m_1 is altered by up to 10%, the number of maintenance days predicted

changes by less than 10%. This indicates that m_1 is not a sensitive parameter, and

fluctuations caused by errors or other factors are not likely to have large impacts on the
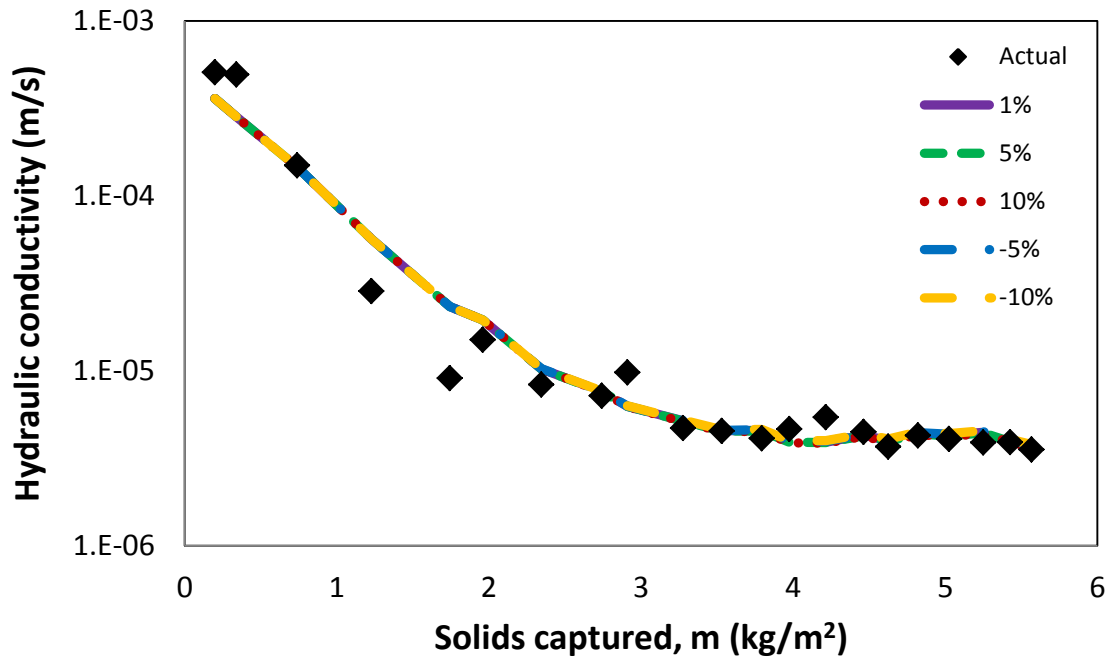
model outputs.

Figure 49. Hydraulic conductivity values as a function of mass of solids captured for

2.P1 data (Actual) and model predicted hydraulic conductivity values using altered *a*

values by 1%, 5%, 10%, -5%, and -10%.

Figure 50. Hydraulic conductivity values as a function of mass of solids captured for 1.P1 data (Actual) and model predicted hydraulic conductivity values using altered *a* values by 1%, 5%, 10%, -5%, and -10%.
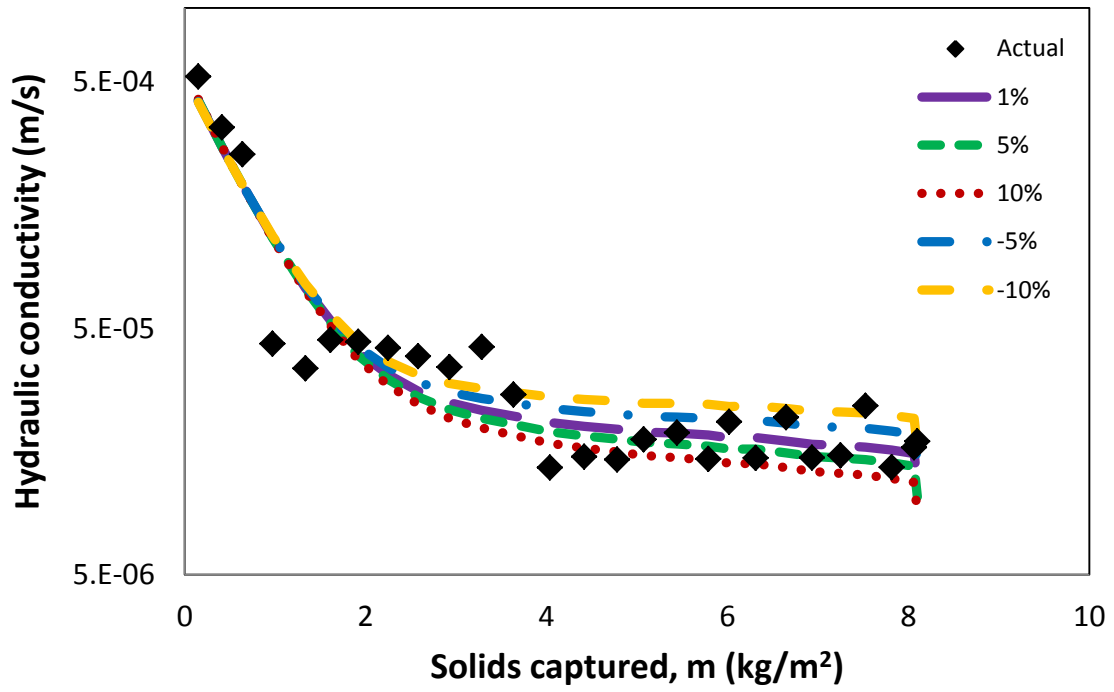
Figure 51. Hydraulic conductivity values as a function of mass of solids captured for

1.P1 data (Actual) and model predicted hydraulic conductivity values using altered *b*

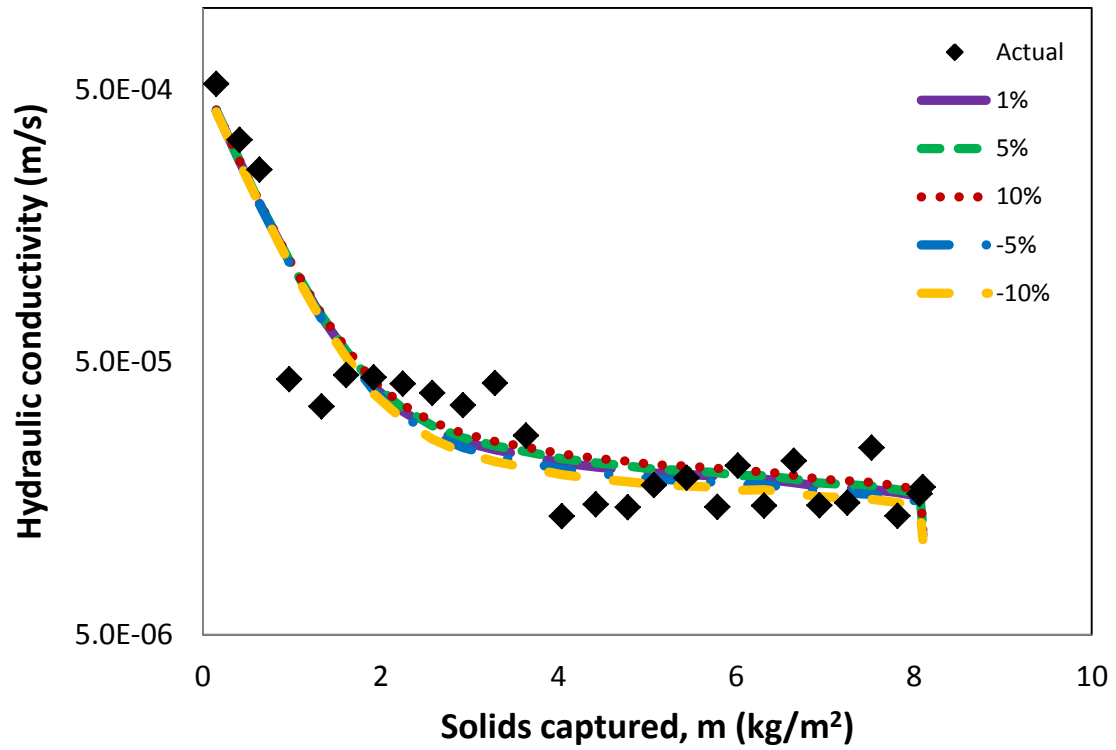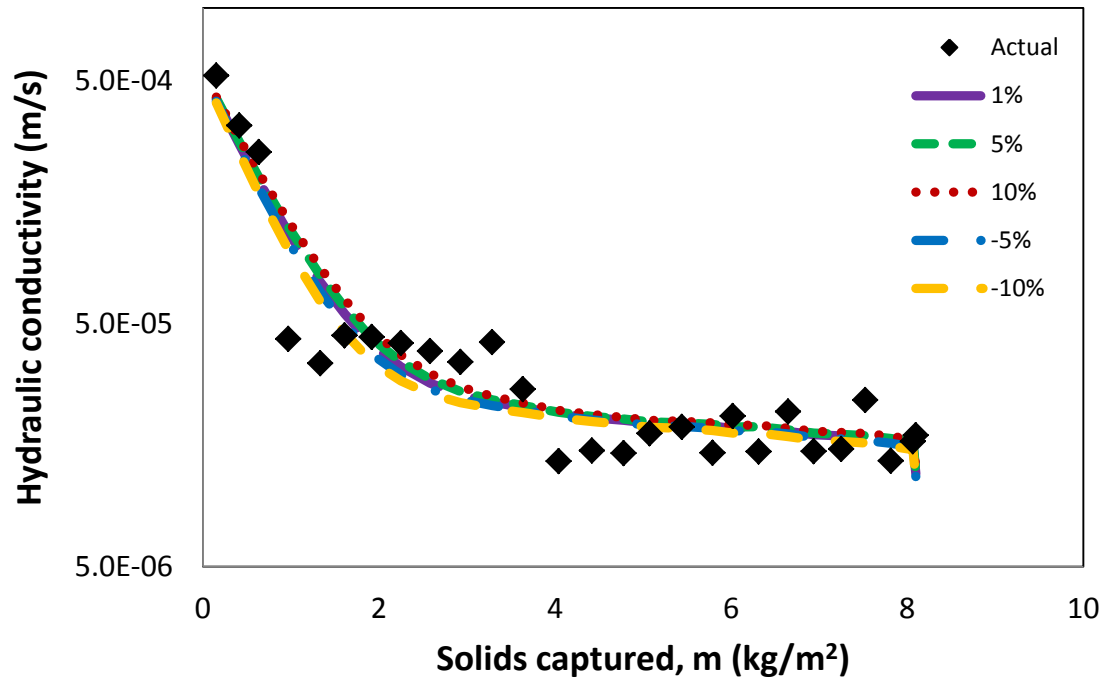values by 1%, 5%, 10%, -5%, and -10%.

Figure 52. Hydraulic conductivity values as a function of mass of solids captured for 1.P1 data (Actual) and model predicted hydraulic conductivity values using altered m_1 values by 1%, 5%, 10%, -5%, and -10%.

EVALUATION OF MODEL PARAMETERS

a

According to Faure et al. (2006), the parameter *a*, is a dimensionless parameter to be

fitted. Faure et al. (2006) states that *a* characterizes the way head loss increases during

the accumulation of particles in series. Larger values of *a* should indicate quicker

accumulation of particles in series and therefore, quicker clogging. This was confirmed

by the data in this study by plotting *a* versus the mass of solids loaded to the filter at the

time of clogging and the mass of solids captured by the filter at clogging in Figure 53.

As seen in Figure 53, as the mass of solids loaded or captured increases, *a* decreases.

Therefore, a larger *a* does indicate quicker clogging in terms of solids loaded to or

captured by the filter.

According to Faure et al. (2006), *a* depends mainly on the structure of the

geotextile and somewhat on the concentration of particles; it is seen to decrease slightly

for decreasing concentrations and is independent of thickness when the structures stay the

same. However, because *a* characterizes the accumulation of particles in series and

indicates how quickly clogging occurs during this phase, it is more reasonable to

hypothesize that the particle sizes play a larger role in determining the value of *a* than the

structure of the geotextile or concentration of particles. Further, particle size should be

the most important parameter defining *a* because it is the filter cake formed by the

particles that is capturing most of the particles in series accumulation rather than the filter

itself. The data in this study confirmed this hypothesis; the greatest correlations between

a and a study parameter, such as particle size or opening size, were seen with D_{60} and D_{10},

as well as D_{60}/D_{10}, the coefficient of uniformity of the soil particles. Figures 54 and 55 show the correlation between a and D_{10} and D_{60}, respectively. As D_{10} or D_{60} increases, a decreases. This result follows the theory that larger particles form a more porous and open cake than smaller particles, and larger particles do not cause clogging as quickly as smaller particles in terms of solids loading. Values of a as a function of the uniformity coefficient are shown in Figure 56. As the coefficient of uniformity increases, a increases. This indicates that as the difference between particle sizes in a distribution increases, the rate of clogging increases, which is reasonable because the smaller particles will fill the spaces between the larger particles in the filter cake leading to more immediate clogging of the filter (Eliasson 2002).

Although there is a correlation between a and D_{60}/D_{10} ($R^2 = 0.5$ for a linear relationship), there are limitations to using the relationship between these parameters given in this study. As stated earlier, the model output is very sensitive to small changes in a. A 10% error in a could produce a nearly 40% change in the number of filter operating days predicted by the model, and the values of a for one D_{60}/D_{10} value vary by more than 10% (Fig. 56). Therefore, more research is needed to more precisely define the relationship between a and D_{60}/D_{10} before use in the hydraulic conductivity model.
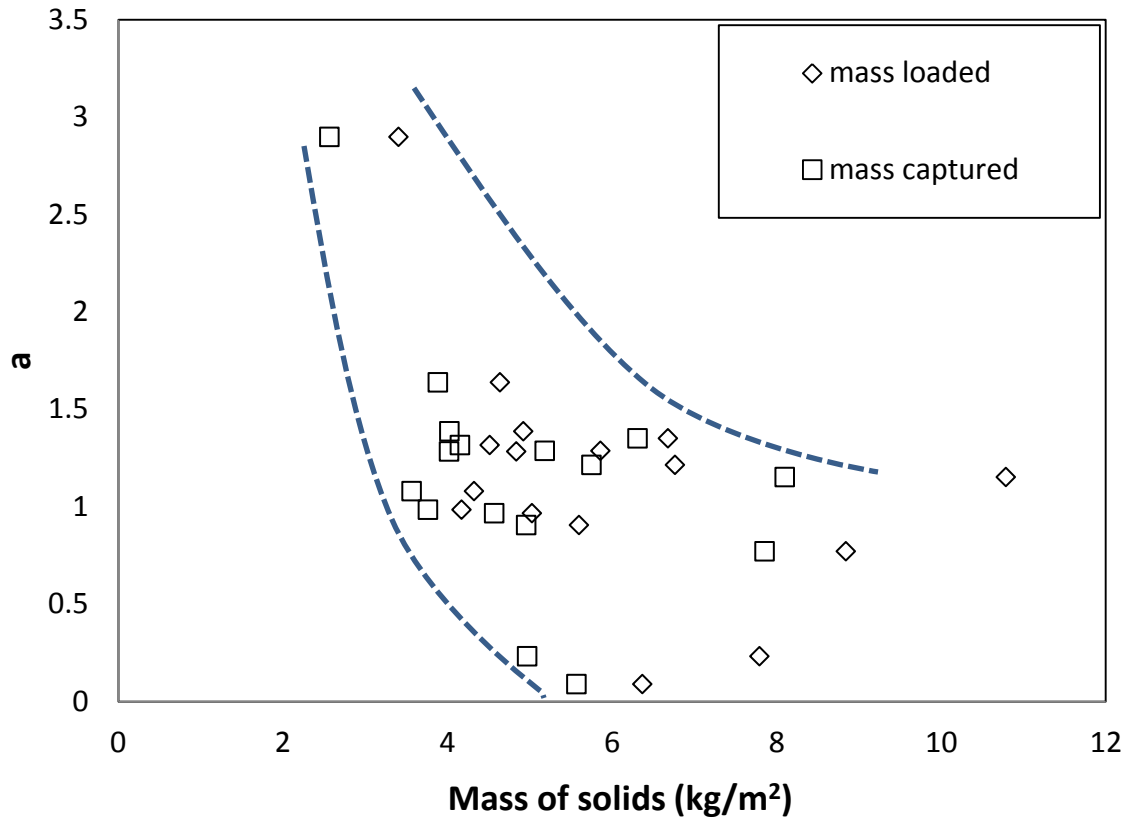
Figure 53. Values of *a* as a function of the mass of solids loaded to the filter and mass of

solids captured in and on the filter at the end of testing, i.e., after clogging. Dashed lines

highlight overall trend in values of *a*.

Figure 54. a values as a function of D_{10} for all data sets with influent TSS concentration of 200 mg/L and influent flow rate of 6 mL/s. Dashed lines highlight overall trend in values of *a*.
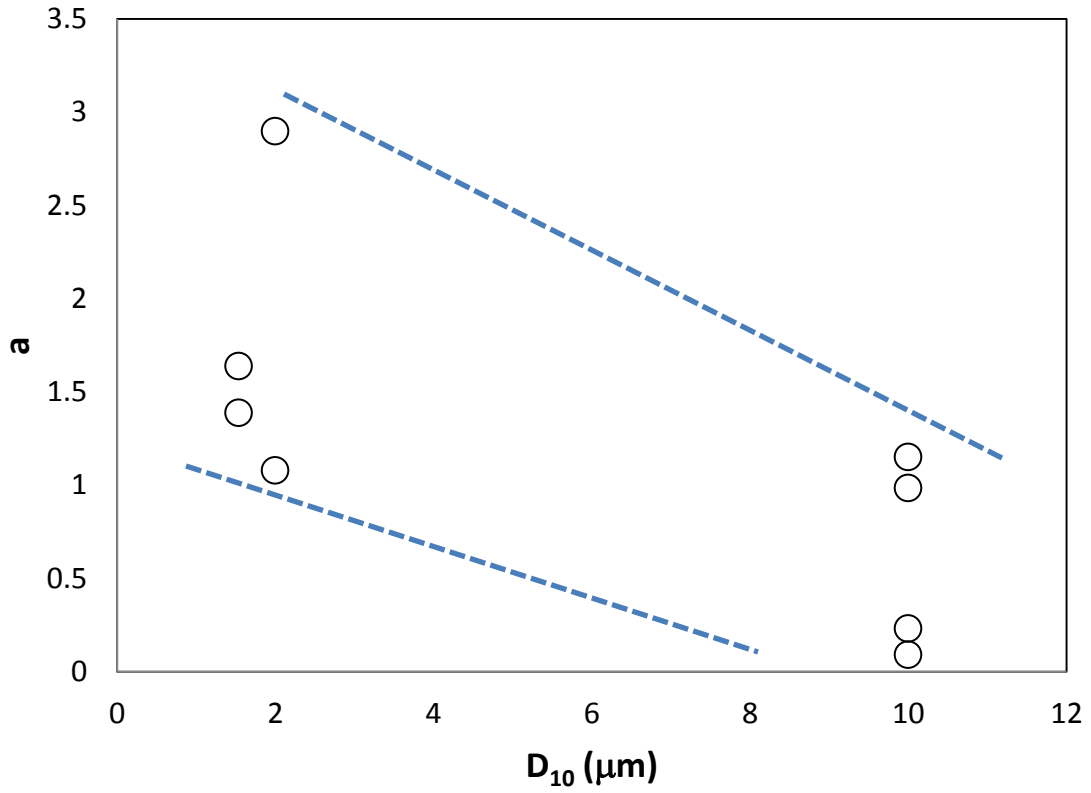
Figure 55. *a* values as a function of D_{60} for all data sets with influent TSS concentration of 200 mg/L and influent flow rate of 6 mL/s. Dashed lines highlight overall trend in values of *a*.

Figure 56. a values as a function of the coefficient of uniformity for all data sets with influent TSS concentration of 200 mg/L and influent flow rate of 6 mL/s. Dashed lines highlight overall trend in values of *a*.
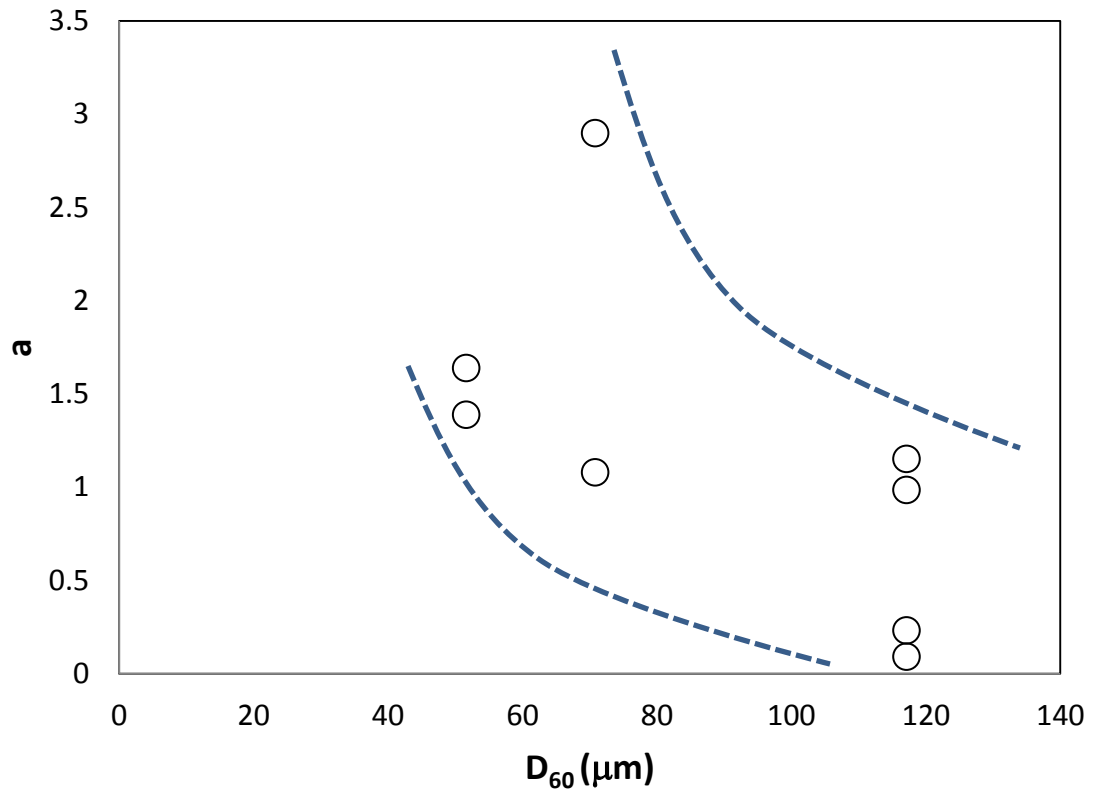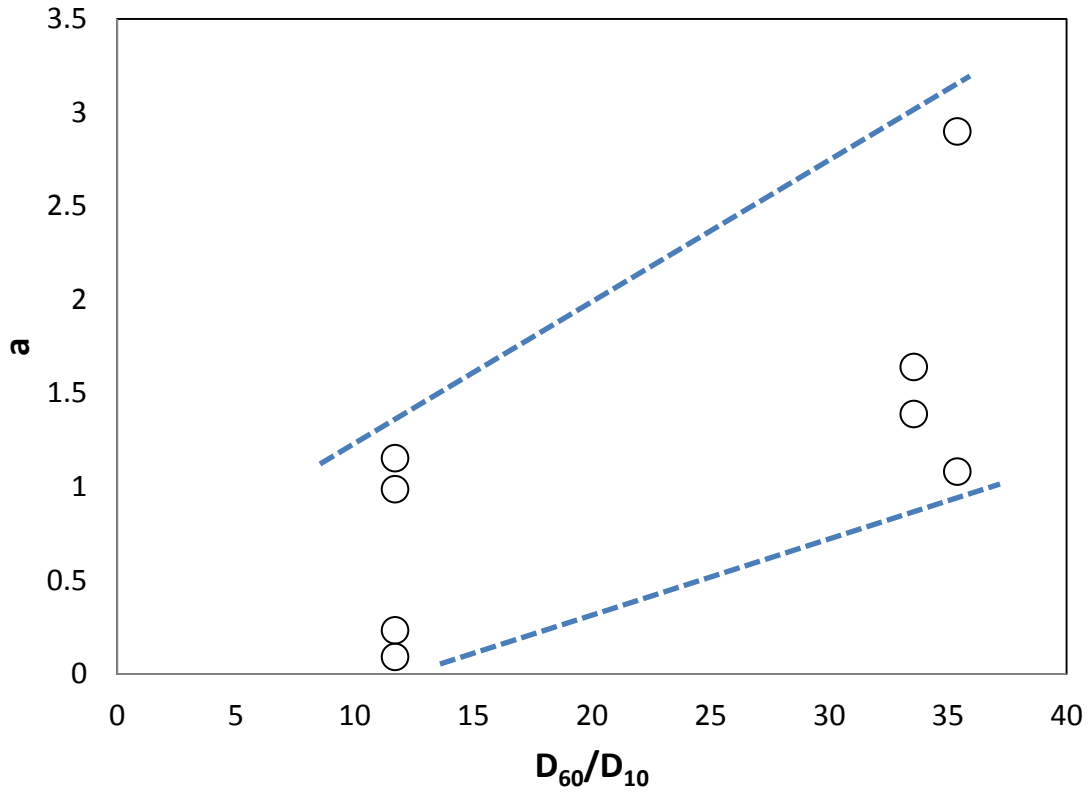
b

The parameter *b*, is a dimensionless parameter in Le Coq's model which characterizes the

relative contribution of accumulation in series versus accumulation in parallel. If *b*

increases, the proportion of accumulation in series will increase as well. According to

Faure et al. (2006), *b* is constant for geotextiles with the same structure, regardless of

concentration, but *b* changes with changing structures and opening sizes. Also, if particle

size of the soil increases, *b* increases because larger particles would clog the pore spaces

faster than smaller particles, filling the vertical channels within the filter and leading to

accumulation in series more quickly (Faure et al 2006). However, the data from this

study does not show an increase in *b* with increasing particle diameter D. An inverse

relationship may exist between *b* and D_{10} and D_{60}, as seen in Figures 57 and 58,

respectively. While no strong correlation existed between *b* and any particular particle

size, D_{10} and D_{60} were chosen to be the particle sizes most likely to have an impact on *b*

because they had the strongest correlation with *a*. A plot of *a* versus *b* in Figure 59

shows that as *a* increases, *b* increases as well. Therefore, it is likely that the parameters

impacting *a* also impact *b*. The relationship between *b* and D_{60}/D_{10} is shown in Figure 60.

The parameter *b* is a function of filter opening sizes because opening sizes in the

filter affect the amount of solids retained within the filter and therefore affect the

proportion of accumulation occurring in parallel (when particles accumulate within the

filter) versus series (when particles accumulate on the filter surface). According to the

data in this study, *b* increases with increasing average of the largest pore sizes in the filter,

(O_{large}) (Figure 61). The same relationship is observed for *b* and O_{small}, an average of the

smallest pore sizes (Figure 62). It should be noted that a strong correlation does not exist

between *b* and these opening sizes, and more data are likely needed to verify any relationship between *b* and opening size. The parameter *b* is difficult to assess intuitively. One might hypothesize that as opening sizes increase, *b* would decrease because more particles would become trapped in the filter before the transition to series accumulation. This may be true; however, more particles becoming captured during parallel accumulation does not necessarily mean that the proportion of accumulation in parallel will be larger than the proportion in series. The parameter *b* only describes the proportion of accumulation in series, not the amount of solids captured during either period of accumulation.

Because ratios of pore sizes to particle sizes play a large role in the criteria used to choose the appropriate geotextile for filtration, the ratios likely impact the values of *b*. The *b* values were plotted as a function of various ratios to determine correlations between them and *b*. The ratio between O_{large}/O_{small} and D_{60}/D_{10} was chosen to be the parameter most likely to impact *b* because there were slight correlations with *b* and O_{large}, O_{small}, D_{60}, and D_{10} as discussed earlier. Although the coefficient of determination (R^2) for each of the trendlines of *b* as a function of each of the parameters O_{large}, O_{small}, D_{60}, and D_{10} (Figures 57, 58, 61, and 62) is low, i.e., approximately 0.3, which is not is in the good range of fit, the correlations between *b* and these parameters were greater than with all other opening sizes and particle sizes (Ayyub and McCuen 2003). Also, O_{large}/O_{small} / D_{60}/D_{10} was determined to be an accurate new retention criteria for effective geotextile in stormwater filtration. The ratio showed the strongest correlation with *b* when compared with other O_x/O_y / D_a/D_b ratios, and the relationship is shown in Figure 63. However, the

correlation is still very small ($R^2 = 0.2$ for a linear relationship), and one should exercise

caution before using this relationship in the hydraulic conductivity model.

Figure 57. *b* values as a function of D_{10} for all data sets with influent TSS concentration of 200 mg/L and influent flow rate of 6 mL/s. Dashed lines highlight overall trend in values of *b*.
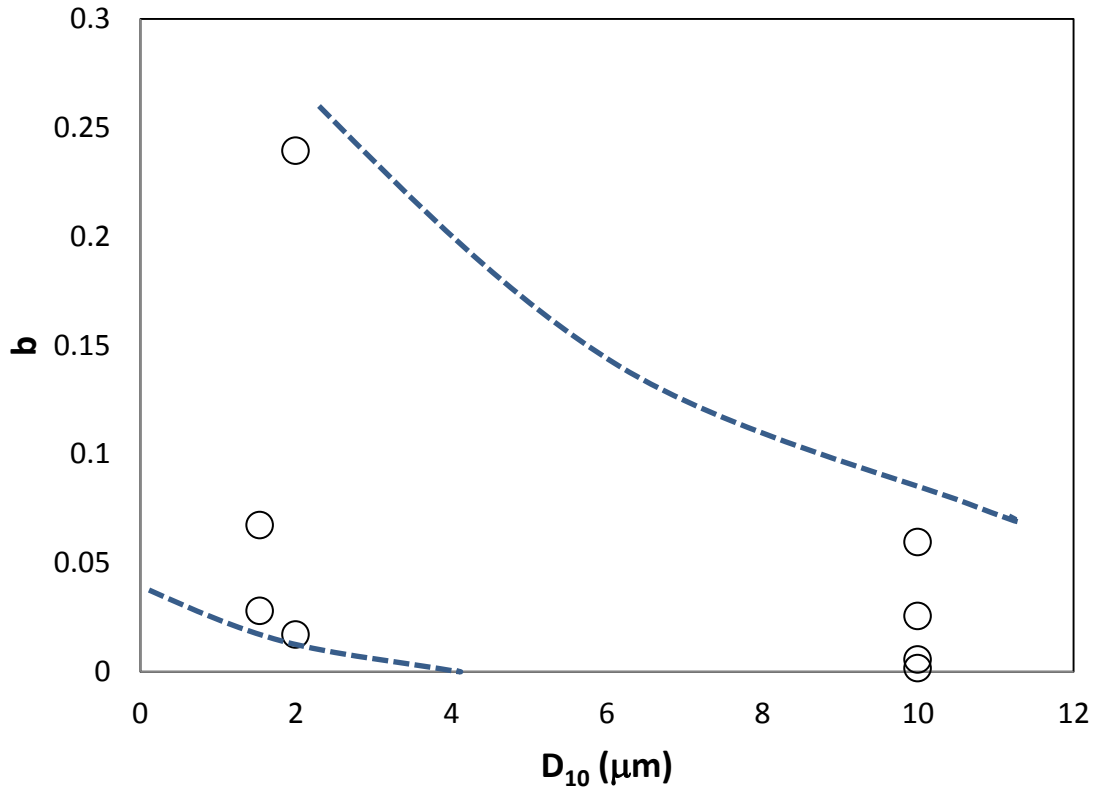
Figure 58. *b* values as a function of D_{60} for all data sets with influent TSS concentration of 200 mg/L and influent flow rate of 6 mL/s. Dashed lines highlight overall trend in values of *b*.

Figure 59. All *b* values as a function of *a*
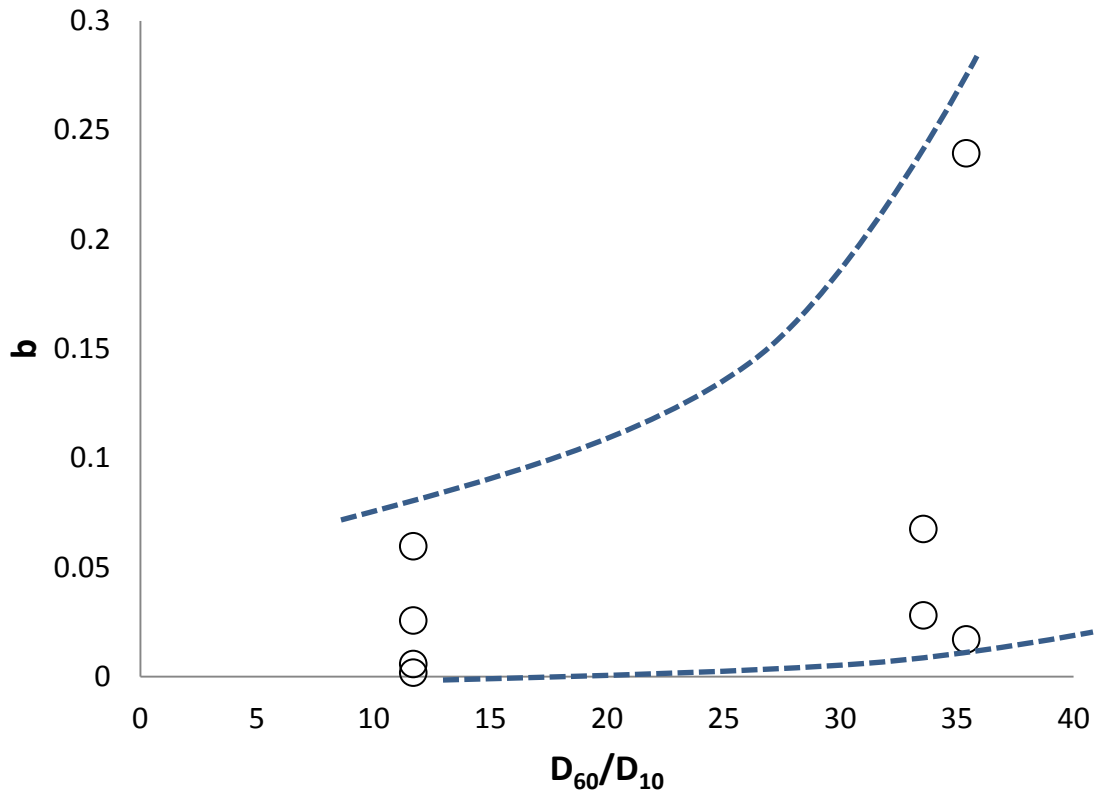
Figure 60. *b* values as a function of the coefficient of uniformity for all data sets with influent TSS concentration of 200 mg/L and influent flow rate of 6 mL/s. Dashed lines highlight overall trend in values of *b*.

Figure 61. *b* values as a function of O_{large} (AVERAGE(O_{95}, O_{100})) for all data sets with influent TSS concentration of 200 mg/L and influent flow rate of 6 mL/s. Dashed lines highlight overall trend in values of *b*.

Figure 62. *b* values as a function of O_{small} (AVERAGE(O_{10}, O_{20}, O_{30})) for all data sets with influent TSS concentration of 200 mg/L and influent flow rate of 6 mL/s. Dashed lines highlight overall trend in values of *b*.
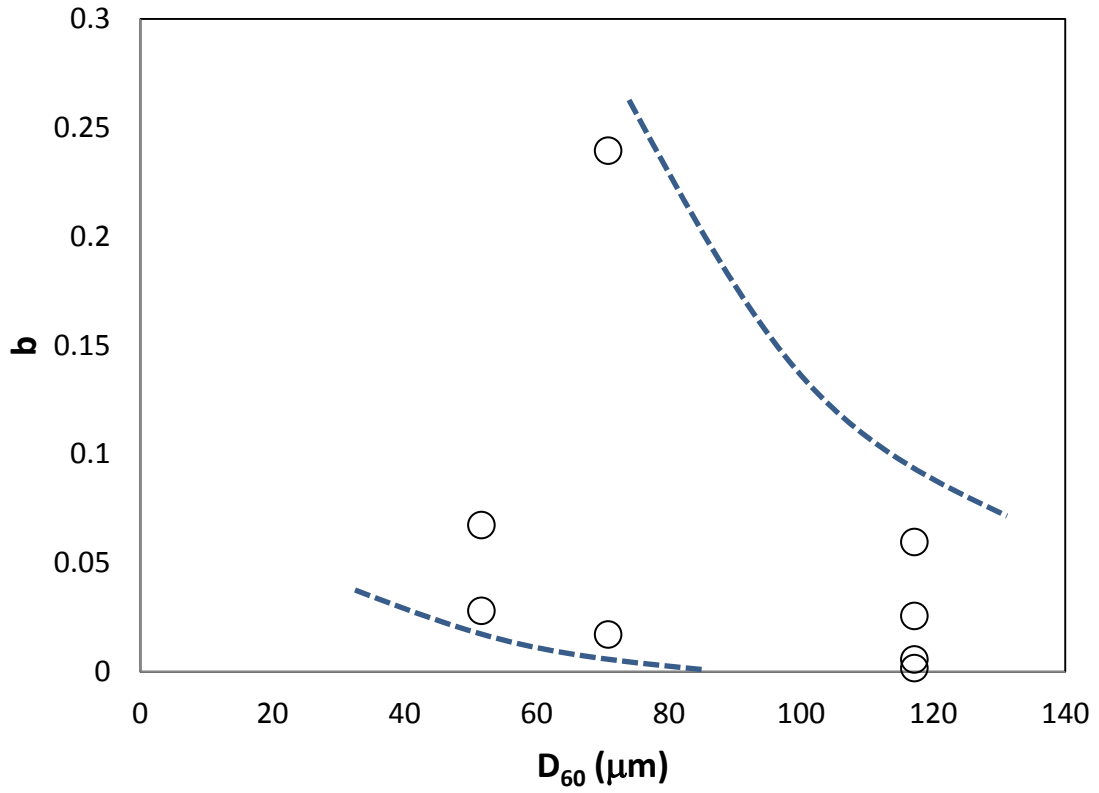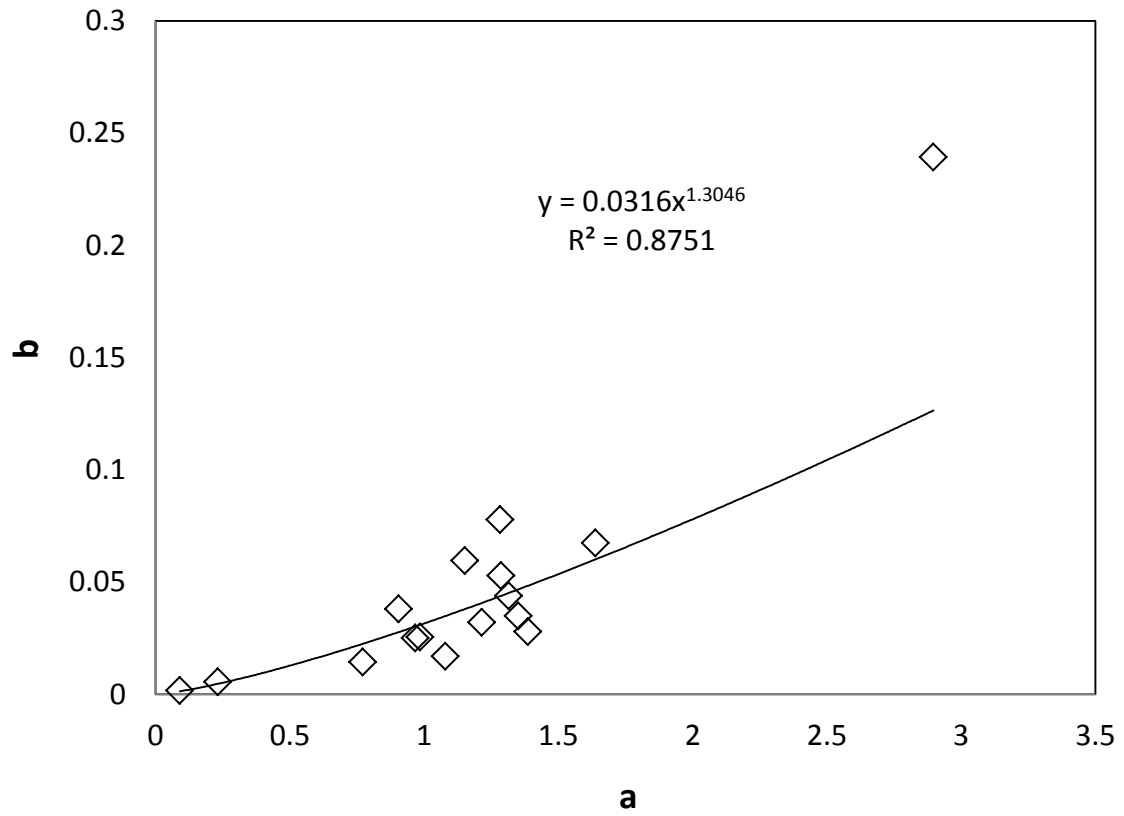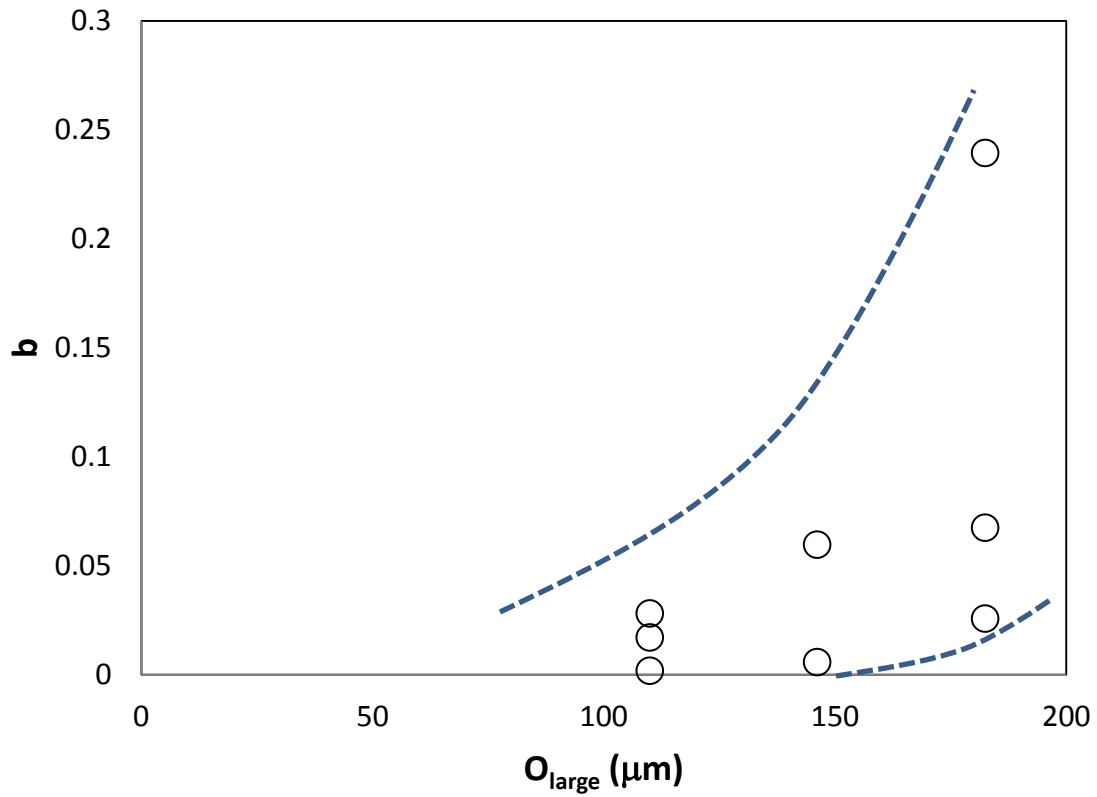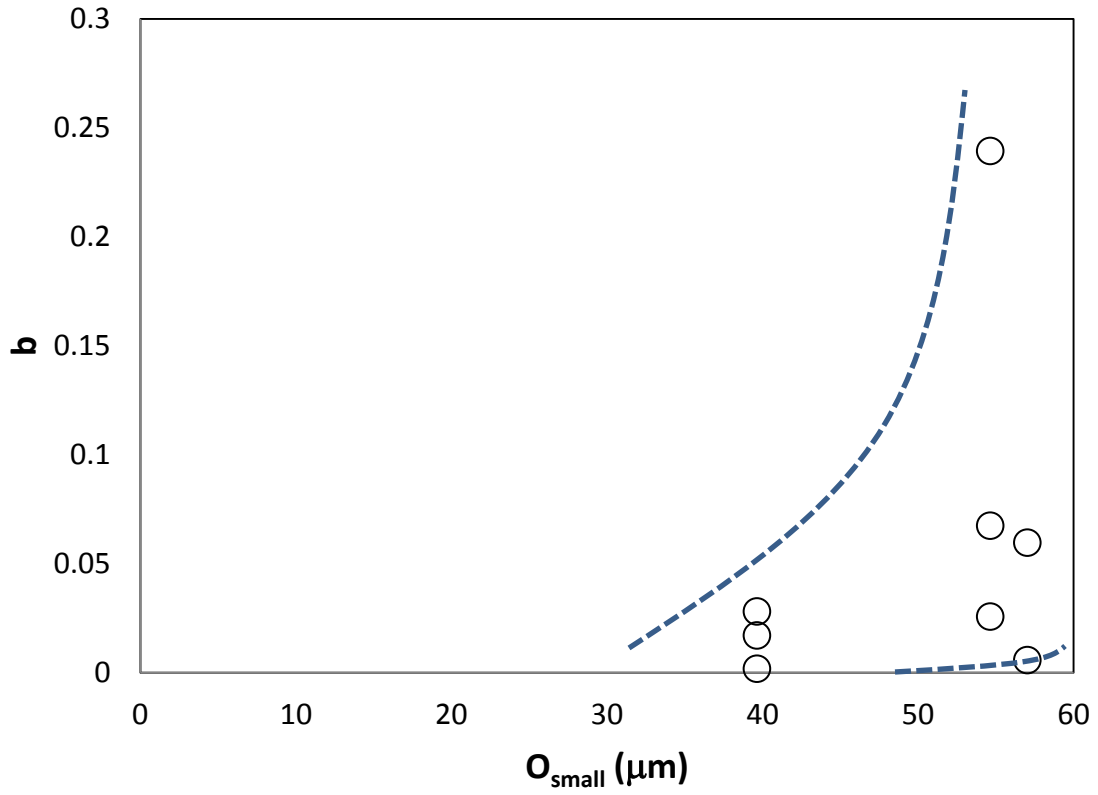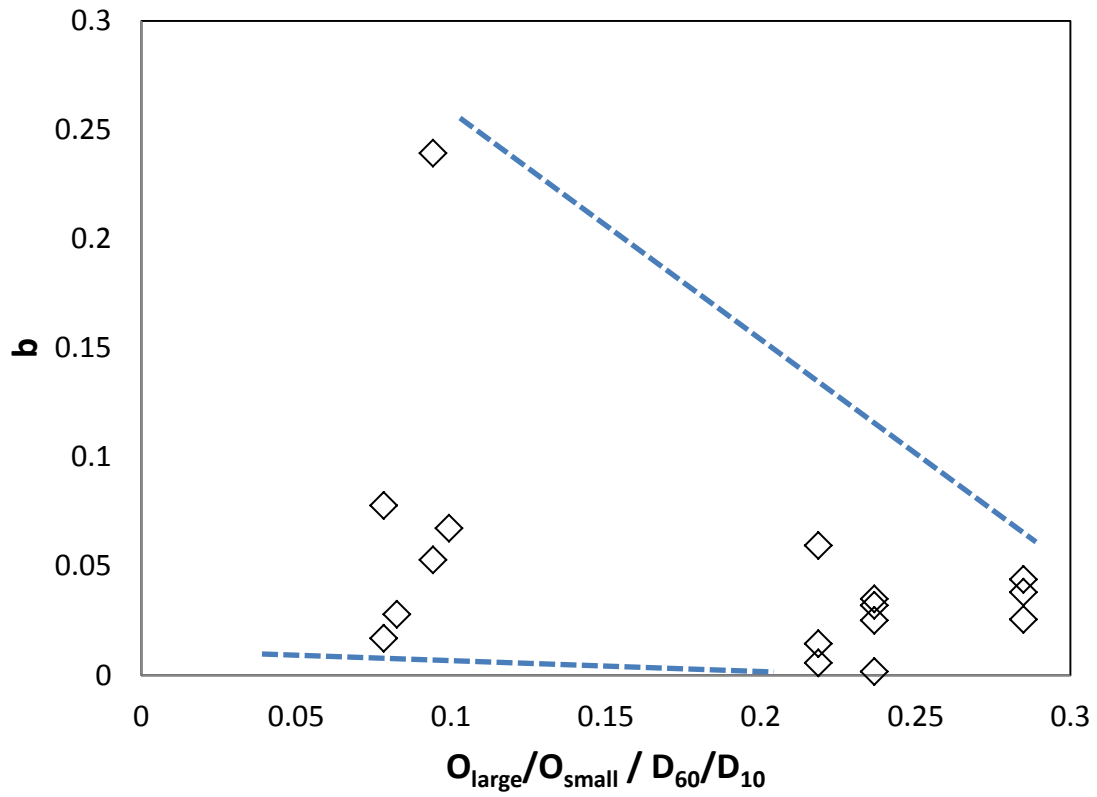
Figure 63. All *b* values as a function of O_{large}/O_{small} / D_{60}/D_{10}. Dashed lines highlight overall trend in values of *b*.

167

m₁

A smaller m_1 value for a given geotextile indicates more rapid clogging (Faure at al., 2006). To confirm that a smaller m_1 indicates an earlier final clogging point in terms of total mass of solids loaded to the filter, m_1 values from this study were plotted against the mass of total solids loaded to the filter at the final clogging point in Figure 64. As seen in Fig. 64, as the m_1 values increase, total mass of solids loaded increases as well, confirming the findings of Faure et al. (2006). Also, with a greater amount of solids captured within the filter at the transition from parallel to series accumulation, it is reasonable that a larger amount of solids could be captured at the final clogging point and thus a greater amount of solids could be loaded to the filter.

The parameter m_1 is dependent on particle sizes and opening sizes because both affect the mass of solids that the filter can capture before the transition from parallel to series accumulation. Values of m_1 were plotted against various O_x/O_y / D_a/D_b ratios and the ratio with the strongest correlation with m_1 was O_{large}/O_{small} / D_{95}/D_{30} where correlation is defined by the correlation coefficient, R, which is greater than 0.8 for the trendline shown in Figure 65. Also, O_{large}/O_{small} / D_{95}/D_{30} was one of the new retention criteria ratios developed for choosing the appropriate geotextile for stormwater filtration. Figure 65 shows that as this ratio increases, m_1 increases.

The parameter m_1 depends on the concentration of particles, C_0. Although Faure et al. (2006) states that m_1 is nearly independent of the concentration C_0, it was hypothesized that m_1 is actually dependent on C_0 in order for m_1 to have the correct units involving mass. Plotting m_1 values against various parameters in this study showed that

m_l is a function of both influent TSS concentration and influent flow rate. More simply, m_l is a function of m_L, the mass of solids loaded to the filter per each 75 minute test.

$$m_L = \frac{C_0 q (75 \min)}{A} \tag{25}$$

m_l is a function of both m_L and O_{large}/O_{small} / D_{95}/D_{30}. Figures 66 and 67 show m_1 as a function of $m_L \times O_{large}/O_{small}$ / D_{95}/D_{30}, and Figure 67 includes linear trendlines with a coefficient of determination, R^2 for each trendline. Both coefficients of determination are above 0.6 which means that the correlation coefficient, R, for each trendline is greater than 0.7 indicating a good fit. Therefore, the linear equation for the trendline of all of the data in this study could be an accurate predictor of m_1 for future use of the model in predicting hydraulic conductivity of a geotextile filter during stormwater filtration. However, as with a and b, caution should be used with the relationship given between m_1 and $m_L \times O_{large}/O_{small}$ / D_{95}/D_{30} because a limited number of data points were used to determine the relationship and because one of the points in Figure 66 is around 25% greater than the value predicted by the trendline. According to the sensitivity analysis performed earlier, 5% and 10% changes in m_1 result in 3 – 4% and 7% changes in number of maintenance days predicted by the model. Therefore, a 25% change in m_1 would likely result in an 18% change in maintenance days, which could mean a delay in maintenance of the filter by over two months for a filter that lasts 365 days.

Thickness of geotextile filter may also play a role in the value of m_1. Intuitively, a thicker geotextile would be able to retain a greater amount of solids before the transition to series accumulation. According to Faure et al. (2006), smaller m_1 values were observed for thinner geotextiles under the same conditions at thicker geotextiles. However, the geotextiles used in this study had very similar thicknesses (2.3-3.2 mm); no

significant differences in m_1 were observed between the thickest and the thinnest geotextile. More studies with geotextiles of varying thicknesses may be needed to address the effect of thickness on m_1.
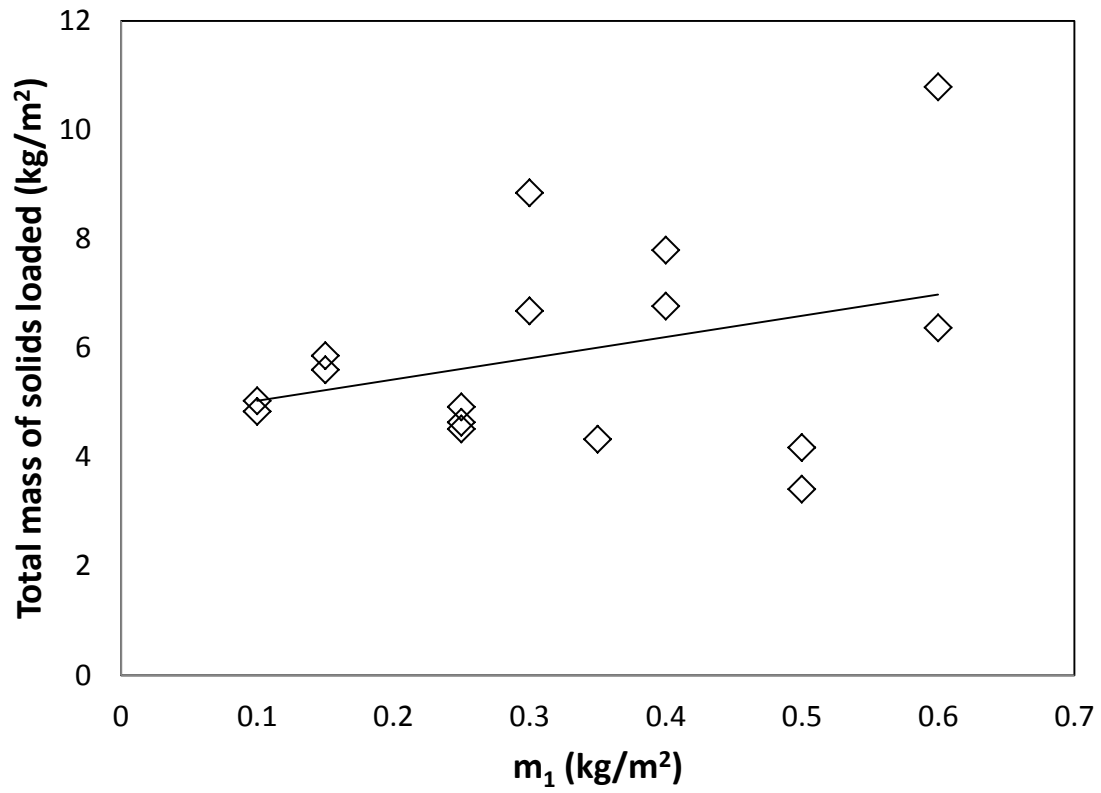
Figure 64. The total mass of solids loaded to the filter at the final clogging point as a function of all *m₁* values.
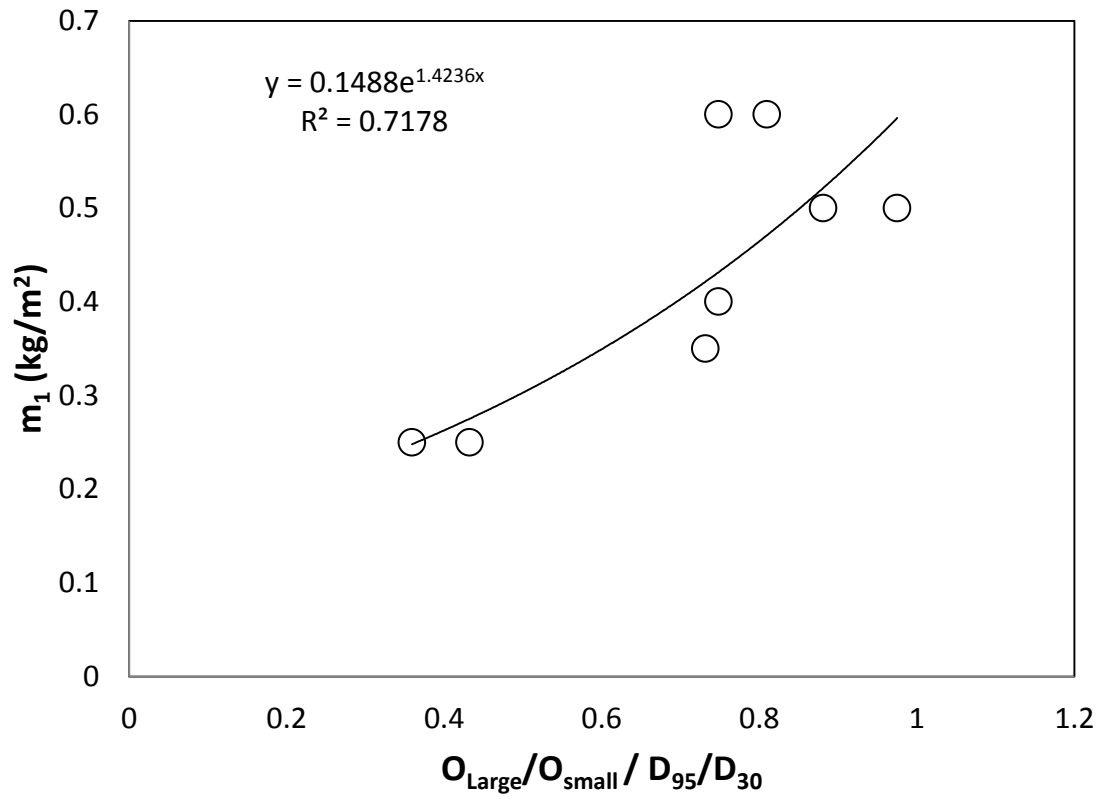
Figure 65. m_1 as a function of of O_{large}/O_{small} / D_{95}/D_{30} for all data sets with influent TSS concentration of 200 mg/L and influent flow rate of 6 mL/s.
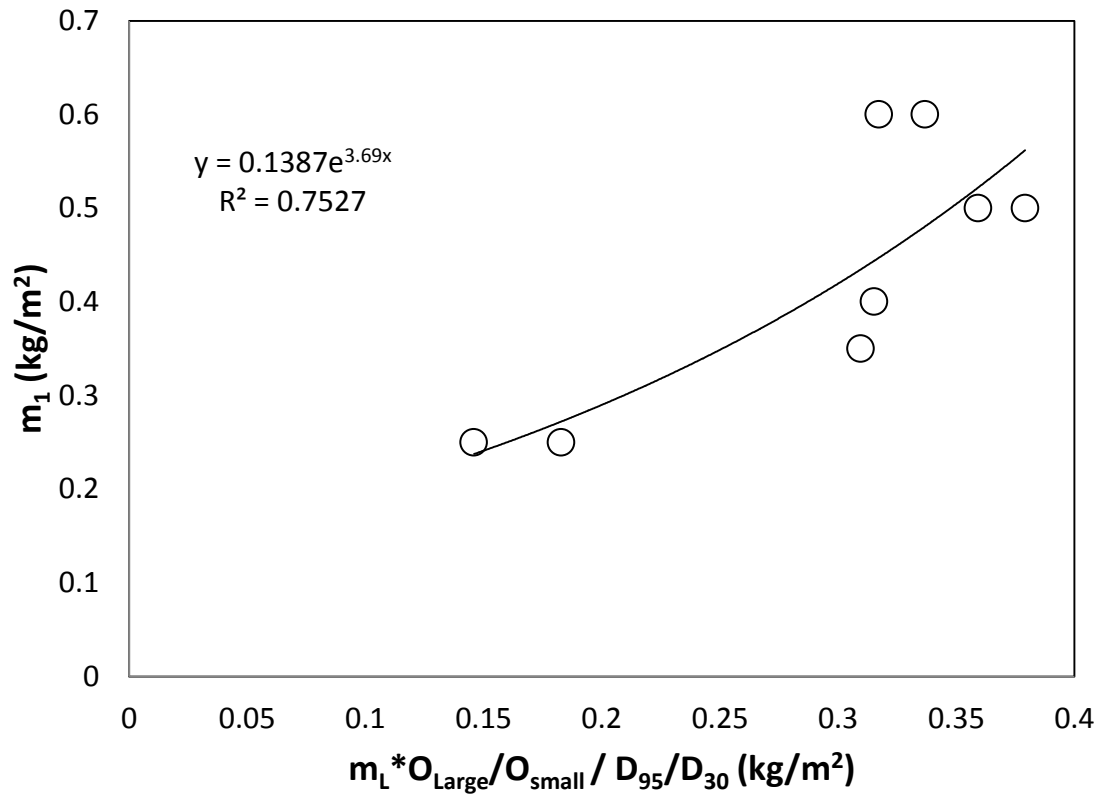
Figure 66. m_1 as a function of of m_L*O_{large}/O_{small} / D_{95}/D_{30} for all data sets with influent

TSS concentration of 200 mg/L and influent flow rate of 6 mL/s.
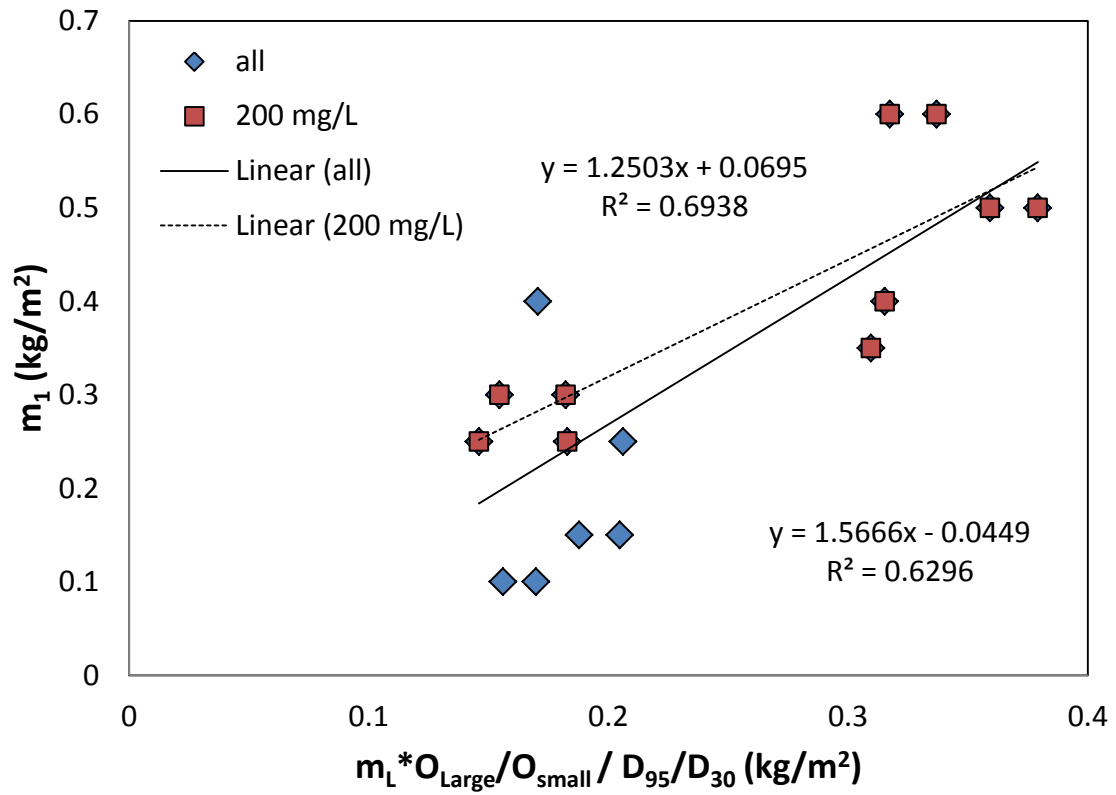
Figure 67. All values of m_1 as a function of of $m_L*O_{large}/O_{small} / D_{95}/D_{30}$.

v/v$_{in}$

The outlet flow rates throughout testing were found to be dependent upon the mass of solids captured by the filter and were input directly into the model to find the appropriate *a* and *b* values. Analysis of the flow rates as a function of solids captured led to the assessment that when $m < m_1$, $q = q_{in}$, and when $m > m_1$, q/q_{in} is a linear function of *m*. Averaging the slopes and y-intercepts of q/qin versus m for every test in this study gives an average slope of -0.07444 and an average y-intercept of 1.0540. Therefore, an estimate of q/q_{in} (or v/v_{in}) when $m > m_1$ is:

$$\frac{v}{v_{in}} = -0.07444m + 1.0540 \tag{26}$$

CONCLUSIONS

The model developed in Equation 19 provides a means of predicting hydraulic conductivity of a geotextile filter in stormwater filtration with good accuracy. The model provides a way in which stormwater management professionals can predict the lifespan of the filter. Knowing the duration of treatment by the geotextile filter will allow for more accurate estimations of when maintenance or replacement of the filter is needed. Precise maintenance plans can minimize the cost and labor of underground filter maintenance.

The model in Equation 19 can also provide a means of predicting hydraulic conductivity of a geotextile filter in other applications additional to stormwater treatment. The model predicts hydraulic conductivity values as a function of solids captured. The solids captured by a geotextile filter do not have to be specifically those from stormwater runoff for the model to be applicable.

The parameters a, b, and m_1 in the function were analyzed as functions of the most important parameters in geotextile filtration of suspended solids in stormwater. The assessments provided by this study form a foundation for the development of the specific functions that can be used to predict a, b and m_1 with knowledge of a few parameters. However, these functions require further study as a result of the sensitivity of the model to errors in a, b, and m_1.

Chapter VI: FIELD TESTING

INTRODUCTION

This section of the research project was initiated in order to better understand the application of a geotextile filter for stormwater treatment under actual field conditions. A prototype was constructed which represented a filter system that would be placed directly inside the upper portion of a storm drain, approximately 30-60 cm (1-2 ft) below the storm drain inlet at the side of a roadway. First, preliminary laboratory testing was performed on this prototype. Next, the prototype was set up at the end of concrete channel where stormwater from a heavily trafficked parking lot was funneled in order to evaluate the filtration of real runoff by the geotextile.

LABORATORY TESTING OF THE PROTOTYPE

METHODOLOGY

The prototype, pictured in Figure 68, consisted of a 132 cm^2 (20.5 in^2) sheet of nonwoven geotextile attached to a 135 cm^2 (21 in^2) metal frame with metal walls approximately 5 cm (2 in) in height on all four sides and a metal screen on top of the filter to catch leaves and other large debris. The geotextile was attached to the frame by 20 small bolts, and 2 metal posts which hold extendable bars for placement in a storm drain extended across the frame. NW1 was chosen for use in the prototype. Although NW1 was not as successful at reducing suspended solids concentrations in laboratory tests as the NW2 and NW3 filters, NW1 was chosen because the application of the prototype is to capture

suspended solids from runoff directly flowing off of a parking lot, highway or other impervious surface. The assumed application for geotextiles tested in column studies in the laboratory was to retrofit urban sand filter systems in which stormwater runoff must first flow through a retention basin. When the runoff is not directed into a retention basin as with the prototype application, the particles are assumed to generally be larger because the flows are faster allowing less settling (Sansalone et al. 2009). NW1 had a larger apparent opening size and permittivity than NW2 and NW3 which means that it may not fine particles as effectively as NW2 and NW3, but it should maintain a larger hydraulic conductivity throughout its lifespan than the other filters. Also, with a larger distribution of particle sizes in actual runoff, clogging is likely to occur faster regardless of the geotextile chosen (Eliasson 2002).

In order to collect the effluent from the filter during laboratory testing, the prototype was set on top of a 91 cm ×61 cm ×20 cm (36" ×24" ×8") plastic tub which was lined with sloped plastic sheets and plastic drop cloth to ensure that the water would flow continuously out of the outlet. At the outlet, i.e., a hole drilled in one end of the tub, vinyl tubing was inserted to direct the effluent to sampling bottles. The remaining materials consisted of a pump, pump tubing, plastic sampling bottles, and a mixer. The testing setup is pictured in Figure 69.

A simulated stormwater suspension was created using the same soil that was used for geotextile column studies (i.e., a silty soil collected from a landfill cover in Polson County, Montana) with a particle size distribution P1 described in the Chapter II.

Approximately 20 g of soil were added to a container of 100 L filled with tap water at room temperature to achieve a TSS concentration of approximately 200 mg/L

which is slightly higher than the average event mean concentration (EMC) for TSS in stormwater runoff events occurring in urban areas (Sansalone et al. 1998; Furumai et al. 2002; Taebi and Droste 2004; Sansalone et al. 2005; Barrett et al. 2006; Flint and Davis 2007; Hallberg and Renman 2008; Kim and Sansalone 2008; Li and Davis 2008). Several 100 L batches of simulated stormwater were used per test. The total volume of water used was dependent upon the duration of the test and flow rate of the influent suspension. A mixer powered by a Minarik motor vigorously mixed the simulated stormwater solution at approximately 100 RPM in order to keep the soil particles suspended. Initially, the simulated stormwater was applied to the prototype at an influent flow rate of approximately 8 L/min. For a geotextile filter with an area of 0.27 m^2, the influent flow rate corresponded to a hydraulic loading rate (HLR) of 0.49 mm/s (69 in/hr). Assuming a runoff area-to-drainage area ratio of 50, the HLR corresponds to an approximate rainfall rate of 3.6 cm/hr (1.4 in/hr), approximately 10 times greater than the rainfall rate for the highest frequency of rainfall events for the state of Maryland (0-0.254 cm, 1 hr; Kreeb 2003). Once the prototype tray began to fill up with water within 5 minutes of testing, the flow rate was reduced to 2.5 L/min, which corresponds to an HLR of 0.15 mm/s (21 in/hr). With a runoff area-to-drainage area ratio of 50, this HLR corresponds to an approximate rainfall rate of 1.1 cm/hr (0.44 in/hr), approximately double the rainfall rate for the highest frequency of rainfall events for the state of Maryland (Kreeb 2003).

Several measurements were taken during testing. Head losses were measured using rulers taped to the inner walls of the tray to assess water levels. Outlet flow rates were calculated by measuring the volume of water exiting the tub in a given amount of

time. After the suspension passed through the geotextile filter, samples of effluent were collected in plastic containers every 8 minutes, and TSS concentration measurements were conducted using Standard Method 2540 B (Eaton et al. 1995). Each test was run for 75 minutes because rainfall events between 0 and 2 hours occur at a higher frequency than all other rainfall events in the state of Maryland (Kreeb 2003). Nine effluent samples were collected during each test, and the TSS concentrations of all nine samples were used to calculate an effluent TSS EMC value for each test using Equation 1 and the method described in Chapter II. Influent samples were collected twice for each 100 L tub of suspension used, once at the onset of use when the tub was full and once at the end of use when the tub was nearly empty. After 75 minutes of treatment, the test was stopped and the filter was allowed to dry by exposing the surface to the atmosphere for 2 or more days. Subsequently, the suspension loading was continued for another 75 minutes, and effluent samples were collected. The process was repeated for several tests, stopping at 75 minutes or whenever the ponded water level reached the top of the tray (4.5 cm). Clogging was defined to occur when the height of standing water on the filter reached the top of the prototype tray within 20-25 minutes of testing because this was the criteria established for the smaller-scale laboratory column tests. The initial test in which the higher influent flow rate (8 L/min) was primarily used is addressed as Test 1P in this study, and the second test in which the lower influent flow rate (2.5 L/min) was solely used is addressed as Test 2P.
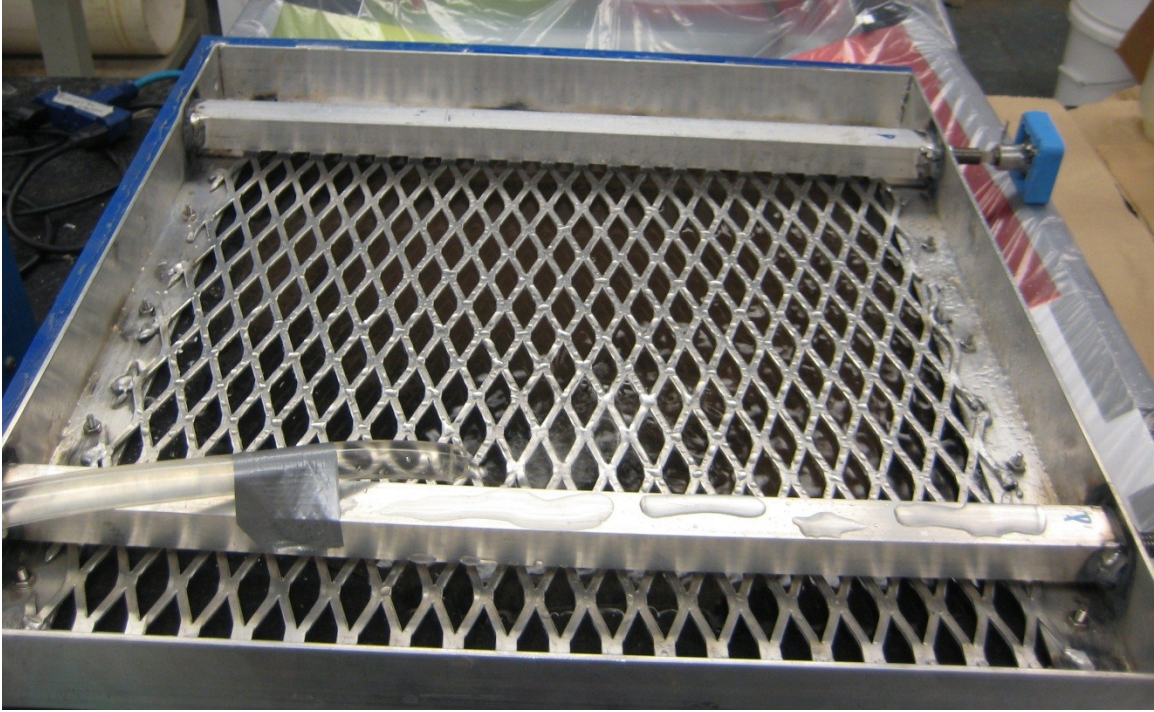
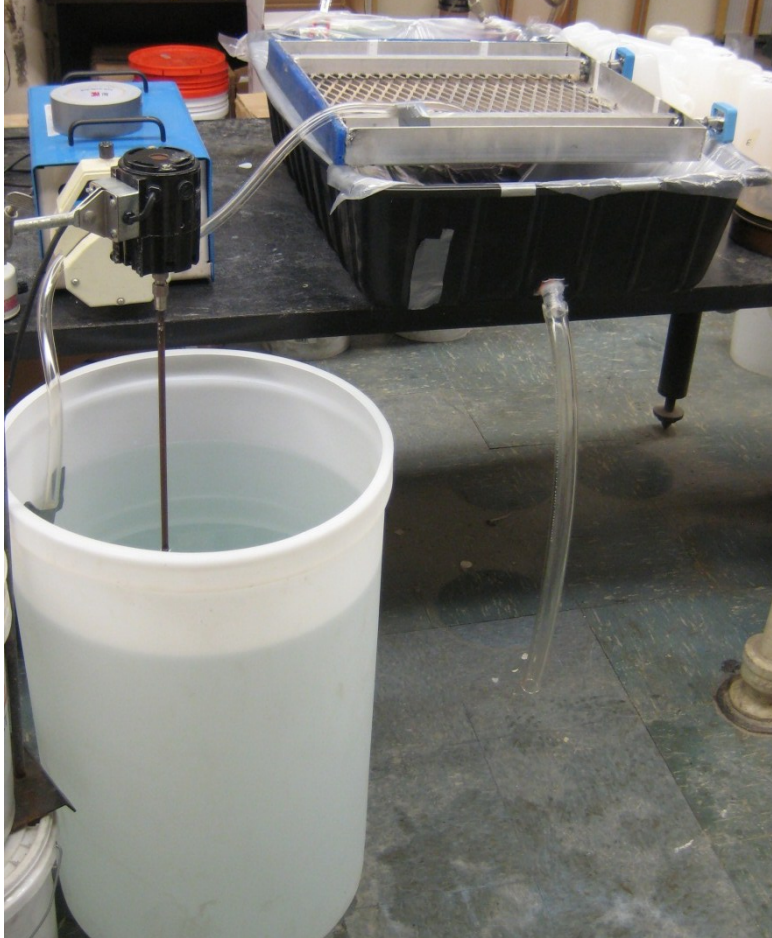*Figure 68*. Prototype of storm drain geotextile filter. (Geotextile filter is below the metal screen.)

Figure 69. Laboratory testing setup of geotextile filter prototype.

RESULTS

Two sets of tests were performed on one type of geotextile. Particle capture and hydraulic conductivity changes were evaluated as a function of solids loading to each filter. The results were compared with results observed in smaller-scale geotextile column test studies.

TSS Removal

The primary purpose of using the geotextile filter to treat stormwater is to remove suspended solids from runoff. The water quality goal was selected as 30 mg/L, as discussed in Chapter II. The effluent TSS concentrations were compared to this water quality goal. Figure 70 shows an example of the influent and effluent TSS concentrations found for one 75 minute test (from Test 1P). The influent concentrations were constant at approximately 200 mg/L. The first effluent concentration measured at 5 minutes was above the target concentration of 30 mg/L, while all others were below the 30 mg/L limit. This phenomenon, i.e., the highest concentration observed in the earliest effluent sample and then a decrease in effluent concentration with time, was observed in most of the other 75 minute tests on the prototype filter because like the geotextile column tests, the filter cake was disturbed by the initial influent flow and with time, the soil particles settled back onto the filter.

Figure 71 displays the influent and effluent TSS EMCs for each 75 minute test performed on the prototype. For each test, the TSS concentration is greatly reduced (by 88-96%), and all of the effluent EMCs are below the target concentration of 30 mg/L.

The prototype was able to capture 90% and 94% of the total solids loaded for tests 1P and 2P, respectively. Figure 72 shows how effective the prototype was at capturing suspended solids. The figure also displays the data for the first four 75 minute tests performed on the same type of geotextile loaded with the same particle size distribution and TSS concentration as the prototype but within the smaller column (described in Chapter II). In general, the geotextile filter in the two tests performed within a column (Tests 1.P1 and 1.P1(3)) did not capture as large of a percentage of TSS as the prototype (70-90% vis-à-vis 90-94%). This could be a result of side leakage around the geotextile due to the larger ratio of perimeter to area of the column filters than for the prototype (0.8 versus 0.2). Also, with a larger area of filter in the prototype and no support mechanisms underneath the filter, the prototype filter was allowed to sag under the weight of the water and solids. This sagging may have resulted in less side leakage at the walls and a greater amount of suspension was forced to travel through the geotextile in the most clogged area of the filter (Fig. 73).

Statistical analysis of the data in Figure 72 gives a comparison of the results from the column studies and the prototype laboratory studies. The slopes (b_1) and y-intercepts (b_0) of the regression lines of the solids captured as a function of solids loaded data for the prototype tests 1P and 2P and the column tests 1.P1, 1.P1 (repeat), and 1.P1 (3) are given in Table 14. The critical levels of significance, as determined by hypothesis testing described in Chapter II, for the values in Table 14 are given in Table 15. The b_1 values for 1P and 1.P1(3) are statistically equal to each other at the 5% level of significance (Tables 14 and 15), indicating that the mass of solids captured per solids loaded is equal between the prototype test at a higher HLR and the column test at a lower HLR. Because

the prototype test with the lowest total percentage of solids captured had the same b_1 value as the column test with the highest total percentage captured, it could be concluded that the geotextile filter within the prototype fixture performs just as well or better than the geotextile filter within a column in terms of suspended solids capture.

The geotextile filters in the column studies discussed in Chapter II were able to be loaded with more than 3 kg/m^2 (3.4 – 10.8 kg/m^2 for all column tests performed) of particle size distribution P1 solids before reaching a final clogging point, whereas, the prototype filters reached a final clogging point at less than 1.5 kg/m^2 (0.62 – 1.1 kg/m^2) solids loading. The values of the total solids captured at the final clogging point (defined in TSS Removal chapter) were also much smaller for the prototype tests than the column studies (0.58 – 1.01 kg/m^2 vis-à-vis 2.57 – 8.10 kg/m^2). This result was primarily due to the much smaller height of the walls of the prototype tray versus the column walls (4.5 cm versus 30 cm) which would force the head loss in the prototype to reach the maximum height within 20-25 minutes of testing at a much lower solids loading than the column studies. (Figure 93 in the Appendix shows the solids build-up on the filter and the tray and the rising water level within the tray.)
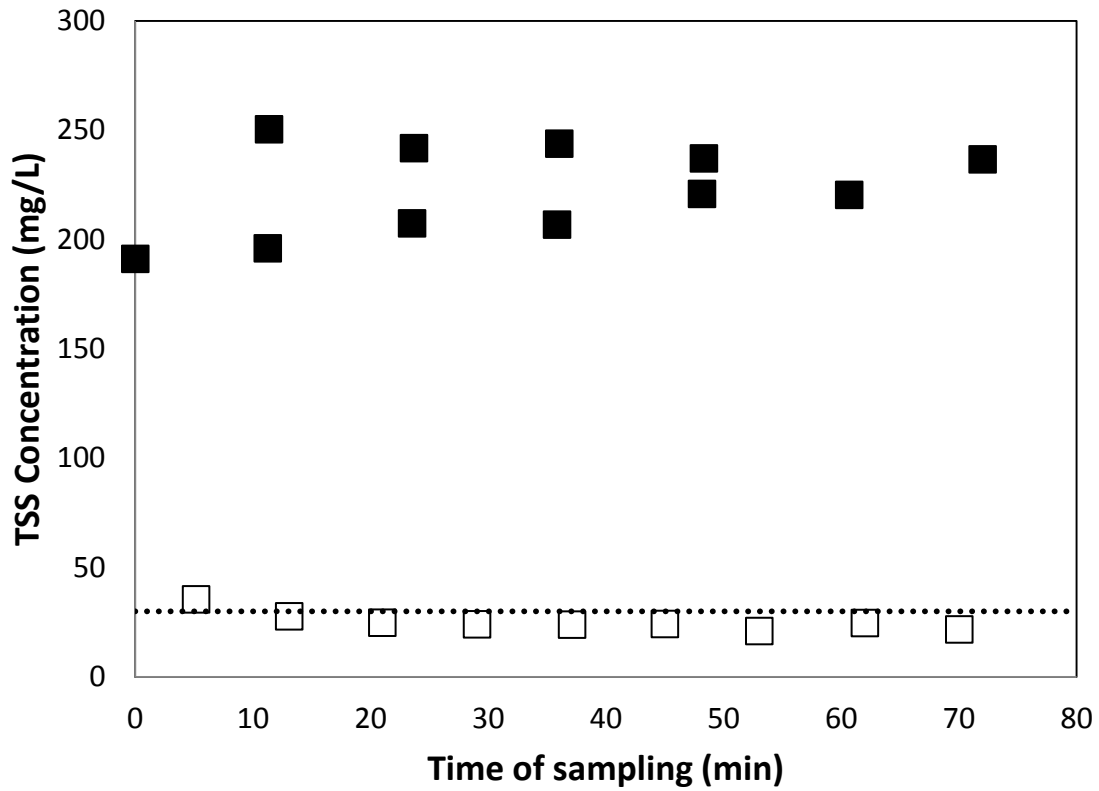
Figure 70. TSS concentration as a function of time during the first 75-min test of Test 1P. Closed symbols indicate influent values. Open symbols indicate effluent values. Dashed line indicates the target concentration of 30 mg/L.
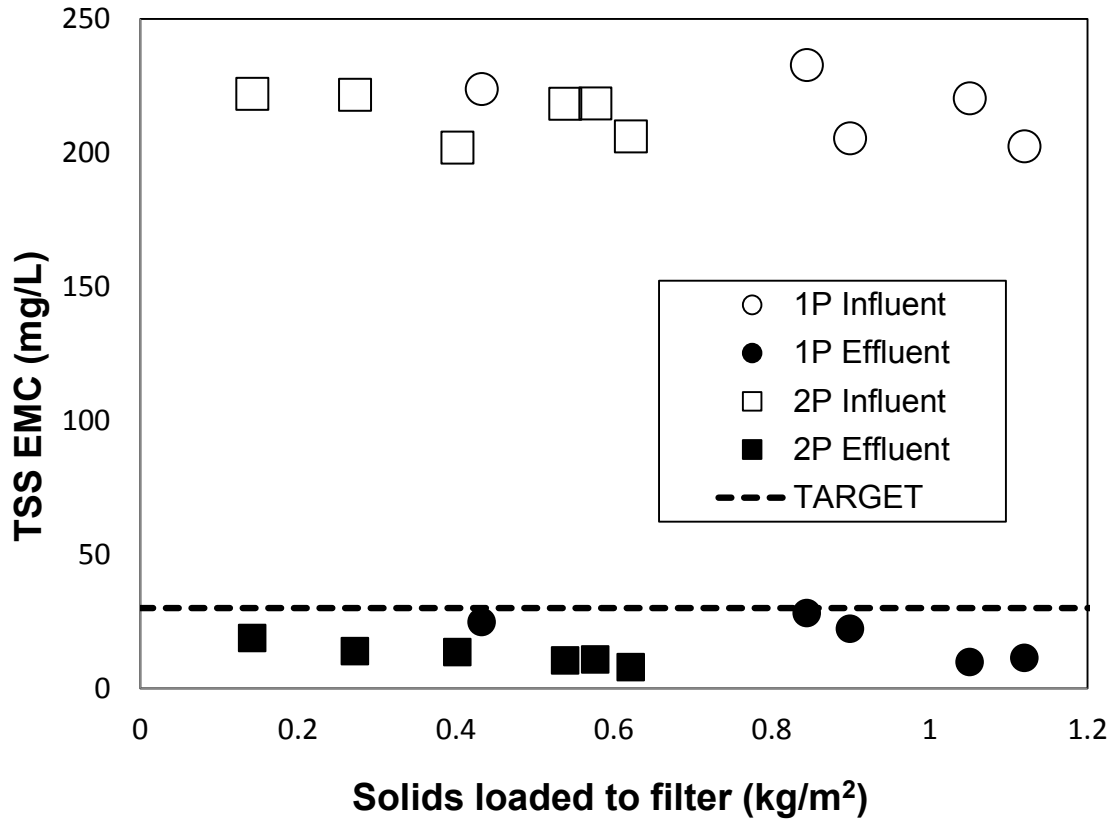
Figure 71. Total suspended solids event mean concentrations as a function of total solids loaded to the filter during laboratory prototype testing. Closed symbols indicate influent values. Open symbols indicate effluent values. Dashed line indicates the target concentration of 30 mg/L.
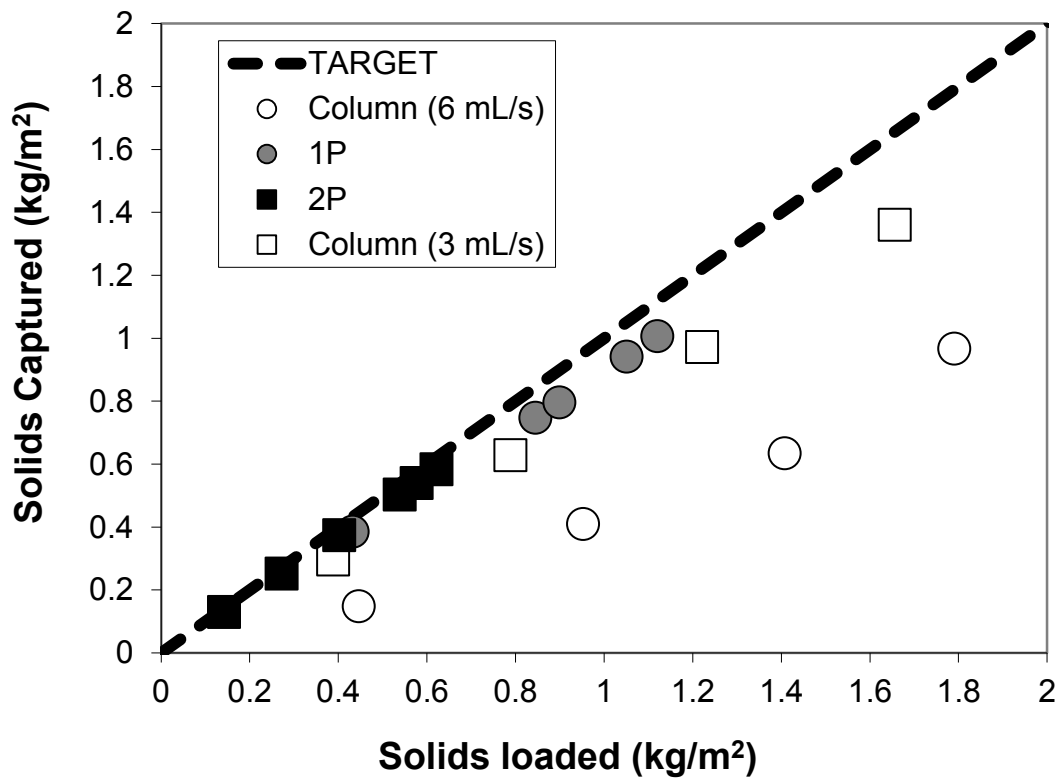
Figure 72. Total P1 solids captured by the NW1 filter as a function of the solids loaded to the filter. Dashed line represents 100% solids capture by a filter. Circle symbols represent tests performed at an HLR of 0.49 mm/s. Square symbols represent tests performed at 0.15 mm/s (2P) and 0.25 mm/s (1.P1(3)).
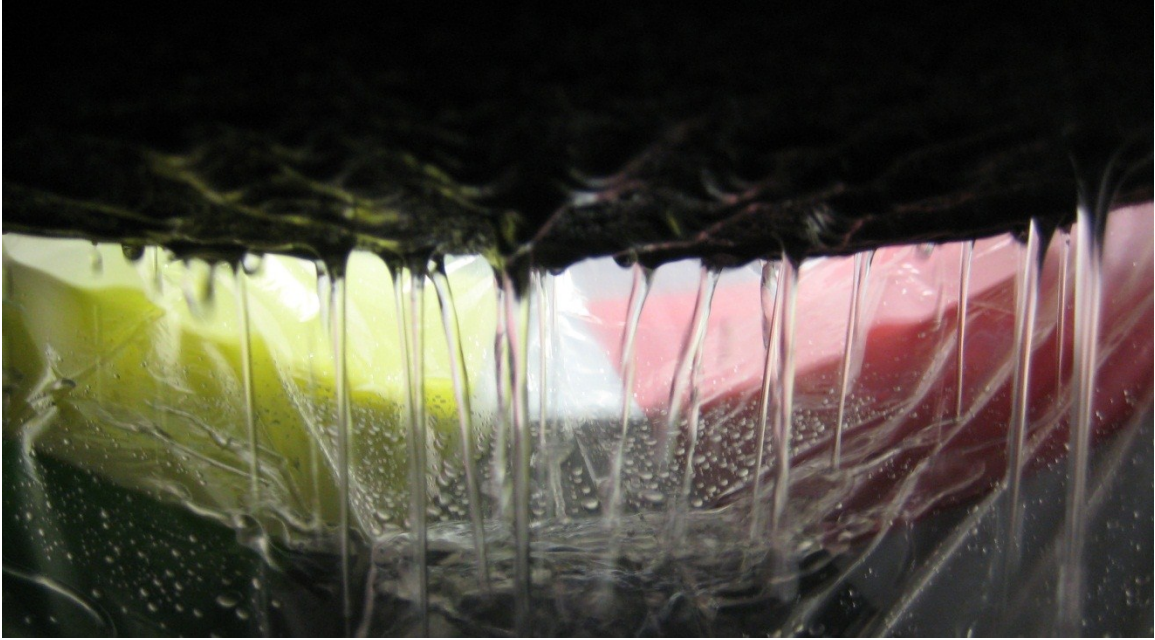
Figure 73. View from below the filter, showing filter sagging and water passing through the center of the filter.

Table 14. Slope and y-intercept values (b_1 and b_0 respectively) and their corresponding standard error values for the solids captured as a function of solids loaded data shown in Figures 72 and 82. Values listed are from tests with particle size distribution P1 and influent TSS concentration of 200 mg/L.

Test type	Influent HLR (mm/s)	b_1	Se (b_1)	b_0	Se (b_0)
	0.5	0.79	0.004	-0.39	0.027
Column	0.5	0.70	0.046	-0.86	0.212
	0.25	0.90	0.002	-0.11	0.010
Prototype	0.49*	0.90	0.011	-0.01	0.010
	0.15	0.94	0.002	-0.0005	0.001
Field-total	variable	0.41	0.018	-0.23	0.172
Field	variable	0.84	0.010	0.06	0.044

*first 56% of test run at HLR=0.49, remaining test run at 0.15

Table 15. Critical levels of significance for two-tailed t-tests setting either b_1 or b_0 (given in Table 14) for the each test listed at the top of the chart equal to the corresponding b_1 or b_0 for each test listed at the left side of the chart. Bold indicates those meeting the standard significance level of 0.01 (1%). Values italicized indicate those meeting both standard significance levels of 0.01 (1%) and 0.05 (5%).

	Test type	Column			Prototype		Field	
Parameter in linear regression	Test Name	1.P1	1.P1 (repeat)	1.P1 (3)	1P	2P	Field data-total	Field data
b_1	1.P1	1	**0.0462**	<0.0001	0.0035	<0.0001	<0.0001	0.0045
		<0.0001	1	<0.0001	0.0004	<0.0001	<0.0001	<0.0001
	1.P1 (3)	<0.0001	0.0003	1	***0.6676***	<0.0001	<0.0001	0.0002
	1P	<0.0001	0.0004	***0.1089***	1	<0.0001	<0.0001	0.0003
	2P	<0.0001	<0.0001	<0.0001	0.0381	1	<0.0001	<0.0001
	F total	<0.0001	<0.0001	<0.0001	<0.0001	<0.0001	1	<0.0001
	F	<0.0001	0.0075	<0.0001	**0.0101**	<0.0001	<0.0001	1
b_0	1.P1	1	**0.0416**	<0.0001	<0.0001	<0.0001	0.0018	<0.0001
		<0.0001	1	<0.0001	<0.0001	<0.0001	0.0010	<0.0001
	1.P1 (3)	<0.0001	0.0032	1	0.0036	<0.0001	***0.4983***	0.0061
	1P	<0.0001	0.0009	<0.0001	1	0.0133	*0.2559*	*0.1700*
	2P	<0.0001	0.0009	<0.0001	***0.6174***	1	*0.2449*	*0.1913*
	F total	<0.0001	0.0063	<0.0001	<0.0001	<0.0001	1	0.0003
	F	<0.0001	0.0005	<0.0001	0.0077	<0.0001	***0.1433***	1

Hydraulic Conductivity

The hydraulic conductivities calculated for prototype tests 1P and 2P are similar to the final stabilized hydraulic conductivities recorded for the NW1 column tests. The hydraulic conductivities are listed in Table 16 along with the hydraulic loading rates of each test. Lower hydraulic loading rates correspond to lower final hydraulic conductivities. Too few hydraulic conductivity measurements were recorded for the prototype tests to verify that the hydraulic conductivity of a geotextile filter can be fitted by a power model as in the column tests.

Table 16. Hydraulic conductivity values for prototype tests.

Test Type	Test	HLR (mm/s)	Final Hydraulic Conductivity (m/s)
Prototype	1P	0.49*	7.73×10^{-6}
Prototype	2P	0.15	6.20×10^{-6}
Column	1.P1	0.49	1.57×10^{-5}
Column	1.P1 (repeat)	0.49	1.36×10^{-5}
Column	1.P1 (3)	0.25	6.62×10^{-6}
*first 56% of test run at HLR=0.49, remaining test run at 0.15			

FIELD TESTING OF THE PROTOTYPE

METHODOLOGY

The prototype which was used in the laboratory studies was tested in the field to filter stormwater runoff from a parking lot on the University of Maryland campus. The runoff reaching the prototype filter in-field was approximately ½ of the runoff from a 0.24 ha section of a heavily-trafficked asphalt surface lot. The lot, which has an asphalt curb around its perimeter to funnel runoff flow to the corner of the lot where the prototype filter was located, is used year-round by commuter students and sporting event attendees (Davis 2008).

In order to capture effluent samples within a 91 cm ×61 cm ×20 cm (36" ×24" ×8") plastic tub without allowing rainwater or other debris to enter the tub, a lid made of sheet metal was placed on top of the tub with the prototype attached. This lid ensured that only stormwater passing through the geotextile filter could enter the tub (Figure 74). At the opposite end of the tub at which the filter was placed, a v-notch weir was cut into the side of the tub to allow water to exit. Inside the tub, a bubble line tube was placed just below the v-notch weir to measure the water level above it from which the water flow rate could be calculated (Figure 75). A tube connected to the ISCO 6712 Portable Sampler with a strainer attached to the end of it was also placed inside the tub to collect samples of filter effluent (Figure 75).

The prototype filter tub was placed at the end of a concrete channel through which stormwater runoff from part of University of Maryland Parking Lot 11 flowed. Because of area constraints due to the presence of nearby trees and a bioretention cell liner with a

wall of soil behind it, the filter tub had to be placed at an angle, and a channel extension constructed of plastic sheets and a concrete block was placed between the concrete channel and the tub (Figure 76). The soil in the area following the v-notch tub outlet was dug out to form a channel so that the water could flow freely out of the tub (Figure 77). The ISCO 6712 Portable Sampler which collected effluent samples from the tub was placed nearby and secured to a tree (Figure 77).

The influent stormwater samples were collected in a 15 cm Tracom Parshall flume within the concrete channel (Figure 78). A bubble line tube attached to a second ISCO Portable Sampler was placed at the entrance of the flume in order to measure water levels which could be used to calculate the influent runoff flow rates.

The influent and effluent sampling programs were enabled to collect up to 24 samples. The first 9 samples were collected every 20 minutes, the 10th and 11th samples were collected after 60 minutes, the 12th, 13th and 14th were collected after 80, 100 and 120 minutes respectively, and 15th through 24th were collected every 60 minutes. The length of the sampling program was to ensure that samples were collected for the entire duration of the storm event. The influent sampler was set to enable sampling at a water level of 0.02 ft, and the effluent sampler was set to enable sampling at a water level of 0.05 ft. By trial and error, these levels were determined to be the levels to best represent the onset of a typical storm event.

The flow rates entering the influent flume and exiting the v-notch weir were calculated using the measured water levels. For flow into the Parshall flume, the following formula was used:

$$q_{in} = C_f z^u \tag{27}$$

where q_{in} is the flow rate of the influent runoff, z is the water level in the channel, C_f is a coefficient, and u is an exponent. C_f and u are determined by the throat width of the flume. For a 6 in flume, C_f and u are 2.06 and 1.58 respectively (USBR 2001). The effluent flow was calculated using the following weir equation:

$$q = C_{wt} \frac{8}{15} \tan\left(\frac{\Theta}{2}\right) \sqrt{2g} H^{5/2} \tag{28}$$

where q is the flow rate of the effluent runoff, C_{wt} is the triangular weir constant, Θ is the angle of the triangular weir, g is gravitational acceleration, and H is the weir head measured by the bubble line tube. The C_{wt} and Θ for the v-notch weir were 0.58 and 120˚, respectively (Munson et al. 2006).

Laboratory testing was performed on the samples collected by the ISCO samplers to determine total suspended solids concentrations for each sample. TSS concentration measurements were conducted using Standard Method 2540 B (Eaton et al. 1995). TSS concentrations of all samples were used to calculate a TSS EMC value for influent samples and an EMC for effluent samples using Equation 1 and the method described in TSS Removal chapter. The total flow volumes between samples were determined by averaging the flow rates measured by the ISCO Sampler between sampling events and multiplying that average by the amount of time between samples.

Figure 74. Prototype filter and tub used in-field to collect stormwater effluent.

Figure 75. Side of prototype filter tub where effluent exited the tub.

Figure 76. Prototype filter tub in place at end of runoff channel.

Figure 77. View over the area inside of a bioretention cell where the prototype filter tub

and ISCO sampler where placed.

a. Side view of Parshall flume

b. View over Parshall flume

Figure 78. Parshall flume (6 in) for influent flow rate measurements **a**. Side view **b**.

Bird's-eye view

RESULTS AND ANALYSIS

Total Suspended Solids Removal

Two in-field test sets were performed on a prototype geotextile filter. The first test set collected preliminary data and assessed problems with the testing set-up. For the second test set, TSS removal was evaluated as a function of total solids loaded to the filter. A brief discussion of the peak flow reduction by the prototype filter is provided in the Appendix. All discussion below refers to the results of the second test set.

Eleven storm events were recorded while testing the prototype geotextile filter under field conditions. The test set was ended when a large storm flooded the system, causing water which had pooled in the soil of the bioretention cell to back-up into the tub collecting the effluent. This back-up would cause any future effluent samples to be inaccurate due to the soil which had been flushed into the system from the cell. The characteristics of the 11 storm events and the data collected on influent and effluent samples are provided in Table 17.

Every storm event recorded in this study exhibited a first flush of total suspended solids. The largest reductions in TSS by the prototype filter occurred for the first two influent and effluent samples collected. Figure 79 shows the very high TSS concentration of the first influent sample (699 mg/L) and the significantly lower (by 84%) TSS concentration of the first effluent sample (112 mg/L).

The prototype filter reduced TSS concentration in the stormwater runoff for every storm event recorded. TSS reduction from the channel influent to the filter effluent ranged from 71 to 99% throughout the storm events. This reduction is shown in Figure

80, where there is a significant difference between the lines of best fit for the influent

concentrations and effluent concentrations (150% difference between the y-intercepts).

A probability exceedance plot shown in Figure 81 also displays the reduction in TSS

concentration by the geotextile filter. As seen in Fig. 81, there is a less than 5% chance

that the effluent TSS EMC would exceed the target concentration of 30 mg/L, but an

approximately 70% chance that the influent TSS EMC would exceed the target

concentrations. Additionally, the effluent TSS EMC at 50% exceedance probability was

less than 10 mg/L while the influent TSS EMC at 50% was over 30 mg/L.

None of the effluent EMCs exceeded the target concentration of 30 mg/L,

indicating that that prototype filter is effective at reducing TSS concentrations to a water

quality goal equivalent to a point source discharger. However, it is important to note that

the prototype filter was not large enough to treat all of the runoff water that reached it due

to the extremely large runoff area to filter area ratio. Assuming that the runoff area is one

half of the 0.24 ha section of parking lot because of the divergent concrete channel, then

the runoff area to filter area ratio is approximately 4400, nearly 100 times the typical

drainage area to filter area ratio for stormwater runoff controls. According to the flow

rates calculated using Equations 27 and 28, the prototype filter treated between 27% and

87% of the runoff volumes per event and around 50% of the total runoff over all of the

events.

Figure 82 shows the total solids captured as a function of solids loaded to the

prototype filter in-field in comparison with the laboratory column test results for the

NW1 filter. The total solids loaded values were calculated in two different ways. For

"Field data-total", the solids loaded values are equal to the total solids that passed

through the influent runoff in the concrete channel. These values are also listed in Table 17. However, as stated earlier, the filter was not able to treat the entire influent runoff volume. Therefore, for "Field data", the solids loaded values are equal to the amount of solids that would be loaded to the filter if the influent volume of runoff was equal to the effluent volume. As seen in Figure 82, if the filter were able to treat the entire influent runoff volume (as in "Field data"), the total solids captured as a function of solids loaded appears very similar to the NW1 column tests, specifically 1.P1(3).

Table 14 gives the slopes (b_1) and y-intercepts (b_0) of the data in Figure 82 along with the standard errors of those values, while Table 15 gives the critical levels of significance for the comparisons of the b_1 and b_0 values between the prototype tests, the laboratory tests, and the in-field tests. The critical levels of significance from statistical analysis (Table 15) do not show that the slopes of the field test regression lines (Figure 82) are equal to any of the slopes of the laboratory column or prototype tests (Figure 72). However, when comparing the slopes given in Table 15, the slope of the "Field data" (0.84) is within the range of the slopes of the laboratory column tests (0.70-0.90). This indicates that the geotextile filter is as successful at capturing suspended solids in field conditions with actual runoff as it is in simulated laboratory column testing.

The values of total solids loaded to the prototype filter at the end of in-field testing were comparable to the total solids loading at the end of the laboratory column tests. The "Field data" calculation and "Field data-total" calculation values of total solids loaded to the filter were 5.84 and 12.24 kg/m^2, respectively, and the total solids loaded to the geotextile filters in the column studies discussed in Chapter II ranged from 3.41 to 10.8 kg/m^2. These results indicate that the prototype filter system is able to effectively

treat as much stormwater runoff as the geotextiles in the column studies assuming as equivalent influent TSS concentration. Additionally, the prototype system may be able to continue treating stormwater runoff beyond 5.84 or 12.24 kg/m^2 solids loading because the testing was not ended at a failure point as the laboratory tests were. The tests were ended after the system flooded, which was discussed earlier. Therefore, the results show that the prototype filter can treat runoff for at least a solids loading of 5.84 or 12.24 kg/m^2.

Figure 83 shows the total solids captured as a function of solids loaded to the prototype filter in-field in comparison with the laboratory prototype test results. As seen in the figure, the total solids captured data points for the Field data align very closely with the total solids captured values for the laboratory prototype tests. The prototype filter in-field was able to capture a greater total solids captured than the prototype filter during laboratory tests (4.99 kg/m^2 versus 0.58 – 1.01 kg/m^2) because testing on the prototype in-field was not stopped when the water pooling above the filter reached the top of the tray. The influent flow rates to the in-field filter were larger than the influent flow rates in the laboratory studies. The peak flow rates and average flow rate of influent runoff per filter area to the in-field filter were 8.1×10^{-4} – 7.4×10^{-3} m/s and 7.7×10^{-4} m/s, respectively, and the influent flow rates to the prototype in-lab were $1.5 – 4.9 \times 10^{-4}$ m/s. The difference is due to the extremely large runoff area-to-drainage area ratio for the in-field tests (4400) as discussed earlier. A more typical runoff area-to-drainage area ratio, such as 50, would likely result in a more effective geotextile filter and a longer lifespan in terms of total solids loaded to the filter because less of the runoff would flow over the sides of the prototype tray.

Table 17. Summary of storm events from field testing

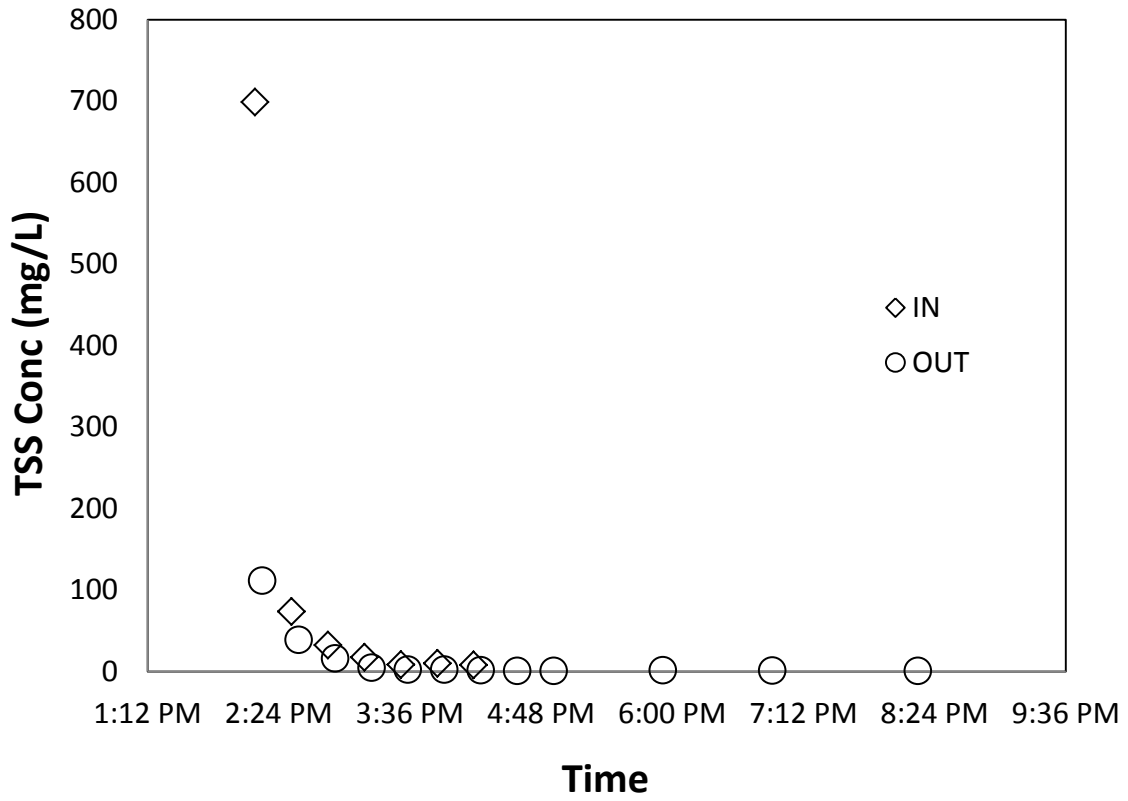| Date	Rain depth (in)	Input volume (L)	Output volume (L)	Input TSS EMC (mg/L)	Output TSS EMC (mg/L)	TSS EMC reduction (%)	Cumulative solids loaded (Field data-total) (kg/m^2)	Cumulative solids loaded (Field data) (kg/m^2)	Cumulative mass captured (kg/m^2)	Total mass TSS reduction (%)
2/11/2012	0.048	1172	589	23.2	1.7	93	1.21	0.05	0.04	4
2/24/2012	0.128	4763	3135	168.9	15.6	91	4.04	1.91	1.74	43
2/29/2012	0.548	23745	9221	22.2	3.9	82	5.89	2.63	2.33	40
3/2/2012	0.256	11308	4058	72.1	22.4	69	8.76	3.66	3.04	35
3/20/2012	0.124	4012	2481	114.4	9.9	91	10.38	4.66	3.95	38
3/24/2012	0.12	4190	2625	26.6	7.6	71	10.77	4.91	4.13	38
4/2/2012	0.036	439	157	184.6	2.3	99	11.06	5.01	4.23	38
4/29/2012	0.06	1187	316	30.9	2.3	93	11.19	5.04	4.26	38
5/1/2012	0.048	1543	646	42.7	5.9	86	11.42	5.14	4.34	38
5/8/2012	0.016	278	0	29.9	no outflow	100	11.45	5.14		
5/21/2012	0.076	5647	4930	40.0	2.9	93	12.24	5.84	4.99	41
	2.674	<---total rainfall estimate								

206

Figure 79. TSS concentrations measured for samples from Feb. 24, 2012 storm event.
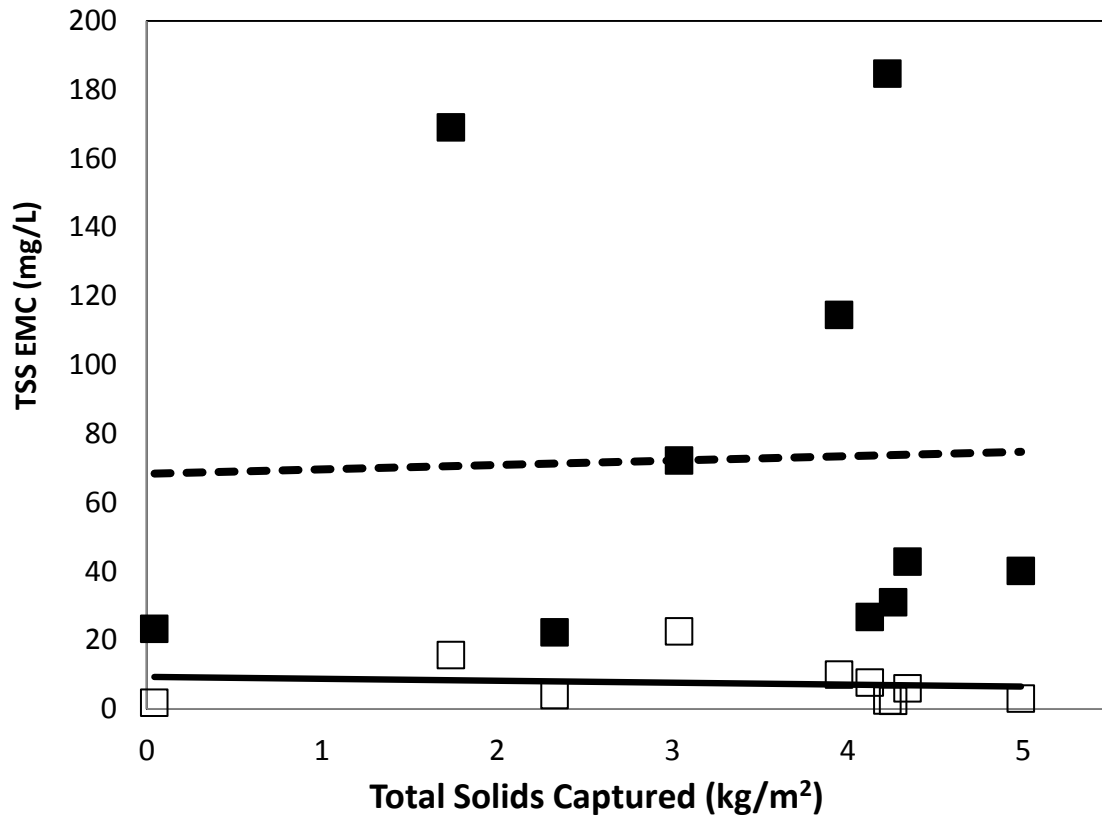
Figure 80. Event mean concentrations of total suspended solids as a function of total

solids captured by the filter. Closed symbols indicate influent values. Open symbols

indicate effluent values. Dashed line is line of best fit for influent EMCs, and solid line is
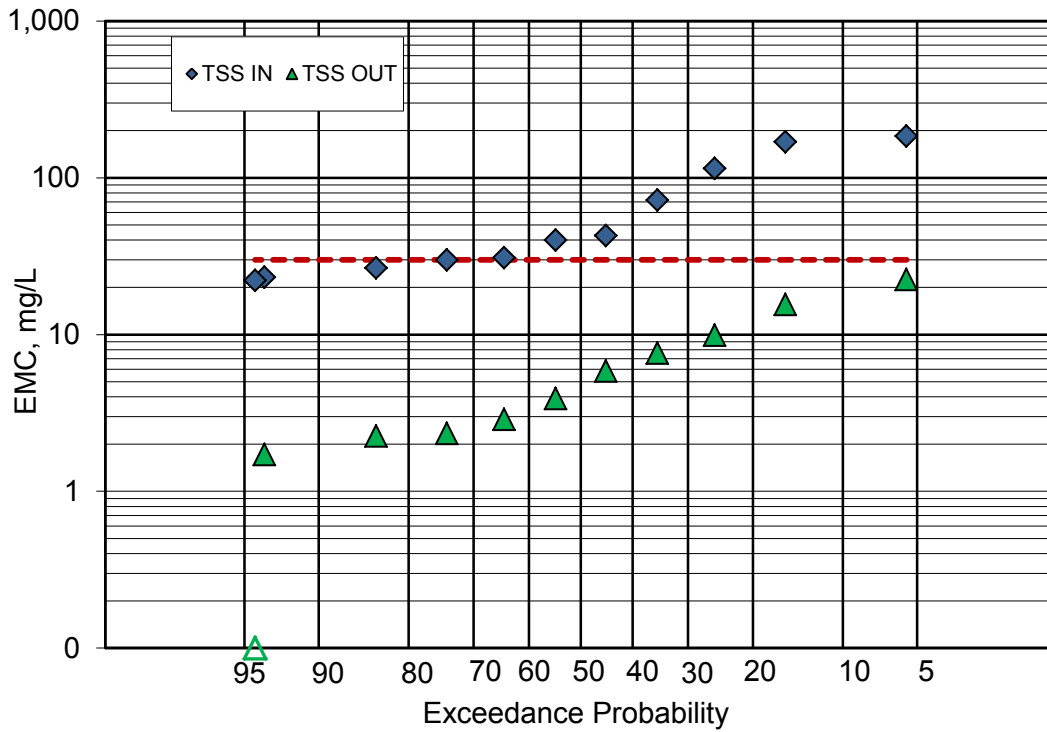
line of best fit for effluent EMCs.

Figure 81. Exceedance probability plot of TSS EMC values for each storm event recorded. Open symbol indicates no outflow detected.
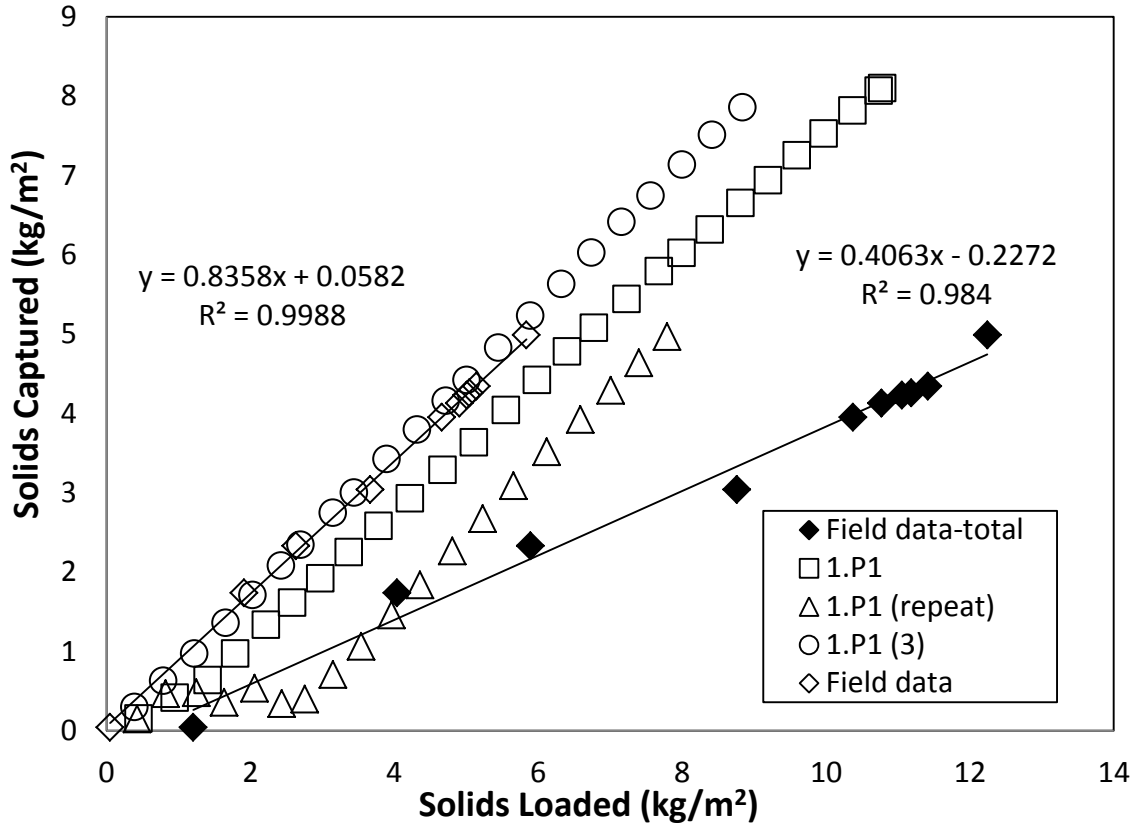
Figure 82. Total solids captured by the NW1 filter as a function of the solids loaded to the filter for the prototype field studies and the column studies with TSS concentration of 200 mg/L, particle size distribution P1, and influent flow rates of 6 mL/s and 3 mL/s.
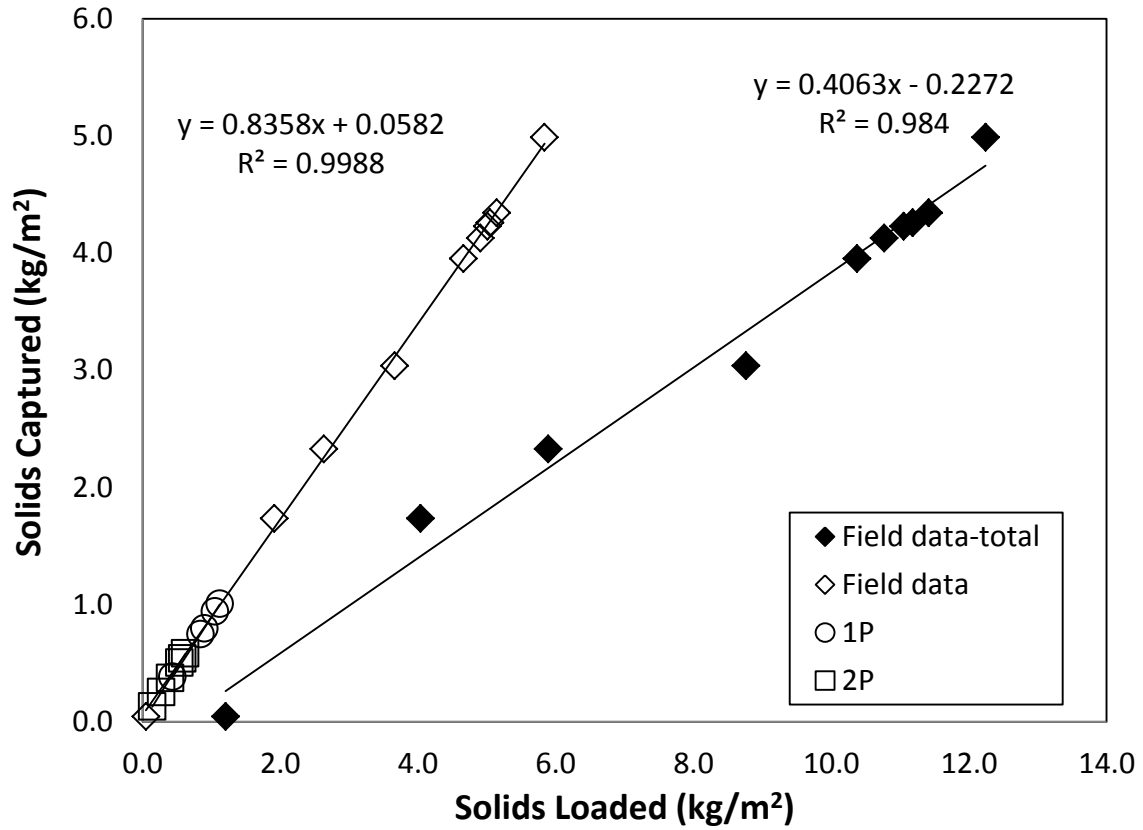
Figure 83. Total solids captured by the geotextile prototype filter as a function of the solids loaded to the filter for the prototype laboratory studies (1P and 2P) and the in-field studies.

Applicability of Geotextile Criteria

The results of the in-field tests were analyzed considering the geotextile filtration criteria established in Chapter III in order to assess the validity of the new criteria. However, some knowledge of particle sizes in the runoff is needed to use the criteria, and no tests were performed to determine the particle size distribution within the runoff for the in-field tests of this study. Therefore, an assumption was made that the particle size distribution was similar to the distribution from a highly-trafficked urban paved area in Baton Rouge, LA (Sansalone et al. 2009). Using the D_{10}, D_{30}, D_{60}, and D_{95} values measured by Sansalone et al. (2009), the NW1 filter, which was used in the prototype, met the criteria of $\dfrac{O_{95}/D_{60}}{O_{30}/D_{10}} > 0.05$ and $\dfrac{O_{large}/D_{60}}{O_{small}/D_{10}} > 0.076$, which means that these two criteria accurately predict the success of the NW1 filter at capturing urban runoff particles. The NW1 filter did not meet the criteria of $\dfrac{O_{95}/D_{95}}{O_{30}/D_{30}} > 0.48$ and $\dfrac{O_{large}/D_{95}}{O_{small}/D_{30}} > 0.68$ because the D_{95} value for the particles measured by Sansalone et al. (2009) was very large (approximately 10000 µm) compared with the D_{95} values chosen for the laboratory column studies in Chapter II (97 – 171 µm). Therefore, for stormwater runoff which either flows too quickly or does not enter a retention basin to allow for settling of larger particles before reaching the filter, criteria involving any of the larger particle sizes such as D_{95} should not be used to choose the appropriate geotextile for use.

Applicability of Hydraulic Conductivity Model

Assuming once again that the particle sizes in the runoff for the in-field tests were equal to the particle sizes in measured by Sansalone et al. (2009), the failure point of the geotextile prototype in-field can be predicted by the model developed in Chapter V (Equation 19). First, the parameters, a, b, m_1 and K_0 must be determined. Using the equations for the lines of best fit for a and b in Figures 56 and 63 to calculate the values of a and b for the in-field tests, a and b are 0.856 and 0.0568, respectively. Because the equation for the trend line for m_1 in Figure 66 includes the ratio D_{95}/D_{30} and the D_{95} ratio may cause inaccuracies when there is little settling occurring before the runoff reaches the filter (as discussed earlier), the equation for the trend line in Figure 101 (in the Appendix) was used to calculate the m_1 value for the in-field test. The equation in Figure 101 which has the ratio D_{60}/D_{10} instead of D_{95}/D_{30} which was previously determined to be more accurate at predicting success of a geotextile filter in the geotextile filtration criteria. Using the average TSS EMC (68.7 mg/L) and the average influent flow rate (0.219 L/s) for the in-field test set, m_L, an approximation of the mass of solids loaded to the filter during each storm event, was calculated for the in-field tests using Equation 25 as 0.239 kg/m^2. Using this value of m_L, m_1 was calculated using the trend line equation from Figure 101 (Appendix) as 2.65. Using Equation 2 and the average influent flow rate (0.219 L/s), the initial hydraulic conductivity, K_0, is equal to 7.7×10^{-4} m/s.

Using these values of a, b, m_1, and K_0, and the relationship between v/v_{in} and m given in Equation 26, the hydraulic conductivity values throughout treatment of stormwater runoff by the prototype filter were calculated as a function of the mass of solids captured by the filter, m, and given in Figure 84. From the laboratory column tests

discussed in Chapter II, the hydraulic conductivity at the clogging or failure point of the filter is equal to $6.62 \times 10^{-6} - 1.64 \times 10^{-5}$ m/s for the NW1 filter. According to the output from the model (Equation 19), the mass of solids captured by the prototype filter in-field at these hydraulic conductivity values is $10.7 - 12.6$ kg/m^2 (Figure 84). To convert this mass to the mass of solids loaded to the filter, one must assume a removal rate of solids by the filter. The removal rates determined by the slope of solids captured as a function of solids loaded for in-field prototype testing were 40.6 % and 83.6 % for "Field data-total" and "Field data", respectively (Figure 82). Using these TSS removal rates, the total solids loaded to the prototype filter at the clogging point is $12.8 - 31.5$ kg/m^2. Assuming an average runoff event of 75 min, influent flow rate of 0.219 L/s, TSS concentration of 68.7 mg/L, and a TSS removal rate of 83.6 %, the prototype filter will retain suspended solids and maintain adequate drainage for approximately 53 rainfall events. For a runoff area equivalent to the ½ of the 0.24 ha parking lot and an assumption of 10% infiltration for the highly impervious area, the total volume of stormwater runoff that this prototype filter could treat for 53 rainfall events, is the equivalent of approximately 4.8 cm (1.9 in) of rainfall (Davis 2009). The value is much smaller than the annual rainfall total for the state of Maryland (40.8 in) (MSA 2012). However, as stated previously, the runoff area-to-drainage area ratio for the in-field prototype testing was 4400, which is 88 times that of a typical stormwater runoff area-to-drainage area ratio for an underground sand filter (50). If the prototype filter area were scaled up to an area that is 50 times smaller than the runoff area, the volume of runoff which could be treated before the clogging point would be the equivalent of 414 cm (163 in) of rainfall. Therefore, if all assumptions are

correct, the model predicts that a larger geotextile filter could successfully treat stormwater runoff for nearly 4 years in the state of Maryland.

Stormwater management professionals calculate the mass of suspended solids per runoff area per year in the influent and effluent runoff in order to assess TMDL regulations. Using the data predicted by the model (Equation 19) discussed earlier, the total solids captured by the prototype filter after 4.8 cm (1.9 in) of rain is 10.7 – 12.6 kg/m^2 which corresponds to 522 – 615 kg/ha/yr (using the runoff area-to-drainage area ratio of 4400 and the annual rainfall total for Maryland). The total solids loaded to the prototype filter after 4.8 cm of rain is 12.8 – 31.5 kg/m^2 which corresponds to 625 – 1537 kg/ha/yr. The large range of values is a result of the varying removal rates (40.6 % and 83.6 %) which is largely dependent upon the volume available for hydraulic head above the filter.
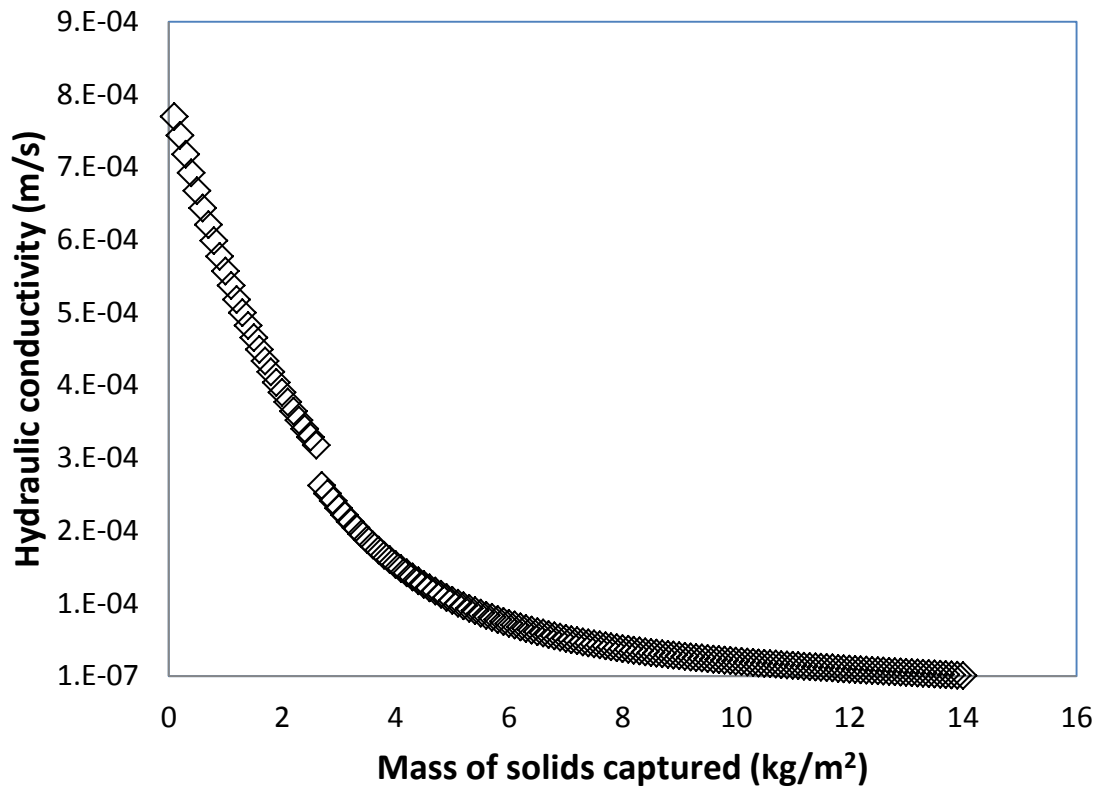
Figure 84. Hydraulic conductivity values for the in-field prototype filter as a function of the cumulative mass of solids captured by the filter as predicted by the model (Equation 19) developed in Chapter V.

CONCLUSIONS

The prototype geotextile filter system greatly reduced TSS concentration and was more effective at removing suspended solids than similar, smaller-scale column tests. The measured hydraulic conductivities of the prototype system were similar to the hydraulic conductivities of column tests performed at the same hydraulic loading rate. Because the prototype exhibited similar behavior to the laboratory column studies, it was expected that the prototype would be effective under field conditions.

The prototype filter was successful at reducing TSS concentrations to below the target concentration in field conditions, and when assuming an influent volume of runoff equal to the effluent volume, the percentage of total solids captured is within the same range as the percentages of total solids captured by geotextile filters in laboratory column studies.

Two of the geotextile filtration criteria developed in Chapter III were applicable to the results of the in-field. With specific assumptions made about the particle sizes in the stormwater runoff, the criteria were effective at predicting success of the prototype filter (NW1 geotextile) in the field application. Additionally, the model developed in Chapter V was used to assess the lifespan of the prototype filter in terms of suspended solids capture and rainfall.

Chapter VII: SUMMARY AND CONCLUSIONS

SUMMARY

Establishing innovative stormwater treatment methods is critical for combatting the detrimental impacts of stormwater runoff. The treatment method of geotextile use for suspended solids filtration from urban stormwater runoff was thoroughly evaluated in this research using laboratory column studies, in-field testing, and theoretical modeling.

Laboratory column studies were performed on three geotextiles at two flow rates, three particle size distributions, and two influent TSS concentrations. During testing, influent and effluent TSS concentrations were measured along with influent and effluent flow rates and head losses above the geotextile filter. Performance of the geotextile filters was assessed by the total masses of solids loaded to and captured by the filter at the point of failure (or final clogging). The column studies confirmed that larger permittivity values and pore size distributions of the filters decreased the effectiveness of suspended solids retention and increased the hydraulic conductivity values of the filter-filter cake system throughout testing. The particle size distribution of the suspended solids in the influent also impacted the hydraulic conductivity values measured throughout testing. In general, a coarser particle size distribution led to larger hydraulic conductivity values due to a more porous and open filter cake formation. Neither the influent flow rate nor the influent TSS concentration had an effect on the total amount (or percentage) of suspended solids retained during testing. However, both parameters had a slight effect on hydraulic conductivity, which was addressed in the mathematical model developed to estimate hydraulic conductivity throughout the lifespan of the filter.

Using the results of the laboratory column studies, new retention criteria were developed to accurately predict success of a geotextile filter at retaining suspended solids in stormwater runoff. Established criteria for geotextiles in geotechnical applications were not adequate for this use of geotextile because they do not incorporate enough information about the filter opening size distribution or the runoff particle size distribution in each criterion ratio. The criteria developed in this study included at least two filter opening sizes and two particle diameters in each criterion ratio. These new criteria were tested at three particle size distributions and two geotextile filter types. Two of the new criteria, $\frac{O_{95}/D_{60}}{O_{30}/D_{10}} > 0.05$ and $\frac{O_{large}/D_{60}}{O_{small}/D_{10}} > 0.076$, were accurate when predicting success or failure of a geotextile for any of the three particle size distributions in this study, as well as for the in-field testing of a geotextile prototype filter. The other two criteria, $\frac{O_{95}/D_{95}}{O_{30}/D_{30}} > 0.48$ and $\frac{O_{large}/D_{95}}{O_{small}/D_{30}} > 0.68$, were accurate for use in choosing a successful geotextile filter for particle capture. However, these two criteria may exclude viable geotextiles for stormwater treatment by predicting failure of a filter type for when that filter would actually be successful at retaining suspended solids of those particular sizes.

A laboratory sand filter column study was developed for this research. The sand filter was meant to simulate the sand filters in urban areas such as Washington, D.C., and the testing was performed in the same manner as the geotextile laboratory column tests in order to produce a direct comparison in performance between the two types of filters. Performance was assessed by the total masses of solids loaded to and captured by the filter at the point of failure (or final clogging). Results showed that the sand filters were

able to retain a larger total percentage of suspended solids than the geotextile filters. However, the sand filters clogged sooner than the geotextiles in terms of total solids loaded.

A theoretical model was developed in Equation 19 to provide a means of predicting hydraulic conductivity of a geotextile filter in stormwater filtration throughout the lifespan of the filter. The parameters in the model were analyzed as functions of the most important parameters in geotextile filtration of suspended solids. The model can be used to predict the lifespan of a geotextile filter in stormwater treatment.

The geotextile filter was tested under actual stormwater runoff conditions where it filtered runoff from a heavily-trafficked parking lot on the University of Maryland campus. Influent and effluent samples were collected using ISCO Portable Samplers. Influent flow rates were measured using a flume, and effluent flow rates were measured using a v-notch weir. The results of the prototype tests were compared with the laboratory column test results, and the model developed in Equation 19 was used to estimate the lifespan of the prototype filter under field conditions.

CONCLUSIONS

The following conclusions were reached as a result of the activities performed:

1. Geotextiles are effective at removing suspended solids from simulated stormwater runoff, but the filtration of suspended solids by geotextiles is dependent upon the filter opening sizes and permittivity and particle size distribution of the suspended solids. Larger permittivity values such as $1.2 \ s^{-1}$ and opening sizes (AOS: 180 μm) correspond to lesser removal rates of suspended solids than smaller permittivity values

$(0.54 - 0.8 \text{ s}^{-1})$ and opening sizes (AOS: 150 μm), but also a longer lifespan due to greater hydraulic conductivity values for a given mass of solids loaded to the filter. Larger particles and ranges of particle sizes such as PSD P1 are generally more easily captured by geotextile filters than smaller particles and smaller range of particle sizes (P2 and P3). Larger particle size distributions also contribute to greater hydraulic conductivity values during testing, and thus longer filter lifespans, than smaller PSDs because they form a more porous and open filter cake at the surface of the geotextile.

2. Geotextile filtration criteria for stormwater treatment must address the phenomena discovered during laboratory column studies discussed in the TSS removal chapter. Filter permittivity, which is influenced by permeability, opening sizes, and thickness, played a greater role in affecting TSS removal than the AOS, which indicated that using permittivity or more than one opening size provides greater accuracy in predicting the appropriate geotextile for the stormwater treatment need. Because particle size distribution also affected TSS removal, a range of particle sizes or at least two particle sizes, enhances the design parameter selection for geotextiles in stormwater treatment. The four geotextile filtration criteria developed in this research given in Table 3 incorporate at least two opening sizes and at least two filter opening sizes and two particle diameters in each criterion ratio. Any of the four criteria can be used to choose a geotextile for successful suspended solids capture.

3. Sand filters are very effective at capturing suspended solids, but clog quicker in terms of solids loaded to the filter, than geotextiles. In laboratory test comparisons, both geotextile and sand filters were successful at reducing the TSS concentration to below the target concentration of 30 mg/L, but the geotextile filters were able to be

loaded to a greater mass of solids per unit area before clogging than the sand filters. For

an average influent TSS concentration of 200 mg/L, a runoff area-to-drainage area ratio

of 50, and an annual rainfall depth of 1.04 m (40.8 in), the sand filters would need

maintenance approximately 71 days before the geotextile filters.

4. The mathematical model given in Equation 19 can be used to estimate the

hydraulic conductivity of a geotextile filter during stormwater treatment. With

knowledge of 2 particle sizes in the runoff, 2 opening sizes of the filter, and estimates of

influent TSS concentration and flow rate, one can predict the amount of total solids

captured by and loaded to the filter at the failure, or clogging point, of the filter and thus,

will be able to estimate how long the filter can be used for suspended solids removal

before replacement or maintenance is necessary.

5. The geotextile filter prototype is effective at reducing TSS concentrations to

less than 30 mg/L in large-scale laboratory testing and under field conditions. According

the to the model developed to determine hydraulic conductivity values as a function of

the mass of solids captured by the filter, the prototype filter could last up to 4 years

before replacement is needed.

PRACTICAL IMPLICATIONS OF THE FINDINGS

The practical implications of the analyses performed on the filtration of urban stormwater

runoff by geotextile filters are summarized as follows:

1. The successful retention of suspended solids and maintenance of adequate

drainage of a geotextile filter discussed in this research indicates that a geotextile filter

will be an effective new best management practice (BMP). A BMP is defined as "a device, practice, or method for removing, reducing, retarding, or preventing targeted storm water runoff quantity, constituents, pollutants, and contaminants from reaching receiving waters" (Strecker et al. 2001). Development of new BMPs and continued analysis and improvement of current BMPs is very important because the US Environmental Protection Agency (EPA) continues to make regulatory improvements to strengthen its stormwater program. A new rule to strengthen the national stormwater program should be proposed by the EPA by June 10, 2013 and a final action regarding the rule should be completed by December 10, 2014. New BMPs may be needed to meet the higher regulatory standards set by the EPA (EPA 2012). The filter could be used to meet Total Maximum Daily Load (TMDL) requirements of TSS for non-point source dischargers, and it could be installed as a retrofit to existing storm drains. Therefore, no new infrastructure would be needed to begin using geotextile filters as a BMP.

The geotextile filter is a device for removing suspended solids from storm water runoff and thus, is a new option for a BMP. It was proven effective in laboratory and field conditions under extreme conditions, i.e., heavy influent flows and large TSS concentrations.

2. New filtration criteria have been established for use in choosing the appropriate geotextile filter for stormwater treatment. Criteria for this use of geotextile have never been established before this research. These criteria ratios can tell municipalities and others responsible for urban stormwater runoff which geotextile(s) can reduce TSS concentrations to a target concentration of 30 mg/L. With this information, educated decisions regarding geotextile use as a BMP can be made.

3. The results from the laboratory tests performed on a sand filter indicate that underground sand filters should be modified or replaced by another media, such as a geotextile, in order to improve drainage during stormwater treatment. More specifically, the laboratory results showed that the sand filter clogs faster than a geotextile filter in terms of total solids loaded to the filter. This information will help stormwater management decision-makers choose better BMPs in order to maximize the lifespan of the BMP and avoid detrimental situations such as flooding in streets from filter bypass.

4. The mathematical model produced in this research (Equation 19) can be used to predict the time of failure of a geotextile filter in stormwater treatment. The model predicts hydraulic conductivity values of the filter as a function of solids captured in and on the filter. With knowledge of an approximate average of total suspended solids concentration in the runoff and influent runoff flow rate along with 2 particle sizes and 2 opening sizes, one can use the information in this research on final stabilized hydraulic conductivity values at the failure point of the filter and the model given in Equation 19 to determine how long the filter will function properly in practice before maintenance or replacement is necessary.

5. This study evaluated the performance of geotextile filters from installation of the clean material to the point of the first instance of clogging. At this point, a cleaning procedure could be performed and the same geotextile filter could continue to perform stormwater treatment or the clogged geotextile could be replaced with an unused geotextile filter. Because the cost of nonwoven geotextile is so low, approximately $1/m^2$, replacement with clean geotextile would not significantly increase the overall cost of

maintenance of the geotextile filter system (MaineDOT 2012). Therefore, a cleaning procedure was not evaluated in depth for this study.

6. This study used one type of soil (described in Chapter II) for the laboratory tests on the geotextile filter columns, the sand filter columns, and the geotextile prototype tray. In practical applications, the user must be aware that there are many types of soils, and the geotextile criteria and hydraulic conductivity model may need to be adjusted to account for soils with higher or lower clay contents than the soil which was used for this study. Soils types vary widely across the United States and certain 2:1 phyllosilicate clay types, such as montmorillonite, can expand greatly when exposed to water (USC 2012). This expansion could impact the ability of the geotextile to capture suspended solids and could also alter the total mass of solids captured at the point of geotextile clogging.

RECOMMENDATIONS FOR FURTHER RESEARCH

The following research topics are recommended to succeed the activities of this study:

1. The three geotextiles chosen for evaluation in this research were excellent choices for suspended solids removal from stormwater runoff; had a geotextile with a larger permittivity and AOS been chosen, it would not have retained the fine particles in PSDs P2 and P3 and had a geotextile with a smaller permittivity and AOS been chosen, it would have retained more of the finest particles in the particle size distributions, but it would not have maintained adequate drainage through the system. However, there are other types of geosynthetics with similar opening sizes and permittivities that could be evaluated for use in stormwater treatment. One example is a geocomposite which is a material that consists of more than one type of geosynthetic material. The ideal

geocomposite for evaluation is a geotextile-geonet composite, where a geotextile is used on one or both sides of a geonet. A geonet is a polymeric netlike material with the sole design function of drainage. A geotextile-geonet composite has an improved drainage function than geotextile alone (Koerner 2005). Plus, if geotextile material is placed on both sides of the geonet, the filtration ability could vastly improve as well because the surface area of geotextile filter doubles with the addition of a second geotextile.

2. Although different PSDs were evaluated, the laboratory testing in this study utilized only one type of soil (silt) for the simulated stormwater suspension. It may improve the accuracy of laboratory testing to subject the geotextile filters to at least one other type of soil besides the silty soil from Polson County, Montana.

3. Further laboratory data could be collected using more particle size distributions and other geotextile filters in order to validate the geotextile filtration criteria developed in this research and establish more criteria for stormwater runoff filtration. Additional ratios which incorporate various particle sizes and filter opening sizes could be created for geotextile use in stormwater filtration so that no matter how much or how little data one has on the particles in the runoff or the opening sizes of the geotextiles, the best choice of geotextile could be made for the present need.

4. Further laboratory testing could be performed using various particle size distributions and geotextiles with different opening size distributions in order to collect data which would verify the functions which define the parameters *a* and *b* in the mathematical model in Equation 19. Correlations were drawn between *a* and *b* and various particle sizes and filter opening sizes in this research. However, specific

functions for *a* and *b* would be very beneficial for those using the model to assess the lifespan of a geotextile filter in practice.

5. Improvements to the geometry of the geotextile filter could be made in order to create the most effective BMP. For example, instead of a flat filter surface, a filter bag could be proposed, which would eliminate any side leakage that would normally occur for geotextile within a column or attached as a retrofit in a former underground sand filter system. Another example of a new geometry for the geotextile filter is a series of panels or baffles where initial panels of geotextile might serve as pre-treatment before the final panels.

6. While it is assumed that capturing suspended solids will remove a large percentage by mass of pollutants such as heavy metals and nutrients, it may be beneficial to also directly test the geotextile filters for their ability to retain these pollutants. Analysis of total phosphorus removal by the geotextile prototype system under field conditions has been initiated in a subsequent project. Nitrogen and phosphorus are two important nutrients that should be addressed by any BMP. Their presence is a result of fertilizers and natural sources, and they are of great importance because they cause eutrophication which leads to algal blooms and anoxic conditions in receiving bodies.

7. As mentioned in the Chapter I, hydrocarbons are a potential pollutant in urban stormwater runoff. Evaluations on the effectiveness of hydrocarbon removal by geotextile filters could be of great value. The adsorbent properties of polypropylene could aid in the attraction and retention of oil to geotextile filters (Monsu et al. 2011).

8. Finally, an economic evaluation of geotextile use as a BMP would be of great value to decision-makers in stormwater management. This research determined that a

geotextile would have a longer lifespan than a sand filter under similar stormwater runoff conditions. However, this study did not address the cost-savings that would result from the longer lifespan and reduced amount of maintenance needed. There would also be economic benefit from the installation of geotextile because of the ease of transport and handling of a roll of geotextile fabric compared to containers of sand.

Chapter VIII: APPENDIX

Theoretical Derivation of the Le Coq model

In order to theoretically develop Le Coq's model, Darcy's Law must first be applied to a filter.

$$\Delta p = \frac{\gamma_w v L}{k}$$

(29)

where Δp is pressure loss or head loss in the filter, γ_w is specific weight of water, L is length of the flow in the filter; and k is equivalent permeability, either in parallel accumulation (k_p) or series accumulation (k_s).

$$k_p = \frac{\sum_i k_i A_i}{\sum_i A_i} \quad \text{where} \quad \sum_i A_i = A$$

(30)

$$k_s = \frac{\sum_i L_i}{\sum_i L_i / k_i} \quad \text{where} \quad \sum_i L_i = t$$

(31)

A_i is area of elementary element number i of filter media, L_i is length of elementary element i of filter media, and k_i is permeability of elementary element i of filter media. Since both types of accumulation occur simultaneously, the pressure loss is a combination of pressure loss due to series accumulation (Δp)$_s$ and pressure loss due to parallel accumulation (Δp)$_p$, weighted by the coefficients N and (1-N) respectively.

$$\Delta p = N(\Delta p)_s + (1 - N)(\Delta p)_p$$

(32)

where (Δp)$_s$ and (Δp)$_p$ are functions of k_s and k_p, respectively (Faure et al. 2006).

Le Coq (1996) proposed that relative pressure loss $\Delta p / \Delta p_0$, is a function of the mass of accumulated particles in the filter, m.

$$(\Delta p / \Delta p_0)_p = \exp\left(\frac{m}{m_1}\right) \quad \text{for parallel accumulation,} \tag{33}$$

$$(\Delta p / \Delta p_0)_s = \left(\frac{m}{m_1}\right)^a \quad \text{for series accumulation,} \tag{34}$$

where Δp_0 is initial pressure loss in the filter, and m_1 is the critical value of mass of accumulated particles.

When $m<m_1$, accumulation is in parallel, and when $m>m_1$, accumulation is in series. The weighting coefficient N is related to the ratio m/m_1 by:

$$N = \tanh\left(b\frac{m}{m_1}\right) = \frac{e^{2b\frac{m}{m_1}} - 1}{e^{2b\frac{m}{m_1}} + 1} \tag{35}$$

where a and b are fitted parameters. Faure et al. (2006) suggest that m be considered as the mass of injected particles rather than accumulated particles because the first quantity is much easier to measure, but accumulated particles is more accurate. Therefore, m shall remain mass of accumulated particles in order to attain the most accurate results.

In the experimental set-up by Faure et al. (2006), pressure is measured at a specific height above a geotextile filter when a pump imposes a flow rate of clear water onto it, p_0. Then, the filter is exposed to a flow with a concentration of dispersed particles and the pressure is measured at the same height. This pressure is called p, and is recorded continuously as the filter encounters the concentrated flow. Once the mass of accumulated particles reaches m_1, p suddenly increases until the safety valve is switched. The downstream pressure in the filter set-up is constant; therefore, the excess pressure δp is the difference between p and p_0.

$$\delta p = p - p_0 = \Delta p - \Delta p_0 \tag{36}$$

Combining Equations (34)-(36), results in Le Coq's model:

$$\delta p = \Delta p_0 \left[(1-N)\exp\frac{m}{m_1} + N\left(\frac{m}{m_1}\right)^a - 1 \right]$$

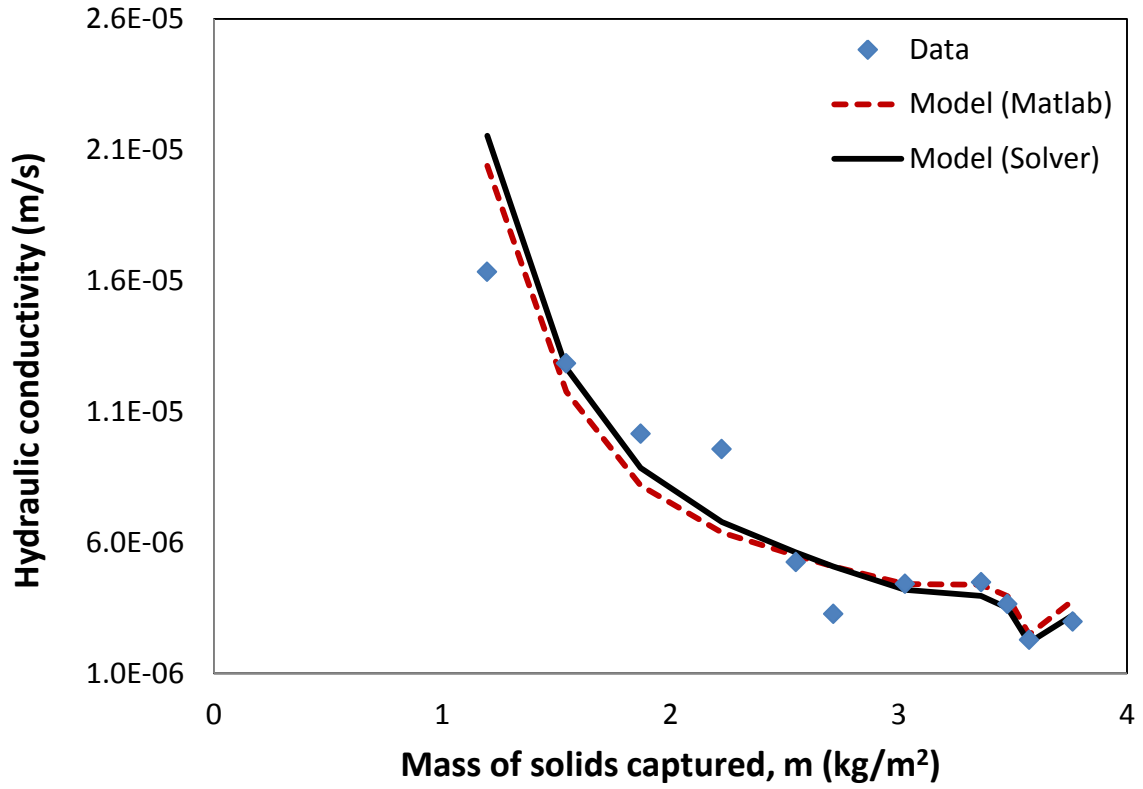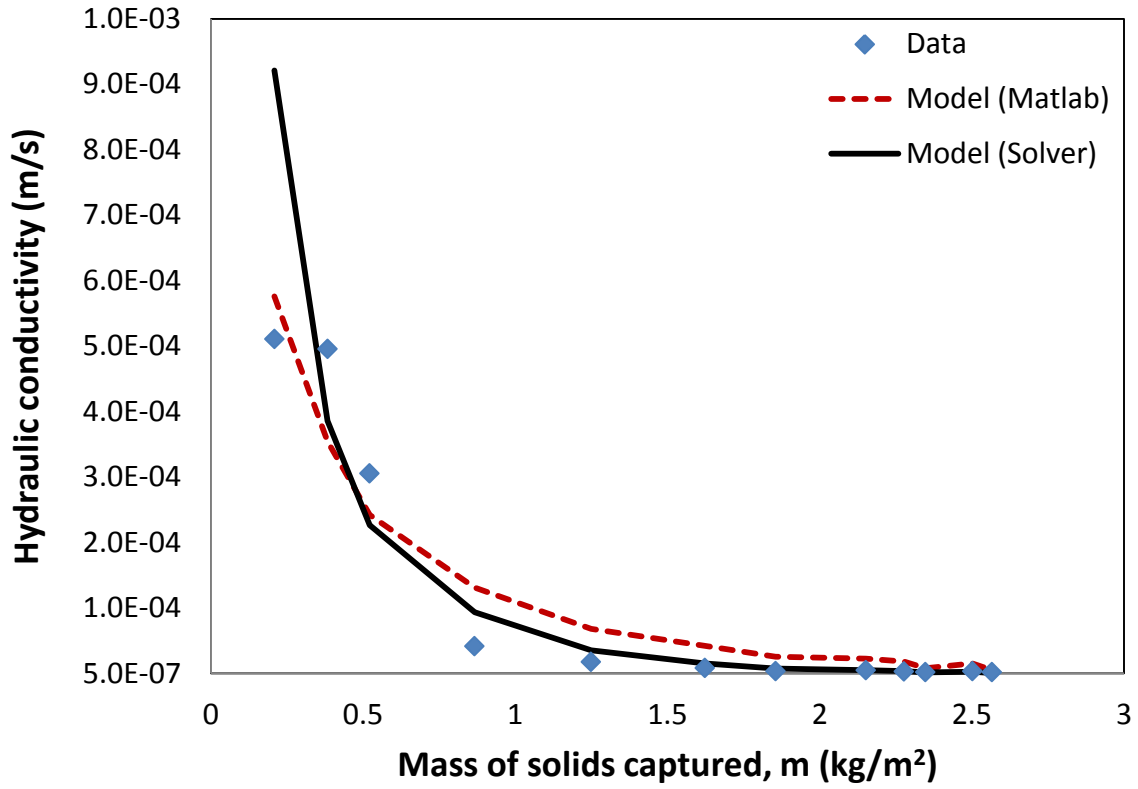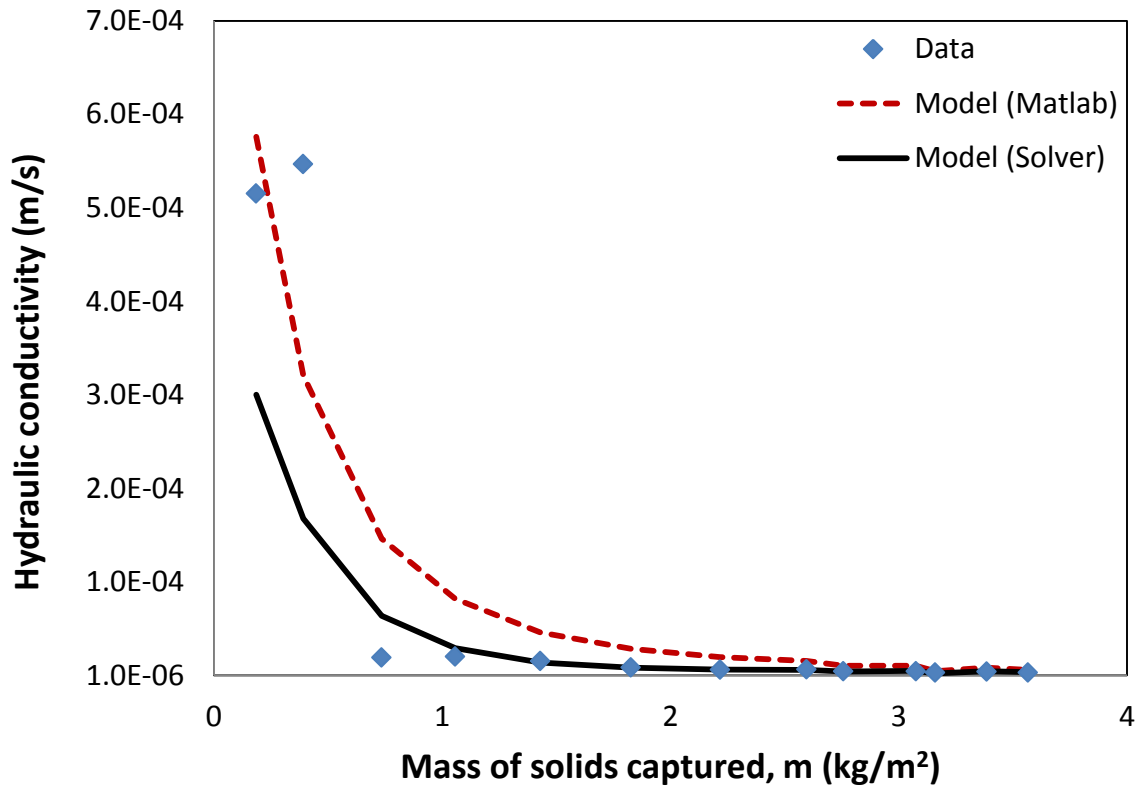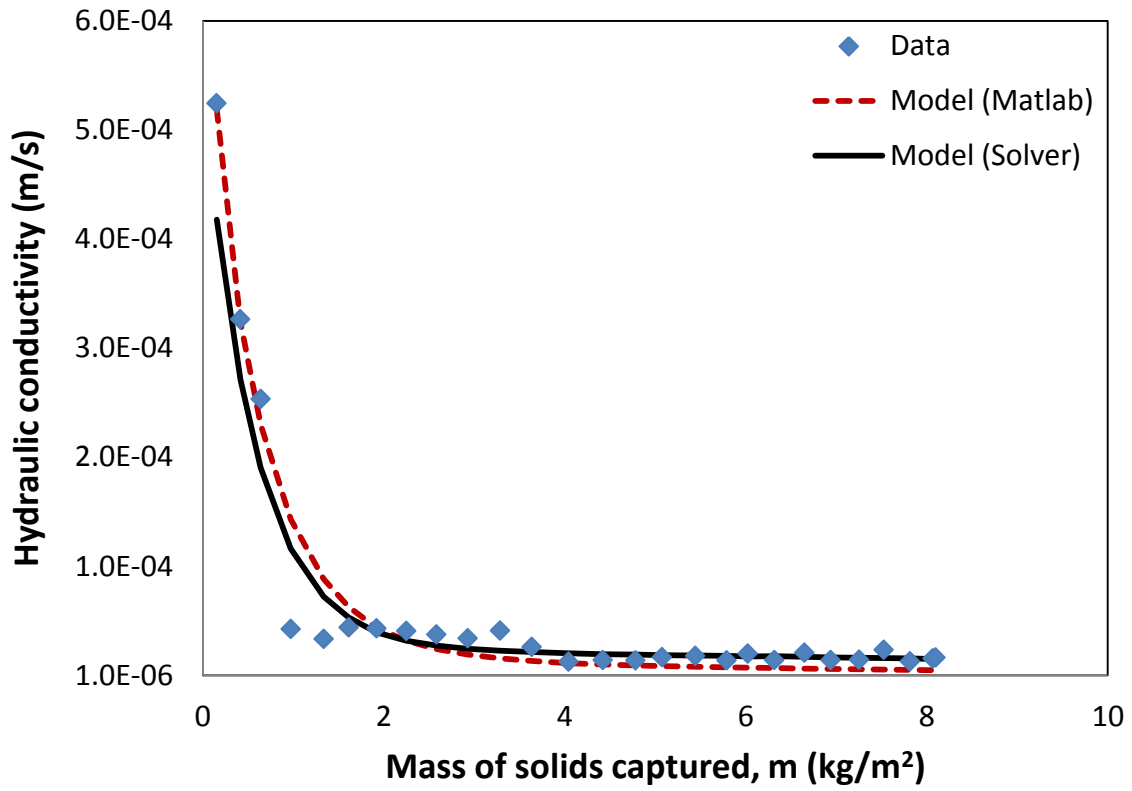$$N = \tanh\left(b\frac{m}{m_1}\right). \tag{37}$$

Figure 85. Hydraulic conductivity values measured during laboratory testing and
hydraulic conductivities predicted by the theoretical model (Equation 19) as a function of
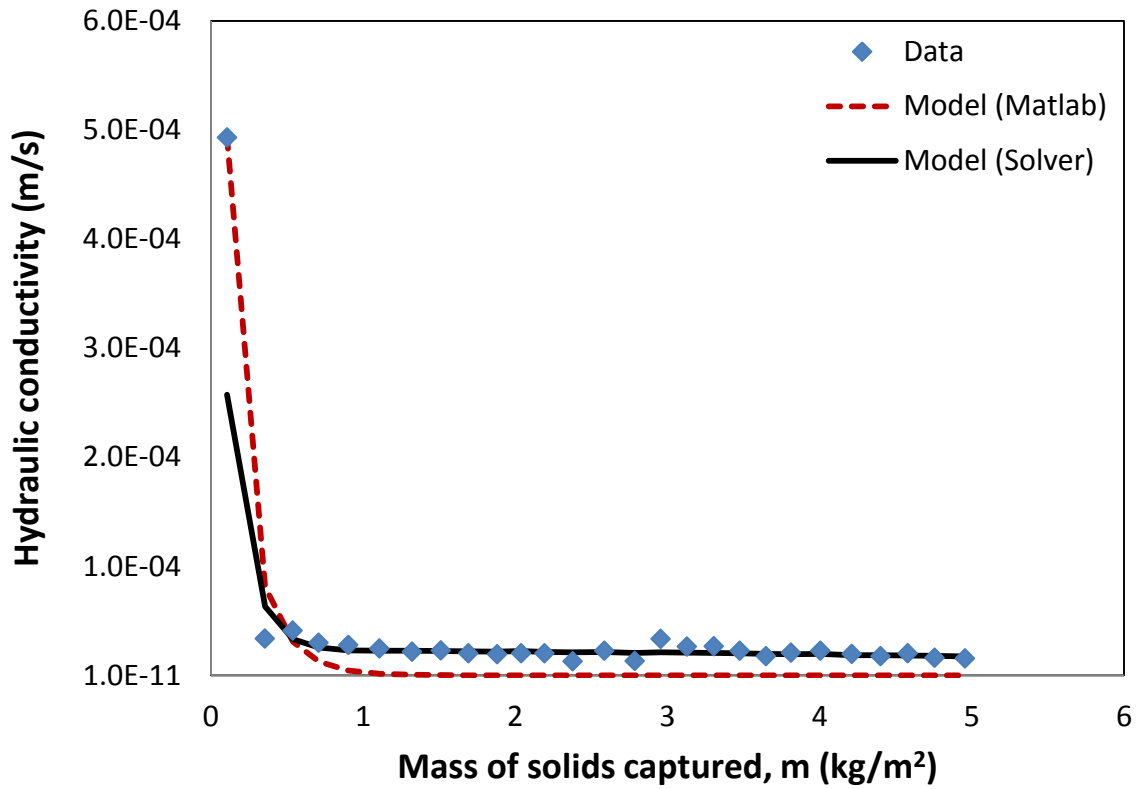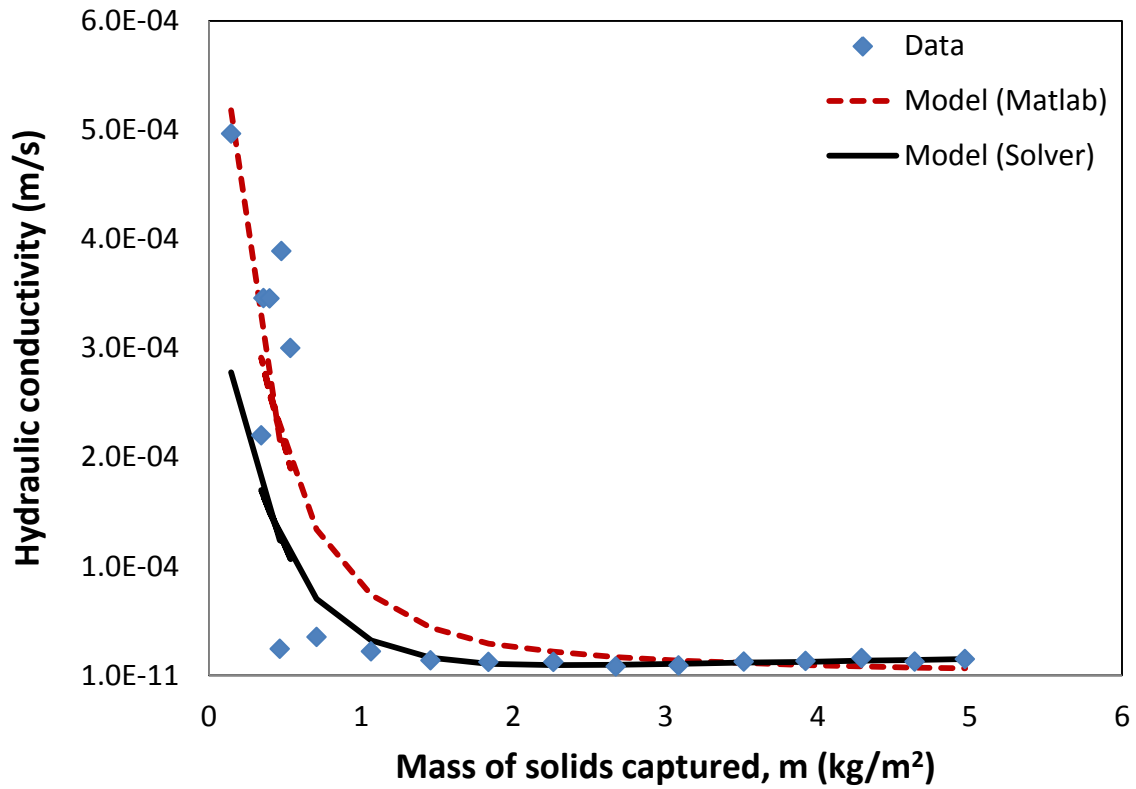the mass of solids captured by the filter for Test 3.P1.

Figure 86. Hydraulic conductivity values measured during laboratory testing and hydraulic conductivities predicted by the theoretical model (Equation 19) as a function of the mass of solids captured by the filter for Test 3.P2.
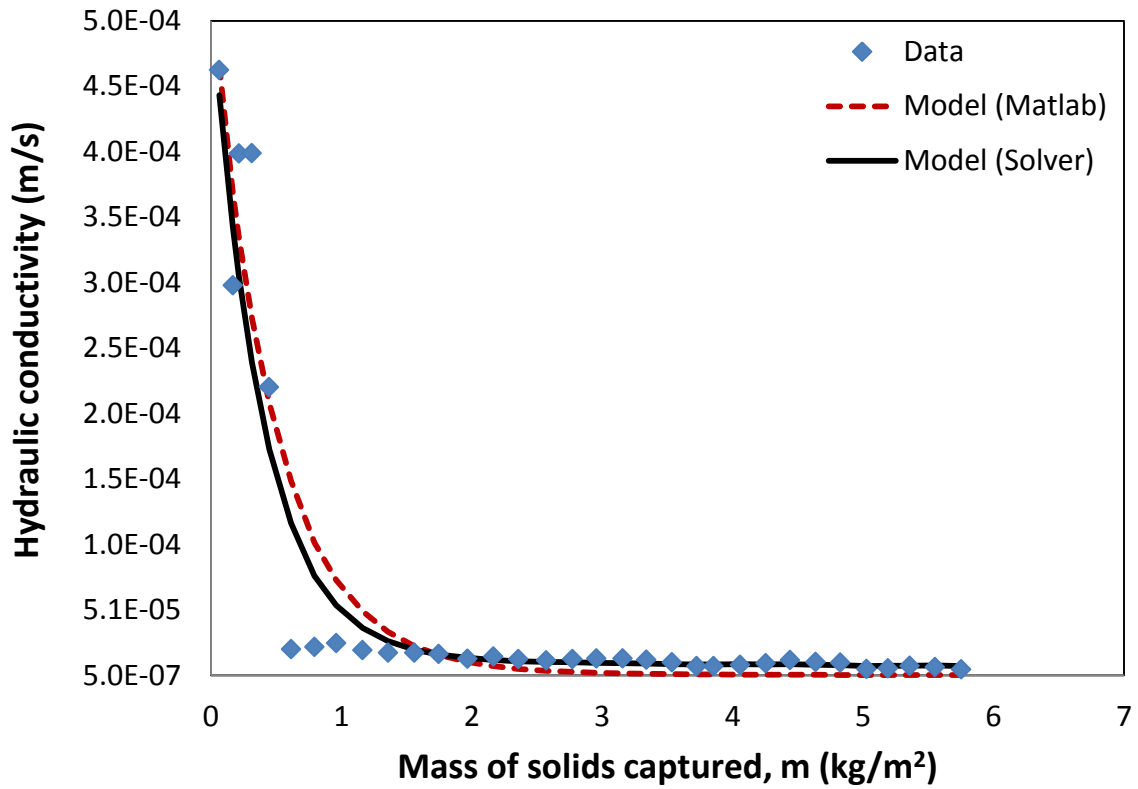
Figure 87. Hydraulic conductivity values measured during laboratory testing and hydraulic conductivities predicted by the theoretical model (Equation 19) as a function of the mass of solids captured by the filter for Test 2.P2.

Figure 88. Hydraulic conductivity values measured during laboratory testing and
hydraulic conductivities predicted by the theoretical model (Equation 19) as a function of
the mass of solids captured by the filter for Test 1.P1.

Figure 89. Hydraulic conductivity values measured during laboratory testing and

hydraulic conductivities predicted by the theoretical model (Equation 19) as a function of

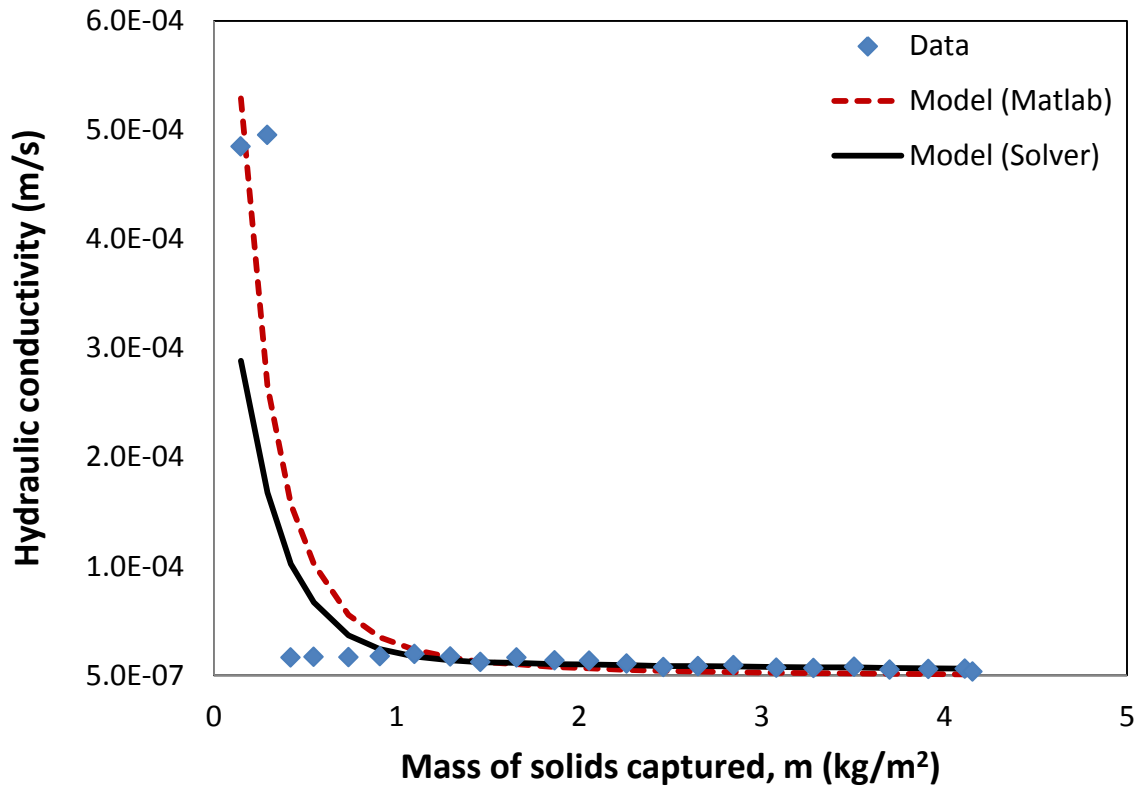the mass of solids captured by the filter for Test 3.P1(100).

Figure 90. Hydraulic conductivity values measured during laboratory testing and hydraulic conductivities predicted by the theoretical model (Equation 19) as a function of the mass of solids captured by the filter for Test 1.P1(repeat).
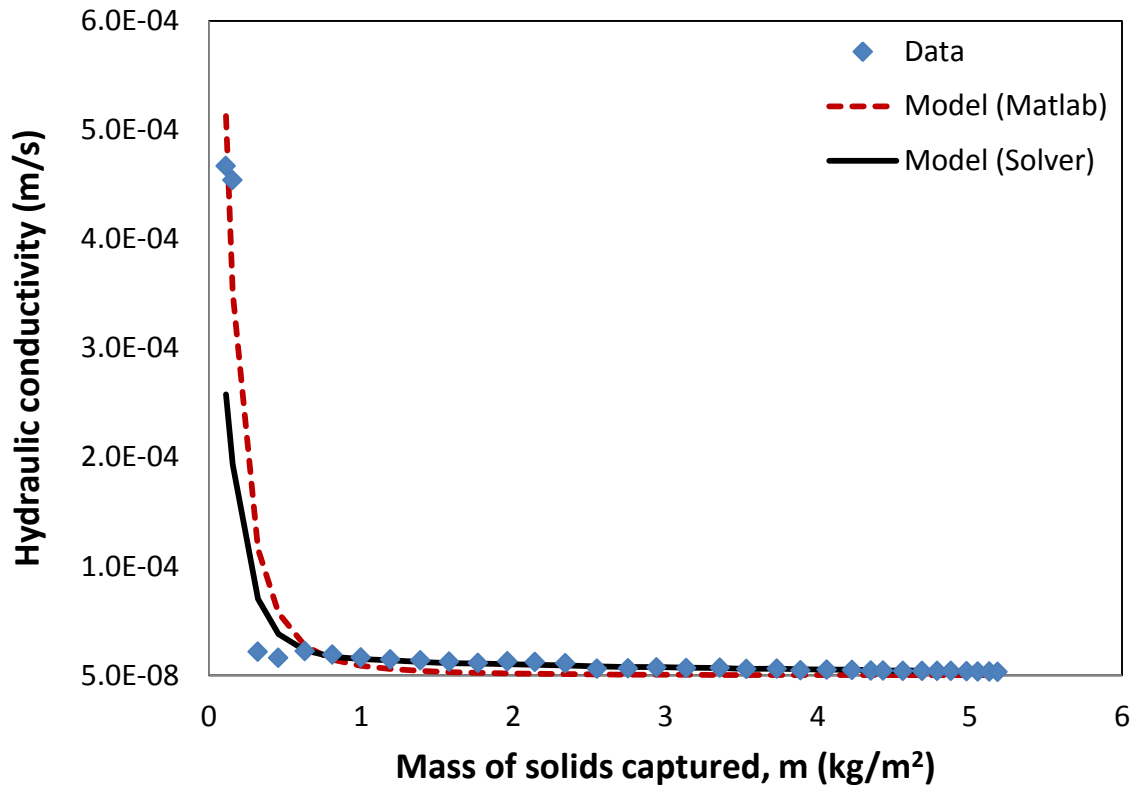
Figure 91. Hydraulic conductivity values measured during laboratory testing and hydraulic conductivities predicted by the theoretical model (Equation 19) as a function of the mass of solids captured by the filter for Test 2.P1(100).

Figure 92. Hydraulic conductivity values measured during laboratory testing and hydraulic conductivities predicted by the theoretical model (Equation 19) as a function of the mass of solids captured by the filter for Test 3.P1(100).
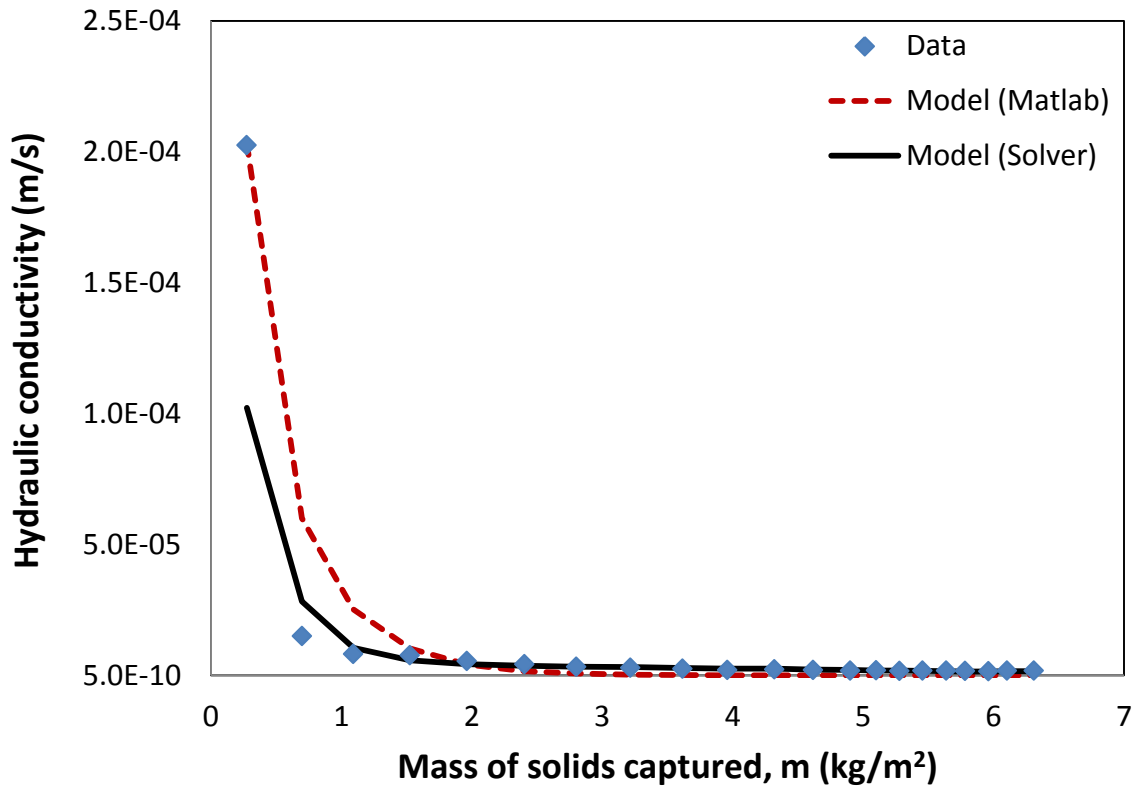
Figure 93. Hydraulic conductivity values measured during laboratory testing and hydraulic conductivities predicted by the theoretical model (Equation 19) as a function of the mass of solids captured by the filter for Test 3.P2(100).

Figure 94. Hydraulic conductivity values measured during laboratory testing and
hydraulic conductivities predicted by the theoretical model (Equation 19) as a function of
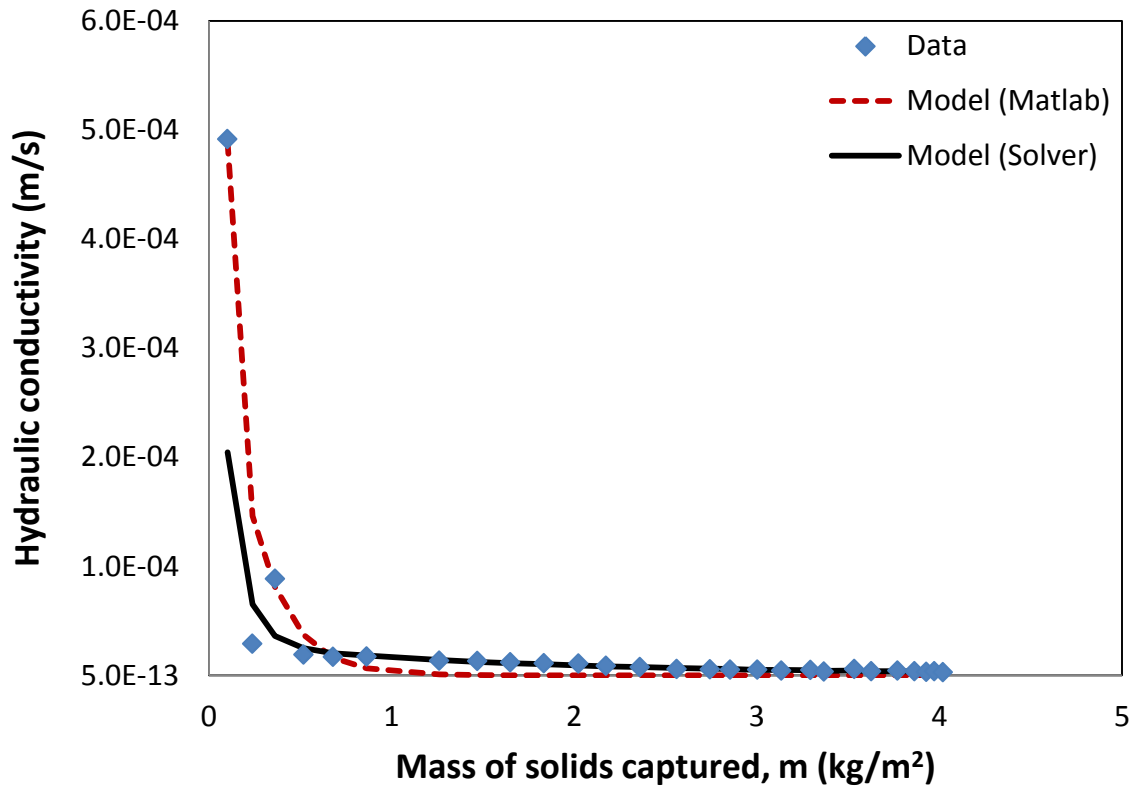the mass of solids captured by the filter for Test 2.P1(3).

Figure 95. Hydraulic conductivity values measured during laboratory testing and hydraulic conductivities predicted by the theoretical model (Equation 19) as a function of the mass of solids captured by the filter for Test 2.P2(100).
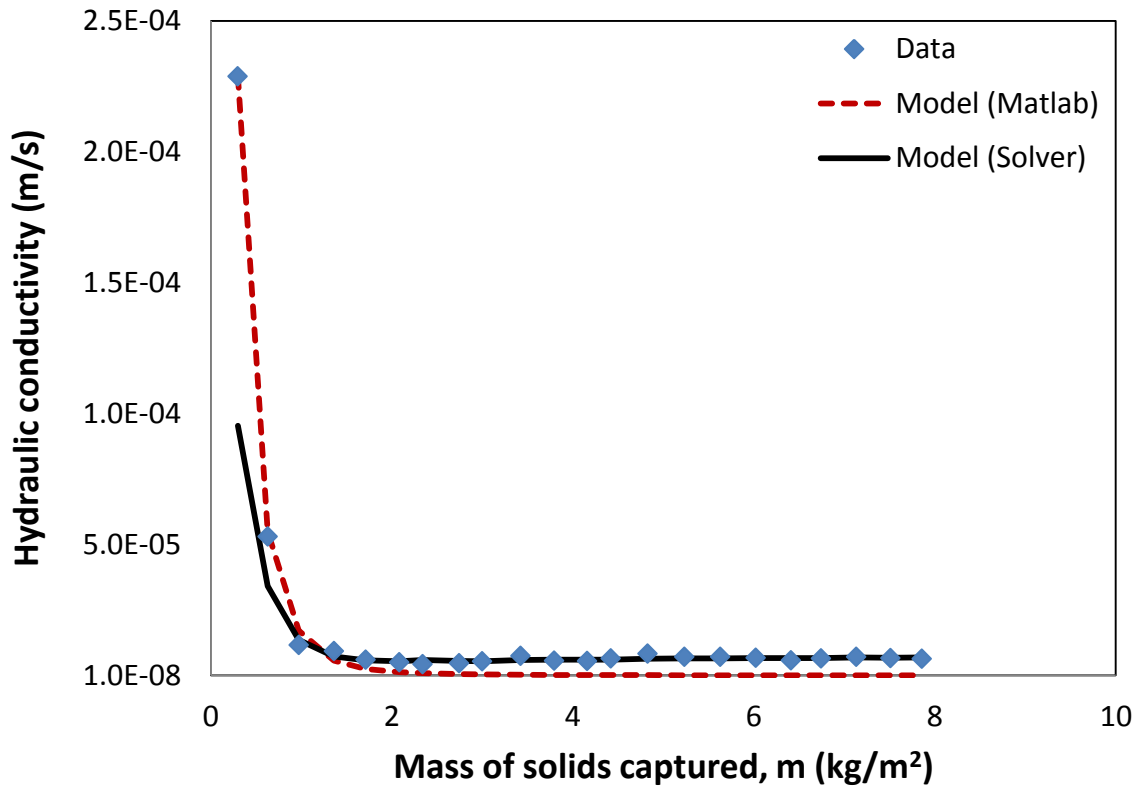
Figure 96. Hydraulic conductivity values measured during laboratory testing and hydraulic conductivities predicted by the theoretical model (Equation 19) as a function of the mass of solids captured by the filter for Test 1.P1(3).
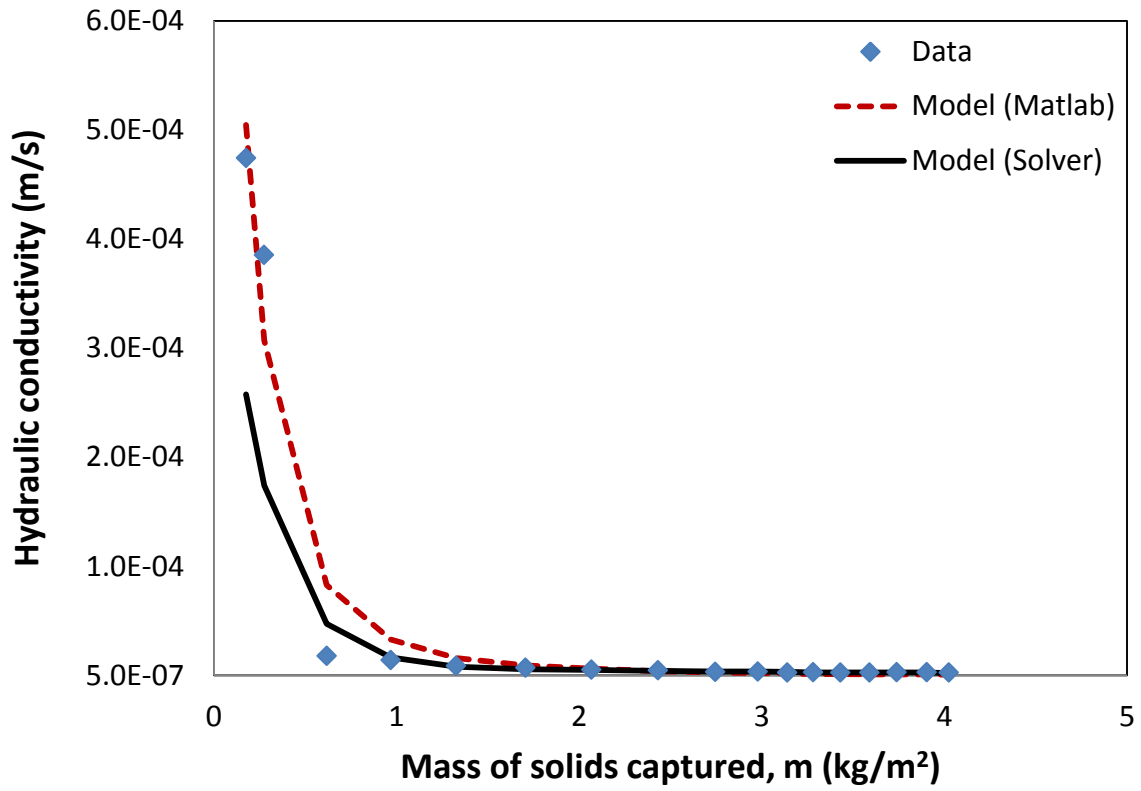
Figure 97. Hydraulic conductivity values measured during laboratory testing and hydraulic conductivities predicted by the theoretical model (Equation 19) as a function of the mass of solids captured by the filter for Test 2.P3.

Figure 98. Hydraulic conductivity values measured during laboratory testing and hydraulic conductivities predicted by the theoretical model (Equation 19) as a function of the mass of solids captured by the filter for Test 3.P3.
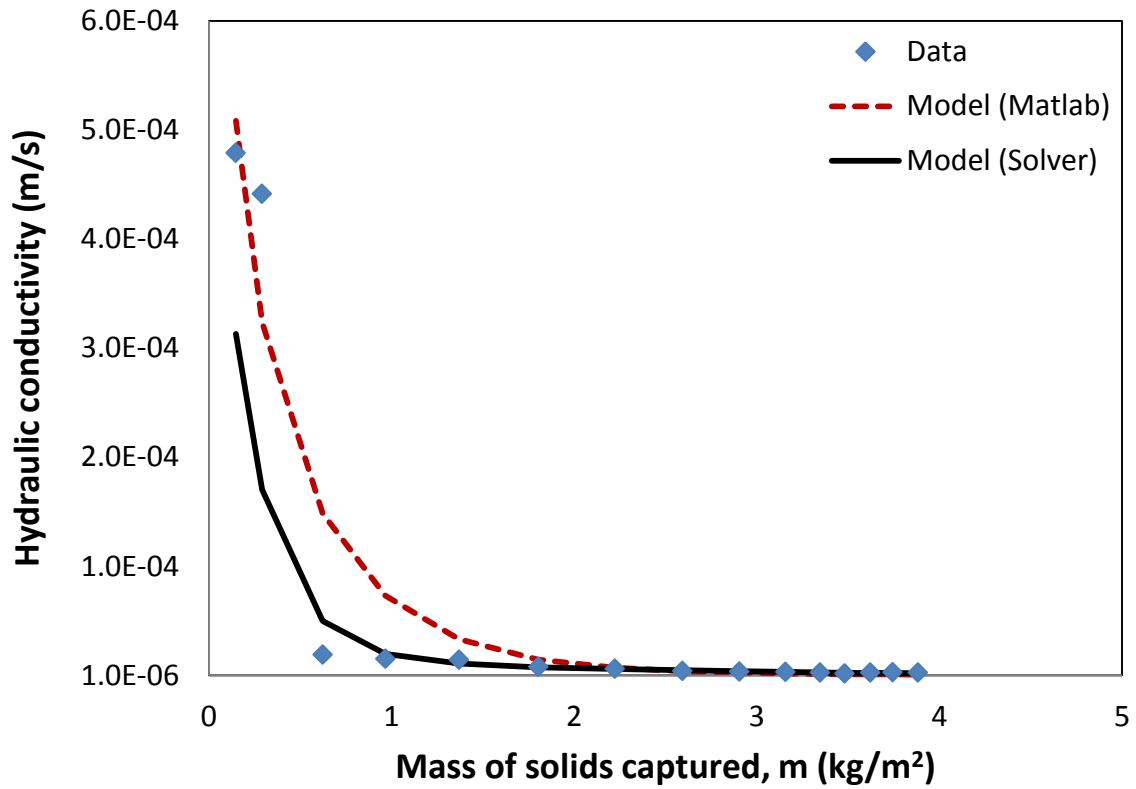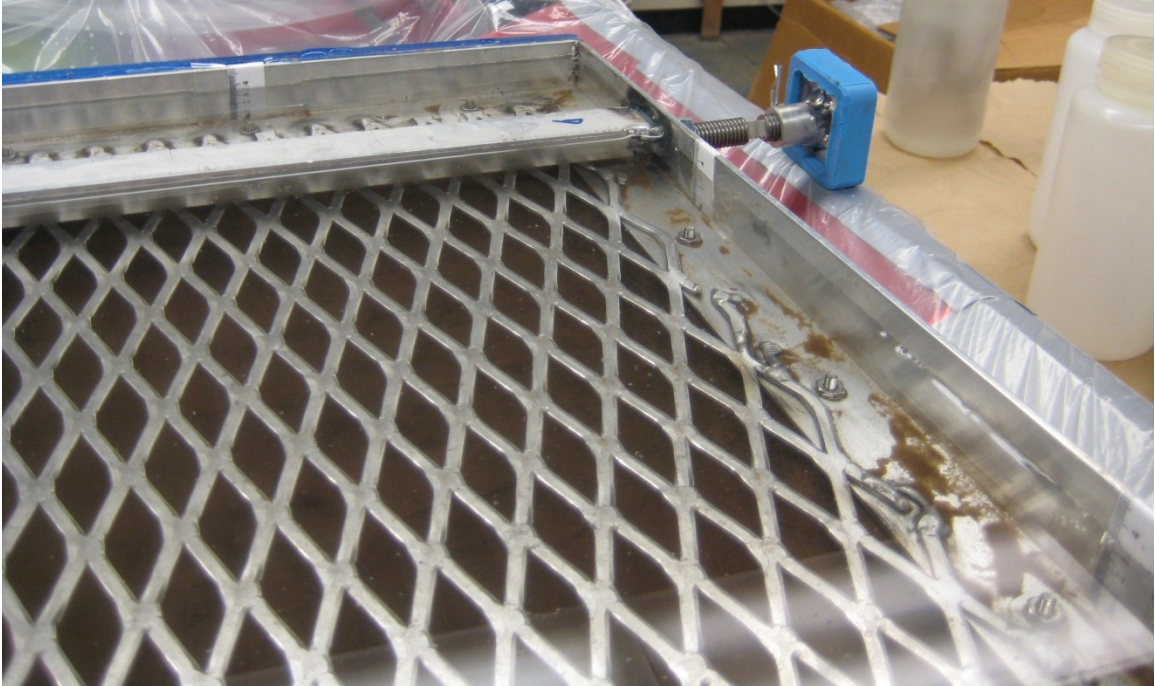
Figure 99. Prototype filter system after solids build-up.

Peak Flow Reduction by Prototype Filter In-Field

The prototype filter effectively reduced peak flow rates for each storm event. The peak flow reductions ranged from 48 to 81%, with an average peak flow reduction of 69% during the storm events. Figure 100 shows the peak flow reductions for each event as a function of the total influent runoff volume.
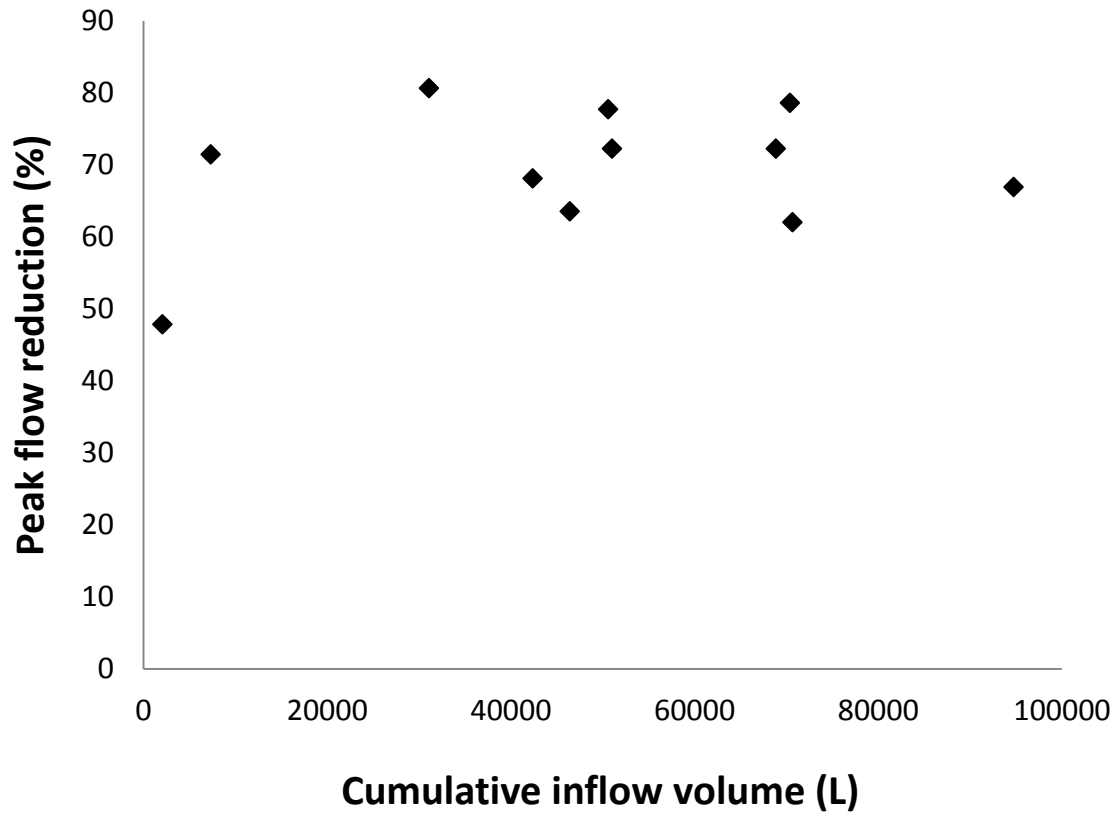
Figure 100. Peak flow reduction of each storm event as a function of the total inflow
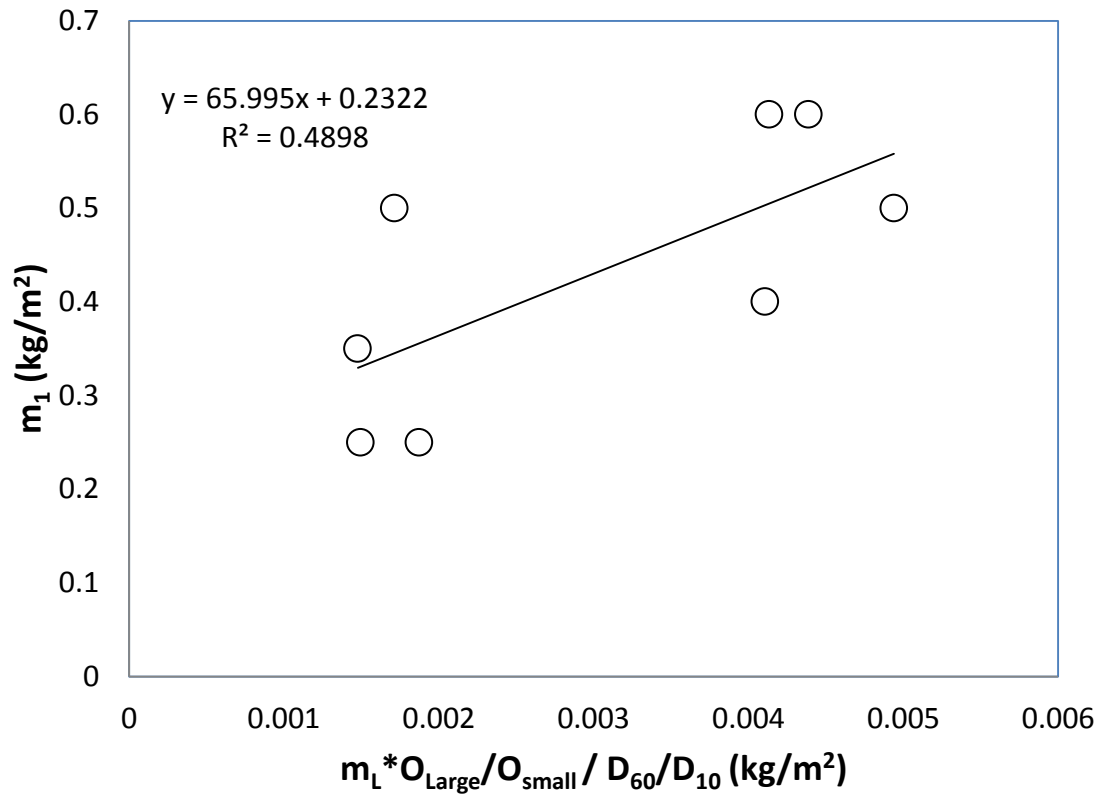
volume of runoff

Figure 101. m_1 as a function of of $m_L*O_{large}/O_{small} / D_{60}/D_{10}$ for all data sets with influent

TSS concentration of 200 mg/L and influent flow rate of 6 mL/s.

REFERENCES

AWWA (American Water Works Association) (1999). *Water Quality and Treatment*, 5th edition. McGraw-Hill, New York.

Aydilek, A. H. (2011). "*Filters and Drains", Chapter 3, Handbook of Geosynthetic Engineering*, Ed. Shukla, S.; Telford, T., Inc., pp. 67-87.

Aydilek, A. H., D'Hondt, D. and Holtz, R. D. (2007). "Comparative evaluation of geotextile pore sizes using bubble point test and image analysis." *Geotechnical Testing Journal*, 30 (3), 1-9.

Ayyub, B. M., and McCuen, R. H. (2003). *Probability, Statistics, and Reliability for Engineers and Scientists*, 2nd edition. Chapman & Hall/CRC, Boca Raton, FL.

Barrett, M. E. (2003). "Performance, Cost, and Maintenance Requirements of Austin Sand Filters." *Journal of Water Resources Planning and Management, ASCE*, 129(3), 234-242.

Barrett, M., Kearfott, P., and Malina, J. (2006). "Stormwater quality benefits of a porous friction course and its effect on pollutant removal by roadside shoulders." *Water Environ. Res.*, 78, 2177-2185.

California Stormwater Quality Association (CASQA) (2003). California Stormwater BMP Handbook, New Development and Redevelopment, California Stormwater Quality Association, January 2003. http://www.cabmphandbooks.com/Documents/Development/TC-40.pdf (Aug. 1, 2012).

Cedergren, H. R. (1989). *Seepage, Drainage, and Flow Nets*, 3rd edition, Wiley-Interscience, New York, USA.

Clark, S. E., and Pitt, R. (2009). "Solids removal in storm-water filters modeled using a power equation." *J. Environ. Eng.*, 135(9), 896-899.

Davis, A. P. (2008). "Field performance of bioretention: Hydrology impacts." *Journal of Hydrologic Engineering*, 13(2), 90-95.

Dullien, F. A. L. (1975). "New network permeability model of porous media." *AIChE J.*, 21 (2), 299-307.

Eaton, A. D., Clesceri, L. S., and Greenburg, A. E. (1995). *Standard Methods for the Examination of Water and Wastewater*, 19th edition. American Public Health Association, Washington, DC.

Eliasson, J. (2002). Sand/Media Specifications, Rule Development Committee Issue Research Report Draft, Washington Department of Health, Wastewater Management Program. November 26, 2002. (Aug. 28, 2012).

Environmental Protection Agency (EPA), (2012). Proposed Rulemaking to Strengthen the National Stormwater Program-National Pollutant Discharge Elimination System (NPDES). July 10, 2012. http://cfpub.epa.gov/npdes/stormwater/rulemaking.cfm (Aug. 15, 2012).

Faure, Y. H., Baudoin, A., Pierson, P., and Ple, O. (2005). "A contribution for predicting geotextile clogging during filtration of suspended solids." *Geotextiles and Geomembranes*, 24, 11-20.

Fischer, G. R. (1994). *The Influence of Geotextile Pore Structure on the Behavior of Geotextile Filters*, Ph.D. Dissertation, University of Washington, Seattle, Washington.

Fischer, G. R., Christopher, B. R., and Holtz, R. D. (1990). "Filter criteria based on pore size distribution." *Proceedings of the Fourth International Conference on Geotextiles, Geomembranes and Related Products*, The Hague, The Netherlands, 1, 289–294.

Flint, K., and Davis, A. P. (2007). "Pollutant mass flushing characteristics of highway stormwater runoff from an ultra urban area." *J. Environ. Eng.,* 133(6), 616-626.

Furumai, H., Balmer, H., and Boller, M. (2002). "Dynamic behavior of suspended pollutants and particle size distribution in highway runoff." *Water Science and Technology*, 46(11-12), 413-418.

Gironas, J., Adriasola, J. M., and Fernandez, B. (2008). "Experimental analysis and modeling of a stormwater perlite filter." *Water Environ. Res*., 80(6), 524-539.

Giroud, J. P. (1982). "Filter Criteria for Geotextiles"*, Proceedings of the Second International Conference on Geotextiles*, Las Vegas, 1, 103-108.

Hallberg, M., and Renman, G. (2008). "Suspended solids concentration in highway runoff during summer conditions." *Polish J. of Environ. Stud*., 17(2), 237-241.

Holtz, R. D., Christopher, B. R., and Berg, R. R. (1998). *Geosynthetic Design and Construction Guidelines-Participant Notebook*, U.S. Federal Highway Administration, FHWA HI-95-038, McLean, Virginia.

Kandasamy, J., Beecham, S., and Dunphy, A. (2008). "Stormwater sand filters in water-sensitive urban design." *Water Management*, 161(WM2), 55-64.

Kim, J. -K., and Sansalone, A. H. (2008). "Event-based size distributions of particulate matter transported during urban rainfall-runoff events." *Water Res*., 42, 2756-2768.

Koerner, R. M. (2005). *Designing with geosynthetics*, 5th ed., Pearson Prentice Hall, New Jersey.

Korkut, E. N., Martin, J. P., and Yaman, C. (2006). "Wastewater treatment with biomass attached to porous geotextile baffles." *Journal of Environmental Engineering*, 132(2), 284-288.

Kreeb, L. B. (2003). *Hydrologic efficiency and design sensitivity of bioretention facilities*. Honors Research, University of Maryland, College Park, MD.

Kutay, M. E., and Aydilek, A. H. (2004). "Retention performance of geotextile containers confining geomaterials". *Geosynthetics International*, 11(2), 100-113.

Kutay, M. E., and Aydilek, A. H. (2005). "Filtration performance of two-layer geotextile systems." *Geotechnical Testing Journal*, 28(1), 1-13.

Lafleur, J., Mlynarek, J., and Rollin, A. L. (1989). "Filtration of Broadly Graded Cohesionless Soils.", *Journal of Geotechnical Engineering*, ASCE, 115(12), 1747-1768.

Le Coq, L. (1996). "Mise en oeuvre et modélisation de médias filtrants à base de fibres minérales pour le filtration des huiles en avionique." Thèse de Doctorat de l'Institut national polytechnique de Grenoble, Ecole Française de Papeterie et Industries Graphiques de Grenoble, Novembre 1996, 280p.

Le Coq, L. and Silvy, J. (1999). "Fibrous media plugging modeling for liquid filtration." *Chemical Engineering Communications*, 174, 145-166.

Li, H., and Davis, A. P. (2008). "Urban particle capture in bioretention media I: Laboratory and field studies." *J. Environ. Eng.,* 134(6), 409-418.

Li, Y., Lau, S. -L., Kayhanian, M., and Stenstrom, M. (2006). "Dynamic characteristics of particle size distribution in highway runoff: Implications for settling tank design." *J. Environ. Eng.,* 132(8), 852-861.

Madigan, M. T. and Martinko, J. M. [ed.s] (2006). *Brock Biology of Microorganisms*, 11th ed., Pearson Prentice Hall, New Jersey.

MaineDOT (2012). MaineDOT, Geotextiles. http://www.maine.gov/mdot/mlrc/geotextiles.php (Sept. 18, 2012).

Mao, N., Otani, Y., Yao, Y., and Kanaoka, C. (2006). "Modeling the filtration process with a flat-type fabric filter." *Advanced Powder Technol.*, 17(3), 237-256.

Maryland State Archives (MSA) (2012). Maryland at a Glance, Weather. Maryland State Archives, http://www.msa.md.gov/msa/mdmanual/01glance/html/weather.html (Feb. 27, 2012).

Mathworks (2012). Product Documentation, Statistics toolbox.
http://www.mathworks.com/help/toolbox/stats/nlinfit.html (July 19, 2012).

Millar, P. J., Ho, K. W., and Turnbull, H. R. (1980). *A Study of Filter Geotextiles for Geotechnical Applications in New Zealand*, Ministry of Works and Development, Central Laboratories Report No.2-80/5, New Zealand.

Monsu, N., Timko, K., and Caracciolo, W. (2011). "Learning from the Deepwater Horizon oil spill and preparing for the future." ASEE Middle Atlantic Regional Conference. Apr. 29-30. http://www.asee.org/documents/sections/middle-atlantic/spring-2011/Learning-from-the-Deepwater-Horizon-Oil-Spill-and-Preparing-for-the-Future.pdf (July 1, 2012).

Mulligan, C. N., Davarpanah, N., Fukue, M., and Inoue, T. (2009). "Filtration of contaminated suspended solids for the treatment of surface water." *Chemosphere*, 74, 779-786.

Munson, B. R., Young, D. F., and Okiishi, T. H. (2006). *Fundamentals of Fluid Mechanics*, 5th ed., John Wiley and Sons, Inc., New Jersey.

Nilsson, L. and Stenstrom, S. (1996). "Effects of serial and parallel pore nonuniformities: Results from two models of the porous structure." *Transport in Porous Media*, 25: 335-350.

Ogink, H. J. M. (1975). *Investigations on the Hydraulic Characteristics of Synthetic Geotextiles*, Delft Hydraulics Laboratory, Publication No. 146.

Pepper, I. L., Gerba, C. P., and Brusseau, M. L. (2006). *Environmental and pollution science*, 2nd ed., Elsevier Inc., Oxford.

Rankilor, P. R. (1981). *Membranes in Ground Engineering*, John Wiley & Sons, New York, 377.

Rollin, A. L., and Lombard, G. (1988), "Mechanisms Affecting Long-Term Filtration Behavior of Geotextiles.", *Geotextiles and Geomembranes*, 7, 119-145.

Sansalone, J. J., and Buchberger, S. G. (1997). "Partitioning and first flush of metals in urban roadway storm water." *J. Environ. Eng.,* 123, 134.

Sansalone, J. J., Hird, J. P., Cartledge, F. K., and Tittlebaum, M. E. (2005). "Event-based stormwater quality and quantity loadings from elevated urban infrastructure affected by transportation". *Water Environ. Res*., **77**(4), 348-365.

Sansalone, J. J., Koran, J. M., Smithson, J. A., and Buchberger, S. G. (1998). "Physical characteristics of urban roadway solids transported during rain events." *J. Environ. Eng*., 124(4), 427-440.

Sansalone, J. J., Lin, H., and Ying, G. (2009). "Experimental and field studies of Type I settling for particulate matter transported by urban runoff." *J. Environ. Eng.*, 135(10), 953-963.

Schober, W., and Teindl, H. (1979). Filter Criteria for Geotextiles, *Proceedings of 7th European Conference on Soil Mechanics and Foundation Engineering*, Brighton. England, 2, 121-129.

Siriwardene, N. R., Deletic, A., and Fletcher, T. D. (2007). "Clogging of stormwater gravel infiltration systems and filters: Insights from a laboratory study." *Water Res.*, 41, 1433-1440.

Southeast Michigan Council of Governments (SEMCOG) (2008). Low Impact Development Manual for Michigan: A Design Guide for Implementors and Reviewers. http://library.semcog.org/InmagicGenie/DocumentFolder/LIDManualWeb.pdf (Jan. 10, 2010).

Strecker, E. W., Quigley, M. M., Urbonas, B. R., Jones, J. E., and Clary, J. K. (2001). "Determining urban storm water BMP effectiveness." *Journal of Water Resources Planning and Management*, 127(3), 144-149.

Taebi, A., and Droste, R. L. (2004). "First flush pollution load of urban stormwater runoff". *J. Environ. Eng.*, 3, 301-309.

United States Bureau of Reclamation (USBR) (2001). *Water Measurement Manual, Chapter 8 Flumes, Part 10 Parshall Flumes*. 3rd ed.-revised. http://www.usbr.gov/pmts/hydraulics_lab/pubs/wmm/chap08_10.html (Jul. 1, 2012)

University of Southern California (USC) (2012). USC online lecture: Clay minerals. http://earth.usc.edu/~dfarris/Mineralogy/17_ClayMinerals.pdf (Sept. 18, 2012)

Urbonas, B. R. (1999). "Design of a sand filter for stormwater quality enhancement." *Water Environ. Res.*, 71(1), 102-113.

Walker, D. B., Baumgartner, D. J., Gerba, C. P. and Fitzsimmons, K. (2006). *Environmental and pollution science*, *Chapter 18: Surface water pollution*, 2nd ed., Pepper, I.L., Gerba, C.P., and Brusseau, M.L. [ed.s], Elsevier Inc., Oxford.